Advanced Vehicle Power Technology Alliance
Fiscal Year 2014 (FY14) Annual Report
(1 Oct 2013 – 30 Sep 2014)

Department of the Army
(RDTA-COS-EB)
Department of Energy

April 30, 2015

Mr. Patrick Davis
Project Director, Vehicle Technologies Office, Department of Energy-Energy Efficiency and Renewable Energy (DOE-EERE).

Dr. Paul Rogers
Director, United States Army Tank Automotive Research, Development and Engineering Center (TARDEC), United States Army Research Development and Engineering Command (RDECOM), United States Army Materiel Command (AMC).

This Page Intentionally Blank

ACKNOWLEDGEMENTS

The Advanced Vehicle Power Technology Alliance (AVPTA) between the Department of Energy (DOE) and the Department of the Army (DA) was publicly announced in July 2011. The Alliance underscores the urgency for energy security; in particular, an emphasis on developing advanced technologies that enable military ground vehicles to become significantly more energy efficient. Individually and collaboratively, the DOE and DA have a long history of successfully developing innovative vehicle technologies. The Alliance is chartered to accelerate the conceptualization and transition into deployment of inventive and creative energy-saving concepts that the Nation needs to achieve energy security.

This report summarizes the third year of technical effort and output of the Alliance's Technology Focus Area (TFA) working groups that were established in July 2011. The TFAs are respectively led by DOE and DA Subject Matter Experts (SMEs) that jointly recommend and oversee project portfolios in areas of interagency mutual technical interest.

We acknowledge the significant contributions of the DOE and DA administrative and technical personnel who in three short years have grown the Alliance from a notional concept into a self-sustaining and highly-productive entity. Work product generated by the Alliance has migrated into commercial and military applications through industry partners. In parallel with ongoing activities, DOE and DA personnel are pursuing opportunities to extend the AVPTA enterprise into new areas of engagement including: autonomy-enabled technologies, advanced / modular manufacturing, the 21st Century Truck Partnership, exploring leading edge technology development with the Advanced Research Projects Agency – Energy (ARPA-E), other Department of Defense (DOD) service branches; and Local, State and other Federal Government agencies.

We specifically acknowledge Mr. Edwin Owens who recently retired from distinguished service in the DOE Vehicle Technologies Office (VTO). Mr. Owens contributed to the Alliance from its inception providing both administrative and technical leadership, the latter in the role of the VTO's Lightweight Structures & Materials TFA Lead.

Mr. Patrick Davis
Project Director, Vehicle Technologies Office, Department of Energy-Energy Efficiency and Renewable Energy (VTO, DOE-EERE).

Dr. Paul Rogers
Director, United States Army Tank Automotive Research, Development and Engineering Center (TARDEC), United States Army Research Development and Engineering Command (RDECOM), United States Army Materiel Command (AMC).

This Page Intentionally Blank

CONTENTS

This Page Intentionally Blank

EXECUTIVE SUMMARY

The AVPTA Mission is to leverage "resources to improve transition of technologies into both the commercial and military marketplace," and "industrial research and development (IRAD) involving commercial automotive and defense ground vehicle manufacturers to transition technologies and increase precompetitive research and development."

The following summaries document the work product of thirty (30) projects contained within the AVPTA portfolio. Project performers include Automotive Industry Original Equipment Manufacturers (OEMs) and Tier 1 / 2 Suppliers, Defense Industry OEMs and Suppliers, DOE National Laboratories, DOD Research Laboratories, Contract Research Organizations, Universities and Colleges, Small and Other Category Businesses.

Some of the projects reported upon herein were among the seven (7) original projects that formed the Alliance's foundation and enabled its rapid start-up. In many instances, DOE and DA mutually leveraged respective ongoing projects by infusing personnel, contributing resources, and providing mutual experience/expertise. This quickly expanded the Alliance technical network and reach, and provided access to activities beyond those directly funded by the Alliance. An example is TARDEC SME engagement in the VTO Annual Merit Review (AMR) during which TARDEC personnel are exposed to the complete VTO project portfolio including participating/contributing as review panel members. Joint participation in the AMR helps to formulate areas of mutual technical interest (AOIs) that contain the description, scope and deliverables for future new-start projects.

Also reported upon herein are projects that were jointly selected for start-up in Fiscal Years 13 & 14. The Alliance has developed and instituted a sustainable, new-start project review and selection process based upon VTOs annual Funding Opportunities Announcements process and timeline. The process leverages DOE's National Energy Technology Laboratory Contract Office to rapidly obligate and efficiently track project funding by individual performer.

Through FY14, DOE and DA have jointly contributed to the Alliance funds totaling $85.3M. The result has been a level of effort/output that neither agency would have realized without the interagency collaboration.

AVPTA has become a reference model for interagency collaboration, and is the prototype after which the Office of the Secretary of Defense/Operational Energy proposed Ground Vehicle Capabilities Improvement Program is structured.

Report Prepared by:

Scott Schramm, Sr. Engineer, TARDEC/RDECOM/AMC

Stacy Mills, Special Projects Officer, TARDEC/RDECOM/AMC

William Haris, Liaison Officer (to DOE), TARDEC/RDECOM/AMC

Gurpreet Singh, Program Manager, DOE-VTO, EERE

This Page Intentionally Blank

INTRODUCTION

There are two high level drivers that led to the development of the AVPTA. The first is the elevation of energy efficiency and security as points of emphasis throughout the Army and the Department of Defense (DOD) as a whole. For the Army, a major milestone in this was the development of the Army Energy Security Implementation Plan (AESIP) in 2009. Within the AESIP goal to Increase Energy Efficiency across Platforms and Facilities, there was an objective to increase the efficiency of tactical equipment. At the DOD level, the Operational Energy Strategy is a principle-guidance document for the Department's approach to ensure energy security for operational forces.

The second was a call by the DOD for strengthened interagency partnering. This was set forth in its 2010 Quadrennial Defense Review. Energy security was identified as an excellent opportunity area for such a partnership. To this end, the DOE and DOD worked to craft a Memorandum of Understanding (MOU) to establish a partnering framework to enhance national energy security. This MOU is included as Appendix A. The MOU calls for the Departments to work together in a wide range of technical areas; including efficient transportation and overall energy efficiency.

DA and DOE worked together under the auspices of this MOU to develop a charter for working together in a wide range of vehicle technologies. This charter describing the Alliance was signed by the Honorable Daniel B. Poneman, Deputy Secretary of Energy and the Honorable Joseph W. Westphal, Under Secretary of the Army and is included as Appendix B.

The DOE mission is to develop technologies that will reduce petroleum consumption and greenhouse gas emissions. A critical step in any new technology development is having it accepted and deployed in the marketplace. Teaming with DOD provides an attractive pathway for early utilization of the novel energy-saving ideas coming from the DOE research portfolio. These agencies strategic goals are summarized in the following table:

DOD & DOE Strategic Goals

DOD Operational Energy Strategy	DOE Vehicle Technology Program
Reduce Energy Demand: – Reduce: • Overall Operational Energy Demand • Mission Risks & Costs – Improve Energy Usage Efficiency	Reduce Petroleum Consumption
Expand & Secure Energy Supply: – Diversify Energy Sources – Protect Energy Supply Access	Reduce Green House Gas (GHG) Emissions[1]
Integrate Operational Energy Considerations Into: – Planning Activities and Force Development	

[1] Corresponds to DOD Strategic Driver

With strong support from senior leadership, the agencies collaborated at the Executive and SME Levels to identify AOIs that are the founding principles for describing each of the Alliance's Technology Focus Areas (TFAs). The respective TFA descriptions follow.

TECHNOLOGY FOCUS AREA (TFA) DESCRIPTIONS

TFA1: Advanced Combustion Engines & Transmissions

Advanced air-fuel management systems and novel combustion regimes have the potential to dramatically increase efficiency and power density, while at the same time reducing emissions. Meeting the challenge of developing and optimizing the combustion of common petroleum fuels, including Jet Propellant-8 (JP8), or biofuels in advanced engines requires a new level of the understanding of the physical and chemical phenomena of the Direct Injection (DI) diesel engine, which will be strongly affected by the different fuel properties which in turn affect fuel/air mixture preparation, combustion and emissions.

Advanced transmissions can allow the engine to operate more frequently in regions of high efficiency and transmit more torque while maintaining drivability. Of particular interest for further Research & Development (R&D) are approaches and devices to increase launch-assist device efficiency, and to increase the number of gear ratios. Among possible options for investigation are higher gear count automatic transmissions, Dual Clutch Transmissions (DCT), wet and dry clutch launch devices, multi damper torque converters, Continuously Variable Transmissions (CVTs), and binary transmissions.

TFA2: Lightweight Structures & Materials

Reduction of vehicle gross weight is an effective approach to reduce energy consumption during the vehicle usage, regardless of their energy sources (e.g., liquid fuels or electric batteries). Lightweight materials such as aluminum (Al) alloys, magnesium (Mg) alloys, high-strength steel, and carbon-polymer composites have been considered to replace low carbon steels conventionally used in automotive components. Challenges exist, however, to integrate components made of these lightweight materials into vehicle structures to achieve maximum weight reduction, while maintaining structural rigidity, crash safety, production quality and cost parity.

TFA3: Energy Recovery & Thermal Management

In current vehicles, approximately 60% of the chemical energy of fuel is lost in the form of waste heat, dissipated by the exhaust and cooling systems. The former offers high-grade heat that approaches temperatures of 800^{o}C while the latter is a considerably more modest heat source at approximately 120^{o}C. Of significant interest are exhaust heat recovery systems, including Organic Rankine cycles, as well as mechanical and electrical turbo-compounding. In addition, through the development of cost-competitive advanced second generation thermoelectric (TE) devices for vehicle applications vehicle fuel efficiency, performance, and emissions can be improved. Thermo-electric devices can

convert engine waste heat to useful electrical power, to be used either assisting propulsion or for powering hotel loads. By integrating high Figure of Merit TE devices in the vehicle architecture, thermal management of vehicles can become significantly more efficient.

TFA4: Alternative Fuels & Lubricants

Alternative fuels and lubricants can facilitate or enhance conventional engine technology, as well as advanced combustion regime engine operation such as Homogeneous Charge Compression Ignition (HCCI) or Low Temperature Combustion. For alternative fuels, the focus should be on drop-in fuels or blend stocks that displace petroleum-derived fuels in vehicle applications without significant infrastructure changes or requirements. New developments in base oil and additive packages can reduce viscosity while maintaining temperature requirements, thereby improving engine and transmission efficiency.

TFA5: Electrified Propulsion Systems

Electric drive options range from mild battery-alternator systems to full parallel and series systems or all electric drive, and require engineering trade-offs between fuel consumption benefit and system complexity, reliability and cost. However, to achieve efficient solutions, electrical materials and devices will require higher conversion efficiencies and power/energy densities than are currently possible. The next generation electric drive vehicles will benefit from improved and lower cost batteries, novel electric motors, thermoelectric waste heat recovery, and power electronic devices and electrical topologies that are capable of handling increased loads and multiple combinations of sources and accessories. Activities will focus on hybrid system power electronics and electric machines.

TFA6: Energy Storage & Batteries

Stakeholders desire to improve existing battery chemistries, develop advanced battery technologies (high power and high energy systems), and conduct ultra-capacitor research. Military goals are to improve the availability of onboard power, reduce energy demand/consumption, expand the energy supply to military operations and build energy security into future forces in the specific areas of: silent watch capability, electromagnetic armor and starting/lighting/igniting (SLI). Civilian/commercial goals are to reduce the petroleum demand, reduce greenhouse gas emissions and promote US economic competitiveness in advanced hybrid electric vehicles and electric vehicles. Advanced lead-acid batteries, ultra-capacitors, lithium-ion batteries, lithium sulfur and lithium-air batteries are joint areas of interest. Both agencies are also interested in improving on-board safety, developing battery test protocols and promoting codes and standards.

TFA7: Activities Suspended - Analytical Tools (Simulation & Modeling)

Diverse fuel sources, advanced combustion modes, hybrid/electrified powertrains, energy harvest/waste heat recovery technologies, and using lightweight materials substantially elevate the complexities of efficient vehicle powertrain systems and impose critical challenges for system integration and control. These efficient vehicle powertrain sub-systems, with new characteristics and strongly interactive dynamics, necessitate research on system integration and advanced control strategies. An integrated and analytical systems approach ensure that the various sub-systems of the vehicle work seamlessly, reliably and synergistically to optimize coordination so as to maximize vehicle energy efficiency, power density and emission reduction potential in real-world applications. Through state-of-the-art modeling and analysis, concepts and strategies can be screened during the vehicle design stage, and most promising candidates and key pathways to bring them to realization in an effective time frame can be identified. Critical components and/or systems needing specific development can also be identified and analyzed with simulation tools.

Effective 21 May 2014, TFA7 activities were suspended by joint agreement of the respective agency Directors. Activities were suspended because no unique, stand-alone projects were identified, and as a regular course of business, Modeling & Simulation is embedded within essentially every AVPTA-related project. TFA7 may be reactivated at any time upon respective agency Directors concurrence.

TFA8: Proposed – Advanced / Modular Manufacturing

As new capabilities, functionalities, materials, structures and related technologies mature and migrate into legacy and next generation ground vehicles, added emphasis will be placed on advanced manufacturing techniques, especially focusing on modularity that enables multiple configurations from a single, basic platform. TFA8 will investigate emerging and unique component, sub-system, system and full-vehicle manufacturing processes and equipment.

TFA9: Starting-up – Autonomy-enabled Technologies

Autonomy-enabled technologies have the promise to significantly decrease fuel consumption through a variety of mechanisms. For example, platooning, where vehicles travel close to each other in order to reduce aerodynamic drag at high speeds, can only be achieved through connectivity and automation. A significant source of excess fuel consumption comes from vehicle operators driving in a sub-optimal manner, such as exceeding optimal speeds and accelerating and decelerating too quickly. Intelligent systems can help increase fuel efficiency by providing information to the driver to improve operational behavior, by determining more efficient routes based on topography or traffic

conditions, or by taking control of certain vehicle functions. An automated traffic management system, implement through a system of autonomous vehicles connected with intelligent roadway infrastructure, could greatly reduce vehicle start/stops and slowdowns, optimizing traffic flow, and improving mobility in urban driving. Preliminary research by the National Renewable Energy Laboratory (NREL) indicates that platooning could increase fuel efficiency by 10%, eliminating driver inefficiencies another 15%, and completely automating the vehicle transportation system could yield a 40% improvement. However, these estimates are based on a limited number of experiments, which may not include the full range of variability that a real world system would experience, nor potential second-order effects, such as an increase in vehicle miles traveled. Accordingly, additional analysis and targeted experimentation are needed to more fully explore the limitations that these autonomy-enabled technologies may have in regards to increasing fuel efficiency across the transportation system.

PROJECT TECHNICAL REPORTS

(Start on Next Page)

AVPTA Technology Focus Area 1: Advanced Combustion, Engines & Transmissions

Ignition Models for Heavy Hydrocarbon Fuels

DOE-VTO TFA Lead: Gurpreet Singh
TARDEC TFA Lead: Dr. Peter Schihl

Principal Investigators:
Lyle Pickett and Mark Musculus

Combustion Research Facility
Sandia National Laboratory (SNL)
Livermore, CA

Start: 2012
Projected Completion: Q1 FY15

Objectives:

- Examine the ignition behavior, spray formation behavior, and evaporation characteristics of two, Army-provided military fuels of interest.
- Measure the ignition delay, liquid length penetration, and transient spray formation using an optical accessible constant volume combustion vessel and an optically accessible single cylinder engine.

Strategic Context:

- The data and knowledge generated from this project will help the technical community to better understand the combustion behavior of military fuels in Diesel engines. Such information will aid in the development of future engines and also in troubleshooting combustion issues within existing military production Diesel engines.
- This effort supports the future development of high power density propulsion systems.
- The project-generated knowledge will be used to support other TARDEC engine research, development and engineering efforts, and supplements both internal data generated by TARDEC along with other TARDEC-funded efforts at various universities.
- Follow-on project activity is not currently planned.

Accomplishments:

- Completed all experimental work associated with each fuel. Data is currently under analysis.

Introduction:

The U.S. Army currently is using JP-8 as its primary ground vehicle fuel. This particular fuel has 'loosely' controlled combustion affecting parameters including the cetane number and the distillation curve. Historical sampling of various global regions that have provided fuel to the Army has shown that the ignition quality can vary between 30 and 60 (cetane index), though most of the fuel consumed by Army systems resides in the 43 to 45 range. These outlaying fuels can lead to potential reliability issues with ground system engines and thus various forms of research and testing has been underway to better understand the impact of such fuels on Army diesel engines. Such efforts have included production engine testing and also basic/applied research measurements to better understand the associated spray and ignition behavior of such fuels.

Approach:

Two measurement devices were used to acquire fundamental combustion data on the two fuels provided by the Army. One fuel was a poor ignition quality, research grade type and the second fuel was also a research grade type though with an ignition quality much higher than most military type jet fuels. Each fuel was evaluated in both a constant volume combustion vessel and a single cylinder engine in order to better understand the ignition event under representative light load operating conditions in military diesel engines using representative military relevant mean injection pressures.

Results and Discussion:

All the experimental work is complete and currently under analysis. Initial results show that one of the two fuels exhibited unusual ignition behavior near 700°K though further analysis to better understand this behavior is under investigation. More results are coming within the next quarter.

AVPTA Technology Focus Area 2: Lightweight Structures & Materials

Light Weight Vehicle Structure (LWVS)

DOE-VTO TFA Lead: Patrick Davis
DOE-VTO Project Lead: William Joost
TARDEC TFA Lead: Dr. Richard Gerth

Principal Investigator
Richard Gerth, Ph.D.

Ground Systems Survivability
US Army TARDEC

Start: October 2013
Projected Completion: June 2016

Objectives:

- Design, manufacture, and evaluate lightweight, multi-material military vehicle structure that is both affordable and 30% lighter weight.
- Evaluate commercial defense barriers to lightweight material technology adoption.

Strategic Context:

- The lightweight turret structure created within the project will provide US Army, Marine Corps and commercial stakeholders with performance and cost-effectiveness information about the application of lightweight materials in combat vehicles.
- The project directly supports the TARDEC Strategy by providing input for business case analysis and technical performance assessment of the applicability of lightweight materials for turrets.
- The project-derived information will be applied to the Combat Vehicle Prototype (CVP) virtual turret and by extension the Future Fighting Vehicle (FFV).
- Follow-on intent is to continue the technical development with the CVP virtual turret which is significantly larger and required to withstand increased loads. The project output will influence requirements regarding the capability of these materials to meet increased size and load conditions.

Accomplishments:

- Validated all classified and unclassified requirements
- Completed Preliminary and Critical Design Reviews (PDR & CDR) with significant redesign to ensure sufficient stiffness for gun firing accuracy.

- Initiated production tooling manufacture.

Introduction:

Vehicle light-weighting is a priority for the US. Army. Due to increased survivability requirements, additional protection measures have been added to vehicles resulting in decreased fuel economy, decreased reliability and associated vehicle availability, and in some cases, decreased fording capability.

Light-weighting of ground vehicle structures, including passenger car bodies, follows a logical and predictable path (see Figure 1):

1. Single material component substitution
2. Single material subsystem substitution
3. Multi-material subsystem substitution
4. Multi-material complete structure substitution

The incumbent material in most cases is advanced high strength steel (AHSS). The alternative lightweight materials are aluminum (Al), magnesium (Mg), titanium (Ti), and fiber reinforced resin composites (FRC). Lightweight vehicle demonstrators have been built before, most notably the composite HWMV by TPI and the aluminum body by Alcoa for the Fuel Efficiency Demonstrator (Johnson, 2010). These studies were based on a single material dominant solution, i.e., the structures were constructed primarily from a single material.

But any subsystem or system made from a single material cannot be as light weight as a weight optimized system composed of multiple materials. This is the target of the industry; to effectively design, manufacture, and assemble vehicle structures and systems that are as light as possible and able to meet functional and cost requirements.

Approach:

A true multi-material structure for a military vehicle has not yet been produced for production. The FCS Aries was a hybrid monocoque / space frame architecture that was predominantly aluminum and composites (Pike and Filar, 2009). It was a multi-material structure which demonstrated the state of the art. The LWVS program is not designed to show the state of the technical art, but rather the state of the commercial art. In other words, it is not a study in how much weight can technically be eliminated through material optimization, but rather how much weight can be eliminated from a current military vehicle using commercially available and affordable technologies. The project tests the hypothesis that multi-material technologies developed for the commercial automotive industry can be adapted for military applications to significantly reduce vehicle weight for an acceptable cost. The ultimate goal of the project, if successful, is to transition the adapted technologies into a current military vehicle through a future upgrade program.

The demonstration platform for the LWVS is the Marine Light Armored Vehicle (LAV). The LWVS program is a multi-year program structured in three phases:

1. Trade study and technology development
2. Detailed design and manufacture
3. Test & evaluation

Phase I developed approximately 20 concepts and reduced the analysis to two multi-material versions: a metallic monocoque of steel and aluminum. This was a low risk approach capable of using the current armor solution and reducing the weight by approximately 25% at $250 / pound saved. A more aggressive multi-material design resulted in over 30% weight savings at approximately $300 / pound saved. It was decided to pursue this design to determine whether the design could be produced, evaluate its performance, and quantify the barriers to adoption.

Results and Discussion:

This project has a threshold weight reduction goal of 339 pounds (38%) for a LAV turret (see Figure 2). The roof is replaced with lighter weight armor steel; the steel side walls and base plate are replaced with carbon fiber composite. The aluminum basket will remain. The trunnion is also being replaced by an aluminum-steel bi-metallic casting.

The normal challenges include meeting the structural strength requirements defined in the operating load cases, and this has been achieved with composite gages similar to the steel turret. The composite design allowable of 68 ksi tension and 33 ksi shear were more than adequate to provide healthy Margins of Safety for all FEA load cases. The material system selected was Tenax 34 MSI fiber and SAC79 epoxy resin. The composite layup is 25/50/25. The selected fabrication process is resin infusion with single side tool / vacuum bag.

Whenever a material substitution project is undertaken there are always “typical “issues to resolve such as strength, joining, and environment. For this project there were some additional challenges that had to be dealt with.

1st Challenge – Maintain the Same Ballistic Protection as the Steel Turret:

The existing steel turret structure is composed of high hard plates which contribute to the armor protection. Since much of this steel is replaced with non-contributing composite. This necessitates utilizing stronger add-on armor than that used over the steel turret. An armor recipe was selected that defeats the specified threat, but is 5 pounds per square foot heavier than current armor. This added up to approximately 100 pounds which was factored into the weight budget.

2nd Challenge – Provide Sufficient Stiffness to Achieve Main Gun Automatic Fire Stability:

The 25mm main gun is supported by a steel rotor, which in turn is supported at the end bearing trunnion supports. The ability of the gun to stop vibrating between shots is necessary for accurate automatic mode operation. The key performance metrics to achieve this are the stiffness of the rotor, trunnion mounts, actuator, and turret baseplate. The design team knew it was impossible to match the current steel stiffness due the reduced modulus of the composite (10 msi for composite vs. 29 msi for steel). The composite simply could not be made thick enough because of space claims. Even if it could, much of the weight saving would have been eliminated. The question was raised; can the main gun be stabilized with software changes to the fire control computer? A lethality assessment (Figure 3) determined that it could indeed be stabilized if specific azimuth and elevation stiffness targets were met. In order to meet these targets the baseplate was thickened and its fiber specification was changed to a high modulus 50 msi fiber. The added thickness along with local reinforcements added 35 pounds, which was factored into the weight budget. These changes to the composite turret result in azimuth and elevation stiffness values that are within 10% of the current steel design and should allow both stabilized and power mode operation without software changed.

3rd Challenge – Attachment of Armor, Bustle Rack, LRUs, and Other Components.

For light components less than 4lbs, bonded composite tap pads with threaded inserts provide sufficient strength. Heavier parts generate enough force at the attachment points to require a through-thickness connection. A composite / metal appurtenance (Figure 4) was developed primarily for the armor attachment and is used in modified form for all other major components. It uses a 12mm threaded WITTEN insert as the load carrying element and functions as a typical threaded tap pad.

Having met these challenges, the multi-material LAV turret weight reduction is projected to exceed targets by being 375 pounds (42%) lighter than the existing steel turret.

References:

- Gerth, R. (2013). “Trade Study of a Lightweight, Multi-Material Military Vehicle Structure,” *2013 NDIA Ground Vehicle Systems Engineering and Technology Symposium*, Troy, MI, 21-22 August 2013.
- Johnson, C. (2010) "Fuel-Saving Design and Engineering," *Accelerate Special 2010 Edition: "FED Alpha Revealed",* pp. 4-9.
- Pike, T. and Filar,C. (2009) "Advanced Reconfigurable Spaceframe (AReS)," in*19th US Army Ground Vehicle Survivability Symposium,* 19-20 August 2009.

Figures and Tables:

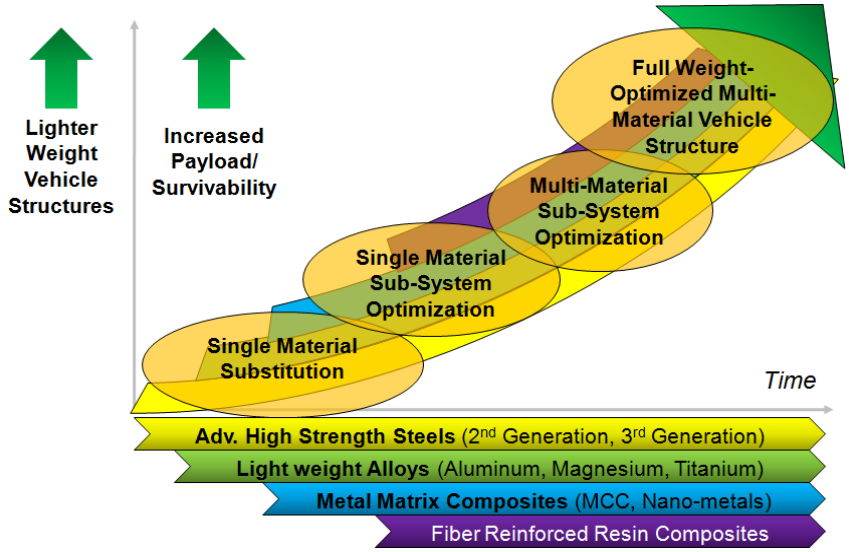

Figure 1. Lightweight Material Adoption Strategy for Structures (Gerth, 2013).

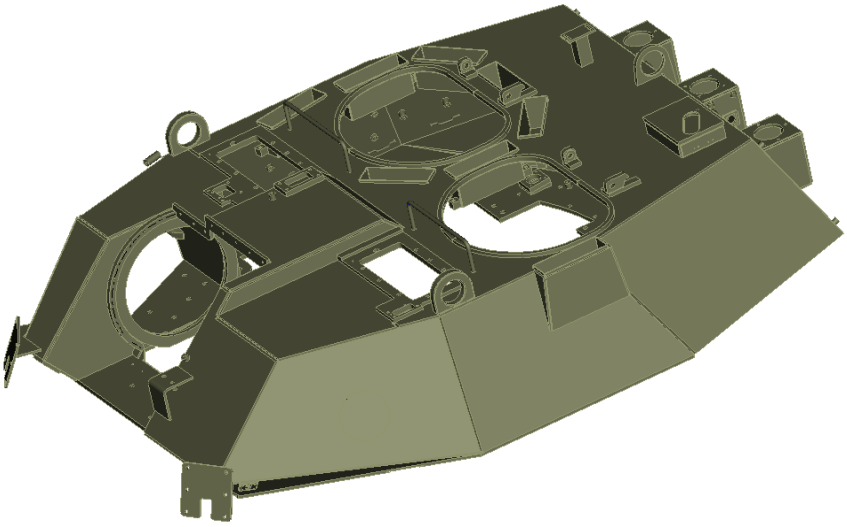

Figure 2. LAV Turret.

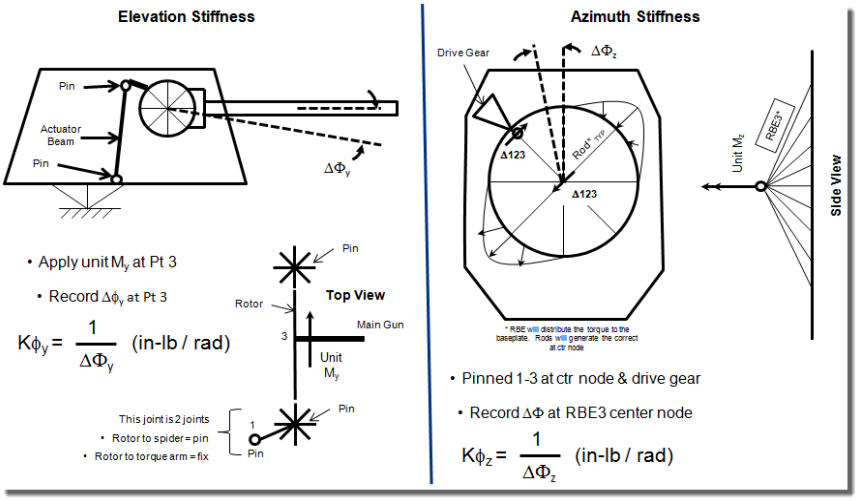

Figure 3. Elevation and Azimuth Stiffness Diagrams and Governing Equations

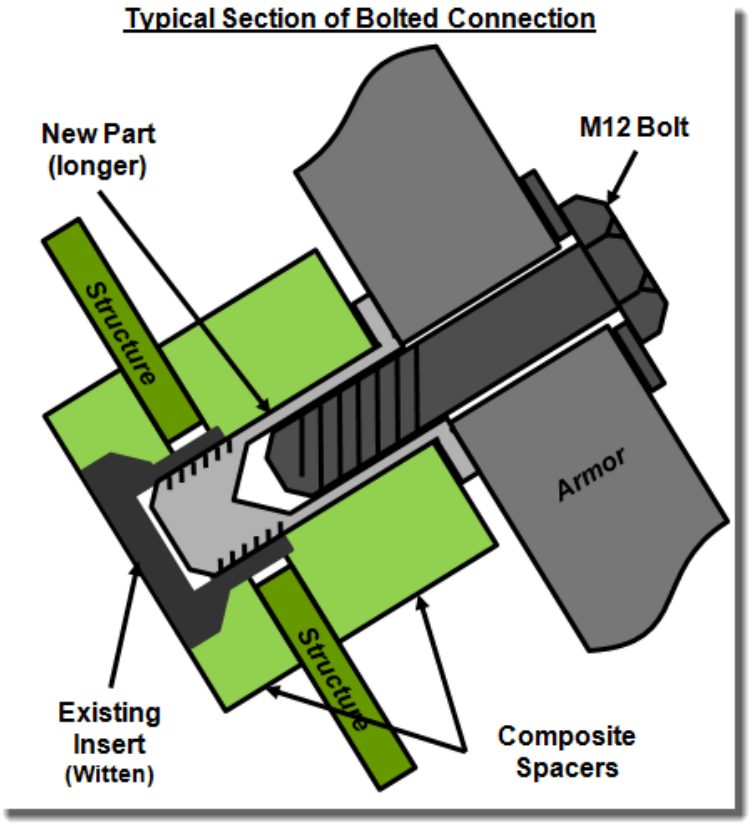

Figure 4. Composite / Metal Appurtenance.

AVPTA Technology Focus Area 2: Lightweight Structures & Materials

Multi-Material Joining (MMJ) - Overview

DOE-VTO TFA Lead: Patrick Davis
DOE-VTO Project Lead: William Joost
TARDEC TFA Lead: Dr. Richard Gerth

Principal Investigator
Richard Gerth, Ph.D.

Ground Systems Survivability
US Army TARDEC

Start: October 2012
Projected Completion: On-going

Objectives:

- Leverage DOE and DOD experience and resources to significantly impact technology development in dissimilar material joining.
- Evaluate performance and understand relative advantages of different technologies for different application and materials.

Strategic Context:

- The MMJ topics are part of TARDEC's efforts to become a Joining Center of Excellence.
- The variety of projects supports all aspects of the TARDEC Strategy, particularly CVP-related activities. The specific applications and transition plans are inclusive within each project summary.
- Both VTO and TARDEC view dissimilar materials joining as a major barrier to industry's increased adoption of advanced lightweight materials.
- Areas of future joint-agency investigation/investment include joint corrosion, adhesives and military-specific, high strain rate events such as ballistic shock.

Accomplishments:

- See individual project descriptions

Introduction:

The lightest weight structure is the one that utilizes the lightest and most cost effective material that meets the engineering design requirements, i.e., a multi-material vehicle structure. Several workshops and studies [1, 2] have documented that one of the greatest barriers to the multi-material vehicle is the lack of effective joining technologies for dissimilar materials. While there are various cost effective materials, the technology to physically join them while meeting production and engineering requirements has been lacking.

Approach:

The Multi-Material Joining effort investigates a variety of technologies to address improving joint strength for both traditional as well as novel parent materials. The technologies investigated in 2014 were:

1. Friction Stir Technologies
    a. Thermal Friction Stir Welding
    b. Scribe Friction Stir Welding
2. Weld Wire Technologies
    a. Durable AHSS Weld Wire
    b. AL6XXX Weld Wire
    c. Filler Wire Characterization
3. Modeling and Simulation
    a. Weld Modeling
    b. Weld Internal State Variable Model Development
4. Additive Technologies
    a. Laser Assisted Cold Spray
    b. Co-Axial Laser Assisted Supersonic Sintering
5. Miscellaneous
    a. Bi-metallic Casting
    b. Bolted Adhesive Carbon Fiber Composite Joints

A technical report for each project follows this overview.

The objective is to develop these technologies to improve structural durability of existing platforms and enable lighter weight, multi-material vehicle structures in future military vehicle platforms.

References:

- AVPTA Workshop, July 2011
- National Research Council, Committee on Benchmarking the Technology and Application of Lightweighting(2012) *Application of Lightweighting Technology to Military Vehicles, Vessels, and Aircraft*.

AVPTA Technology Focus Area 2: Lightweight Structures & Materials

Multi-Material Joining (MMJ) - Thermal Friction Stir Welding

DOE-VTO TFA Lead: Patrick Davis
DOE-VTO Project Lead: William Joost
TARDEC TFA Lead: Dr. Richard Gerth

Principal Investigator:
Richard Miller
Focus Hope Industries, Inc.
1400 Oakman Boulevard
Detroit, MI 60439
Phone: (313) 494-4716
E-mail: richard.miller@focushope.edu

with Martin M. McDonnell III
Ground Systems Survivability
US Army TARDEC

Start: January 2014
Projected Completion: September 2015

Objectives:

- Develop a production-representative manufacturing process to join high hardness armor steel with AA6061 aluminum alloy using a bimetallic Thermal Friction Stir Welding (TFSW) process.
- Demonstrate technical feasibility by producing 36-inch long butt welds.
- Determine optimal process parameters that maximize joint tensile strength.

Strategic Context:

- TSFW will be used by new Programs of Record (PORs) that require welding of steel to aluminum.
- The technology directly supports the TARDEC Strategy as a leap-ahead capability. It will also help ensure that newer lightweight requirements can be met without loss of performance.
- The project work product can easily transition to military stakeholders for utilization on new programs where dissimilar material joining is required. The technology also helps TARDEC's continual growth as the Joining Center of Excellence for the Department of Defense (DOD).
- Follow-on activity includes TARDEC pursuit of MANTECH support to further develop TFSW and Scribe Friction Stir Welding (SFSW).

Accomplishments:

- Designed and constructed a water-cooled welding fixture capable of securing work pieces up to 40-inches long, and 36-inches wide.
- Developed algorithm for the fixture to thermally control the work pieces.
- Successfully demonstrated the capability to produce continuous 36-inch long bimetallic friction stir welds.

Introduction:

Thermal Friction Stir Welding (TFSW) uses a laser to preheat the steel parent material to enable the joining of high hardness steel to aluminum alloy using the friction stir process. Based on a proof-of-concept project that successfully demonstrated the feasibility of TFSW (TARDEC R&D Contract #W56HZV-05-C-0721), this current project expands upon those results to develop the tools, equipment, and manufacturing processes required to produce extended length (36-inches) production-representative bimetallic butt weld joints in thick armor plates.

The key technical issue is temperature control of the parent materials. Under the previous project, TFSW of thick plate in a butt joint configuration was accomplished. Unfortunately the process demonstrated very short tool life. The data from the study indicated that the differential thermal expansion coefficients of steel and aluminum were significant contributors. It was hypothesized that more precise temperature control of the parent materials might result in longer weld lengths. This required both a heating and a cooling process, as the laser heating process is designed to heat quickly but not cool quickly.

Approach:

In Phase 1, a custom weld fixture will be designed and fabricated. This water-cooled fixture will incorporate several thermal management algorithms and techniques that were first demonstrated in the previous project. In Phase 2, the new fixture will be used to conduct a series of experiments to determine the friction stir process parameters (i.e. tool rotation speed, tool travel speed, and tool orientation) that results in maximum bimetallic joint strength. During the course of these experiments, four friction stir tool design configurations (tool geometry, joint geometry) will be evaluated. Finally in Phase 3, after an optimized set of process parameters has been established, a complete set of material joint specimens will be fabricated and used to characterize the bimetallic joint strength and metallurgical properties.

Results and Discussion:

The design of the custom fixture was finalized in May, and the 48-inch wide x 48-inch deep steel plate fixture (Figure 1) was completed and initially tested in September. The

cooling water lines (blue) are visible in the figure. Using a non-optimized set of TFSW process parameters, a full 34-inch long bimetallic weld, which exhibited no visible defects, was completed.

As of December 2014, the project has progressed into the second phase with efforts currently being focused on conducting process parameter optimization experiments.

Two of the four planned TFSW configurations have been used so far: 23 experiments using Tool A and 10 experiments using Tool B. Along with continued experiments with the current tool configurations, evaluations of Tools C and D will begin in January, 2015. Several of these trials results in 36" long welds, which validated the hypothesis that thermal control of the parent material could be used to increase tool life.

After post-weld machining, several test specimens have been extracted from each of the process parameter coupons and tensile-tested by our metallurgical laboratory. The maximum bimetallic tensile strength for each of the tool/joint configurations that have been achieved to date are 169 MPa and 175 MPa, for Tools A and B respectively, which are both significantly below the 205 MPa target.

Conclusions:

While the water cooled fixture has proven to be effective in increasing tool life and weld length, it has not yet been possible to achieve the desired weld strength in the first quarter of planned experiments. Further experiments evaluating two additional tooling configurations and changes in process parameters are planned. Once the optimal parameters and tooling configurations have been achieved, Phase 3 will commend. Phase 3 involves creating a full set of samples for ballistic shock testing in TARDEC's Survivability Armor Ballistics Laboratory (SABL).

Figures and Tables:

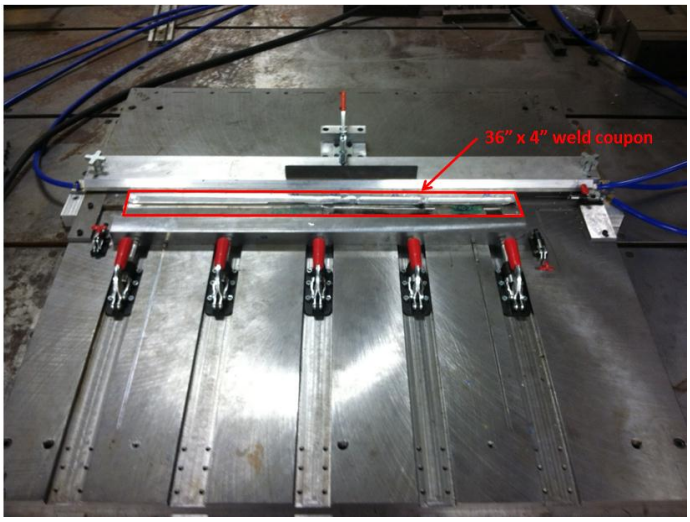

Figure 1 – Bimetallic Water Cooled TFSW Weld Fixture (water cooling lines in blue)

This Page Intentionally Blank

AVPTA Technology Focus Area 2: Lightweight Structures & Materials

Multi-Material Joining (MMJ) – Scribe Friction Stir Welding (SFSW)

DOE-VTO TFA Lead: Patrick Davis
DOE-VTO Project Lead: William Joost
TARDEC TFA Lead: Dr. Richard Gerth

Principal Investigator:
Yuri Hovanski
Pacific Northwest National Laboratory
902 Battelle Boulevard, Richland, WA
99352

with Martin M. McDonnell III
Ground Systems Survivability
US Army TARDEC

Start: Q4FY12
Completion: Q4FY14

Objectives:

- Understanding the scalability of the Scribe Friction Stir Welding (SFSW) process applied to thick sections including the development of parametric tool models to scale critical variables in the design and optimization of tooling for increasingly thick material cross-sections.
- Weld development including understanding the effects of process parameters in the materials of interest.
- Characterizing the interfacial properties of SFSW welds between thick section Al armor and Rolled Homogeneous Armor (RHA).

Strategic Context:

- SFSW technology has been effectively demonstrated for welding dissimilar metal section in sheet sections for the automotive industry. This technology will enable new Programs of Record (PORs) to successfully utilize lightweight aluminum alloys within new designs to achieve reduced weight requirements.
- The technology directly supports the TARDEC Strategy: as a leap ahead capability enabling the joining of alloys otherwise atypically joined providing design flexibility to attain both weight and performance requirements. And when scaled for thicker sections, SFSW will enable steel and aluminum to be welded together.

- SFSW will be applied to the Combat Vehicle Prototype (CVP) program for joining aluminum and steel armors for joints specified throughout the demonstrator. TARDEC will develop SFSW expertise in the solid-state welding of dissimilar materials to further its objective to become the Joining Center of Excellence for the Department of Defense (DOD).
- Additional AVPTA funding will be requested to further develop SFSW, and with MANTECH funds, the continued simultaneous development of SFSW and Thermal Friction Stir Welding (TFSW).

Accomplishments:

- Designed parametric 3-D tool model for scalable design of SFSW tooling.
- Developed SFSW welding parameters for joining AA6061-T6 to RHA in sections up to 38.1mm.
- Demonstrated SFSW welds in lap, step, and sandwich weld geometries.
- Developed design guidelines for scribe geometry, location and size to enable SFSW welding of thick section Al to RHA.
- Characterized interfacial properties showing the effect of hook features and scribe width on mechanical properties.
- Characterized the interfacial chemistry, demonstrating the SFSW process ability to form thin, uniform intermetallic layers along the joint interface.

Introduction:

The emphasis on lightweight vehicle design to improve efficiency and increase performance has led to an increased demand for multi-material structures. While significant increases in the capacity to model multi-material platforms have empowered designers to theoretically optimize materials locally across a global platform, the technology necessitated to join many of these materials has lagged in comparison to the advancements in computational tools enabling the design. Researchers have demonstrated many options for joining aluminum and steel sections [1-5]; however, the scalability of these techniques to thick section aluminum armor is often limited. Traditional friction stir welding (FSW) has shown promise at joining aluminum to steel in both lap and butt geometries of increasingly thick sections [6-10], yet the process is greatly complicated in several ways. First, the tooling requirements for FSW of steel materials are both costly and complicated, with only tungsten based or super-abrasive tools showing promise [11-13]. Additionally, the FSW process depends on solid-state mixing of materials, which is frustrated when trying to mix materials where the hot forming temperatures of one (steel) exceed the melting temperature of the other (Al).

The SFSW process was developed to overcome these and other difficulties associated with joining materials with vastly different melting regimes. Having initially been demonstrated on joining magnesium to various steel alloys [14-16], SFSW technology has been utilized to join many dissimilar material combinations ranging from dissimilar metals to polymer metal combinations. SFSW eliminates the difficulties associated with traditional FSW of dissimilar metal combinations, as the goal is to disrupt the interface of

the two metals in a lap configuration rather than trying to mix them, as is the case with FSW. A scribe cutter placed on the bottom of the pin section of the SFSW tool is utilized to cut the high melting temperature material such that is it allowed to deform at much lower temperatures than localized extrusion required for traditional FSW. As such, the SFSW process simultaneously cuts away a portion of the steel while back extruding the aluminum. The process essentially combines these two technologies into a single process allowing for chemical and mechanical bonding to take place at the joint interface.

This effort focused on demonstrating the scalability of SFSW technology to thick section Al alloys being joined to RHA. The work was divided into three main areas of interest including: 1) SFSW technology scalability, 2) Dissimilar metal weld process development, and 3) Characterization of the joint and interface.

Approach:

This work focused on three primary areas of interest. The first effort tackled understanding the scalability of the process to thick section. This effort included the development of parametric tool models that scaled critical variables in the design and optimization of tooling for increasingly thick material cross-sections. The second effort focused on the weld development. This included developing an understanding of process parameters in the materials of interest. Finally, the work entailed detailed characterization of the joint interface, includes an understanding of properties and their relationships to interfacial chemistry, texture, and interfacial morphology.

Parametric Tool Design:

With an emphasis of demonstrating the capability of utilizing SFSW to join thick section Al armor to RHA, the initial task was to design tooling capable of penetrating thick section Al and cutting the steel beneath it. A parametric 3-D model was developed to provide rapid scalability of critical tool parameters during the design and testing of tools. Tooling was originally designed for welding 25.4-mm thick AA6061-T6 to 12.6-mm RHA in lap geometry, as shown in Figure 1.

Tool geometry was designed to allow the scribe cutter in the bottom of the pin to interface with the steel section without allowing the pin itself to come in contact with the steel as shown in Figure 2. This design both serves to manage the heat and direct the flow of the steel during the cutting process. Additionally, because the main tool body is only in contact with Al, it can be fabricated of low-cost tool steel rather than more costly materials required to traditionally FSW ferrous alloys.

The parametric 3-D solid model was built to accommodate rapid changes to tool features that were necessitated during process development, and was modeled using SolidWorks Pro. The base model was designed for scalability, such that relationships could be modified to change features on the tooling to scale from welding across various thicknesses of Al sections. The nature of the SFSW tooling is such that applying traditional principles of parametric design allow for managing global variables to control

features such as pin length, shoulder convexity, etc. The initial global variables identified are listed in the following table, and identify the variables that feed into each of the more detailed functional relationships that establish an overall tool design.

While additional features to the tool may be modified outside the nine global parameters identified in Table 1, these parameters were globally linked across the initial parametric model to enable rapid 3-D modeling. The following Figure 3 demonstrates how changing a global variable like shoulder convexity effects the overall desin of the tool, while allowing the software to maintain the effective pin length. Figure 3 also shows the effect that shoulder convexity has on the overall shoulder engagement, which ultimately influences the down forces, flash and material flow of the aluminum under the constrainsts of traditional FSW.

Scribe Design:

Having designed the foundational tool with parametric scalability, significant effort was then put into developing scribe geometry that was capable of more rapidly cutting the RHA. As RHA is generally difficult to machine at high velocities, target velocities of 50-150 mm/min were selected based on historical experience machining this material with cutter diameters ranging from 9-13 mm. Various machining bits were employed to demonstrate machining parameters, and were shown to effectively cut depths of 1-5 mm at feed rates of 50-150 mm/min. Cutter geometries including three and four flute end mills with both straight and rounded edges.

Generally, most cutters were demonstrated to effectively cut RHA both lubricated and dry, when the feed rates were appropriately designed for steels with the effective hardness of RHA. Nevertheless, all traditional cutting tools failed in tests when integrated with a SFSW tool. Analysis of failures showed that fluted cutters depended on the ability to throw a chip from the tooth. While this is effective when machining, cutting in SFSW requires that the material being cut is always under a forge load of the upper material induced by the FSW side of the process. Many design evolutions were investigated to determine if these failures could be counteracted, yet ultimately the scribe design shown to be most effective was a simple cylindrical cutter protruding from the base of the pin as shown in Figure 4.

With the cylindrical scribe geometry validated in testing, the next process was to determine the optimal radial offset, diameter, and length. Testing ultimately aided in developing several design rules to assure scribe performance during the welding process. First, scribe diameter should be at least twice the length of the scribe protruding from the pin tip. Scribe diameter should be on the order of $1/6^{th}$ the diameter of the pin tip, and be centered at a radial position half way between the center and the edge of the tool. These design guidelines were developed during the testing and evaluation of numerous tool designs to systematically establish the limitations of the scribe size and location.

Multi-piece Tooling:

Aiming to minimize the overall cost of tooling, tool designs were implemented to allow for interchangeable features and reusable sections. Figures 5 & 6 show 3-D representations of two distinct modular multi-piece tool designs utilized during the development of SFSW for thick section welding of Al to RHA. The first, shown in Figure 5, shows a tool design with interchangeable pin tips. This design was originally utilized to allow for increasing pin tip lengths to be interchanged in the tool shank and shoulder section. Developed to accommodate traditional carbide cutting tools, this design allowed for cutter inserts to be held in place with set screws on the pin section, which could be removed after damage or when utilizing the tool for welding thicker sections of Al.

The second design, shown in Figure 6, was adapted to allow for replaceable tool tips, which included the shoulder, pin and scribe sections. This tool design also allowed for placement of the cylindrical scribes at locations farther from the radial axis of the tool center. This was shown to be critical is increasing the overall size of the hook features and scribe interlock at the interface of the joint. Additionally, this design was shown to be easier to disassemble after welding, as the Al was not able to permeate the interfaces between tool pieces.

Results and Discussion:

A statistically significant number of SFSW welds were made to allow for characterization of the interface and measurement of mechanical properties of select SFSW welds. Figure 7 shows a typical SFSW setup of a sandwich section of RHA embedded into a 38.1 mm thick section of AA6061. The close up view shown in the right image of Figure 7 shows the predrilled hole in the surface of the Al plate. This hole, while only partially through the thickness of the plate, was designed to be approximately 90% of the volume of the pin tip. Holes like these were used to minimize the distortion and material flash associated with the pin plunging into the material. Ultimately this allowed for greater uniformity in weld parameters along the length of the weld.

For mechanical and microstructural characterization welds were sectioned via water jet to 6-12 mm thick samples to avoid introduction of any cutting induced stress. Figure 8 shows representative welds produced via SFSW, with water jet sectioning of the 300 mm weldment shown in the right image. Cross-sections of both lap sections and sandwich sections are shown in Figure 9, showing how weld penetrations of 12.7 mm were used to weld Al section ranging from 12.7-38.1 mm.

Tensile data was normalized by dividing the instantaneous peak load by the width of the welded section. As the area of a lap joint is problematic to characterize, this normalized strength parameter is typically utilized to provide a comparative outlook of joint strength in lap welds. These values are plotted, Figure 10, against the measured

extension during tensile testing for different configuration of welds produced with two tool designs that varied the position of the scribe with respect to the central axis of the tool. Four cases are considered: The first case was a joint made with an early scribe tool design which resulted in relatively narrow scribe path of 9.5 mm (the projected width of the region cut by the cylindrical scribe while rotating). The remaining three plots are all from newer scribe tool designs which allowed for a 12.7 mm wide scribe path. The wider scribe path offered increased interlocking of material and evidently resulted in stronger joint. Whereas the single sided joint exhibited a peak load/length of ~1200 N/mm, the double sided sandwich configuration offered a greater load bearing capacity at 1660 N/mm. The data represented by the blue dotted line is from a sample in a sandwich type configuration that was welded on only one side of the RHA steel thus exhibiting lower load bearing capacity than the C-joint with welds on each side. The data shown in Figure 10 is representative of several weld specimens from each configuration; as such this graph only shows representative plots.

Comparing the scribe joint strength to some baseline to obtain parameter akin to joint efficient in this lap joint is not straight forward. However if load carrying capacity of a solid block of aluminum of the same cross-sectional area is considered the sandwich type join resulted in a joint efficiency of ~ 35% when compared to AA6061-O base metal strength. It is important to point out however that comparison of this type of efficiency is problematic since the joined interface is very small compared to the overall area of the sample being tested. The increase in scribe path (swept area of the scribe hence hook) further will increase the joint strength. However it is important to recognize that a finite FSW tool pin radius imposes practical limit on the width of the scribe path.

Figure 11 shows progression of geometrical hook feature as the tool traverses along the length of the scribe joint to illustrate the evolution of hook feature. The pictures were obtained from polished specimens from different location of the joint. The number of the top right corner of each picture is the distance from tool plunge from where the sample was extracted. Joint cross-section corresponding to start of the plunge sequence to the first 25mm of the SFSW is shown in the top row. Clearly at around 12.7mm from the tool plunge (start of the SFSW) the hook achieved its full size. Along the length of the joint the hook feature mains its general geometric shape providing interlocking feature to the aluminum plate at the top. Figure 12 shows similar SFSW macrostructure at different location of the joint illustrating the consistency of hook feature along the length of the joint. In this case the plunge depth was increased to 14.2mm (compared to 13.8mm in Figure 11) so the scribe engaged 0.4mm deeper into the RHA steel. The direct effect of greater scribe engagement resulted in deeper cut in the steel. Consequently the thickness of the hook feature has increased. This also results in more steel chips being introduced to the aluminum stir zone.

Energy dispersive spectroscopy (EDS) was used to perform elemental identification and mapping using Scanning electron microscopy (SEM) of representative interface region of Friction Stir scribe specimens. Figure 13 shows a representative low magnification optical image of Aluminum/RHA Steel interface showing hook regions. The pictures below in

Figure 14 show low magnification optical image showing the presence of intermetallic layer indicated by red arrows. SEM image of the interface layer at higher magnification using back scattered electron (BSE) is shown in Figure 15. Likewise the aluminum and iron atoms identified by the EDS are shown using color maps in Figures 16 & 17. Figure 17 also shows SEM micrograph and elemental maps of Al and Fe with IMC layer overlap at edge of a steel particle. EBSD orientation maps that shows grain structure for wrought iron and recrystallized grain structure similar to what is obtained during traditional FSW of AA6061-T6. The Crystal structure of the IMC layer could not be revealed by EBSD as no diffraction pattern was visible from the region confirming the presence of IMC. There is a clear intermetallic compound layer (IMC) of ~ 2-3µm thick (See EDS results in Figures 18 & 19). The IMC layer appears to be very homogeneous and similar at different locations that were scanned. No microstructural feature could be identified even with the use of BSE. Upon comparison with Al-Fe binary phase diagram the IMC layer was identified to be monoclinic Al3Fe. Line scans show that the concentration of other alloying elements (Mg, Mn, Cu etc.) changes in a subtle manner across the interface (See Figures 20 & 21).

Conclusions:

With an objective to leverage the DOE investment in the development of SFSW technology to join dissimilar metals, impressive progress was made to demonstrate the ability to join progressively increasing thicknesses up to 38.1mm. While more development and testing would be required to advance the technology to prototypical configurations, tensile testing of welded sections demonstrated the ability to produce stabilized weld properties and an ability to increase strength based on interface geometry and tool design. Design guidelines for tooling to aid in determining the tool geometry were interfaced with a 3-D parametric modeling tool that provided rapid tool configurations for variations in material thicknesses in the weld configurations.

References:

- Kimapong, K. and T. Watanabe, *Friction stir welding of aluminum alloy to steel.* Welding Journal, 2004. **83**(10): p. 277s-282s.
- Murakami, T., et al., *Dissimilar metal joining of aluminum to steel by MIG arc brazing using flux cored wire.* Isij International, 2003. **43**(10): p. 1596-1602.
- Sun, X. and M.A. Khaleel, *Resistance spot welding of aluminum alloy to steel with transition material - Part II: Finite element analyses of nugget growth.* Welding Journal, 2004. **83**(7): p. 197s-202s.
- Kah, P. and M.S.J. Martikainen, *Trends in Joining Dissimilar Metals by Welding.* Advanced Materials & Sports Equipment Design, 2014. **440**: p. 269-276.
- Shah, L.H. and M. Ishak, *Review of Research Progress on Aluminum-Steel Dissimilar Welding.* Materials and Manufacturing Processes, 2014. **29**(8): p. 928-933.
- Kimapong, K. and T. Watanabe, *Lap joint of A5083 aluminum alloy and SS400 steel by Friction Stir Welding.* Materials Transactions, 2005. **46**(4): p. 835-841.
- Watanabe, T., H. Takayama, and A. Yanagisawa, *Joining of aluminum alloy to steel by friction stir welding.* Journal of Materials Processing Technology, 2006. **178**(1-3): p. 342-349.

- Chen, Y.C., et al., *Friction stir lap joining of AC4C cast aluminum alloy and zinc-coated steel.* Advanced Welding and Micro Joining / Packaging for the 21st Century, 2008. **580-582**: p. 371-374.
- Feng, K.Y., M. Watanabe, and S. Kumai, *Microstructure and Joint Strength of Friction Stir Spot Welded 6022 Aluminum Alloy Sheets and Plated Steel Sheets.* Materials Transactions, 2011. **52**(7): p. 1418-1425.
- Habibnia, M., et al., *Effect of tool rotation speed and feed rate on friction stir welding of 1100 aluminum alloy to carbon steel.* Materials and Manufacturing Technologies Xiv, 2012. **445**: p. 741-746.
- Steel, R.J., et al., *Friction stir welding of steel T-joint configurations.* Proceedings of the Fifteenth (2005) International Offshore and Polar Engineering Conference, Vol 4, 2005: p. 1-5.
- Leonhardt, T., *Properties of tungsten-rhenium and tungsten-rhenium with hafnium carbide.* Jom, 2009. **61**(7): p. 68-71.
- Thompson, B., *Tungsten-Based Tool Material Development for the Friction Stir Welding of Hard Metals.* Friction Stir Welding and Processing Vi, 2011: p. 105-112.
- Jana, S., et al., *Effect of Tool Feature on the Joint Strength of Dissimilar Friction Stir Lap Welds.* Friction Stir Welding and Processing Vi, 2011: p. 205-211.
- Jana, S., et al., *Solid State Joining of Magnesium to Steel.* Magnesium Technology 2012, 2012: p. 11-16.

  Jana, S., Y. Hovanski, and G.J. Grant, *Friction Stir Lap Welding of Magnesium Alloy to Steel: A Preliminary Investigation.* Metallurgical and Materials Transactions a-Physical Metallurgy and Materials Science, 2010. **41A**(12): p. 3173-3182.

Figures and Tables:

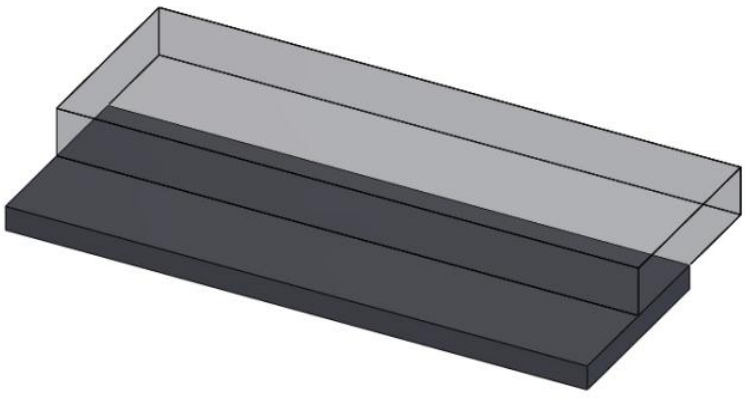

Figure 1. Original lap configuration for development of thick section SFSW joining of Al to RHA.

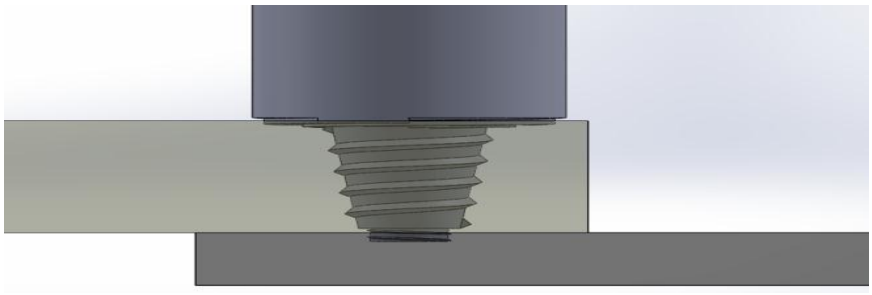

Figure 2. A 3-D rendering of a SFSW tool penetrating the top material in a lap joint. Note the scribe cutter is in contact with the lower material without the pin section of the tool touching the lower material.

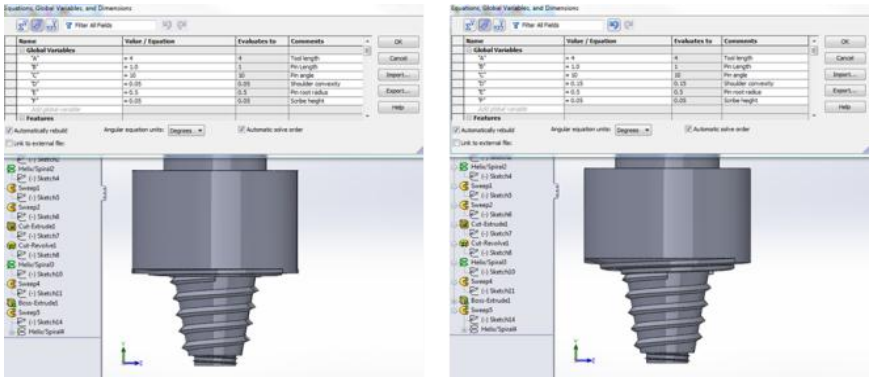

Figure 3. Example of a SFSW welding tool designed for 25.4-mm pin engagement with a shoulder convexity of 1.27-mm (left) and 3.81-mm (right).

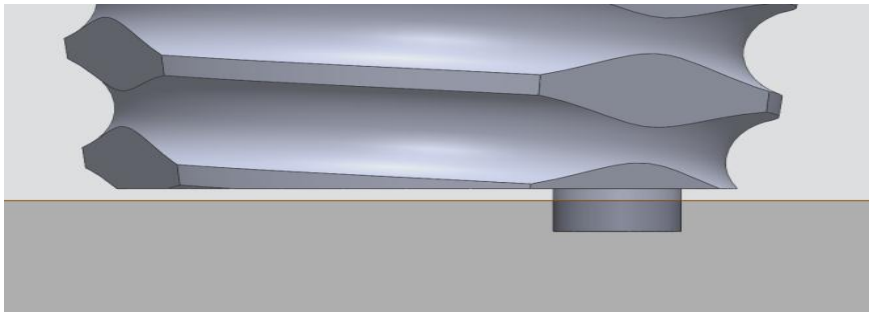

Figure 4. A close-up rendering of the base of a SFSW pin with a cylindrical scribe attached.

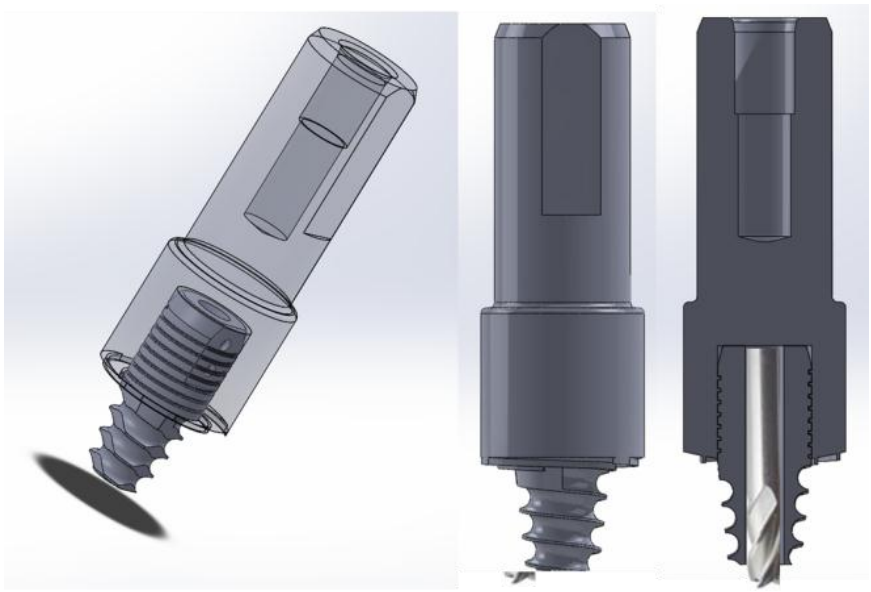

Figure 5. A 3-D representation of a multi-piece tool with a fixed shank/shoulder design.

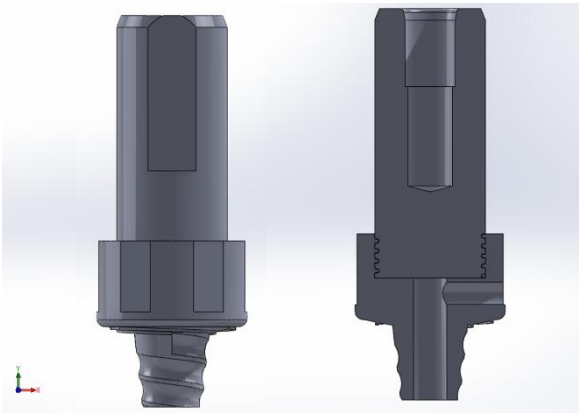

Figure 6. A 3-D representation of a multi-piece tool with a fixed pin/shoulder design attached to a removable shank.

Figure 7. SFSW weld setup ready for joining (left) with inset Configuration as shown in the upper left inset picture. A hole is pre-drilled in the Al plate (right) prior to welding.

Figure 8. Representative SFSW weld between AA6061 and RHA (left). Welds sectioned via water jet as shown right, were used for testing and characterization.

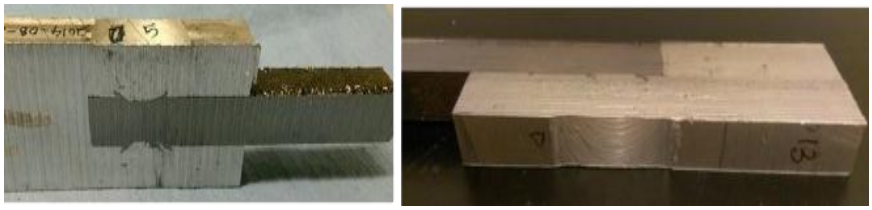

Figure 9. Water jet cut sections of SFSW welds between AA6061 and RHA. Sandwich sections (left) and lap sections (right) were cut for mechanical testing and interfacial characterization.

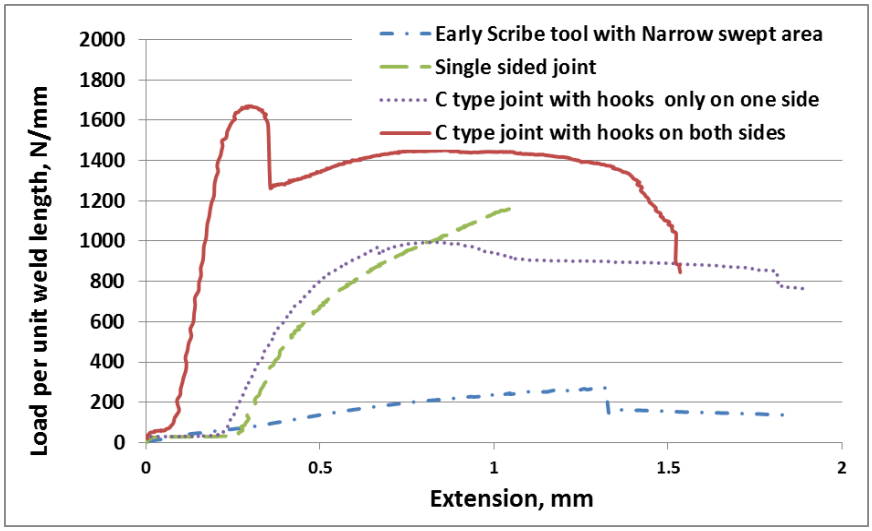

Figure 10. Graph of tensile properties of various SFSW welds demonstrating the ability to influence weld performance with tool design and weld configuration.

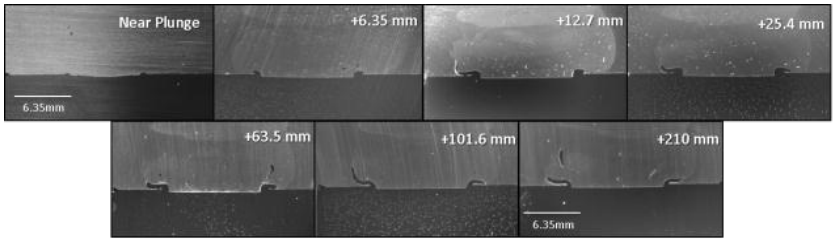

Figure 11. Optical Weld macrostructure revealing the progression of hook feature along the length of the weld traverse. The numbers on top right corner are indicative of distance from the tool plunge. 275RPM, 50mm/min. Plunge force= ~ 29kN, *Plunge depth = 13.8mm*.

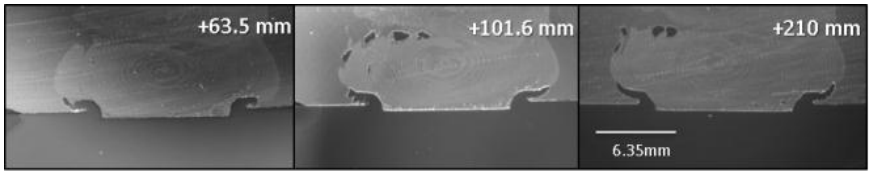

Figure 12. Optical Weld macrostructure along the length of the weld traverse. The numbers on top right corner are indicative of distance from the tool plunge. 275RPM, 50mm/min., *Plunge depth = 14.2mm.*

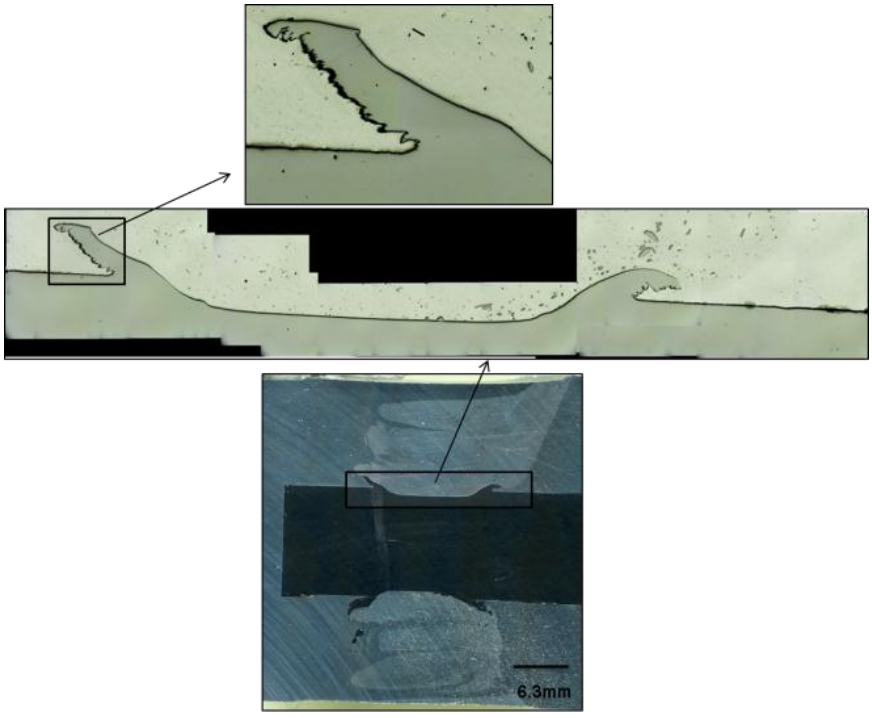

Figure 13: Optical Macrostructure of Sandwich type configuration of scribe joint showing hook feature in both sides of the RHS steel.

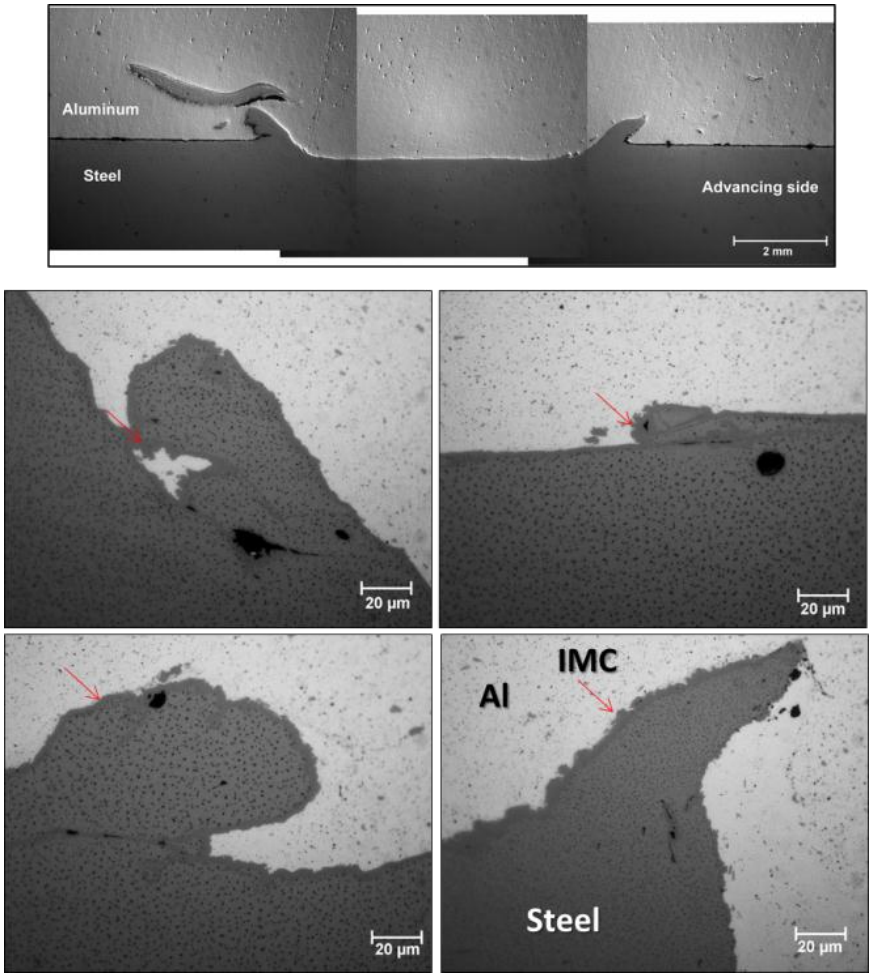

Figure 14: Low magnification optical image of interface (above). Higher Magnification micrographs showing intermetallic layer (IMC) at the interface at the hook region.

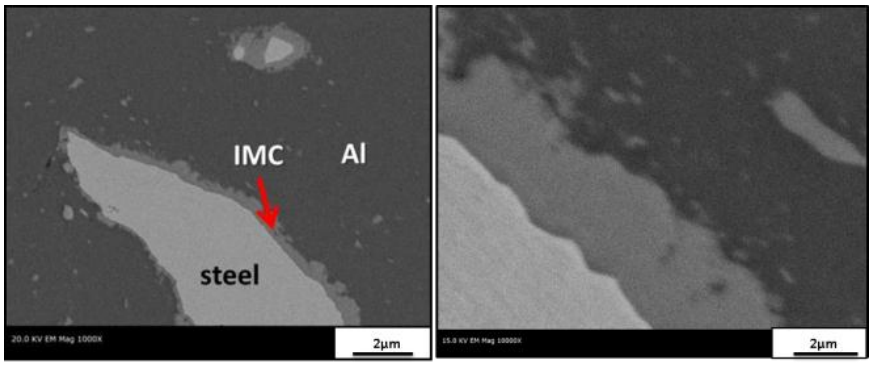

Figure 15: SEM image in BSE (back scattered electron) mode that clearly shows the intermetallic layer along the interface.

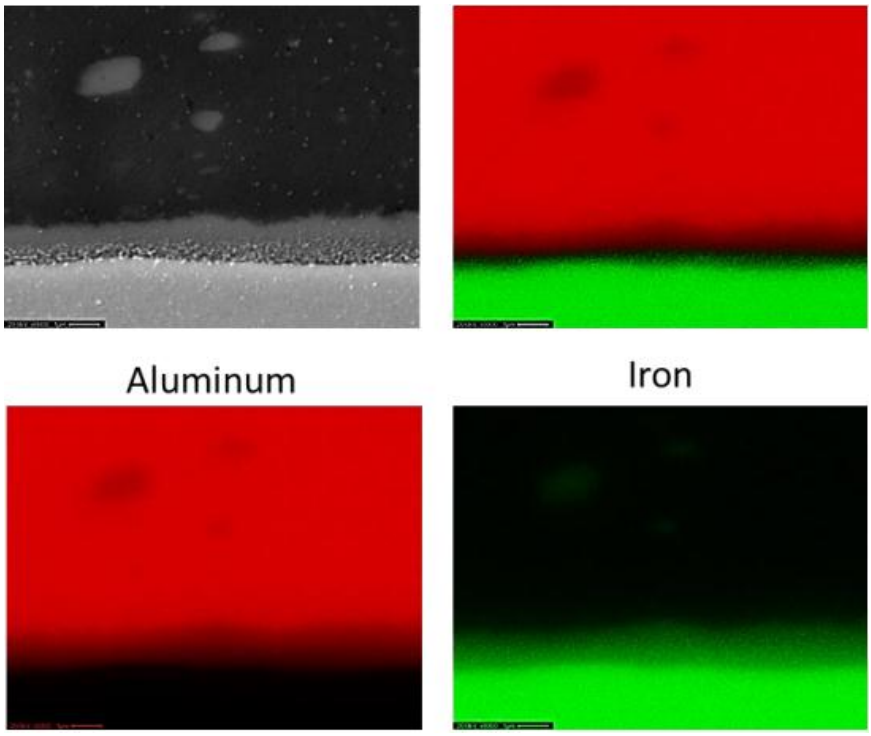

Figure 16: Representative interfacial region of a typical Friction Stir Scribe joint as seen in SEM. Color maps for Fe and Al and overlap layer are shown as obtained from EDS the sample.

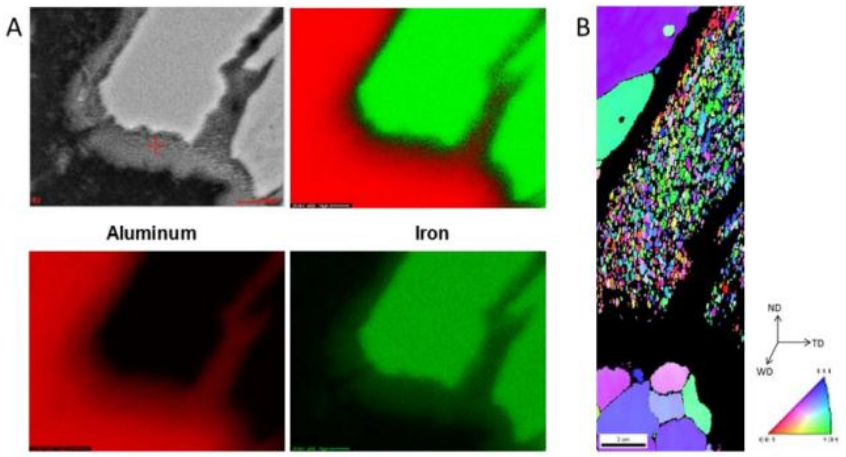

Figure 17: (A) SEM micrograph and elemental maps showing Al and Fe overlap in IMC layer around the edge of a steel particle. (B) EBSD orientation map showing grain structure of AA6061 and RHA steel, but not IMC layer.

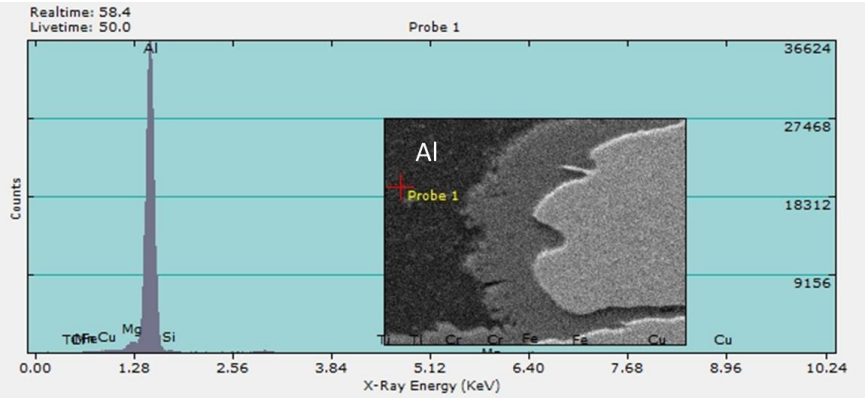

Quantitative Results for Probe 1
Analysis: Bulk Method: Standardless
Acquired 19-Apr-2013, 15.0 KeV @10 eV/channel

Element	Weight %	Std. Dev.	Atomic %	ROI (gross)
Mg	3.02	0.81	3.38	12364.53
Al	94.46	2.06	95.05	314348.16
Si	0.71	0.26	0.69	2833.86
Ti	0.02	0.01	0.01	88.61
Cr	0.01	0.00	0.00	84.18
Mn	0.02	0.01	0.01	103.91
Fe	1.74	0.57	0.85	1358.26
Cu	0.02	0.01	0.01	44.37
Total	100.00			

Figure 18: Typical EDS analysis corresponding to Aluminum near the SFSW interface.

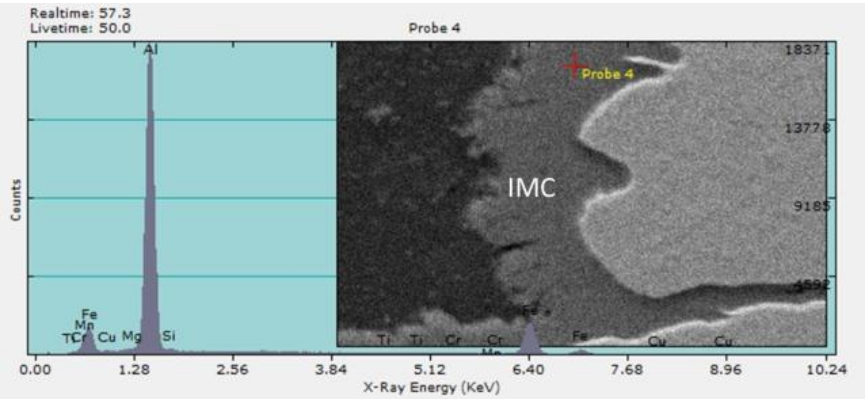

Quantitative Results for Probe 4
Analysis: Bulk Method: Standardless
Acquired 19-Apr-2013, 15.0 KeV @10 eV/channel

Element	Weight %	Std. Dev.	Atomic %	ROI (gross)
Mg	0.87	0.30	1.17	3677.09
Al	65.23	1.47	78.88	157973.05
Si	0.29	0.11	0.34	2820.56
Ti	0.00	0.00	0.00	12.98
Cr	0.00	0.00	0.00	47.14
Mn	0.07	0.03	0.04	249.72
Fe	33.28	1.11	19.44	22128.34
Cu	0.26	0.12	0.13	173.92
Total	100.00			

Figure 19: Typical EDS analysis corresponding to IMC near the SFSW interface.

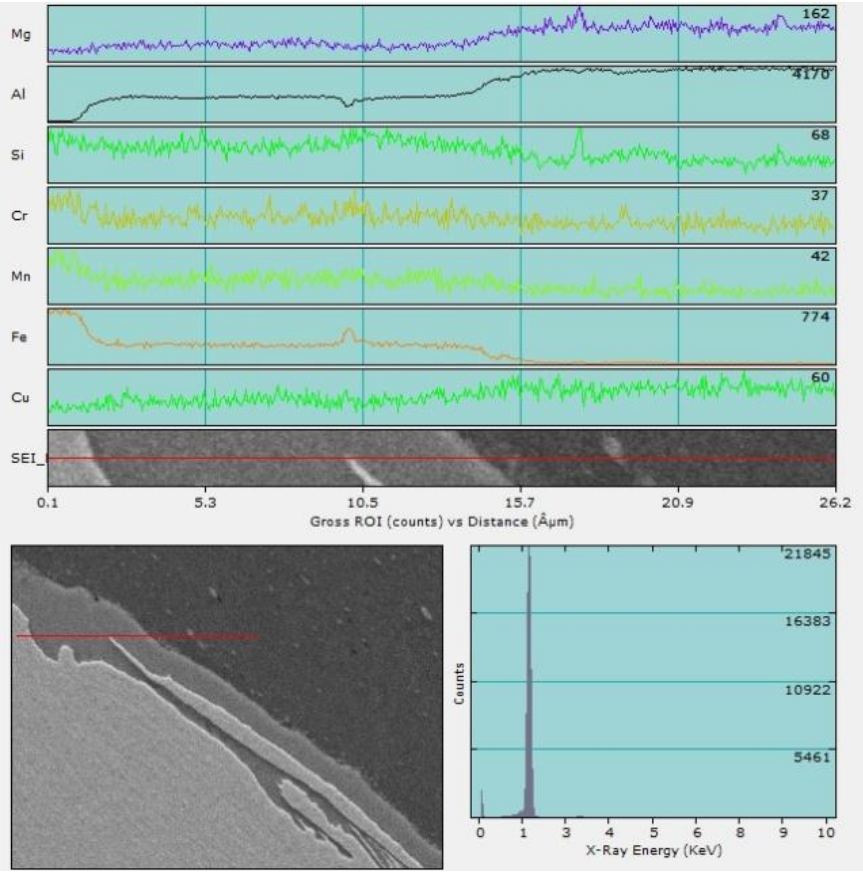

Figure 20: EDS line scan across the intermetallic layer for the line shown in the SEM image.

Figures Continued on Next Page

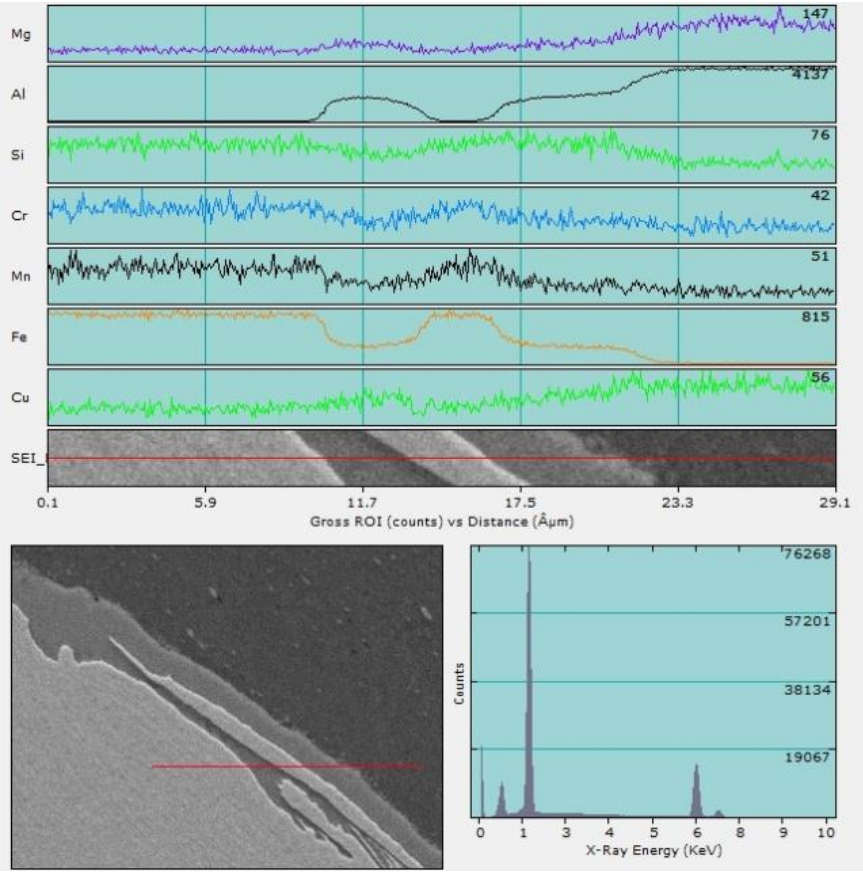

Figure 21: EDS line scan across the intermetallic layer for the line shown in the SEM image.

Pin root radius	Tool Length	Shoulder Convexity
Pin thread pitch	Tool Radius	Pin Angle
Shoulder radius	Pin Length	Pin Radius

Table 1. Global Variable List for Parametric Tool Design.

This Page Intentionally Blank

AVPTA Technology Focus Area 2: Lightweight Structures & Materials

Multi-Material Joining (MMJ) - Thermal Friction Stir Welding (TFSW)

DOE-VTO TFA Lead: Patrick Davis
DOE-VTO Project Lead: William Joost
TARDEC TFA Lead: Dr. Richard Gerth

Principal Investigator
Zhili Feng , Ph.D.ll

Oak Ridge National Laboratory (ORNL)
PO Box 2008, MS6083
Oak Ridge, TN 37831

with Demetrios Tzelepis
Product Lifecycle Engineering
US Army TARDEC

Start: October 2013
Projected Completion: September 2015

Objectives:

- Develop an innovative welding filler wire that can substantially reduce tensile weld residual stress and mitigate the susceptibility of hydrogen induced cracking
- Develop residual stresses measurement techniques using neutron diffraction for welded armor plates
- Demonstrate the effectiveness of new filler wire to reduce HIC on selective welding conditions.

Strategic Context:

- The project was initiated to resolve hydrogen embrittlement during welding of armored vehicles by creating a welding wire that would produce a hydrogen embrittlement-resistant microstructure. An added bonus is that the welding process produces compressive instead of tensile residual stress at the weld toe. This improves fatigue performance that is of interest to the automotive industry.
- The weld wire can be used across all armor steel protected military vehicles.
- The projects supports the TARDEC Strategy by work product being applicable to the sustainment of legacy vehicles, and new Programs of Record (PORs).

- TARDEC and ORNL plan to submit for MANTECH for funding to transition the technology for commercialization. Multiple weld wire manufacturers have expressed interest in commercializing the weld wire, and an Original Equipment Manufacturer (OEM) has verbally offered facilities for component and vehicle-level testing once coupon-level testing is successfully completed.
- A joint TARDEC/ORNL patent application has been submitted on the weld wire, and another joint patent application is planned to be submitted for non-destructive testing.

Accomplishments:

- Established baseline pre-heating procedures of HIC control for MIL-DTL-46100 and MIL-DTL-12560.
- Developed several new weld filler wire chemistries for “in-welding-process” Hydrogen Induced Cracking control.
- Demonstrated the feasibility of eliminating hydrogen embrittlement by means of special weld filler wire in laboratory conditions
- Applied patent on the chemistries of weld filler wire that are effective to suppress HIC in this project.

Introduction:

Hydrogen induced cracking (HIC), or cold cracking, has been a major persistent challenge in welding of high-strength armor steels. Fabricating HIC-free welded structures can be difficult in field fabrication environment and repair. For certain types of applications, pre-heating, post-weld heat treatment, and use of low hydrogen welding practices are mandatory per code/standard specifications. These requirements are often time consuming and represent a significant cost factor in construction. There are also many other applications where it is practically impossible to consistently eliminate the presence of hydrogen, and the hardened microstructure is necessary to maintain the strength of the weld. Yet in other cases, HIC imposes undesirable limitations on the choices of high-strength steels and development of high-strength weld filler wire where the use of these steels and filler wires would be necessary for the intended applications. Therefore, there is a need and demand for new weld wire chemistry and associated welding technology that can be applied to effectively prevent HIC.

Approach:

It is well established that three essential conditions must co-exist for HIC – (i) presence/absorption of hydrogen from welding operation or environment, (ii) sensitive hardened microstructure, and (iii) high tensile residual stresses. Weld residual stresses develop in a welded structure as a result of the non-uniform thermal expansion and contraction of the base metal during welding operation. The weld region typically cools last in the entire weldment. As it cools from the melting point of the materials, the weld region shrinks. It is such on-cooling shrinkage that results in the formation of high-tensile

residual stresses in the weld region that can reach or even exceed the yield strength of the base material. In principle, a volumetric expansion process that takes place during the cooling period could negate the effects of thermal shrinkage. One such volumetric expansion results from the phase transformation of austenite to a low temperature phase such as ferrite, bainite, martensite, or more likely a mixture of these low temperature phases in a steel. The effectiveness of the volumetric expansion to negate the formation of high-tensile residual stress depends on the extent of the volume expansion and temperature range in which the allotropic phase transformation takes place. The formation of martensite, especially at a temperature range close to but above the ambient temperature (or the intended service temperature of the weldments), is most effective.

This project is to develop a special welding filler wire which utilizes low temperature phase transformation (LTPT) to reduce the high-tensile residual stresses in the weldments of high-strength steels to prevent HIC. The filler wire makes it possible for "in-welding-process" HIC control, thereby eliminating the need for pre or post weld heat treatments. This reduces the fabrication cost and enables the use of high-strength steels based on the application needs without the concerns of HIC. Weld filler wire chemistries are systematically based on the LTPT principle and experimentally evaluated in the project to determine suitable weld filler wires to prevent HIC specific for armor applications.

Results and Discussion:

Baseline Pre-heating Procedures of HIC Control:

Since preheating can reduce the level of concentration of accumulating hydrogen significantly, the current study evaluated the base line preheating procedures for two armor steels, MIL-DTL-46100 and MIL-DTL-12560. The ISO 17642-2 Y-Groove weldability test was used to assess susceptibility of HIC. The results are shown in Figure 1. The result show that HIC crack length can be eliminated by preheating 12560 above 100°C and by preheating 46100 above 150°C.

Development of LTPT Weld Filler Wires:

Several weld filler wires with different LTPT characteristics were produced and tested by means of Y-Groove weldability test. The testing revealed a varying degree of success in suppressing HIC by different LTPT weld filler wires. Figure 2 shows some examples of the testing results. The reference is the commercial ER100-S weld filler metal that is commonly used to weld armored steels. A pre-heat of 100 ºC is necessary to eliminate HIC with this reference filler wire in the Y-groove test. The experimental Wire 3 did not show any appreciable improvement over the standard wire. Experimental Wire 1 greatly reduced the susceptibility to HIC, as it reduced the pre-heating temperature to 50 ºC. Finally, a new filler wire, labeled as ORNL's new filler wire in the figure, was effective at eliminating the pre-heat requirement, resulting in no cracking at the ambient temperature.

Figure 3 compared the weld appearance and weld cross-section of MIL-12560 steel welded with the ER100-S weld filler wire and newly developed weld filler wire from the Y-groove test. The ER100-S standard filler wire results in 100% HIC over the entire weld length. On the other hand, HIC was not observed in welds made with the new ORNL filler wire.

Figure 4 shows a hardness map of the new filler wire developed in this work. Weld metal hardness is more or less uniform. Hardness ranges from 360 to 400 HVN, which is much high than the standard filler wire (300 HVN), and generally matches the hardness of the base metal, MIL-12560.

Conclusions:

Our current approach has shown the feasibility of a new HIC resistant high-strength welding filler wire. Our next step is fabricating the filler wire with industrial partners. Several candidate LTPT filler wires are being produced by our industry weld consumable partners, and will be further tested and optimized in FY15.

- Demonstrated preheating procedures to eliminate HIC for MIL-DTL-12560 and MIL-DTL-46100
- Showed feasibility of a new welding filler wire to mitigate HIC without sacrificing strength
- Working with industrial partners on fabricating new welding filler wires.

Figures and Tables:

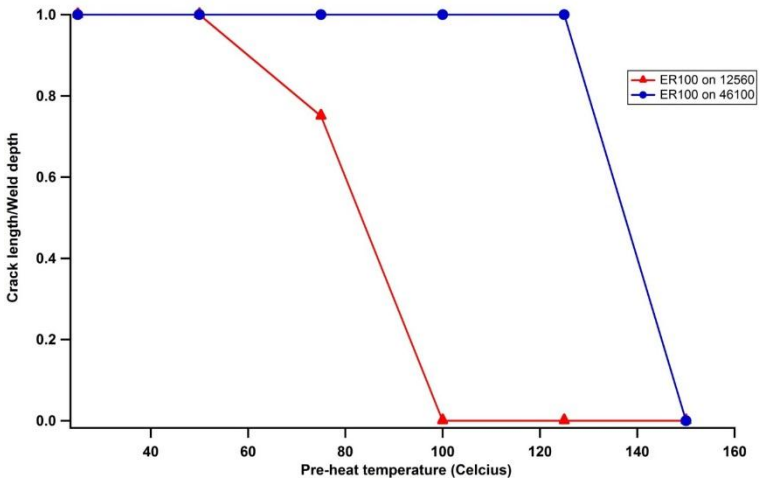

Figure 1. Pre-heating requirement to weld a ultra-strength armored steel.

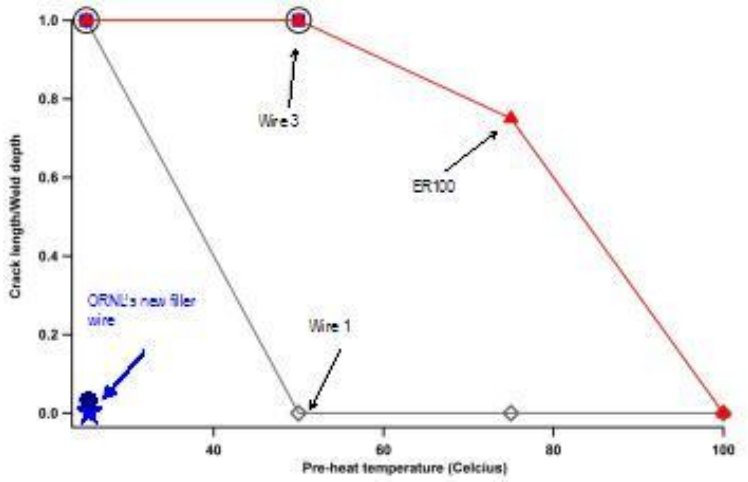

Figure 2. Degree of HIC reduction from different LTPT wires developed in this work.

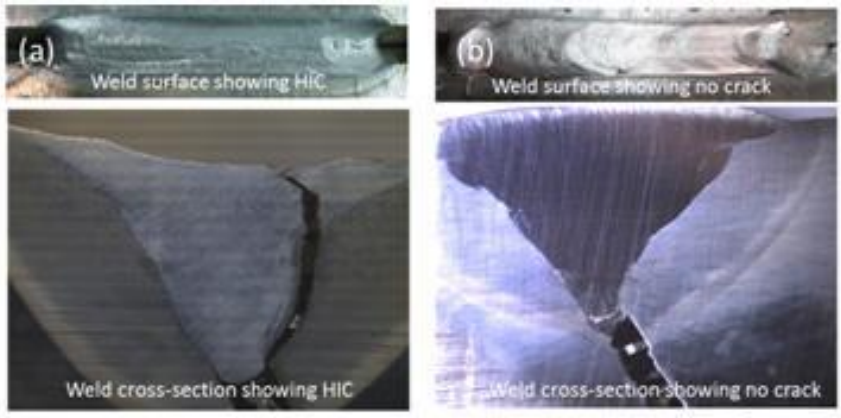

Figure 3. HIC(or lack of it) in ISO 17642-2 Y-Groove weldability test of a high-strength armored steel. (a) Standard filler wire resulting in 100% HIC over the entire weld length, (b) new developed welding filler wire resulting in minimum HIC.

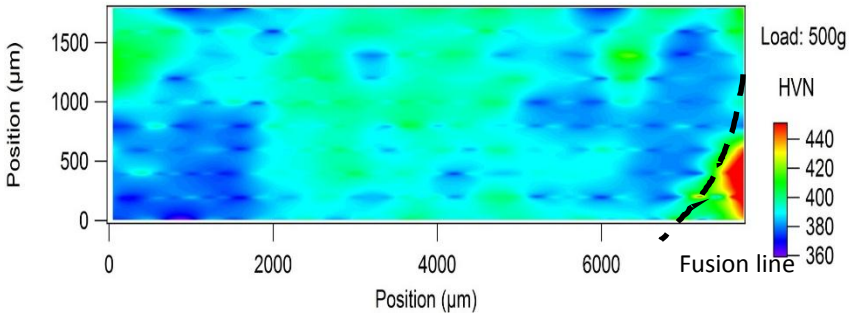

Figure 4. Microhardness mapping of a LTPT weld region in MIL-12560 steel.

This Page Intentionally Blank

AVPTA Technology Focus Area 2: Lightweight Structures & Materials

Multi-Material Joining (MMJ) - High Strength Filler Wire: Suitable for High Strength 6xxx Aluminum Alloys – Phase II

DOE-VTO TFA Lead: Patrick Davis
DOE-VTO Project Lead: William Joost
TARDEC TFA Lead: Dr. Richard Gerth

Principal Investigator
Phillip Smith

Alcoa Defense, Inc.
Alcoa Technical Center
100 Technical Drive
Alcoa Center, PA 15069-0001
Phone: (724) 337-2440
E-mail: philip.smith@alcoa.com

with Martin M. McDonnell III
Ground Systems Survivability
US Army TARDEC

Start: January 2014
Projected Completion: March 2015

Objectives:

- Develop a weld wire for welding high strength aluminum plate, particularly 6055; such that the weld joints exhibit improved mechanical properties and corrosion resistance over the incumbent weld wire material.
- Refine the chemistry of the weld wire in an effort to optimize the corrosion and mechanical properties of the resulting weld joint.
- Aluminum alloy materials (5083 and 6055) will be fusion welded with the newly developed high strength filler wire.

Strategic Context:

- The technology developed within this project will be commercialized for application to aluminum high-performance blast shields and vehicle hulls. The commercial transportation community will gain weight savings via the stronger weld wire enabling less material to be used for each welded joint. Application benefits include: overcoming $MgSi_2$ embrittlement effects from the incumbent 4XXX

aluminum filler materials previously used for welding high-strength 6XXX aluminum alloys, and allowing the welding of 6XXX to 5XXX (e.g., 5083 and 5456) aluminum alloys.
- The technology directly supports the TARDEC Strategy because it can be easily transitioned into legacy and future military systems where higher-strength weld wire is needed.
- The technology will enable the application of newer high-strength aluminum alloys into Capability Demonstrators (CDs).

Accomplishments:

- C56U-1 Chemistry developed
- C56U-1 ingot cast, rod extruded, wire drawn
- C56U-1 weld wire evaluated
- C56U-1 weld wire deemed to have a propensity for corrosion
- C56U-1 weld wire deemed to have a propensity for sensitization
- Emphasis was shifted from developing a weld wire for 6013 to 6055 since the military recently classified 6055 as being weldable.
- Seven new chemistries were developed to weld 6055
- Initial evaluation conducted of the seven new chemistries – Additional refinement needed
- Six new chemistries developed.

Introduction:

During recent conflicts in the Middle East, U.S. combat vehicles have been subjected to steadily increasing levels of mine and blast threats. In response, the armor community has developed quick war time solutions. However, the solutions are usually not optimized for weight, performance, and cost. Additionally, the need for improved fuel efficiency dictates the development of light weight vehicle designs.

Joining method technologies enable the use of new lightweight material systems. High strength 6xxx aluminum alloys, such as 6013 and 6055, have 20%+ higher strength than currently used aluminum alloys. They offer the potential to significantly improve performance, weight, and cost. However, when welding 6xxx high strength alloys (e.g. 6013), the only commercially available filler wires that can weld these high strength 6xxx alloys without cracking are 4043, 4047 and 4145. Unfortunately, the welds produced with these filler alloys have limited shear strength and ductility, which in turn limit their capability to withstand blast type of loads. When welding these high strength alloys to 5xxx (e.g. 5083) parts, the use of 4xxx type filler leads to formation of brittle $MgSi_2$ at the fusion zones of the welds with the 5xxx parent metals. On the other hand, when welding such high strength 6xxx/5xxx alloy combinations with Mg based 5xxx filler alloys (e.g. 5556, 5356, 5183), the formation of Mg_x/Cu_y low melting eutectics at the fusion zones of the welds with the high strength 6xxx alloy leads to their cracking.

Approach:

In Phase I of the High Strength Filler Wire Program a filler wire was developed, to bench scale levels, which could join 6013 plates while maintaining high strength and ductile weld joints.

In Phase II of the program it is proposed to refine the chemistry of the weld wire in an effort to optimize the corrosion and mechanical properties of the resulting weld joint. Additionally, other aluminum alloy materials (5083 and 6055) will be fusion welded with the newly developed high strength filler wire. The corrosion resistance of the weld joints and their mechanical properties will be evaluated. The optimization of the high strength filler wire allows the welding of the incumbent 5083 alloy to the newer 6013 and 6055 higher strength alloys and improves the maintainability and repairability of legacy vehicles. It also permits the light weighting and improved performance of new vehicles, as well as increased protection for the Warfighter.

A test ingot (~100 lbs) of the down-selected chemistry will be cast. Filler wire will be drawn from the test ingot. The filler wire will then be used to join 6013, 6055 and 5083 to themselves, as well as to each other, while verifying the weld parameters for each combination. The mechanical and corrosion properties of the welded joints will be re-evaluated to confirm no adverse effects.

Task Flow Path:

- Develop Candidate Chemistries
- Cast Book Molds
- Machine, Homogenize, Roll Candidate Chemistries
- Bench Scale Test and Evaluate – GTA
  - Weldability Evaluation
  - Corrosion Evaluation
  - Macrographs
  - Microscopy
  - Mechanical Property Evaluations
- Repeat if Necessary or Down-select
- Cast Pilot Scale Ingots - 100#
- Extrude Ingots to Rod
- Draw, Shave and Clean Wire to 0.062”
- Test and Evaluate – GMA
  - Weldability Evaluation
  - Corrosion Evaluation
  - Macrographs
  - Microscopy
  - Mechanical Property Evaluations

- Repeat if Necessary

Results and Discussion:

By the end of Phase I, 200lbs of C56U-1 weld wire was produced. Initial weld evaluations indicated that superior welds were achievable when joining aluminum alloy 6013 to 6013 versus welding with the incumbent 5083 weld wire (see Figures 1 and 2).

Phase II began in April, 2014. Detailed analysis of the weld quality of the weld joint generated in Phase I continued. Although dye penetrant tests and microscopy indicated excellent weld quality, the corrosion evaluation indicated that C56U-1 had a propensity for intergranular corrosion, as well as stress corrosion cracking. The weld nugget in the as-welded condition showed low mass loss (<15 mg/cm^2) in ASTM G67 test, which indicates resistance to intergranular corrosion (IG) and stress corrosion cracking (SCC). After exposure to 100°C/ 1 week, the weld nugget had mass loss of above 25 mg/cm^2, which indicates susceptibility to IG and SCC. This suggests that the weld can become susceptible to SCC after exposure to elevated temperatures and/or after long-term ambient exposure (see Figure 4). This indicates a propensity for sensitization.

Additionally, the ASTM G69 results indicate the weld nugget to be anodic to the Heat Affected Zone (HAZ) and base metal in the 6013-6013 weld with C56U-1 filler. An optimum condition for weld corrosion is that the weld has the same or similar corrosion potential as the base metal. If that is not possible, the preferred configuration is that weld is more noble than the base metal. In the 6013-6013 with C56-1 filler, the optimum or the preferred condition was not evident. The galvanic corrosion potential between the weld and the base will need to be further evaluated (see Figure 4).

A review with TARDEC was conducted in August, 2014. TARDEC expressed their desire to place emphasis on the development of a high strength filler wire for aluminum alloy 6055 rather than aluminum alloy 6013. This desire was based on the fact that the Army Research Laboratory was in the process of classifying aluminum alloy 6055 as a “weldable” alloy based on their recent ballistic shock test results. Since aluminum alloy 6055 was already one of the alloys of choice in the test matrix the expressed desire was easily embraced. Since the corrosion results indicated a need to refine the filler wire chemistry the subsequent developments were directed towards a filler wire material for the welding of aluminum alloy 6055.

Seven candidate chemistries were developed for the joining of aluminum alloy 6055 to 6055 (see Figure 5).

The same flow path as previous defined was used. Book molds were made of the candidate chemistries. The book molds were machined, homogenized, and rolled. Rod was cut from the rolled material. Constrained “T” samples were welded using the GTA process. Sections were cut from the welded samples and polished. The dye penetrant

tests and visual inspection of the cut and polished sections indicted that another round of chemistry refinement is required (see Figure 6).

Conclusions:

FY 14 saw the conclusion of Phase I and the kick-off of Phase II. The Phase I resulted in a C56U filler alloy that had superior weld quality over the incumbent material, but had a propensity for corrosion.

New emphasis was placed of the development of a high strength filler wire for the joining of aluminum alloy 6055 to itself, as well as to aluminum alloy 5083.

The results from the first round of candidate chemistries for the fusion welding of aluminum alloy 6055 were not favorable. Further refinement of the candidate filler wire chemistry and evaluations are expected to continue into FY15.

Figures and Tables:

Figure 1. Aluminum Alloy 6013 + 6013 Welded with 5183 Filler Wire.

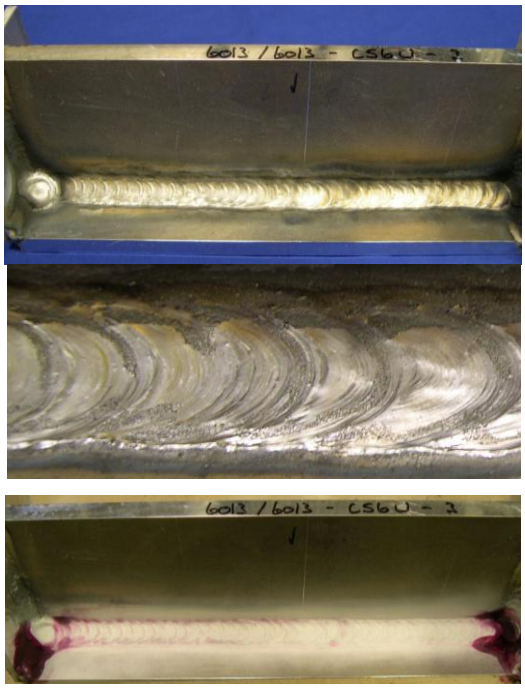

Figure 2. Aluminum Alloy 6013 + 6013 Welded with C56U-1 Filler Wire.

			G67 Mass Loss (mg/cm^2)								
			As-Welded Condition				After 100°C/ 1 Week Sensitization				
Weld Description	**Area Tested**	**Gauge** (inches)	**S#**	**Sample 1**	**Sample 2**	**Average**	**S#**	**Sample 1**	**Sample 2**	**Average**	**Comments**
6013-T651 to 6013-T651 with C56U filler	Weld Nugget	0.5	904746	5.50	5.45	**5.48**	905426	38.34	36.98	**37.66**	**Current Study**
5083-H32 to 5083-H32 with 5183 filler	Weld Nugget	0.5	845016	2.02	2.06	**2.04**	846253	7.64	6.83	**7.24**	**Previous results**

Figure 3. IG and SCC Corrosion Evaluation of Weld Nugget.

Sample Description	Samples	Solution Potential (mV vs. SCE)		
		Weld Nugget	HAZ (6013)	Base Metal (6013)
904746 6013/6013 with C56U Filler As Welded	Sample 1	-752.4	-729.5	-721.9
	Sample 2	-750.0	-728.9	-721.1
	Average	-751.2	-729.2	-721.5
904526 6013/6013 with C56U Filler After 100°C/1 week	Sample 1	-750.1	n/a	
	Sample 2	-751.3		
	Average	-750.7		

Figure 4. Galvanic Corrosion Evaluation.

Proposed Alloy Compositions

Alloy	Si	Fe	Cu	Mn	Mg	Zn	Potential
6055	0.9	0.1	0.75	0.05	0.9	0.7	-0.858
4943	5.5				0.3		-0.732
W1	0.1	0.1	**0.25**	0.3	5.9	**0.25**	-0.875
w2	0.1	0.1	**0.5**	0.3	5.9	**0.25**	-0.862
W3	0.1	0.1	0.75	0.3	5.9	**0.25**	-0.850
W4	0.1	0.1	**0.25**	0.3	5.9	**0.5**	-0.900
W5	0.1	0.1	**0.5**	0.3	5.9	**0.5**	-0.887
W6	0.1	0.1	0.75	0.3	5.9	**0.5**	-0.875
W7	0.1	0.1		0.63	5.9		-0.846

Figure 5. Candidate Filler Alloy Chemistries.

Best
4145
4943
4043
W6
W5
W2
W1
W4
C56U
W3
W7
Worst

Figure 6. Ranking of Weld Quality

This Page Intentionally Blank

AVPTA Technology Focus Area 2: Lightweight Structures & Materials

Multi-Material Joining (MMJ) - Weld Wire Characterization in Welding Armor Grade Steel

DOE-VTO TFA Lead: Patrick Davis
DOE-VTO Project Lead: William Joost
TARDEC TFA Lead: Dr. Richard Gerth

Principal Investigator:
Matthew Rogers

Ground Systems Survivability
US Army TARDEC

Start: October 2013
Projected Completion: December 2015

Objectives:

- Understand the joint quality and welding process efficiency of welded armor steels.
- Establish weld wire selection criteria for the new MIL-Standard on the welding of armored steel.
- Provide practitioners a point of comparison between current joining practices and future welding practices.
- Create validation data for ballistic and blast models of welded armor plates.

Strategic Context:

- The data developed within the project will be transitioned within TARDEC and to vehicle manufacturers through the MIL Weld Standard to enhance vehicle design. The data will identify optimal weld wire / material combinations to maximize weld wire filler material properties.
- The project supports the TARDEC Strategy by providing the platform Program Managers (PMs) with data and standards for improving the weld quality of all vehicles. The same data and standard can be adopted by the automotive industry.
- The project builds upon TARDEC's AVPTA MMJ investments leading to becoming a Joining Center of Excellence.
- Future plans include expanding the study to include 2XXX, 5XXX, 6XXX and 7XXX aluminum alloys.

Accomplishments:

- Research planning complete.
- Weld fixtures, program, and process parameters identified and validated.

- Material procured and 100% of Phase I plates welded.

Introduction:

The chemical and mechanical properties of armor steel used by the US Army are similar to advanced high strength steels used in the automotive industry. The ultimate tensile strength ranges from 150 ksi to 300 ksi depending on the armor grade selected. The last MIL standard for welding armor was canceled in 1998 and replaced with the Ground Combat Vehicle Welding Code (GCVWC)-Steel, which has never been updated and has no engineering guidance for the selection of weld wire. Additionally, neither the old MIL standard nor the GCVWC-Steel include any recommendation based on newer armor grades and new welding techniques. There are also no published industry guidelines for welding of advanced high strength steels, which the government could use to weld armor. This has led to a proliferation of welding techniques by the defense contractors, which in turn has led to a general decrease in weld quality and the proliferation of defects, such as cracks induced by hydrogen embrittlement.

Performance of welded joints is critical to the performance and reliability of ground vehicles. The performance depends on many factors associated with the welding. One key factor is the type of weld wire, of which there are many. A weld wire is classified by weld process and tensile strength. The preferred process for welding plate armor in ground vehicles is Gas Metal Arc Welding (GMAW) pulse. Weld wire tensile strength ranges from 70 ksi to 120 ksi; some ground vehicle manufactures have even used austenitic stainless steel filler metals. Unfortunately, the weldments made from these wires in combination with modern armor materials have not been characterized. There is also a general lack of knowledge of the mechanical and ballistic performance, in terms of joint efficiency, of these wires. Joint efficiency is defined as the ratio of the properties of the welded armor to the properties of the base metal armor. If the joint efficiency of each weld wire is known, then proper filler metal selection criteria can be established and implemented through a the new weld standard.

In addition to establishing selection criteria for the welding of armor steel, the data obtained in this study will be used to validate material models for ballistic and blast modeling and simulation. This data can be used by both TARDEC engineers and vehicle manufactures to further optimize vehicle design.

Approach:

The project is divided into three phases.

Phase 1:	Investigate the mechanical and metallurgical properties of welded armor using various weld wires.
Phase 2:	Perform high strain rate events using a ballistic shock test with a welded H-Plate.
Phase 3:	Perform penetration testing to determine magnitude of vulnerability.

Phase 1:

Involves robotically welding MIL-DTL-12560 class1,MIL-DTL-46100 class1, and ASTM A514 Grade A to themselves in 14" x 21" x 1/2" single V-groove sample. Filler materials are solid wire, stainless steel, and metal core filler. Various tensile strengths ranging from approximately 70ksi-140ksi will be used. All samples will be welded internally at Center for System Integration (CSI). The samples will then undergo tensile, hardness, fatigue, charpy impact, hydrogen embrittlement (see Figure 1). Once this is complete the samples will be ranked for performance. The highest performers will move to Phase 2.

Phase 2:

This phase will involve taking the highest filler performers from Phase 1 and robotically welding them into a 3'x 3' x 1/2" H-plate configuration. The same single V-Groove configuration will be used throughout this test as well. Once the plates are welded and radiographicaly tested they will be sent over to the TARDEC SABL lab for Ballistic Shock (see Figure 2). If the samples pass they will be used for Phase 3.

Phase 3:

This phase will involve taking the performers from Phase 2 and robotically welding 2' x 2' x 1/2" single V-groove plates. Penetration testing will be conducted to determine the joint efficiency as defined by the magnitude vulnerability (see Figure 3). These tests will be performed with a high speed camera and flash x-ray to record the dynamic deformation during the ballistic shock test. Understanding the dynamic deformation response is crucial to improving our understanding of weld responses to high strain rate events.

Results and Discussion:

In the first year the overall study plan was completed and the welding material and weld wires procured. In addition, it was necessary to develop an automated manner to weld standard I plates and H plates for testing. Figure 4 shows the hardware fixture that was developed to robotically weld the large sample of I and H plates. Figure 5 shows a completed I plate weld, and 6 shows how an H-Plate looks by comparison.

One issue that was not anticipated was that the MIL-DTL-46100 (high hard) material became highly magnetic from the shoot penning cleaning process. This required adding the additional step of demagnetizing the material before welding to prevent arc blow (see Figure 7).

The Phase 1 I plates welding has been completed. Figure 8 shows a sample hardness scan of a completed weld zone. Figure 9 shows how all the weld characterization samples are cut from a single plate. Three samples will be cut from different plates for each weld wire / parent material combination to obtain statistical validity of the results.

Conclusions:

The Phase 1 plates will be tested and analyzed. Upon completion, Phase 2 and Phase 3 will be conducted and completed. The remaining Phase 2 plates and Phase 3 will take approximately 3 months to weld. Once the data is collected, it will be statistically analyzed and provide input to the development of a new MIL-STD for welding. MIL-STD will utilize the data and testing criteria to develop mechanical acceptance criteria.

This data will transition and be used by both TARDEC engineers and vehicle manufactures to further optimize vehicle designs. This data will transition to Industry, PM's, Depot's, and Arsenals through the new welding mil standard, by creating filler metal selection charts. The data from this project will also be easily transitioned to help industry, such as the automotive and heavy equipment companies, in the selection of weld filler materials for their types of AHSS due to the similarities in properties. The data obtained in this study will also be used to refine material models for modeling and simulation.

Figures and Tables:

Test	Locations	Time Frame
Robotically welded samples	TARDEC CSI weld area	FY14
Tensile Testing	TARDEC Metallurgical Lab	FY14/FY15
Hardness Testing	TARDEC Metallurgical Lab	FY14/FY15
Charpy Impact	TARDEC Metallurgical Lab	FY14/FY15
Fatigue Testing	Mississippi State University	FY14
Hydrogen Embrittlement Test	Oak Ridge National Lab	FY15

Figure 1. Phase 1 Test, Test Location and Time Frame.

Test	Locations	Time Frame
Robotically welded samples	TARDEC CSI weld area	FY14/FY15
Radiographic Test	ANAD	FY15
Ballistic Shock Test	TARDEC GSS SABL	FY15

Figure 2. Phase 2 Test, Test Location and Time Frame.

Test	Locations	Time Frame
Robotically welded samples	TARDEC CSI weld area	FY15
Radiographic Test	Outside Contractor	FY15
Penetration Test	TARDEC GSS SABL	FY15

Figure 3. Phase 3 Test, Test Location and Time Frame

Figure 4. Fixture for Robotic Welding of I-Plate

Figures Continued on Next Page

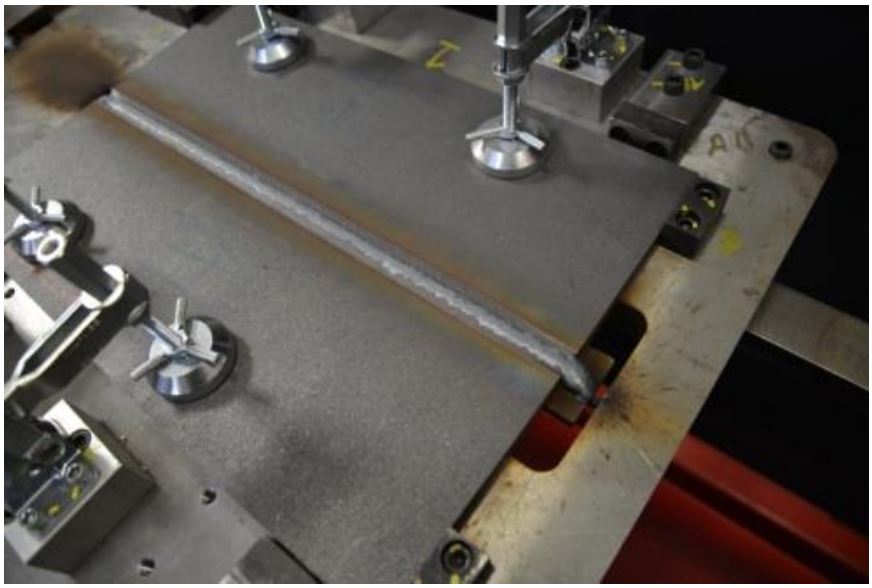

Figure 5. Completed I-Plate Weld.

Figure 6. H-Plate Clamped and Ready for Welding.

Figures Continued on Next Page

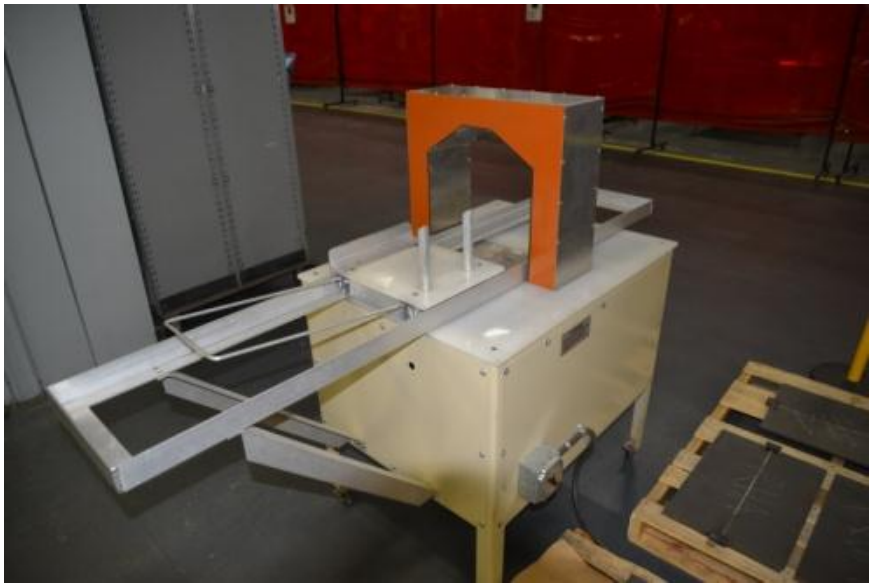

Figure 7. Demagnetizing Process.

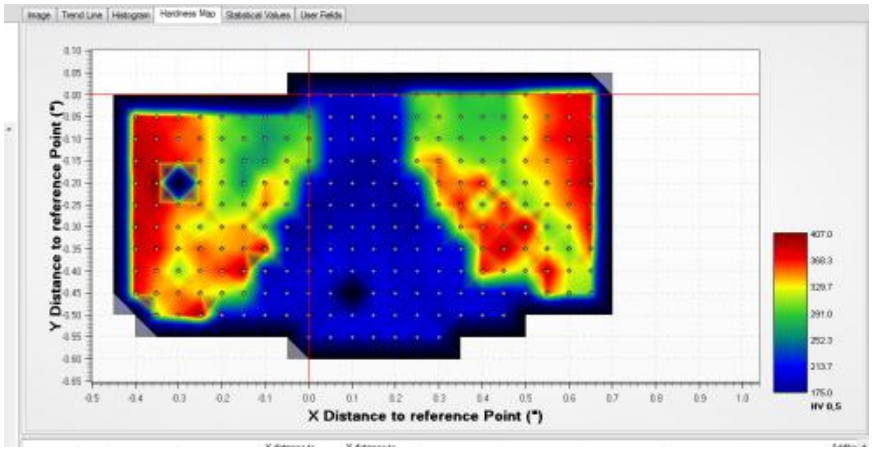

Figure 8. Hardness of I Plate Weld (Heat Affected Zone in Blue).

Figures Continued on Next Page

Figure 9. I-Plate Marked Samples for Standardized Weld Characterization Tests.

AVPTA Technology Focus Area 2: Lightweight Structures & Materials

Multi-Material Joining (MMJ) – Fatigue Performance of Welded Rolled Homogeneous Armor (RHA) Plates

DOE-VTO TFA Lead: Patrick Davis
DOE-VTO Project Lead: William Joost
TARDEC TFA Lead: Dr. Richard Gerth

Principal Investigator:
Justin Hughes

with Hongjoo Rhee, Mark Horstemeyer, Wil Whittington
Center for Advanced Vehicular Systems
Mississippi State University (MSU)
200 Research Boulevard
Starkville, MS, 39759
Phone: (662) 325-9221
E-mail: hrhee@cavs.msstate.edu

w/ Shabbir Hussain
Analytics
US Army TARDEC

Start Date: FY12
End Date: FY14

Objectives:

- Develop Multi-Stage Fatigue and Damage models that can predict weld life for rolled homogeneous armor (RHA) weld joints.
- Calibrate and validate models based on physical measurements.

Strategic Context:

- The modelling developed / assessed within the project will assist to develop techniques to simulate ballistic impacts, design test fixture structures, and reduce testing with resultant cost and time decreases.

- This project provides TARDEC with new capabilities for Finite Element Analysis (FEA) of H-Plate weld joints.
- The technology will be applied to supplement physical testing and identify / develop areas identify as potentially susceptible to physical testing.
- The technology will be directly support the TARDEC Strategy providing modeling support to the Combat Vehicle Prototype (CVP) and other Program of Record (POR) vehicles requiring ballistic impact analysis of welded joints.

Accomplishments:

- Performed materials characterization (e.g. microstructure, grain size, pore distribution, hardness profile, etc.) on weld joints.
- Carried out quasi-static/high strain rate compression and tension tests on weld joints
- Performed fatigue tests on weld joints.
- Conducted microstructural characterization (e.g. fractography) on tested samples.
- Developed internal state variable (ISV) model and fatigue model for welded joints.

Introduction:

The Material microstructure properties directly influence macro-scale material behavior. The ability to quantify the effects of material microstructures on damage behavior is necessary to accurately model a material's deformation and fatigue performance.

Internal State Variable (ISV) theory allows the production of physics based modeling frameworks capable of capturing the dissipative micro-mechanisms associated with material deformation. Using these modeling frameworks with microstructure sensitive, Multi-Stage Fatigue (MSF) and Damage (DMG) models results in high fidelity weld life predictions.

Approach:

By utilizing Mississippi State University's (MSU's) existing generalized modeling framework, MSF and DMG models specifically for Rolled Homogeneous Armor (RHA) and welded joints can be developed.

Material specific models are generated by calibrating the DMG and MSF models to mechanical test data. These models are then combined in a finite element analysis

(FEA) software package to produce a simulation tool. These models are capable of accurately predicting material performance by utilizing factors such as:

- Inclusion of material microstructure information.

- Rate and temperature dependence on stress-strain behavior.
- Damage evolution during material deformation.

Existing sub-models for the mechanisms responsible for damage and plasticity (and their dependencies) are implemented in the DMG and MSF models within a larger Integrated Computational Materials Engineering (ICME) modeling paradigm. The inclusion of these sub-models with micro-scale information allows for the whole of the framework to make accurate predictions of macro-scale deformation and fatigue performance. Figure 1 shows the ICME framework and how information is shared amongst modeling techniques.

Results and Discussion:

Microstructure characterization of Rolled Homogeneous Armor (RHA:)

Material microstructure properties were quantified via the use of both optical and electron microscopy. Grain sizes were quantified from polished and etched samples of RHA base material and weld sections. Particle size and distribution was quantified from failed tension samples in a scanning electron microscope (SEM).

Mechanical testing and modeling of Rolled Homogeneous Armor (RHA):

A multitude of mechanical tests were performed to fully capture the material's performance with respect to changes in load rates for monotonic testing and strain amplitudes for fatigue testing. Figures 2 and 3 show the behavior of both the welded joint and base material for varying strain rates in tension and compression, respectively. Figure 4 gives the experimental strain-life fatigue curve and shows the changes in the shape of the hysteresis loop as the tests progressed.

Conclusions:

MSU's existing DMG and MSF frameworks were applied to capture the specific behavior of RHA plate material and welded sections. The models were calibrated to mechanical test data for both base material RHA and welded sections.

Pending additional test data, future work will seek to improve the robustness of the material models. By utilizing fatigue crack growth studies, better calibrations of MSF can be obtained. Also, by performing statistical analyses for every model parameter, uncertainty quantification (UQ) for model output can be obtained. The uncertainty related to experimental data can be pushed through the modeling framework to provide uncertainty banding to assess the "degree of goodness" of model calibrations.

Figures and Tables:

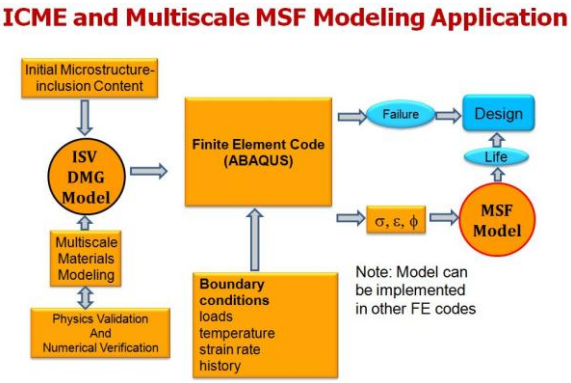

Figure 1: MSU-ISV and MSF Modeling Framework.

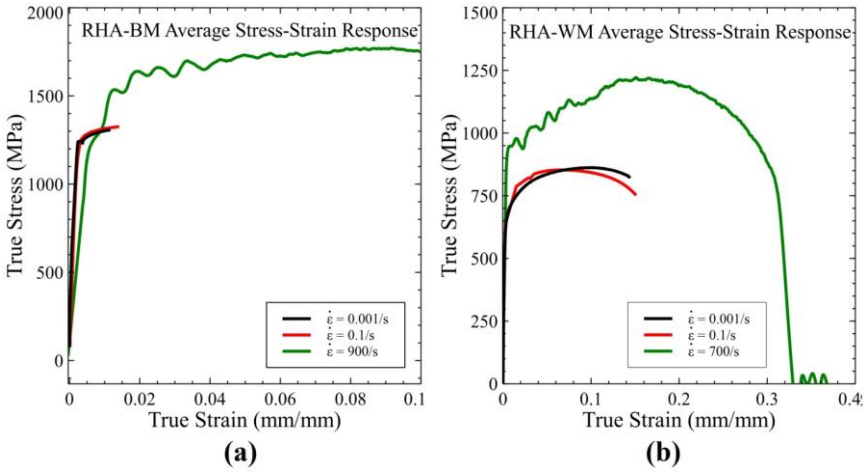

Figure 2: Average tension stress-strain response at 0.001/s, 0.1/s, 700/s, and 900/s strain rates for (a) RHA base material (BM) and (b) RHA weld material (WM).

Figures Continue on Next Page

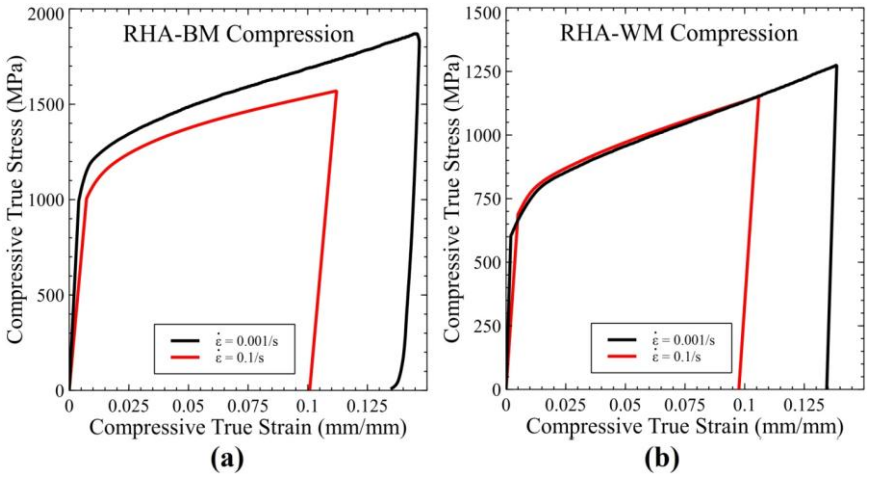

Figure 3: Average compression stress-strain response at 0.001/s and 0.1/s strain rates for (a) RHA base material (BM) And (b) RHA weld material (WM).

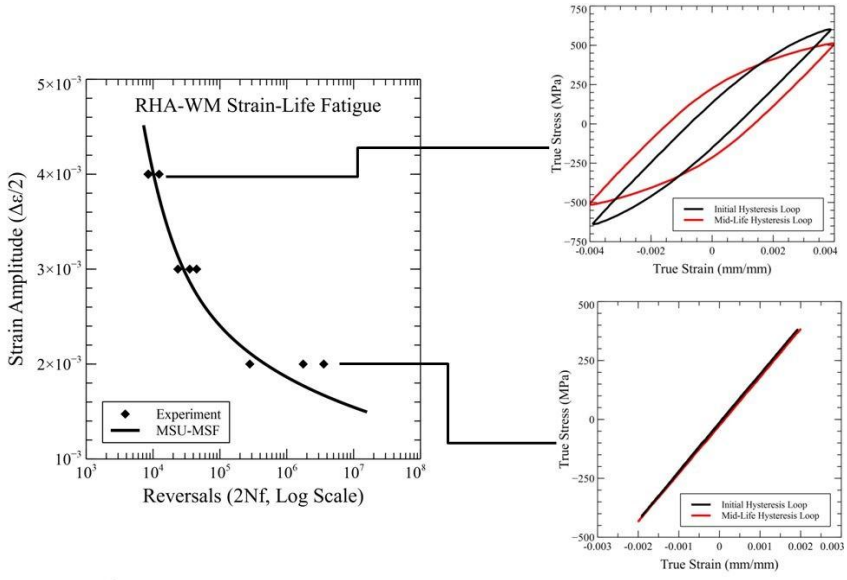

Figure 4: Strain-Life fatigue results for RHA welded joints at an applied strain ratio of R= -1.

This Page Intentionally Blank

AVPTA Technology Focus Area 2: Lightweight Structures & Materials

Multi-Material Joining (MMJ) – Computational Modeling & Simulation of Metal Joints under Ballistic Impact

DOE-VTO TFA Lead: Patrick Davis
DOE-VTO Project Lead: William Joost
TARDEC TFA Lead: Dr. Richard Gerth

Principal Investigator:
Dr. James Sheng

w/ Ron Renke and Shabbir Hussain
Analytics
US Army TARDEC

Start: FY12
Completion: FY14

Objectives:

- Characterize armor materials and weld filler materials for utilization in computational modeling and simulation of ballistic impact.
- Develop an analytical simulation capability of an armor plate weld seam under high speed impact loading (ballistic impact).
- Use the analytical capability to design and fabricate a test set up to test armor plates and weld seams subjected to a ballistic impact.
- Validate the computational finite element models by using physical ballistics impact test measurement.

Strategic Context:

- The modelling developed / assessed within the project will assist to develop techniques to simulate ballistic impacts, design test fixture structures, and reduce testing with resultant cost and time decreases.
- This project provides TARDEC with new capabilities for Finite Element Analysis (FEA) of H-Plate weld joints.
- The technology will be applied to supplement physical testing and identify / develop areas identify as potentially susceptible to physical testing.

- The technology will be directly support the TARDEC Strategy providing modeling support to the Combat Vehicle Prototype (CVP) and other Program of Record (POR) vehicles requiring ballistic impact analysis of welded joints.

Accomplishments:

- Successfully tested 14 materials (with 3 samples each) and fitted the measured properties to the internal state variable (ISV) material models.
- Analytical methodology was successfully utilized to verify the test fixture design for conducting the ballistic impact tests.
- Validated analytical models of ballistic impacts on armor material and weld seam within 11% of physical test data.

Introduction:

Vehicle modeling and blast simulation analyses requires high fidelity in the material characterizations, to improve accuracy of predicting material failure/rupture and to design a vehicle system with better survivability performance. This is especially true when it comes to characterizing the weld filler material in armor plates because the welding process usually reduces the material strength and is therefore the weak spot of the structure under ballistic loading.

TARDEC has developed a finite element modeling capability to simulate a ballistic projectile impact on an armor plate and weld seam. This analytical methodology was used to verify the structural integrity of the test fixture before fabricating the hardware and to predict the performance of armor plate along with welding seam under ballistic impacting. However, detailed models that capture the material changes in the heat affected zone (HAZ) post weld are a complex function of the parent materials, the weld wire, and the welding process used. Accurate material characterization is crucial to the prediction improvement of the armor plate impacting. These material models developed in this project is integrated into developed FEA models to predict the weld seam integrity when subjected to the effects of a ballistic projectile impact.

The models developed in this project will help reduce the number of tests needed in the lab by using simulation and also identify the areas that need to be targeted for hitting the projectile on the plate. If the analytical models can be validated to accurately predict weld seam failures with the ballistic shock data, it is believed that the FEA techniques can be extended to blast events.

Approach:

The multiple objectives of this project are an attempt to get more accurate performance predictions of various hull structural configurations when subjected to blast events.

Material Characterization:

Material test samples were cut from armor plate weld samples and subjected to high strain rate testing and fatigue testing. The results of these tests (Figure 1) were used to define the necessary material parameters and coefficients for the analytical material models.

Test Configuration Design:

A series of H-plate tests were designed to measure the ballistic impact performance of these welded joints. The H-Plate consists of four rectangular shaped metal plates that were joined by weld seams. The plates were used for ballistic impact tests with projectiles, to determine their structural integrity during the impact. Total six impact tests have been conducted, and 2 of the impact locations are illustrated in Figure 2.

A test fixture was also designed to hold the H-plate for the impact tests, as shown in Figure 3. The fixture will support both sides of the H-plate (cyan). The H-plate can be positioned from either side or top into the holding slot. Once the testing plate is in position, a 2x4 wood block is wedged in the slot to hold the h-plate in position for impacting.

Analytical Methodology Development:

A finite element model of the test fixture and sample (H-Plate) was created to replicate the test fixture, armor plate, and ballistic projectile. Multiple iterations of the finite element model were run to achieve a stable solution and deformation modes in the plate and projectile that reasonably predicted the results from the hardware testing. The structural integrity of the test fixture was also verified during this process.

Results and Discussion:

The test fixture used to conduct ballistic impacts on weld plates was modeled to develop the process for ballistic impact testing in the lab. The fixture shown in Figure 3 below was first modeled and analyzed to make sure it can withhold the impact of the projectile, before the fixture was built. The FEA simulation model for the fixture with the

projectile hitting it at a certain velocity was modeled as shown in Figure 4. The armor plate material properties were assigned and the fixture material and thicknesses were modeled using simulation.

The displacement contour plot from the FE simulation, showing the maximum displacement due to the impact of the projectile is shown in Figure 5. As expected, the displacements are the highest at the point of projectile contact with the test specimen plate.

The plastic strain plot for the simulation, showing the plastic strain on the plate due to the impact of the projectile, is shown in Figure 6. Both the plastic strain and the displacement plots were used to help guide the design of the test fixture.

The test fixture setup for the H-plate to withstand ballistic projectile impact is shown in Figure 7. The results of the simulation are based on actual test material properties of the filler material and armor plate due to heat affected zones of the armor contact plate material. This simulation will help optimize and reduce the actual projectile shots needed to assess the impact on the H-plate because the validated computational modeling and simulation can be used to substitute many intermediate tests in design welding seam and patterns.

Figure 8 shows the plate after impacting at the welding corner with an impacting speed of 1352 ft/s by a steel projectile. The predicted weld cracking length is 12.19 inches compared with 13.5 inches of measured cracking length, i.e., the prediction was within 11% of the actual measurement. The crater diameter estimated in the computational simulation is 9.7 inches compared with the measured 9.5 inches, i.e., the prediction was within 2.2% of the actual measurement. The results of the developed welding seam models show good agreement with the ballistics impacting test measurement.

In the simulation shown in Figure 9, the impact of the projectile with the H-weld plate does not lead to any separation of the weld or failure of the weld.

Conclusions:

In this project, more than 40 material sample tests have been conducted, and about 14 material ISV models have been developed. These models have been used in computational modeling and simulation of the H-Plate welds to predict ballistic impact performance. The modeling methodology and procedures developed at TARDEC, as part of this effort, provide reasonably good prediction of the physical ballistic impact test measurement.

Analytics plan in the future is to apply these developed material model, methodology and procedures to support other PM and technology development programs.

Figures and Tables:

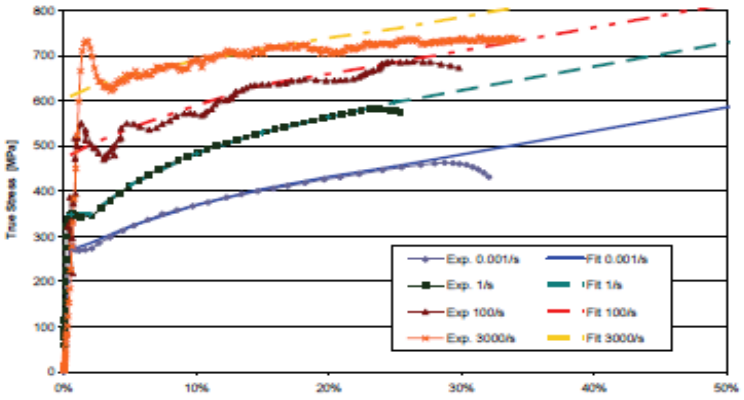

Figure 1 True Stress for different Strain Rates.

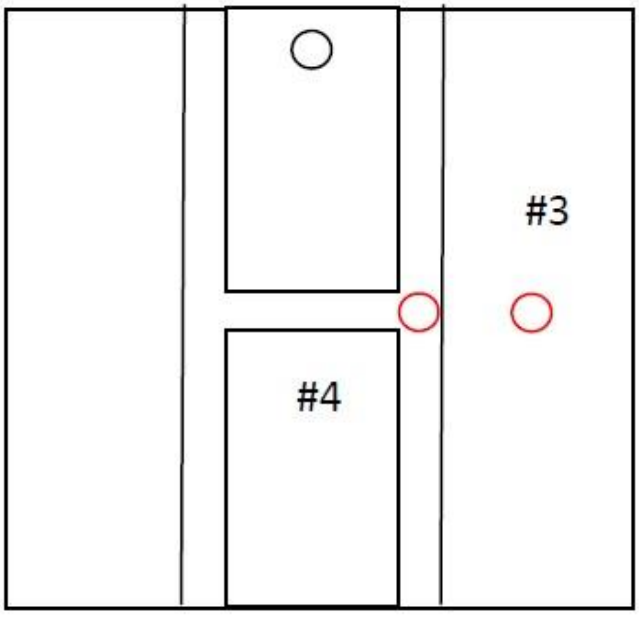

Fig. 2 H-Plate design with 2 impact locations.

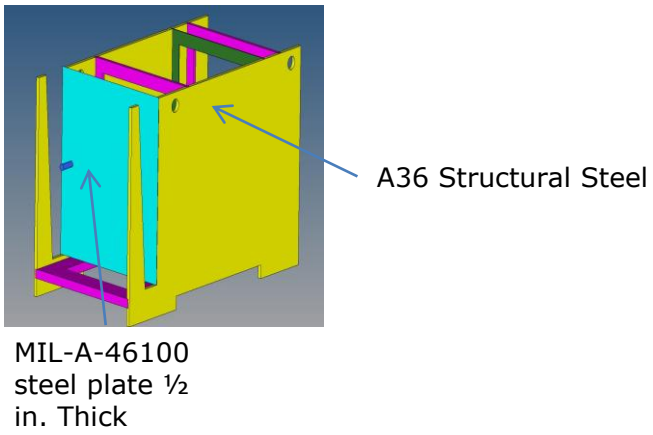

Fig. 3 – Finite Element Model of Ballistic Test Fixture.

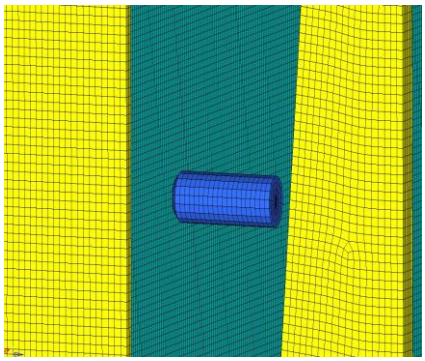

Fig. 4 – Finite Element Model of Projectile.

Figures Continued on Next Page

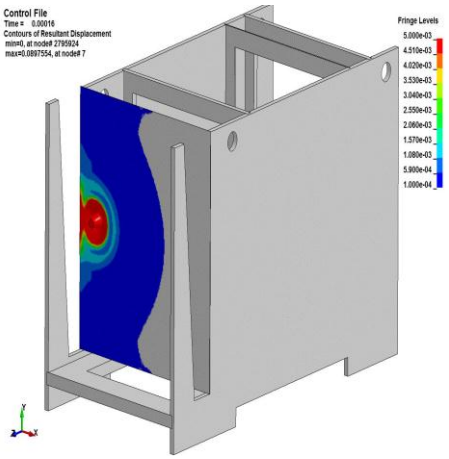

Fig. 5 – Displacement Contour Plot.

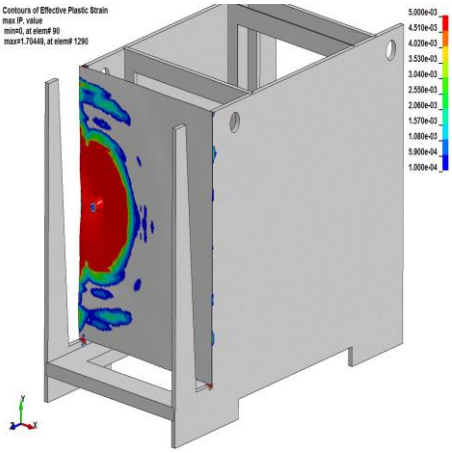

Fig. 6 – Plastic Strain Contours.

Figures Continued on Next Page

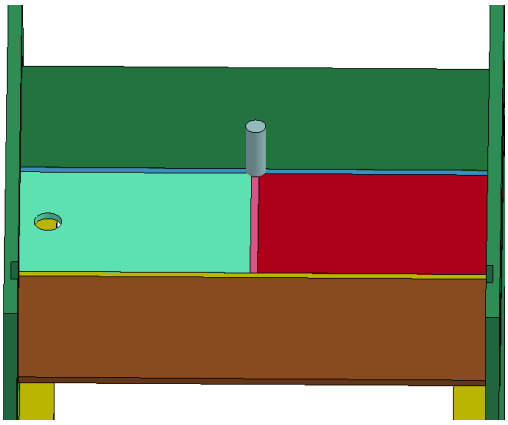

Fig. 7 – Armor H-Plate Weld Test Configuration.

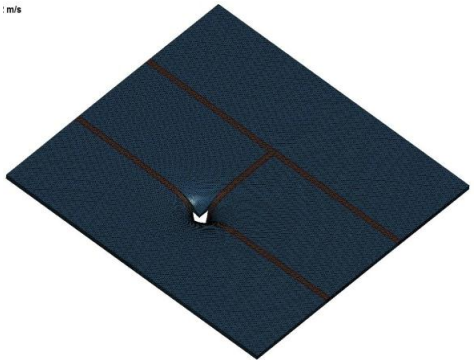

Fig. 8 - Finite Element Model of shot 14309-4-C with penetration.

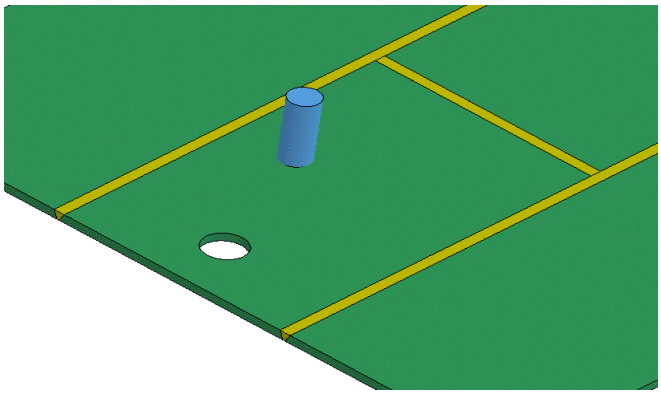

Fig. 9 – H-Plate Weld with no separation.

AVPTA Technology Focus Area 2: Lightweight Structures & Materials

Multi-Material Joining (MMJ) – Laser-Assisted Cold Spray

DOE-VTO TFA Lead: Patrick Davis
DOE-VTO Project Lead: William Joost
TARDEC TFA Lead: Dr. Richard Gerth

Principal Investigator:
Victor Champagne, PH.D.

Director, ARL Center for Cold Spray
US Army Research Laboratory
Aberdeen Proving Ground

w/ Benjamin Eichhorn
Technology Planning
US Army TARDEC

Start: October 2013
Projected Completion: December 2015

Objectives:

- The overall objective of this proposal is to develop *Cold Spray (CS)Technology* as a feasible means to join dissimilar materials including; aluminum to advanced steel for light-duty vehicle body-in-white joints.
- The research will focus on Process Development and Demonstration and Joint Design and Characterization.
- The first materials to be considered are joining
  - Cast ZE41A Magnesium to Wrought 6061 Aluminum.
- Other materials that will be considered for this program include:
  - Aluminum to Magnesium (5XXX, 6XXX and 7XXX series Al to magnesium alloys such as ZE 41A, AZ91C & AZ91E).
  - Titanium to Aluminum (Ti6Al-4V to 5XXX, 6XXX and 7XXX series Al).
  - Aluminum to Advanced Steel (5XXX, 6XXX and 7XXX series Al to low and medium carbon containing steels).

Strategic Context:

- This project is focused on light-weighting tactical wheeled vehicles by replacing cast iron brake rotors with aluminum rotors.
- Additive manufacturing is employed to apply a cast iron wear surface upon the aluminum rotor.
- TARDEC is partnering with the Program Manager – FSOV to support a military product Original Equipment Manufacturer in the development of a next generation tactical vehicle.
- The technology will be used to; apply metallic powder to dissimilar material to improve performance and reduce weight, repair worn metallic components and apply hard wear surfaces onto metallic components.
- The technology can be easily adapted for use within TARDEC and / or by military arsenals and depots.

Accomplishments:

- The results of this work represent a breakthrough in the development of a practical method to join dissimilar materials, specifically, wrought 6061 Al alloy to cast ZE41A Mg, by a combination of the cold spray process (CSP) and friction-stir welding (FSW).
- Materials characterization and analysis of results showed conclusively that cold spray can be used to join aerospace and automotive alloys of Mg and Al. The CSP joint had higher shear strength than the base Mg and exceptional tensile and hardness properties.

Introduction:

The Cold Spray process involves the introduction of a heated high-pressure gas such as helium or nitrogen together with 1- to 50-µm particles of a metal or alloy into a gun onto which is attached a nozzle designed such that the gas exits at supersonic velocities. The powder particles entrained in the gas flow are accelerated to velocities in the range of 200 to 3000 meters-per-second, considerably higher than what are achieved in any thermal spray process, including High Velocity Oxyfuel (HVOF). Because the temperature of the gas generally ranges from 0 to 1,000 ºC, no melting of the particles takes place, plus there is no oxidation, decomposition, or other degradation of the powder material.

Cold spray technology can closely match the properties of the parent substrate material and rapidly restore dimensions without causing heat affected damage. This is significant because cold spray can be applied without exceeding the temperature limitations of the bonded materials. Cold Spray can have a positive impact on force readiness by creating the capability to perform structural repairs and other wear surfaces either in forward areas and/or at the depot level in order to maintain full mission readiness. The repair technology/process has been field tested and found to be feasible/capable of reclaiming components. Cold spray shows a significant improvement over existing

methods, using aluminum alloys as a cost-effective, environmentally acceptable means to provide both surface protection and repair/rebuild capability for a variety of aluminum and magnesium alloy components.

For the purposes of this report, the following definitions will be used:

- "Aluminum" is defined as 5XXX, 6XXX or 7XXX series aluminum alloy 5 mm thick.
- "Advanced Steel" is defined as automotive sheet steel with an ultimate tensile strength (UTS) greater than 580 MPa (~85ksi) and 5 mm thick.
- "Body-in white joints" refers to joints between the materials described above in the body-in-white where constraining the assembly and access to the joint is limited by size of the assembly".

Approach:

Phase 1: Joint Test Protocol (JTP), Modeling of Process Parameters and Automation Integration:

- Develop Joint Test Protocol for selected groups of dissimilar materials (coupon and/or component testing with industry, academia and Government input).
- Calculate gas flow and temperature characteristics of De Laval nozzle by means of isentropic (frictionless) gas dynamic principles and empirical measure by a DPV 2000 laser based particle velocity measuring system.
- Drag and heat transfer coefficients from solid rocket analyses are used to iteratively calculate particle velocity and temperature through the nozzle to determine the “Critical Impact Velocity”.
- An empirical relationship between the particle velocity and particle material characteristics is used to calculate the deposition efficiency or the percent of incoming particles that adhere and form a well bonded deposit, which is used to determine the optimal cold spray process parameters that will result in adequate consolidation and maintain the Nanostructured microstructure.
- Identify automation requirements for robot programming and manipulation, including design of specialized fixtures to hold parts during spraying and machining.
- Procure/fabricate materials for automation, process development and testing.
- Initiate automation integration.

Phase 2 Cold Spray Process Developments:

- Finalize automation integration and establish prototype capability.
- Validate process modeling and critical impact velocity.
- Powder selection and acquisition, materials characterization.
- Nozzle development and fabrication based upon powder characteristics.
- Conduct spray trials and optimization.

Phase 3 Materials Testing and Evaluation: Duration:

- Spray coupons and components for testing and evaluation.
- Perform required materials and component tests.
- Analyze data and make necessary adjustments to the cold spray process.

Phase 4 Joint Designs and Characterization:

- Design various joint configurations and through modeling and simulation.
- Test feasibility of joint design through sub scale testing.
- Characterize cold sprayed joint designs (bend testing, Microstructural analysis).

Phase 5 Transition / Implementation:

- Establish prototype capability for subscale coupons and simple geometry parts.
- Conduct cold spray process prove-out based upon JTP.
- Perform demonstration of cold spray process on actual parts.
- Write final report.

Results and Discussion:

Surface Preparation:

The surface preparation used for all the ZE41A-T5 magnesium substrates was an abrasive blast followed by a solvent rinse. The abrasive blast equipment was a *Port-A-Blast.* This equipment does not recycle the abrasive. The use of uncontaminated abrasive was necessary to minimize the embedding of corrosive materials such as iron into the magnesium substrate. It has been proven that some of these containments are detrimental to corrosion resistance of the magnesium substrate. The abrasive media used was a 60 grit aluminum oxide. This media was sprayed at 100 psi pressure at a 45 degree angle stand-off angles. The stand-off distance was between 4 to 6 inches away from the surface of the part. The solvent rinse was ethanol.

Cold Spray Processing (CSP):

A cold spray layer of 6061 Al was deposited onto the edge of the magnesium plate sufficient in thickness to accommodate a FSW weld, to enable it to be joined to the 6061aluminum plate. The 6061 Al layer was produced using commercially available gas-atomized 6061 Al powder (Valimet, Stockton, CA, USA). The specified particle size cut was -325 mesh which corresponds to a maximum particle size of approximately 44 μm and an average of 18 μm measured using a laser diffraction particle size analyzer. A high pressure cold spray system was used and helium was chosen as the process gas to achieve high impact velocities between incident particles. The pressure and temperature of helium were maintained at 2.8 MPa and 400˚C, respectively. Deposition took place

using a nozzle stand-off distance of 25 mm, 90° deposition angle, medium powder feed rate (12 g min^{-1}), and a high nozzle traveling speed (600 mm s^{-1}). The total deposition thickness of ~ 8.5 mm was achieved in this study. The purpose of the cold spray transitional material was to mitigate the formation of a deleterious inter-metallic layer at the dissimilar metal interface. The cold spray layer would serve as an insulator and minimize any thermal energy from the FSW. FSW allows for minimal heat transfer across the cold spray layer. Figure 1 shows a schematic of the sample, as prepared according to the prescribed method incorporating cold spray and FSW. Figure 2 shows four samples of ZE41A-Mg that have been 'buttered' with a CSP layer of 6061 Al. The samples were approximately 4 inches long, 2 inches wide and ¼ inch thick and then final machined flat and parallel to the original magnesium plate surfaces (Figure 3). After the cold spray layer was applied the FSW process was incorporated to join the materials together. Without the cold spray layer this would not be achievable without the formation of an inter-metallic layer at the dissimilar metal interface.

Triple Lug Shear Strength Test:

The Triple Lug Shear Test method was used to study the adhesive shear behavior of the cold spray buttered edge, where 6061 Al was cold sprayed onto ZE41A-T5 magnesium. Triple Lug procedure methodology is prescribed in military specification, MIL-J-24445A. A deposit with a thickness of greater than 0.125 inches is applied onto the ZE41A-T5 magnesium by the cold spray process. Three rectangular-shaped 'lugs' are machined from the 6061 Al cold spray weld. The lugs are then sheared from the test specimen using a compressive load frame set-up. Only one lug is sheared from the specimen at a time. Failure stress is reported based on the load at failure and the surface area of the lug. Control specimens milled from single pieces of cast magnesium were included in the matrix to establish a baseline for comparison. The specimens were tested in shear in a universal tensile testing machine (MTS, Systems Corporation, Eden Prairie, MN) under displacement control at constant cross-head speed of 1 mm/min. The applied load was measured continuously with a 25 kN load cell. The force required to shear off the coating and the coating/substrate attachment area then yielded the shear strength of the bond. All of the 6061 Al cold spray lugs showed very high adhesion on the magnesium alloys. The average adhesive strength of the 6061 Al cold spray lugs on ZE41A-T5 Mg was about 22ksi and actually exceeded the average strength of the base line ZE41A-T5 Mg samples, which were 17ksi. The 6061 Al cold spray lugs on the ZE41A-T5 broke off by fracturing material well beneath the Al/Mg interface. This substantiates the claim that a structural weld is possible between ZE41A-T5 Mg and 6061 Al utilizing the cold spray process alone, since the weakest point is no longer at the cold spray deposit/magnesium substrate interface. The latter clarifies that the in contrast to conventional joining methods, the Al/Mg interface does not include any inter-metallics.

Micro-structural Analysis of the Cold Spray Buttered Edge:

The micro-structural features of the cast ZE41A-T5 Mg samples 'buttered' with 6061 Al cold spray in preparation for FSW, were evaluated by optical microscopy and scanning electron microscopy (Supra-40, Zeiss, Oberkochen, Germany). Cross-sections of the

edge were taken utilizing a LECO cut-off saw and one inch diameter metallographic samples were mounted in Bakelite and prepared incorporating a series of grinding steps starting at 180 grit and finishing with 2400 grit. Final polishing was accomplished using 3 um diamond paste followed by ¼ um diamond paste and completed using a 0.05 um colloidal silica suspension.

The important aspects of the evaluation were that as anticipated, no evidence of a heat affected zone was observed since the cold spray process is accomplished below any phase transformation temperatures and well below the melting point of both materials (4 and 5). Figure 4 represents an as-polished sample showing the interface of the cast ZE41A-T5 Mg and the cold spray 6061 Al layer taken with the scanning electron microscope (SEM). The interface showed no inherent defects such as porosity, cracks and oxide inclusions or inter-metallic compounds. The CSP layer near the substrate interface has a good deposition quality with no obvious evidence of porosity, triple junction voids, and lack of bonding between powder particles. This demonstrates suitable local particle deformation due to proper selection of cold spray process parameters.

.

Figure 5 shows the same area but using optical microscopy and after being etched with Keller's reagent. It shows no inter-metallic formation at the interface.

Tension Testing of the 6061 Al Cold Spray Deposit:

A total of 6 tensile bars were cut from actual deposits of CSP 6061 Al. The tensile test results showed that the CSP 6061 Al has a very high strength 49ksi, in the as-cold sprayed condition (Table 1). The Yield Strength (YS) and the Ultimate Tensile Strength (UTS) of the cold spray 6061 Al actually exceeds the properties of wrought 6061-T6. The primary strengthening mechanism is the work hardening that occurs during particle impact and consolidation in the solid state. The elongation at failure (%EL) is 5%, which actually exceeds that of the ZE41A-T5 Mg and is comparable with other cast magnesium alloys. The %EL can be increased to approximately 17% after the in process annealing, if necessary. The YS and UTS dropped to values typical of wrought 6061 with T4 tempering. Both the as-deposited and in process annealed data indicate that there is potential for utilizing cold spray to serves as a suitable transition material when joining ZE41A-T5 Mg to 6061-T6 Al by FSW.

Friction Stir Welding Process:

Friction Stir-welding was chosen to join a 'buttered' piece of cast ZE41A Magnesium to a plate of wrought 6061 Al. The purpose of the cold spray transitional material was to mitigate the formation of a deleterious inter-metallic layer at the dissimilar metal interface. The cold spray layer would serve as an insulator and minimize any thermal energy from the FSW. FSW also allows for minimal heat transfer across the cold spray layer.

The 10 mm aluminum 6061 plates were welded to the cold sprayed 6061 ('buttered' pieces of cast ZE41A Magnesium). The process parameters of the tool was 800 RPM, 10 IPM, 1° Lead Angle and a 0.15 IPM Plunge Rate. The two plates to be joined were initially machined to ~0.250" thickness and a pin length 0.130. Pin Tool design Details were: 1- two Piece Adjustable Pin Tool, 2- 0.425" Diameter Shoulder - Concave, 3- 10° tapered pin with 3 flats, and 4- Material Type – H13 tool steel shoulder with MP159 Pin. Figure 6 shows the FSW achieved when joining cast ZE41A Mg to wrought 6061 Al.

Micro Hardness Test:

Vicker's micro hardness measurements were performed on the CSP/FSW samples. Measurements were taken across the various zones, as shown in Figure 7. A micro hardness traverse (collected from a substrate/coating cross-section) was conducted whereby measurements were obtained with a fixed separation of 0.3 mm, traveling from the Mg substrate through the CSP/Mg substrate interface, to the surface of the CSP layer and across the FSW area and into the wrought 6061 Al. The position of the indentation relative to the various regions was measured using optical microscopy in conjunction with image analysis. Vickers hardness testing was performed using a 500g load. The results show the typical hardness gradient across the Dissimilar Materials Integration Zone (DMIZ). The hardness across the nugget was lower than both that of the cold spray 6061 Al as well as the wrought 6061 Al due to mechanical mixing of the materials being FSW.

Micro-structural Examination of the FSW Samples:

Figures 8a and 8b show a cross section of the weld in the as-polished and etched condition respectively as observed optically and electron microscopy (Figure 9) confirmed the absence of an inter-metallic layer. The cold spray material served as the transitional material allowing the two dissimilar metals to be joined without any formation of undesirable inter-metallics or other undesirable Micro-structural features, such as heat affected zones (HAZ) or the formation of an as-cast structure. The welded area was free from porosity and defects often associated with conventional welds. Evidence of an intercalated microstructure with vortexes associated with FSW, as a result of mechanical mixing of the two metals was observed, also reported by Somasekharan and Murr.

Tension Testing of the Cold Spray/FSW joint between ZE41A Mg and 6061 Al:

A total of 12 tensile specimens were fabricated from samples that were prepared by buttering one edge of ¼ inch thick panels of cast ZE41A Mg with 5056 Al by the cold spray process to which a ¼ inch thick piece of wrought 6061 Al was joined by FSW (Figure 1). The tensile test results (see Table 2) show the results of a major breakthrough in the joining of these two dissimilar materials for the ultimate strength of the joint was approximately that of the cast magnesium substrate.

Conclusions:

The results of this work represent a breakthrough in the development of a practical method to join dissimilar materials, specifically, wrought 6061 Al alloy to cast ZE41A Mg, by a combination of the cold spray process (CSP) and friction-stir welding (FSW).

Materials characterization and analysis of results showed conclusively that cold spray can be used to join aerospace and automotive alloys of Mg and Al. The CSP joint had higher shear strength than the base Mg and exceptional tensile and hardness properties.

This work allowed for a better understanding of the Friction Stir Weld Zone and the Dissimilar Materials Integration Zone (DMIZ) through materials characterization.

Presentations / Publications:

- Applied Surface Science, Ms. Ref. No.: APSUSC-D-13-04269, Title: “Microstructural Stability of Ultrafine Grained Cold Sprayed 6061 Aluminum Alloy.” Published 2014
- Applied Surface Science, 305, pp. 797-804, 2014, Title: “Nano crystalline High Energy Milled 5083 Al Powder Deposited Using Cold Spray”. Published 2014
- TMS 2014 Conference Proceedings, Ultrafine Grained Materials VIII, “Processing and Fatigue Crack Growth Behavior of Cold-Spray, 6061 Aluminum Alloys".
- TMS 2014 Conference Proceedings, Ultrafine Grained Materials VIII, "Through-process Modeling of Al Alloy Optimization for Cold Spray Processing".
- Advanced Materials, Processes and Applications for Additive Manufacturing, "Cold Spray Processing of Bulk Nanostructured Aluminum Alloys: Characterization, Evaluation, and Optimization".

Figures and Tables:

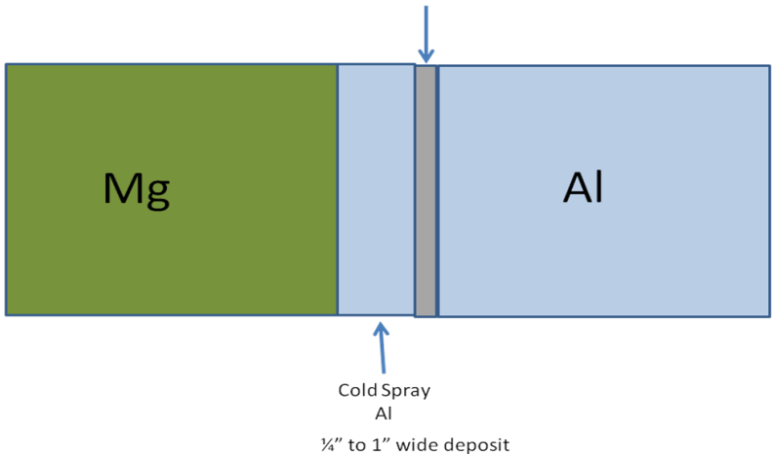

Figure 1. Shows how the samples were prepared to enable ZE41A Mg to be joined to wrought 6061 Al by a combination of the cold spray process and friction-stir welding.

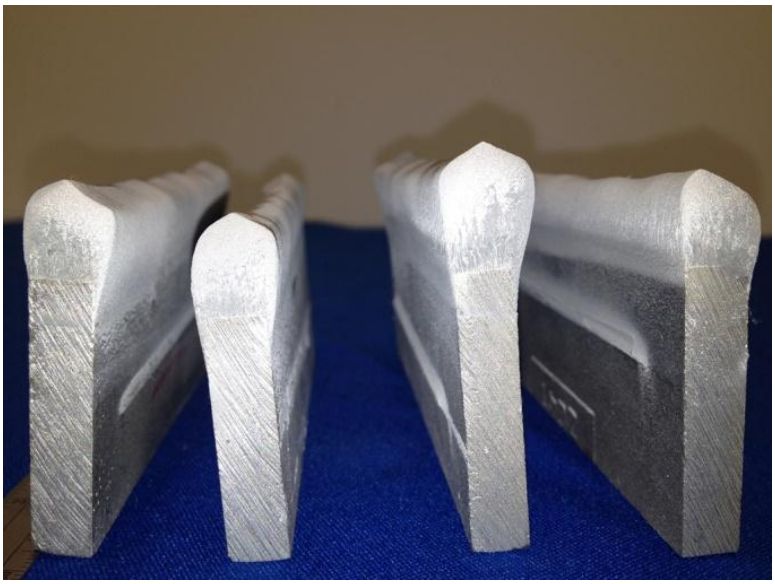

Figure 2. Samples of cast ZE41A-Mg 'buttered' with 6061 Al cold spray to prepare for FSW.

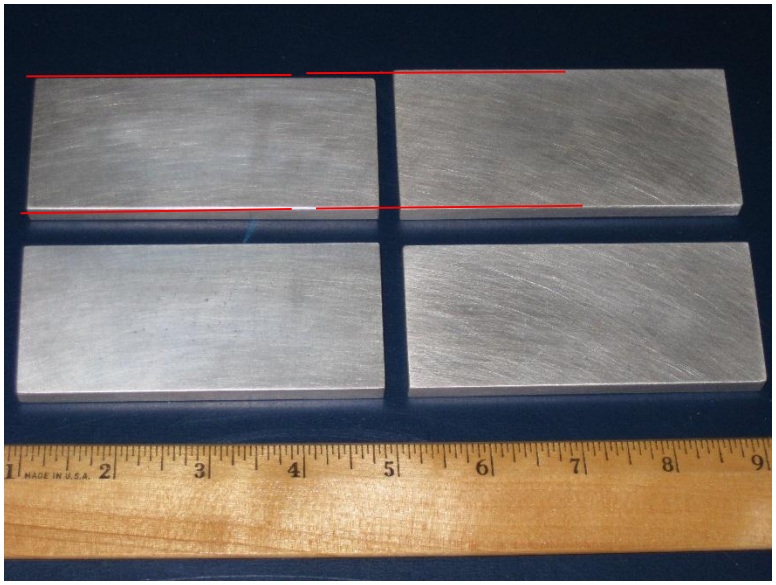

Figure 3. Finished machined samples of cast ZE41A Mg 'buttered' with 6061 Al cold spray. (Red lines denote the Al / Mg interface).

Figures Continued on Next Page

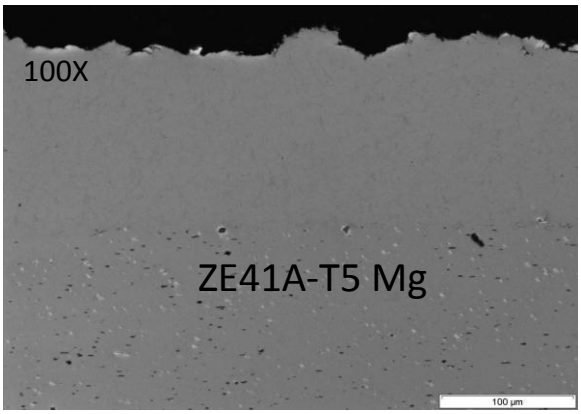

Figure 4. Scanning electron microscope image of an as-polished cross-section of the 6061 Al/ZE41A-T5.

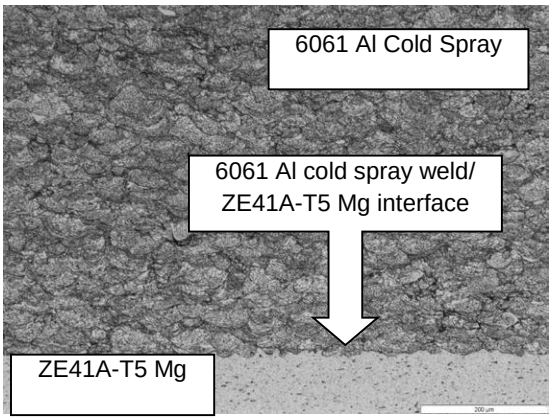

Figure 5. Etched microstructure of 6061 Al deposited onto ZE41A-T5 Mg.

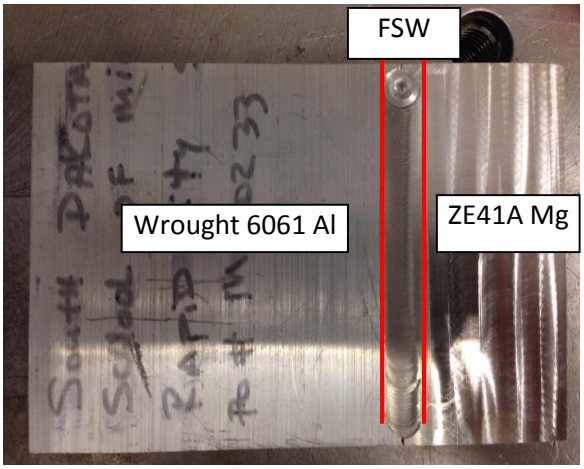

Figure 6. Completed FSW joining cast ZE41A Mg to wrought 6061 Al.

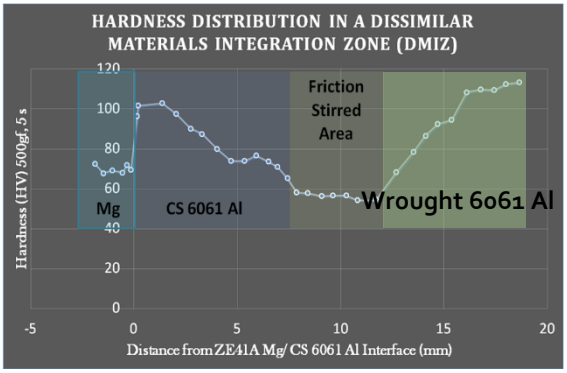

Figure 7. Micro Hardness traverse across the Mg substrate and CSP / FSW into the 6061 Al.

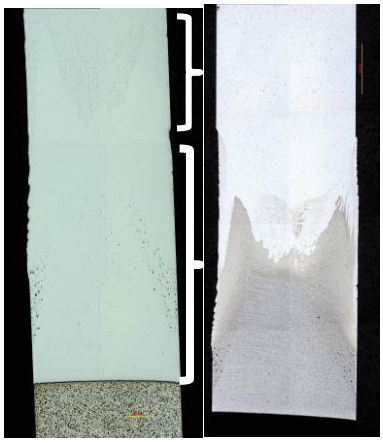

(a) **(b)**

Figure 8. Cross-section of the FSW showing the cast ZE41A Mg. The cold spray 6061 Al and the wrought 6061 Al in the as-polished (a) and etched (b) condition.

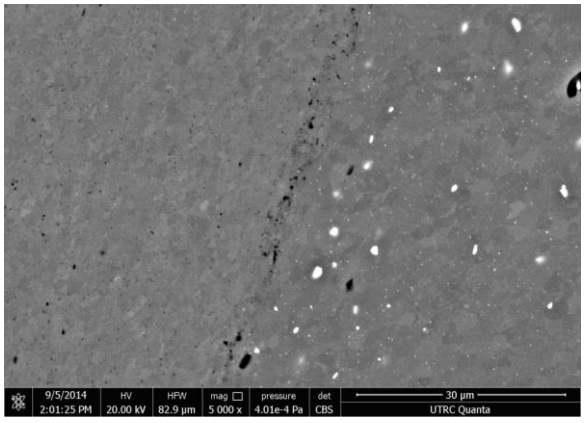

Figure 9. SEM of FSW within a vortex zone. Note the grain refinement across the sample.

6061 Condition	UTS, ksi	YS, ksi	%EL
annealed	18	8	25
T4, T451	30	16	18
T6, T651	42	35	10
cold sprayed	49.3	42.5	5

Table 1. Tension test results of cold spray 6061 Al compared to wrought 6061 Al.

SPEC #	UTS (ksi)	YS (ksi)	Modulus (msi)	%ep @ Failure	Notes
6061-5056-1-					
1	**28.7**	**28.4**	**10.1**	**0.23%**	Clean Mg-Al (interface) break
2	**28.1**	**27.4**	**9.9**	**0.27%**	Clean Mg-Al (interface) break
3	**28.6**	**28.4**	**10.3**	**0.23%**	Clean Mg-Al (interface) break
AVG	**28.5**	**28.1**	**10.1**	**0.24%**	
6061-5056-2-					
1	**28.2**	**25.1**	**9.4**	**0.74%**	Clean Mg-Al (interface) break
2	**26.2**	**25.3**	**9.4**	**0.31%**	Partial Mg-Al (interface) break
3	**28.3**	**25.3**	**9.8**	**4.70%**	Only 2.8 ksi at fracture, significant necking, no Mg-Al (interface) break
AVG	**27.5**	**25.3**	**9.5**	**1.92%**	

Table 2. Tensile Test of Cold Spray/Friction Stir Weld Joining of ZE41A-Mg to 6061 Al.

AVPTA Technology Focus Area 2: Lightweight Structures & Materials

Multi-Material Joining (MMJ) - Co-axial Laser Assisted Supersonic Sintering (CLASS)

DOE-VTO TFA Lead: Patrick Davis
DOE-VTO Project Lead: William Joost
TARDEC TFA Lead: Dr. Richard Gerth

Principal Investigator:
Pravansu Mohanty, Ph.D.

University of Michigan (U of M) – Dearborn
4901 Evergreen Road
Dearborn, MI 48128-1491

w/ Benjamin Eichhorn
Technology Planning
US Army TARDEC

Start: October 2012
Projected Completion: September 2016

Objectives:

- Develop the material systems that support the Co-axial Laser Assisted Supersonic Sintering (CLASS) process.
- Demonstrate the efficacy and flexibility of the CLASS process by creating:
  - Lightweight aluminum brake rotors with comparable performance to a steel brake rotor.
  - Low cost SiC encapsulated armor plates.

Strategic Context:

- Coated aluminum brake rotors will support sustainment of existing Programs of record (PORs) and be available as an option for next generation vehicles.
- The light-weight armor plates developed by encapsulating Silicon-Carbide (SiC) tiles onto a hexagonal Ti_6Al_4V matrix will be used as a light-weight applique armor solution on legacy and next generation POR vehicles.
- The technology directly supports the TARDEC Strategy for the sustainment and light-weighting of legacy and next generation POR vehicles.
- TARDEC Ground Systems Survivability (GSS) will be able to utilize the new light-weight armor applicable to legacy and next generation POR vehicles.

- Follow-on activity is conditional to results of pending testing and evaluation.

Accomplishments:

- Development of material system that exhibits galvanic and CTE compatibility with aluminum brake rotor.
- Development of finite element model to simulate heat dissipation with coated rotor solution.
- Successful encapsulated SiC tiles with titanium alloy with lean manufacturing.

Introduction:

The ability to strategically position material can lead to lighter, robust components. For example, a hard dense material in conjunction with a lighter material can enhance performance and weight reduction. A ductile material surrounding a hard material can improve impact resistance. While the applications might appear diverse, the common barrier to these multi-material systems boils down to the ability to hold them together. This joining technique and choice of materials then determine structural integrity and useful life of the component.

Conventional joining techniques rely on melting to fuse components together. Difference in melting points and formation of brittle intermetallic phases prevent it for use with dissimilar materials. The choice of materials also plays an important role. These govern corrosion potentials which can accelerate galvanic corrosion. Mismatch in coefficient of thermal expansion can also cause excessive stresses leading to premature component failure.

The focus of the presented report is to enable effective use of multi-material components to achieve weight reduction in military vehicles. This can increase mission lengths or payload. Optimization of two components; brake rotor discs and ballistic armor plates are addressed in this investigation.

Brake rotor discs: Coated aluminum brake rotor:

Brake rotors are a heavy unsprung vehicle mass that serves to act a heat sink to dissipate the kinetic energy of the vehicle in order to decelerate or stop. In addition the rotor surface provides stable friction across its operating regime. Weight reduction in rotors can increase mission lengths (via fuel efficiency) but also ride and maneuverability. Coated Aluminum brake rotors present a viable light weighting solution. The coating withstands the grunt braking action while the aluminum serves an efficient heat sink and keeps temperatures low. Key issue with this concept is the lack of feasible joining process and compatible material system. The present investigation will develop a potential coating material and deposition process to fabricate coated aluminum brake rotors.

Ballistic armor plates - Hexagonal Ti-6Al-4V enclosure for SiC encapsulation:

The objective of this project was to create lightweight armor plates by encapsulating Silicon carbide (SiC) tiles onto a hexagonal Ti6Al4V matrix. Light weighting increase the fuel efficiency of the military trucks and also the capability to increase the payload for combat missions. The critical requirements of the outer metal matrix as well the backing plate are lightweight, high strength and toughness, enhanced corrosion resistance which are critical requirements of an armor plate. Titanium has a high strength to weight ratio, excellent ballistic mass efficiency and is corrosion resistant making it a superior material for many combat systems and components. Good ballistic impact resistance and a high strength-to-weight ratio make titanium valuable material. In specific Ti6Al4V, the most popular Titanium alloy provides superior ballistic protection when compared to conventional rolled homogeneous armor (RHA) steel on a weight basis but is far less efficient on both weight and volume basis than the state of the art ceramic armor. Titanium and other metallic armors achieve defeat of hardened (armor piercing) ballistic threats primarily through energy absorption by plastic deformation and shear of the armor and by friction between the ballistic projectile and the armor plate. Ceramic armors achieve defeat by deformation and fracture of the projectile where the ceramic plates are broken. By combining a ceramic material like silicon carbide with Ti6Al4V to form a composite structure, we can combine the different failure modes and thereby produce an enhanced armor plate [1].

Ti6Al4V is an alpha- beta type alloy of Titanium with 6wt% Aluminum and 4wt% Vanadium. Aluminum is an alpha stabilizing element whereas vanadium is a beta stabilizing element thus forming an alpha-beta alloy. The presence of aluminum in the ti6al4v alloy improves the oxidation resistance of the alloy at higher temperatures whereas vanadium which is a beta stabilizer helps improve the fabric ability of the alloy.

Silicon carbide tiles cannot sustain successive impacts without quickly losing much of their protective value. To reduce these effects, the tiles are made as small as possible (30mm thick). These tiles need to be encased within a metal or metal composite matrix. Metal plates are usually machined leading to material wastage and then the tiles are isostatically pressed into the heated plates or glued with an epoxy resin. When the tiles are held under constant compression by their matrix it improves their resistance to kinetic penetrators which cannot be achieved by using glues [2]. This matrix needs to be backed by another plate which can reinforce the ceramic tiles from behind and to prevent deformation of the metal matrix by kinetic impact. Typically the back plates are poured in by casting onto the ceramic tiles leading to intermetallic formation between the tile and the plate and compromising the structural integrity of the whole armor plate. These plates absorb impact and extend the life of the composite inside the matrix.

Machining Ti6Al4V plates are difficult time consuming and very expensive process. Thermal stresses and impact of vibration on the cutting edge leads to tool failure while machining titanium and its alloys. Ti6Al4V block was machined to press fit the tiles as a part of one our schemes (Figure 1). Since the manufacturing route was tedious and the

plate was too heavy which contradicted our goal we decided to pursue the additive manufacturing route.

Approach:

Since FY09, the University of Michigan developed a novel Co-axial laser assisted supersonic sintering process (CLASS). This solid –state deposition technology overcomes the hurdles of multi-material joining process: - melting point, formation of intermetallics and thermal degradation. Akin to cold spray technology, powders of desired materials are accelerated to target area at supersonic velocities (see Figure 2). At these conditions, the powder undergoes adiabatic shear straining to create micro jets at the interface to create metallurgical bonds. A coaxial laser beam irradiates this foot print to relieve excessive stresses to prepare for next layer of deposition. The novelty of the process lies in the ability to switch the laser beam as primary deposition source. Here at significantly lower particle velocity; the process can create finer deposited features. The CLASS process was developed and applied through the course of the investigation.

Development of Coated Aluminum Alloy brake rotor:

Choice of aluminum alloy:

Unlike conventional grey cast iron rotors, the useful life of coated aluminum rotors is clearly limited by a coating thickness threshold. This is necessary to prevent localized hot spots and subsequent warping. Thus if designed conservatively, the potential weight saving drops from 50% down to mid-25. To maximize weight savings, U of M's first approach was to use high temperature strength Aluminum L12 alloys. Of these series of precipitation hardened alloys, hypereutectic Aluminum 398 alloy was selected due to availability of the material in casting foundry. The alloy has higher temperature strength than conventional aluminum alloys (Figure 4). The designed brake rotor and cast prototype prior to deposition are shown in Figures 5 and 6.

Coating material:

The Fe-Mn-Al system has been thoroughly investigated to replace conventional Ni-Cr based stainless steel and is considered as a potential coating material for brake rotor application [3]. The work hardening property of the Mn based ferrous alloy system results in plastic deformation under impact loading with abrasion or erosion. This mechanism obviates the possibility of brittle fracture and spalling [4].

Manganese is an austenite former and a cost effective replacement for Nickel. Disadvantages of manganese are the tendency to segregate forming beta manganese and its high affinity for oxygen at higher temperature [5]. This often results in the alloy with depleted Mn content. This alters the stacking fault energy leading to formation of martensitic phases which could be unwarranted and detrimental. Aluminum also helps

increase the SFE. Therefore it stabilizes the austenitic phase and prevents formation martensite phases. At higher levels of aluminum, the formation of a continuous passive layer has been shown [6, 7].

Silicon is known to reduce SFE and promotes Y to e transformation. Silicon is often added as it improves fluidity during casting and also increases strength by solid solution alloying.

Chromium Additions to Fe-Mn Alloys have been widely studied as means to improve the corrosion properties of this alloy [8,9]. Chromium also increases the yield strength or the flow stress thus enhancing wear property [8]. There is discrepancy on the effect of the stacking fault energy by Chromium. Some prove that it increases while the others prove otherwise.

Carbon and Nitrogen are two other important elements widely researched in Ni-free austenitic alloys. Both these elements have higher solubility in austenite matrix. The disadvantage of these interstitials is precipitation. The maximum amount of carbon that can be added was limited to 1.2% [9] Nitrogen up to .22wt% has shown to reduce work-hardenability [11]. Carbon has been shown to precipitate at 4500C [12].Carbon was however added as it affects the critical resolved shear stress which is necessary for twinning [9, 12].

Thus Fe-Mn-Al-Cr-C Alloy system forms a suitable framework for wear resistant alloy for a brake rotor application. The role of manganese will be to ensure the stability of austenitic phase at all temperatures and compensate for its affinity to oxidize. By Varying Aluminum and Chromium the galvanic potential of the alloy will be brought to match that of aluminum. The role of carbon will be to enhance twinning tendency. Its precipitation will result in strengthening of the alloy and lubrication preventing galling. High temperature wear tests will be conducted to ensure stable wear resistance at upper limits of typical braking surface temperature.

Hexagonal Ti-6Al-4V enclosure for SiC encapsulation:

To reduce the cost of the armor plate and eliminate machining and intermetallic formation, a new manufacturing route has been developed where the outer Ti6Al4V hexagonal walls are deposited onto a Ti6 base plate using the laser based Direct Metal Deposition (DMD) process (Figure 7). The tiles will be press fitted and locked in place so that the tiles don't get dislodged during the high velocities of the Cold Spray process. Ti6Al4V will be deposited on the top the tiles using the cold spray process to encase the tiles within the matrix thus consisting of top and bottom Ti6 backing plates with the tiles encased within.

The laser depositions have to be conducted inside an argon atmosphere due to the close affinity of titanium towards oxygen. Our setup could only deposit one Ti6 hexagonal wall, this lead to the fabrication of new rectangular chamber shown in Figure 8. The increase in bellow sleeves and larger chamber volume allowed for flexibility in

nozzle movement even under pressurized environment. The increase in chamber volume resulted in longer purge times but decreased oxygen ppm.

To ensure there is no oxidation in the Ti6Al4V wall deposits, the process gas flow was increased. Inert gas is blown through the nozzle, which helps both in powder delivery and shielding the deposits from oxidation. Shielding gas strategy is a delicate balance between powder delivery without causing excessive disturbance at the melt pool, but also adequate pressure to drive away the ambient air. Three hexagon tile Ti6Al4V wall structures were built for early conceptual proof.

The surface quality of the hexagonal wall was significant for tile encapsulation. Tighter deposition tolerances and cleaner finish was needed to get a nice press fit for the tiles as well reduce the gap between the tile and the hexagonal wall surface. The argon pressure varies at different locations inside the chamber during deposition and could cause powder disturbance during deposition depending upon the nozzle location. This would result in powder accumulation inside the hexagon which adheres to the hot wall surface as un-melted particles. To alleviate this issue an acrylic shroud was developed to curtain powder flow perturbation.

Silicon Carbide (SiC) Encapsulation by CLASS process:

Once the tiles were locked in place, Ti6Al4V powders were deposited using Laser Assisted Cold Spray process (LACS) onto SiC tiles. Bond tests were done on titanium substrates as machining the SiC tile proved cumbersome. Smaller powder particle deposited showed reduction in deposition porosity. The porosity in the deposits can be finally consolidated when the armor plates gets hipped.

The encapsulated tiles had an approximate 30micron gap between the tile and wall surface after press fit. Despite press fit tolerance of the SiC Tile with respect to the wall structure, there were unavoidable gaps. These emanate from the adherence of powder particles to the built structure during deposition. These gaps are too large for a cold-spray fill operation. The edges around the SiC tile and Ti6Al4V wall interface can be filled up successfully by orienting the nozzle geometry normal to the edge surface (Figure 9).

The edges which did not have permissible gaps were not filled in the middle. These gaps were filled up by laser cladding the Ti6 powder. The complete process schematic for armor plate fabrication is shown in Figure 12. This scheme was successfully tested on a single encapsulated tile structure which can be seen in Figures 10 and 11. Currently the three tile structures are being cold sprayed after which the tile wall interface gaps will be laser deposited. Then the armor plates will be hipped where encased powders can be consolidated to create fully dense materials. Hipping also improves the mechanical properties of these materials.

Results and Discussion:

Complexities with Al398 alloy casting:

The complex precipitation of the high temperature Al398 alloy resulted in difficulties during casting. There was unavoidable porosity on the outer edges of the castings. This is shown in Figure 13A. 13B shows an X ray of the casting showing poor density on the periphery of the casting due to shrinkage issues.

Alloy development for brake rotor coating material:

Corrosion studies:

The results of corrosion compatibility studies of the Fe-Mn alloy are shown in Figures 14 through 16. Various alloy compositions were developed to determine the most compatible materials to Aluminum alloys. Figure 14 shows the open circuit potential which indicates stable potential after long immersion periods in 0.5% NaCl solution. The potentio-dynamic (TAFEL) plot is presented in Figure 15. The Fe-Mn alloys show similar Ecorr and passivation characteristics with aluminum alloy. In order to quantify the galvanic current intensity, zero resistance ammetry was performed in with Fe-Mn alloys and stainless steel (316) with respect to aluminum alloys (Figure 16). The Fe-Mn alloys exhibited very low galvanic coupling unlike 316 alloy.

High temperature wear study:

Pin on disc wear tests were performed at elevated temperatures to quantify the effect oxidative wear on friction. The results shows stable coefficient at elevated temperatures (Figure 17). Cast Iron is also plotted for baseline comparison. Tests were done at 550deg C with a 6N load for 10000 cycles with an Alumina (Al203) counter body.

Coating fabrication:

The efficiency of the coaxial laser assisted deposition process (CLASS) over conventional cold spray process is shown in Figure 18. Dense deposits with higher coating thickness were obtained. Rigorous bond tests were performed on coated rotors (Figure 19). A fourfold increase in bond strength was observed with the CLASS process (Figure 18). Subsequently, deposition was carried out on actual rotor (Figure 20). The rotors are awaiting brake dynamometer tests according to FMVSS recommendations.

Thermal modeling:

Coating minimum thickness requirement through Modeling – FEA model was developed to identify the effect of coating thickness on temperature profile during braking.

The through thickness temperature is shown during a braking cycle and subsequent cool down period (Figure 21). The simulation is carried with using a 3000lb vehicle mass travelling at 60 miles per hour decelerated to 10 miles per hour in 2 seconds. The resulting thermal profile for a 1mm coating thickness is shown. For a peak temperature of 170° C attained on the braking surface, the coating-aluminum interface reaches around 140° C followed by immediate dissipation to 70° C.

Hexagonal Ti-6Al-4V enclosure for SiC encapsulation:

Three Ti6Al4V hexagonal walls were successfully deposited onto Ti6Al4V substrate using the DMD process (Figure 22). The deposited walls were clean and oxide free and did not require any additional machining. The sharp edges of the SiC tiles tend to chip off during encapsulation. The SiC tiles were machined on the edges to get a nice tight press fit into the walls. Near flat top surface was achieved by maintaining an optimum thermal cycle. The process efficiency (powder usage) had been doubled by increasing powder feed rate and subsequent laser power. Excess powder can be reclaimed and recycled for use eliminating wastage.

The complete process schematic for armor plate fabrication is shown in Figure 12. This scheme was successfully tested on a single encapsulated tile structure which can be seen in Figure 23.

Conclusions:

A tailored process and material system to manufacture coated brake rotors and encapsulate SiC tiles for ballistic armor was developed. A novel Fe-Mn alloy was developed with stable wear resistance at high temperature and galvanically compatible with proposed high temperature Al 398 alloy. A lean manufacturing route was optimized for encapsulating SiC tiles with minimized consumption of titanium alloy.

Moving forward, the next phase of the project is testing and evaluation. This will be used as feedback to optimize coating and wall thickness to improve heat dissipation and structural integrity on rotors and armor plate respectively. Additionally, the encapsulated Tile assembly can be HIP'ed (hot isostatic press) to increase structural integrity.

References:

- http://energy.ornl.gov/armor/materials/materials.cgi?nav=1
- Hauver, G.E., Netherwood, P.H., Benck, R.F. and Kecskes, L.J., 1994, "Enhanced Ballistic Performance of Ceramics", 19th Army Science Conference, Orlando, FL, June 20–24, 1994, p. 1633-1640
- H. H. Huang, T. H. Chuang, Materials Science and Engineering: A 2000, 292, 90.
- A. Ball, Wear 1983, 91, 201.
- Y. F. Gong, B. C. De Cooman, steel research international 2011.

- A. Grajcar, S. Ko+éodziej, W. Krukiewicz, Archives of Materials Science 2010, 78, 78.
- I. El-Mahallawi, R. Abdel-Karim, A. Naguib, Materials science and technology 2001, 17, 1385.
- A. S. Hamada, Acta Universitatis Ouluensis C 2007, 281, 1.
- O. Bouaziz, S. Allain, C. P. Scott, P. Cugy, D. Barbier, Current Opinion in Solid State and Materials Science 2011.
- L. Bracke, J. Penning, N. Akdut, Metallurgical and Materials Transactions A 2007, 38, 520.
- Y. N. Dastur, W. C. Leslie, Metallurgical and Materials Transactions A 1981, 12, 749.
- L. Remy, A. Pineau, Materials Science and Engineering 1977, 28, 99.

Presentations / Publications:

- V Varadaraajan, P Mohanty, Laser assisted cold spray process

Figures and Tables:

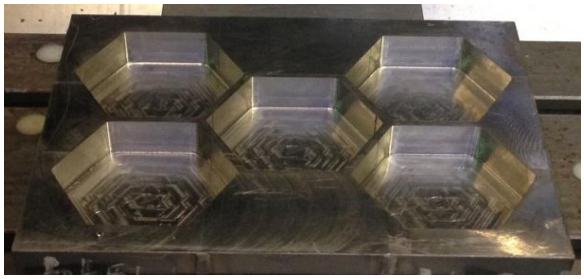

Figure 1. Machined Ti6Al4V block for press Fit of SiC tiles.

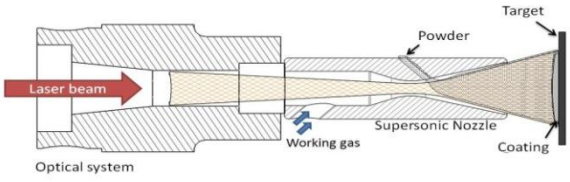

Figure 2. Schematic of the CLASS process.

Figure 3. CLASS nozzle prototype.

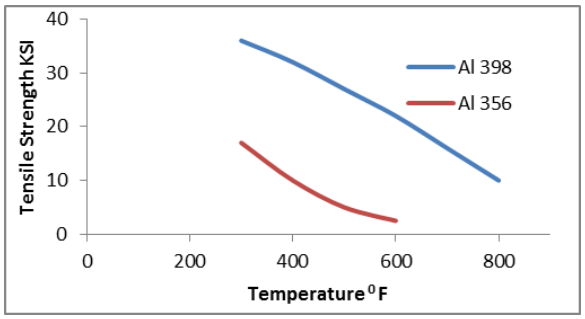

Figure 4. Elevated Temperature property Aluminum Alloys.

Figures Continued on Next Page

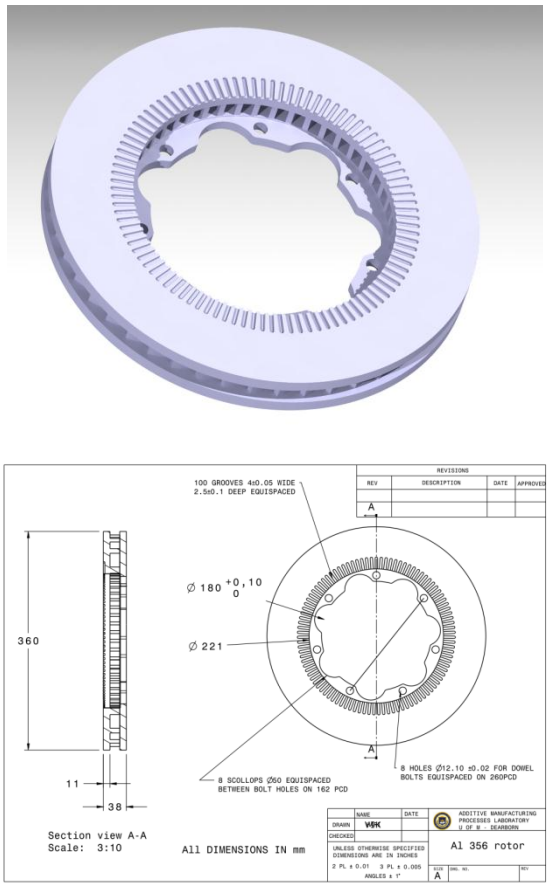

Figure 5. Brake rotor casting specification.

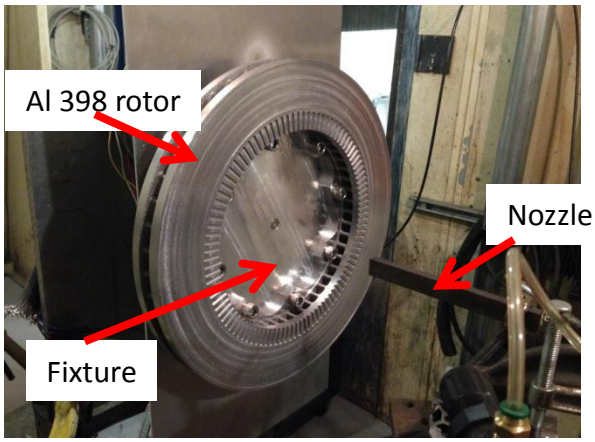

Figure 6. Al 398 rotor with fixture prior to coating deposition.

Figures Continued on Next Page

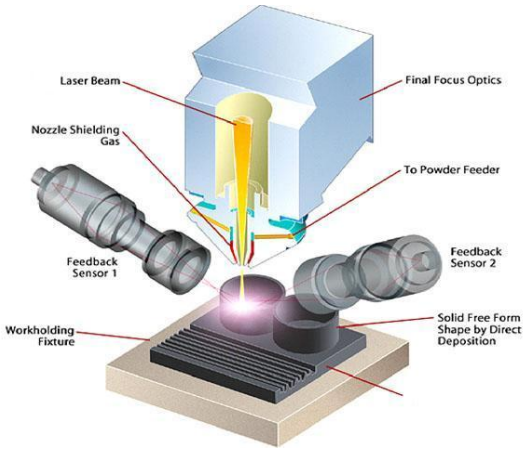

Figure 7. Laser Direct Metal Deposition (DMD) Process.

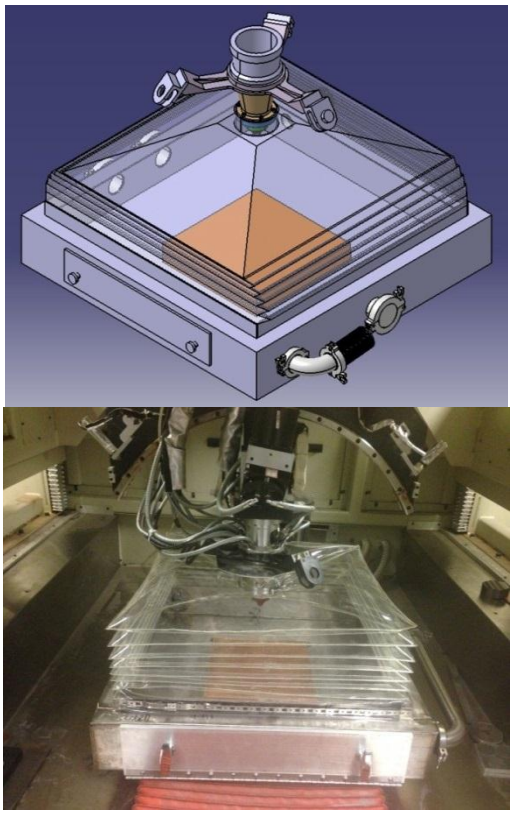

Figure 8. Schematic and fabricated Rectangular chamber setup for multiple tile deposition.

Figures Continued on Next Page

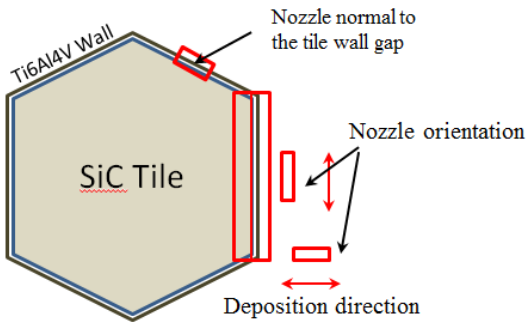

Figure 9. Cold Spray encapsulation scheme with SiC tiles.

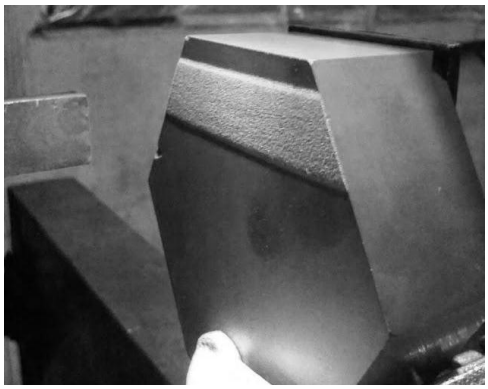

Figure 10. Ti6Al4V cold sprayed onto SiC tile.

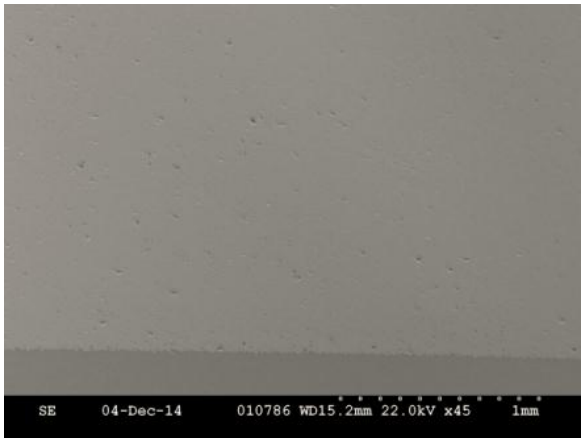

Figure 11. Ti6Al4V (light area on top) cold Sprayed onto Ti substrate (dark grey area on bottom).

Figure 12. Optimized lean manufacturing route to encapsulate SiC tiles using Ti6Al4V alloy.

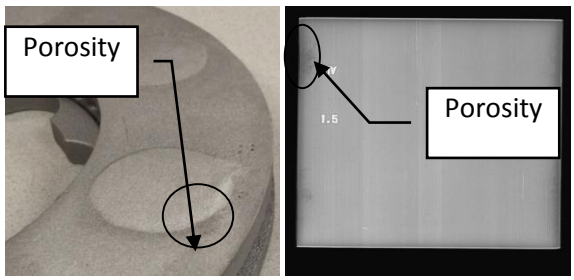

Figure 13. (A) Porosity defect in the casting (B) x-ray of the casting revealing defects.

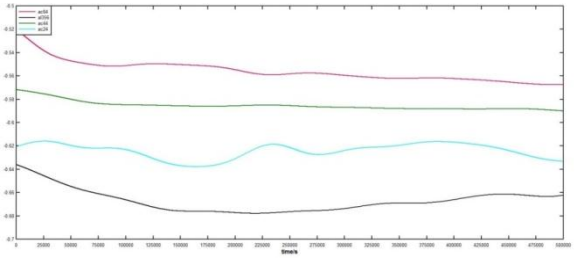

Figure 14. : Electrochemical testing of Fe-Mn-Al-Cr-C alloy in NaCl solution: Open circuit potential vs time.

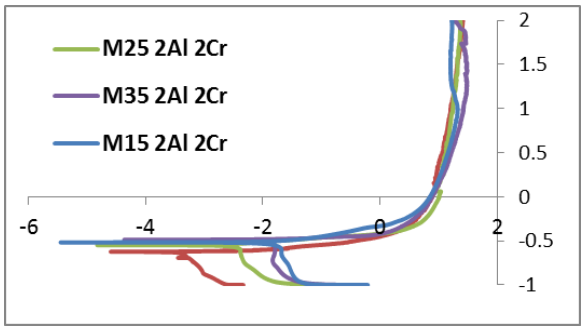

Figure 15. : Electrochemical testing of Fe-Mn-Al-Cr-C alloy in NaCl solution: Potentiodynamic plot.

Figures Continued on Next Page

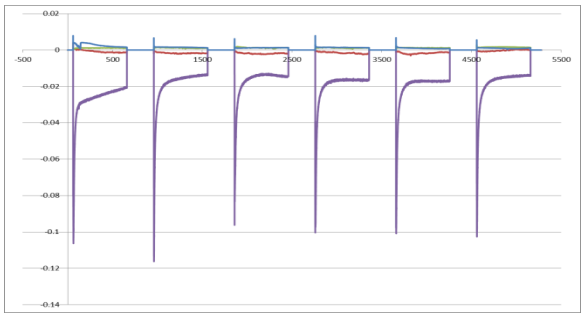

Figure 16. : Electrochemical testing of Fe-Mn-Al-Cr-C alloy in NaCl solution: Zero resistance ammetry to study Galvanic current intensity.

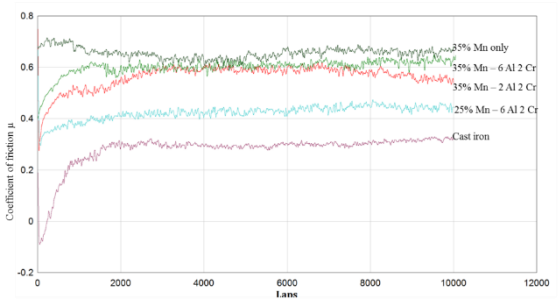

Figure 17. Coefficient of friction at elevated temperatures.

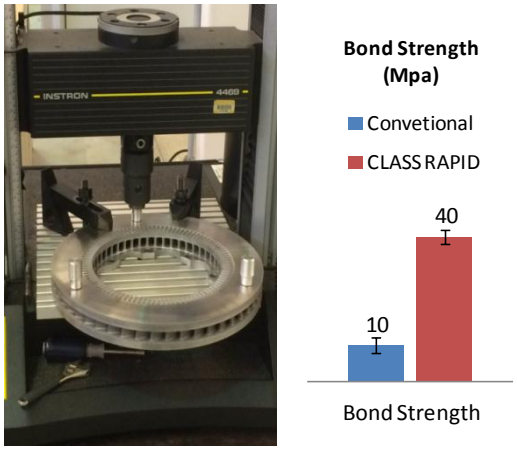

Figure 18. Bond pull test in progress and results.

Figures Continued on Next Page

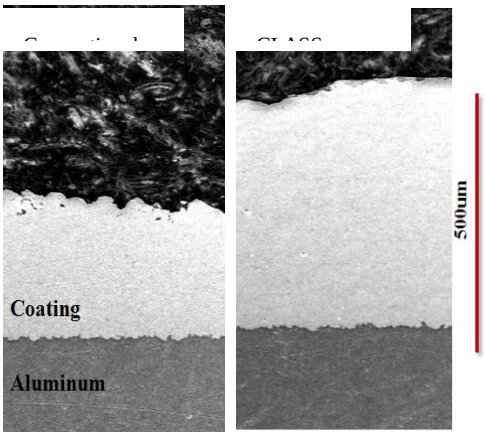

Figure 19. Cross-section of Fe-Mn coating on aluminum with conventional cold spray and CLASS Process.

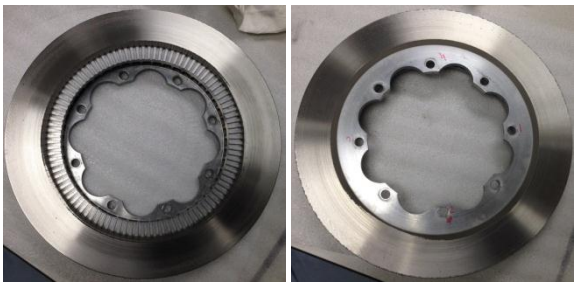

Figure 20. Successful deposition onto full size Al 398 Marauder brake rotor (Left: front; Right: back).

Figures Continued on Next Page

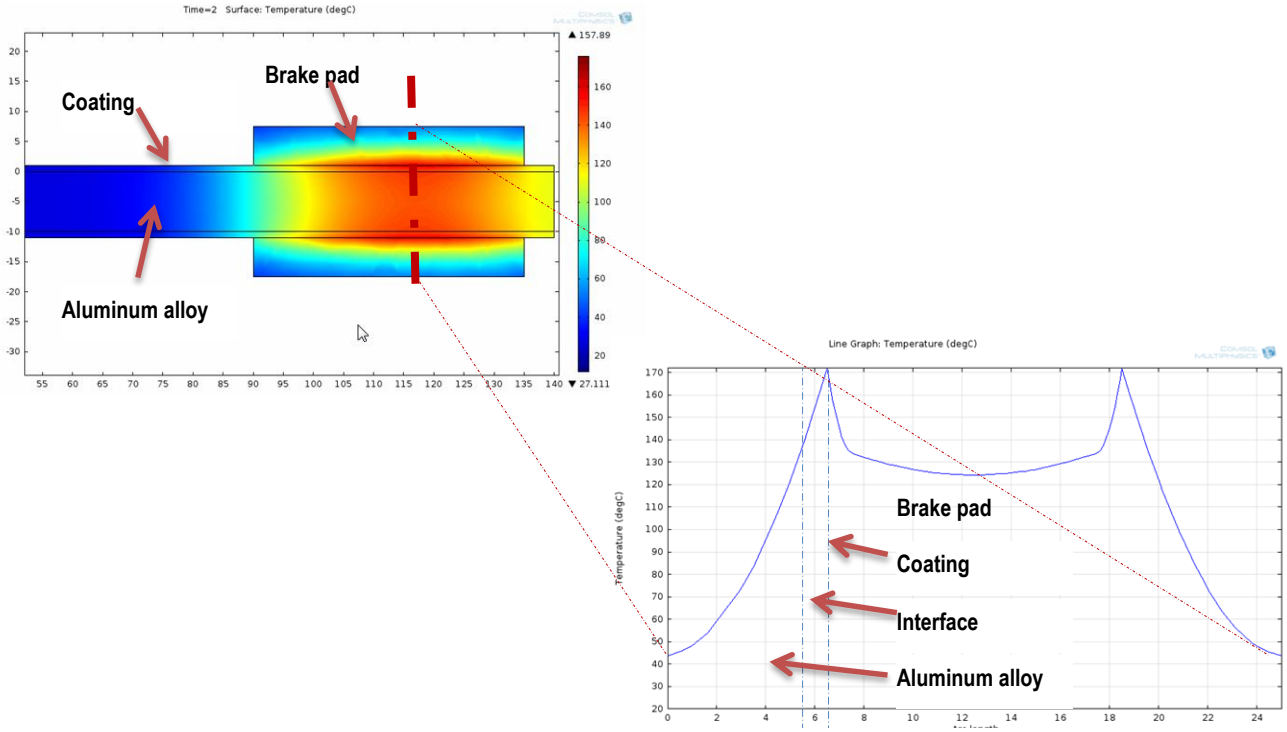

Figure 21: Thermal profile of brake rotor surface during braking.

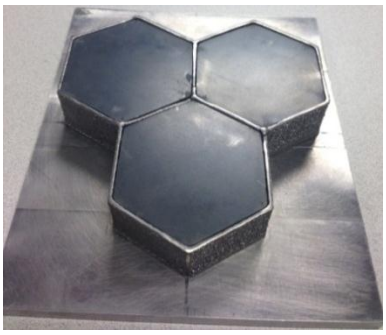

Figure 22. SiC encapsulation onto three Ti6Al4V laser deposited walls.

Figures Continue on Next Page

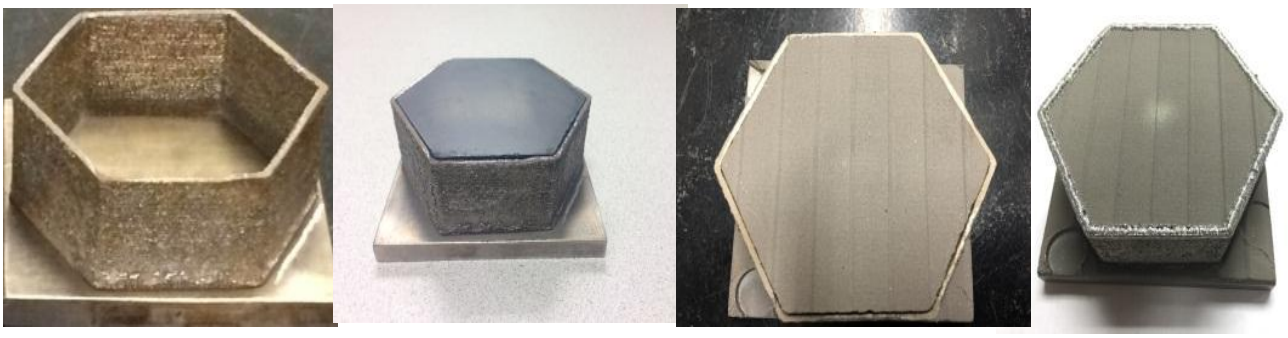

Figure 23: Processing sequence to encapsulate a SiC tile with Titanium (Ti6Al4V) alloy.

AVPTA Technology Focus Area 2: Lightweight Structures & Materials

Multi-Material Joining (MMJ) – Bi-Metal Gunner Rotor Casting

DOE-VTO TFA Lead: Patrick Davis
DOE-VTO Project Lead: William Joost
TARDEC TFA Lead: Dr. Richard Gerth

Principal Investigator:
Adam Loukus

w/ Luke Luskin
REL, Inc.
57640 North 11th Street
Calumet, MI 49913
Phone: (906) 337-3018
E-mail adam@relinc.net

w/ Benjamin Eichhorn
Technology Planning
US Army TARDEC

Start: January 2014
Projected Completion: December 2014

Objectives:

- Develop procedures & techniques to join dissimilar materials utilizing the high pressure squeeze casting process.
- Minimize cost and optimize performance of bimetal cast components.
- Demonstrate bimetal casting technology by manufacturing a light weight cast gunner rotor with bimetal armor inserts.

Strategic Context:

- The bi-metal cast rotor has the same performance at a reduced weight compared to the rotor currently used in the Light Armored Vehicle – 25 (LAV-25) which is the carrier vehicle for the AVPTA Light Weight Vehicle Structures project.
- The project directly supports the TARDEC Strategy by enabling lighter weight rotor availability for legacy and future Program of Record (POR) vehicles.
- Bi-metallic casting is a commercial process.

- Reducing rotor weight is a major area of interest for military and commercial vehicles. Determining the best material for optimal performance, cost and weight is an area of mutual technical interest and ongoing research.

Accomplishments:

- Developed tooling and process plan to cast complex gunner rotor geometry in a high pressure permanent mold casting machine.
- Successfully cast initial prototypes with steel armor inserts in aluminum 206 alloy.

Introduction:

REL has investigated composite insert castings for several years in applications related to armor development. Ceramic inserts were primarily used in armor applications to defeat hard projectile threats but the technology can also be applied to multi-metallic castings. As follow on work REL received SBIR PHIII funding to develop tooling and techniques for casting bi-metal squeeze castings for structural vehicle applications. As a demonstration component, the LAV-25 (Figure 1) gunner rotor assembly was chosen to showcase the technology. This particular component has critical structural demands from vehicle dynamic loading and main artillery recoil loads. The gunner rotor also requires ballistic penetration resistance in specific areas.

Approach:

A multi stage approach was used to develop the bimetal gunner rotor demonstrator. The key development stages are as follows:

- Define geometry and specific locations that require ballistic reinforcement inserts.
- Manufacture and test small coupon samples of the bimetal joint to ensure proper interlock is obtained.
- Complete FEA of rotor design for recoil impulse load and vehicle G loading.
- Design mold tooling and casting process plan for squeeze casting gunner rotor.
- Manufacture molds and support tooling for casting rotor in REL's UBE 900 squeeze casting press.
- Cast initial rotors in aluminum 206 or 356 alloy with mild steel inserts to prove out casting process.
- Cast 3 final rotors with armor inserts.
- Weld and machine to finished geometry
- Test finished rotor for structural load capacity.
- Evaluate options for casting magnesium/steel bimetal gunner rotor.

Results and Discussion:

Design:

The gunner rotor design utilizes the same exterior shape as the steel production version. The walls are increased from .375" to .75" thick towards the interior of the rotor. Four steel armor panel inserts are cast in place to guard shot lines during weapon elevation travel (see Figure 2). The weight of the proposed bimetal design is approximately 71 pounds, or 23% lighter than the steel production version.

Coupon Testing:

Scaled versions of the proposed bimetal joint scheme were designed and cast for evaluation. The samples were pulled in a quasi-static test machine to determine the specific pull-out strength of three different joint variants.

Coupon Types:

- 46100 Steel with cross holes.
- NRX modified mild steel with cross holes.
- NRX modified mild steel without cross holes.

A test sample schematic is shown as Figure 3. Tensile test results are contained within Figures 4 through 6.

The NRX steel samples with cross holes exhibited the highest strength. However, the samples with cross holes only were a close second at 8.25 kip/inch average strength. The NRX modification was relatively costly and the group A joint design was sufficient for the application so it was selected going forward.

Analysis:

Analysis was completed on the gunner rotor for the critical load cases identified in the customer supplied load case and criteria document. No major issues with stress or deflection criteria were identified. The overall stresses in the part were quite low with respect to yield. Some assumptions had to be made on the interfaces between the gun and mounting flanges due to lack of CAD data and information. REL used best judgment for these boundary conditions.

The overall stiffness at these locations was probably exaggerated to some degree. However, due to the low overall stresses and lack of data it was deemed acceptable for the purposes of this study.

Assumptions:

- Rotor is constrained rigidly at end cap mounting flanges.
- Gun mount adds stiffness to rotor gun mount flange. Stiffness is equivalent to .5" steel plate.
- Optics tube will be stiffened by optics housing when installed. Stiffness prevents optics tube from distorting out of round
- Gun center of gravity is approximately 28 inches forward of the rotor gun mount flange.

Load Case: Vertical Acceleration 4G:

- Type: Linear Static
- Stress Criteria: Factor of Safety >= 1.5 wrt Yield
- Deflection Criteria: Upper Rear Corner <= .09 in, Lower Rear Corner <= .09 in.

This load case was considered significant due to the weight and bending moment associated with the M242 Cannon hanging off the front of the rotor with a 4G acceleration. The other acceleration load cases were smaller in magnitude and the other directions did not induce any specific stress magnifications. Overall the stresses seen (Figure 7) in the 4G load case were quite low.

- Peak Stress: 38 MPa = 5.51 ksi
- Safety Factor > 4.3
- Peak Deflection .05mm = .002in

Load Case: Main Armament Firing (9000 lbf Recoil @3.333hz 3 Shot Series):

- Type: Linear Transient
- Stress Criteria: Factor of Safety >= 1.5 wrt Yield
- Deflection Criteria: None

The recoil load case resulted in low overall stress. Although the recoil load is substantial the duration is relatively short. The load is assumed to be transferred to the gun mount flange via a .5" thick steel plate flange bolted to the 4 mount holes. This plate distributes the load and acts to stiffen the rotor. The walls of the REL cast gunner rotor are quite thick at .75in. This tends to stiffen the overall structure and appears to support the recoil load very well. The 3 shot group resulted in similar stress because loading is fully elastic and the rotor recovers completely between each shot.

- Peak Stress: 31 MPa = 4.5 ksi
- Safety Factor > 5.3

Molds & Tooling:

REL developed a mold design (Figures 9 through 11) to cast the gunner rotor in a high pressure squeeze casting process. Due to the complex geometry involved the die consists of 10 precision surface machined inserts that interlock to form a complete mold assembly. The die parts have been successfully machined and fit up accurately.

Casting Trials:

Initial casting trials have begun with aluminum 206 alloy and mild steel inserts. Some issues with complete die pressurization and shrinkage cracking have been identified. Complete die filling was achieved and inserts were completely encapsulated. Overall the first two castings (Figures 12 and 13) look very promising. REL is setting up to run more casting trials with some sight die modifications to improve metal flow and pressurization. Some trials in 356 alloy will also be run to determine the sensitivity to alloy selection.

Conclusions:

Successful bimetal gunner rotor castings have been manufactured at the initial prototype stage. Some issues such as shrinkage cracking and improved metal flow/pressurization are being solved. The next steps will be to complete a high integrity casting and complete final welding and machining to create a finished part. The finished components will be ready for testing on a load frame and for vehicle fit-up.

Figures and Tables:

Figure 1: Gunner Rotor attaches M242 25mm Cannon to the LAV-25 turret.

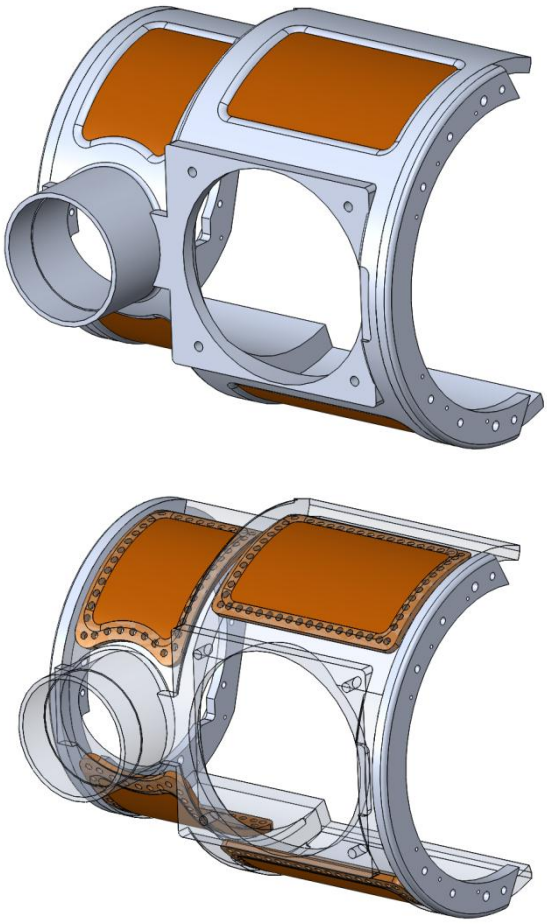

Figure 2: REL Bimetal Rotor Design with Steel Inserts.

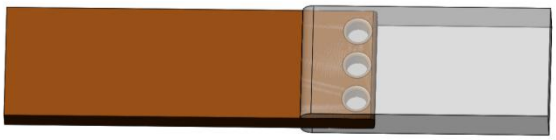

Figure 3: Coupon Joint Design.

Figures Continue on Next Page

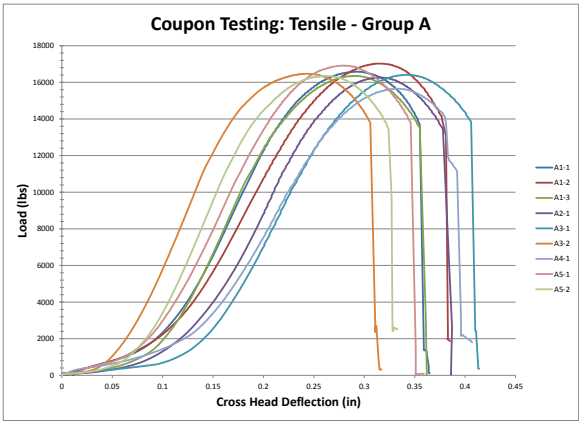

Figure 4: Tensile results of the armor steel samples with cross holes.

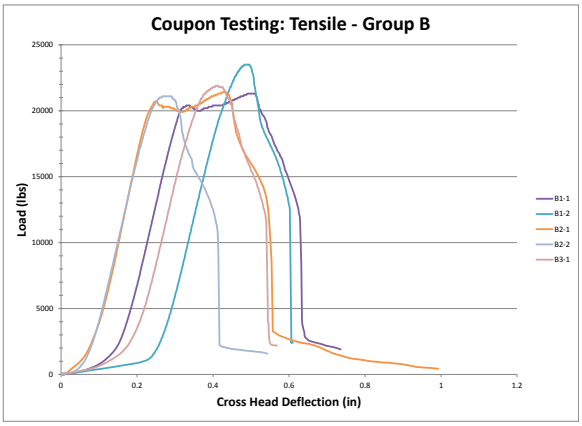

Figure 5: Tensile Results with NRX and Cross Holes.

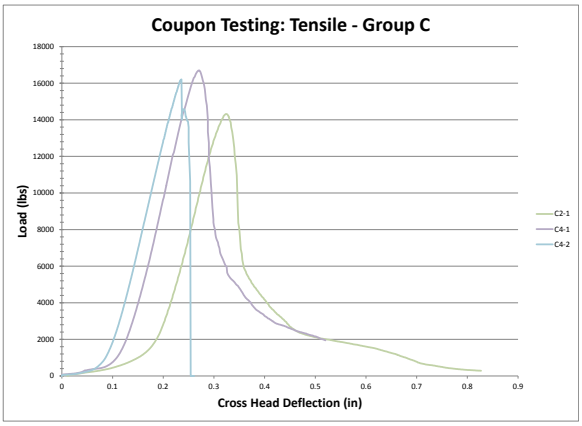

Figure 6: Tensile Results with NRX, No Cross Holes.

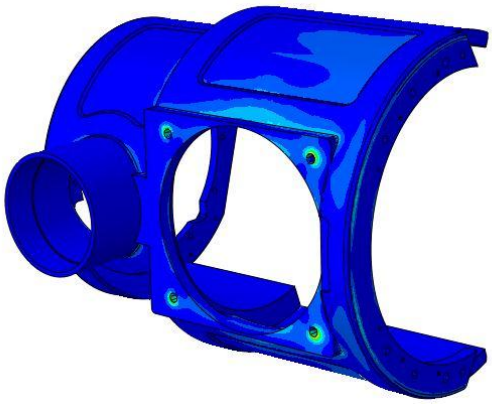

Figure 7: 4G Stress Distribution.

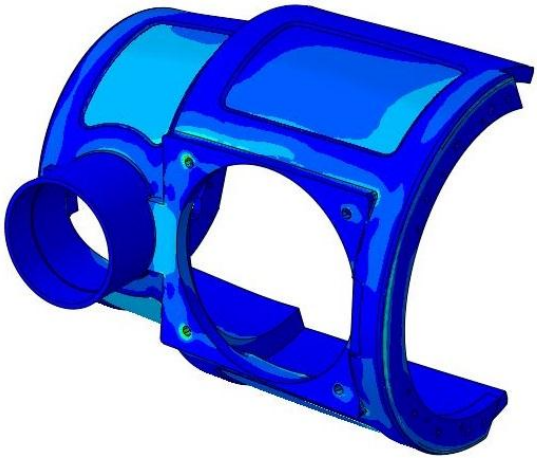

Figure 8: Recoil Load Case Stress Distribution.

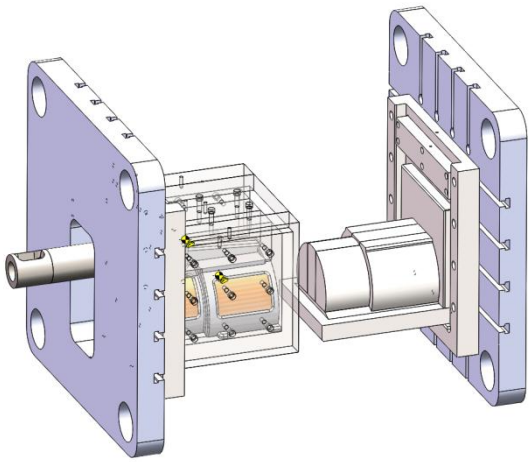

Figure 9: Gunner Rotor Die Design Schematic.

Figure 10: Inner rotor die assembly.

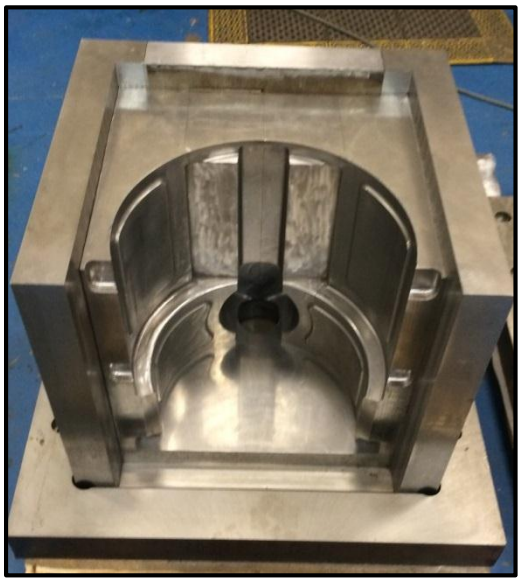

Figure 11: Outer rotor die assembly.

This Page Intentionally Blank

AVPTA Technology Focus Area 2: Lightweight Structures & Materials

Multi-Material Joining (MMJ) – Mechanical Composite Joint Failure

DOE-VTO TFA Lead: Patrick Davis
DOE-VTO Project Lead: William Joost
TARDEC TFA Lead: Dr. Richard Gerth

Principal Investigator:
Riley Woodham

Seemann Composites
12481 Glascock Drive
Gulfport, MS 39503
Phone: (228) 314-8000
E-mail:
rwoodham@seemanncomposites.com

Sub-Contractor
Material Science Corporation
Ted Campbell
135 Rock Road
Horsham, PA 19044
Phone: (215) 542-8400
E-mail: Campbell@materials-sciences.com

w/ Bernard Sia
Bridging Team
US Army TARDEC

Start: FY11
Projected Completion: FY14

Objectives:

- Assess how an applied load is distributed between a metallic (17-4PH stainless steel) component and intermediate modulus fiber reinforced composite component joined by a series of bolts.
- Determine the effect of bolt hole size and bolt hole pattern on the performance of a composite component bolted to a metallic component.
- Determine the potential failure modes for joints comprised of a composite component bolted to a metallic component.

Strategic Context:

- The project directly supports development of the Composite Joint Assault Bridge as a replacement for the Armored Vehicle Launched Bridge on the Joint Assault Bridge (JAB) program. The technology developed within the project will be applied to the JAB mid-span joint.
- Information developed during this project may be applied where stainless steel is bolted to an intermediate modulus carbon fiber composite. Information includes but is not limited to: design specifications for successful joint configurations, and identification of potential failure modes resulting from joint configurations.
- The project supports the TARDEC Strategy by introducing advanced materials into the JAB Program of Record (POR), and providing longer span capability and load capacity than the incumbent bridge design.
- Follow-on work includes: continuing development of the joint design; specifically bolt bearing and by-pass tensile load testing, combined compression and shear load testing, fatigue testing and corrosion testing; development of the Composite Joint Assault Bridge design; and full-scale bridge treadway testing.

Accomplishments:

- Two tensile bolt-bearing and by-pass tests were carried out in FY14, with the specimen failing at 243% and 156% of the design load, respectively.
- The test demonstrated that bolt size affects the joint's ability to successfully meet the targeted load level, but does not affect how load is transferred between the metallic and composite component.
- Finite element models run prior to both tests agree well with the actual test results, validating the assumptions made in developing the model.

Introduction:

The Composite Joint Assault Bridge (CJAB) is a composite bridge being designed for use on the Joint Assault Bridge system. One of its design elements is a mid-span joint consisting of a stainless steel hinge bolted to an intermediate modulus carbon fiber composite tension rail. The bridge's mid-span sees the highest amount of load during bridge crossing, making it the most critical component of the structure and a candidate for risk reduction. Unknowns exist with respect to how load is actually distributed between the metal and composite when connected using bolts, as well as the failure modes which may result. To resolve these unknowns, a test program was started to assess the behavior of joints comprised of intermediate modulus carbon fiber composite components bolted to stainless steel components.

Approach:

In lieu of building a full scale structure, it was decided to exercise the critical behavior of the joint through component testing utilizing associated fixtures. Figures 1 and 2 show the test article design and its derivation from the full Composite Joint Assault Bridge

design. The test article consists of a stainless steel hinge fitting bolted to an intermediate modulus carbon fiber composite tension rail. These components are then placed into a steel box used to approximate the joint's boundary conditions in the overall bridge structure. Based off of the results of Test 1 in April 2013, a simulated bulkhead was added to the steel box in October 2013 to provide additional resistance to vertical loads. Figure 3 shows the test specimen inside of the test box with the simulated bulkhead installed.

A finite element model was run prior to each test to simulate the results. To run the model, assumptions were made with respect to the following aspects of the specimen:

- Fit of the tension rail in the slotted fitting and associated friction
- Fit of bolts in normal prep holes and minimal torque
- Fit of pins in multi-lug hole and associated friction
- Geometric variations within practical tolerances
- Clearance of side walls away from the box structure and of assembled test specimen from steel box bottom plate/ rails (areas where bearing on steel is possible)
- Clamp up forces at minimum torque.

Displacements were also imposed to the test frame interfaces to run the model.

Figure 4 shows the full test specimen placed onto a 3000-kip Southwark-Emery universal testing machine at the University of Illinois Urbana-Champaign's Talbot Laboratory. The steel box attached to the testing machine through the use of a pair of loading tangs and a link adapter which were originally designed for the Advanced Modular Composite Bridge program, a previously completed program performed by Seemann Composites.

The test machine applies an axial tension load to the test article, and the test box reacts this load to the test specimen through a double shear, bolted connection. Within the test box, the test specimen is oriented at an angle of approximately 4 degrees with respect to the pull load to more accurately simulate the loads seen in the full bridge. This orientation also introduces an out-of-plane load to the specimen.

Each test consisted of seven test runs performed at the following load levels:

- Run 1: Up to 70 kips for System Checkout
- Run 2: 50% design load (175 kips)
- Run 3: 100% design load (350 kips)
- Run 4: 150% design load
- Run 5: 180% design load
- Run 6: 200% design load

- Run 7: Load specimen to failure

Visual inspections of the specimen were performed after each run. Cracking and other audible events were also listened for throughout testing. Strain, load and displacement were measured and recorded for each test.

Results and Discussion:

The first test performed in FY14 occurred in October 2013. The test specimen successfully completed Runs 1-6 without any audible or visible signs of damage. At Run 7, the specimen experienced net section failure at a load of 849 kips, or 243% of the design load. Failure occurred at the first row of bolts attaching the specimen to the test box and was caused by the detachment of fiberglass tabbing reinforcing the tension rail. This caused the bypass tension stress to exceed the material's tension allowable, resulting in fiber failure with no load redistribution path. This failure propagated as net section failure, and also caused the hinge fitting to collide with the text box and bulkhead, resulting in additional damage, including bolt shear failure.

The following conclusions were made from review of the strain gage data:

- Average axial strain mid-length in the composite tension rail was comparable to the prediction. Some strain jumps were seen in a few gages (see Figure 5), which may indicate seating of the bolted joints or the start of delamination of the fiberglass tabbing.
- Strain readings at the upper and lower edges of the lugs of the hinge fitting were very non-linear, due to the change of the bearing load and area as the pin seats (see Figure 6). Side-to-side symmetry of the strain readings had been predicted.

- Behavior at weak points of the steel hinge, as determined from von Mises stresses in the model, indicated yielding and non-linear strain response at the load corresponding to the material allowable. This was as predicted.

A uniform change in strain from one gage to the next was observed in the set of gages positioned between the bolts along the length of the steel fitting (see Figure 7). This confirms the uniform unload of the steel into the composite and proves that the joint behaved as intended per its design.

Post-test inspection of the specimen revealed the following:

- Net section yielding of the steel hinge at a section through the first row of bolts.
- Elongation in the first row of bolts. The deformation seen was that of a propped hole in bending, not a tear-drop shape indicative of bearing yield.

- Some bearing damage in the composite, near the region of the hinge fitting, which appeared to be uniform over the bolt pattern.
- The 0.5 inch diameter end bolts experienced some bending and shear yielding.

Each observation agreed well with the simulation performed prior to the test. Inter-laminar shear and tension damage was also found in the composite near the site of net tension failure. The end bulkhead also experienced yielding damage and bolt failure.

The second test, performed in September 2014, looked to verify the results of the first test performed in FY14. Prior to this test, the following changes were made to the test specimen:

- Bolt size at the composite-to-hinge fitting was changed from ½" to 5/8" diameter.
- A different taper region was used for the fiberglass tabbing.
- Washer/ head orientation for the bolts securing the end bulkhead was changed.

The test box from the October 2013 test was reused for this test. The test specimen completed Runs 1-4 with no visible or audible signs of damage. At Run 5, an attachment to the fixture failed at 156% design load, resulting in the occurrence of net section failure at the first row of bolts attaching the specimen to the steel box. Similar to the October 2013 test, the failure appeared to be caused by the detachment of fiberglass tabbing used to reinforce the tension rail laminate. Significant amount of damage was also observed in the curved edges of the composite at the occurrence of the second audible sound. Review of strain gage data indicated the following:

- Similar to the October 2013 test, some strain jumps were observed in the gages used to measure axial strain mid-length in the composite tension rail, indicating seating of the bolted joints or delamination of the fiberglass tabbing.
- Non-linear strain readings at the steel bulkhead, as illustrated in Figure 8.
- No indication of yielding at the weak points of the steel hinge. The response does appear to trend toward small volume yielding beginning at 600 kips (see Figure 9). Strains in these areas also appeared to be higher than that predicted by simulation and seen in the October 2013 test.
- Uniform change in strain from one gage to the next was observed in the set of gages positioned between bolts along the length of the steel fitting, similar to that observed in the October 2013 test.
- Indication of asymmetry at start up, based on the response of gages placed on the fitting positioned on the inner mold line side between the last 2 bolts on the left and right side, shown in Figure 10. Equal side-to-side tension was then observed at higher loads. This suggested that the composite tension rail experienced a combination of twist and in-plane bending.
- Highly non-linear response exhibited by the lugs of the hinge fitting, similar to that seen in the October 2013 test.

Post-test examination found no permanent deformation of the metallic hinge, hinge fasteners, hinge fastener holes, and composite tension rail fastener holes. Mid-thickness delamination was found, through ultrasonic testing, in the hinge area of the composite. This failure grew from a corner and extended into the bolted region.

Comparisons were made with results from the October 2013 test. Figure 11 shows that the strains on the upper side of the tension rail were lower in the September 2014 test (labeled Round 3) than in the October 2013 test (labeled Round 2). This indicates the application of a different bending load, for the same axial component, in the section. Reasons for this include: 1) less clamp-up of the tabbed specimen to steel based on thickness and/or bolt torque, 2) different and/or higher normal bending due to fit/ alignment, 3) twisting of the specimen incurring torque in the flat section due to fit/ alignment, 4) progressive debonding of the tabbing under lower loads. Figures 12 and 13 show that strain measurements on the outer and inner mold line sides of the hinge were similar for the two tests. This suggests that the change in bolt size from ½" to 5/8" diameter did not change how load is transferred to the composite tension rail.

Conclusions:

Based off of the results of testing performed in FY 14, the following conclusions were made:

- The joint generally exhibited similar behavior during both tests, and the viability of this multi-material joint has been demonstrated.
- Designing a test specimen/ fixture to fully replicate the boundary and loading conditions of a joint in a complex structure is a challenge.
- A compression capable end bulkhead is a requirement for structural integrity of this joint.
- The steel hinge/ composite bolted joint appear to be more bearing critical. This is preferred to the occurrence of bolt shear failure.
- Bypass stress concentration adjacent to bolts in the hinge fitting did not incur ultimate failure.
- Bolt size does not alter how load is transferred between a metallic component and composite component, but affects a joint's overall ability to meet a targeted load level.
- Modeling and simulation of the test agreed well with actual test results, validating the assumptions made in the creation of the model.

Future work for this project will include the following:

- Explore design changes to the composite rail to address the delamination found after the October 2014 test.

- Modify the test box and interface between the test specimen and test box to eliminate specimen pull out.
- Perform a fourth bolt bearing and by-pass test.
- Integrate a newly designed compression bulkhead.

Perform fatigue testing, combined load (compression + shear) testing, and corrosion testing to facilitate future development of the joint.

Figures and Tables:

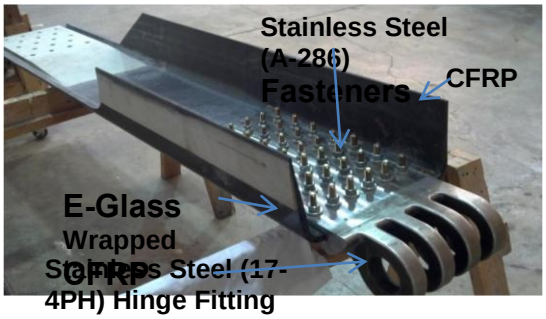

Figure 1: Joint Test Specimen.

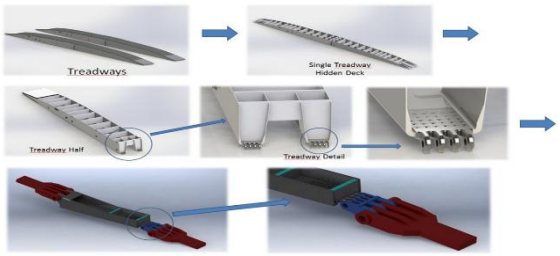

Figure 2: Derivation of Test Specimen from Bridge Design.

Figure 3: Joint Test Specimen within Steel Box.

Figure 4: Test Specimen Installed In Test Machine

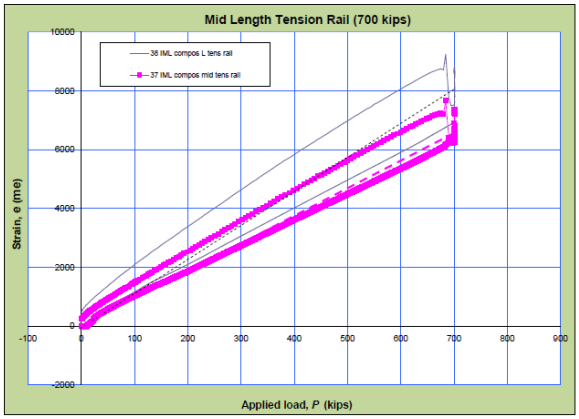

Figure 5: Jumps in Strain vs Load Plot May Indicate Bolted Joint Seating or Fiberglass Delamination.

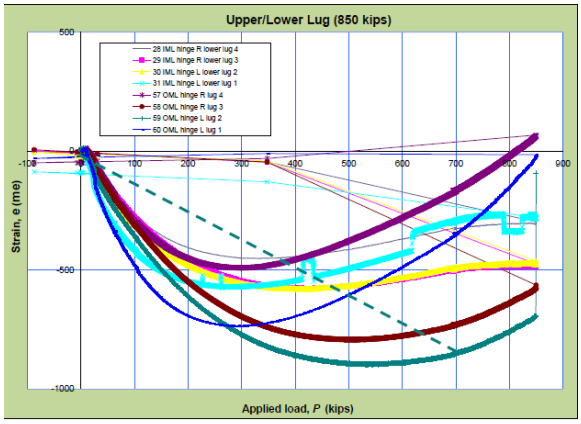

Figure 6: Non-Linear Strain Behavior Observed in Hinge Fitting Lugs.

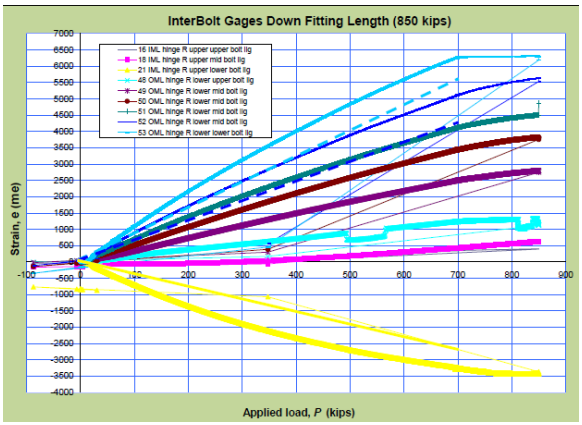

Figure 7: Uniform Change in Strain between Strain Gages along Length of Steel Fitting Observed.

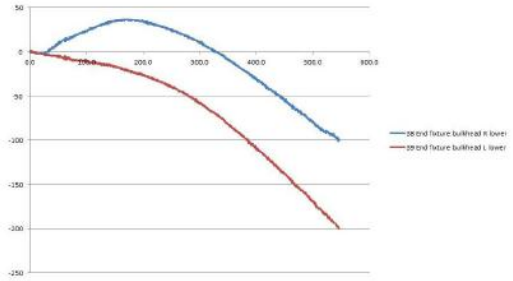

Figure 8: Strain Response at End Bulkhead.

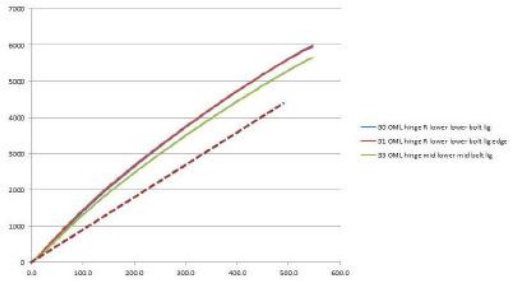

Figure 9: Strain Response at Steel Hinge Weak Areas.

Figures Continued on Next Page

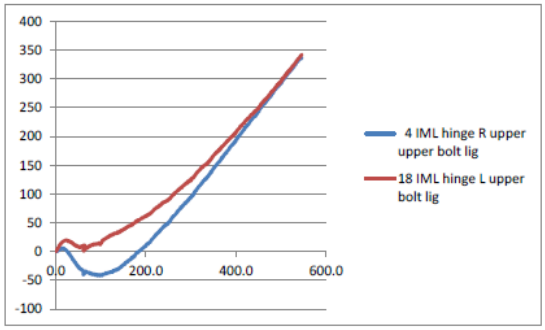

Figure 10: Response on Left/ Right Gages on Fitting Indicates Twist and In-Plane Bending of Composite Rail.

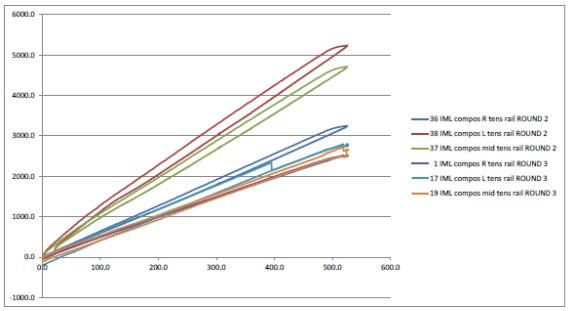

Figure 11: Tension Rail Gage Comparison.

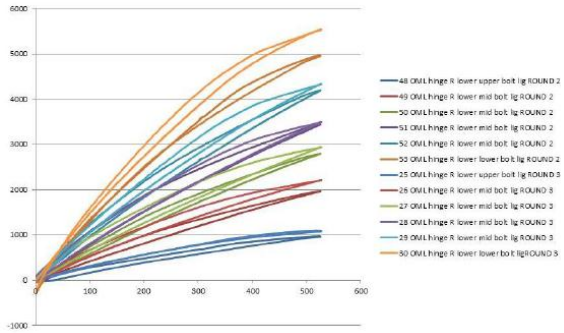

Figure 12: Fitting OML Gage Data Indicates No Change in Load Transfer due to Increased Bolt Size.

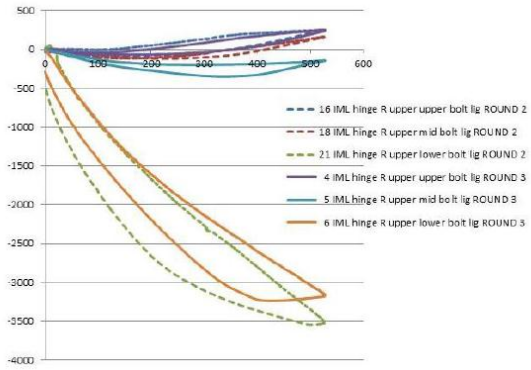

Figure 13: Fitting IML Gage Data Indicates No Change in Load Transfer due to increased Bolt Size.

AVPTA Technology Focus Area 2: Lightweight Structures & Materials

Breakthrough Techniques for Dissimilar Material Joining - Overview

DOE-VTO TFA Lead: William Joost
TARDEC TFA Lead: Dr. Richard Gerth

Principal Investigator
Richard Gerth, Ph.D.

Ground Systems Survivability
US Army TARDEC

Start: October 2013
Projected Completion: On-going

Objective:

- To establish new techniques for producing dissimilar material joints in vehicle structures.

Strategic Context:

- These are investigations into Technology Readiness Level (TRL) 2 & 3 technologies for which the performance and scalable applicability are unknown.
- The technologies directionally support the TARDEC Strategy because they are both early TRL and because they focus on dissimilar material joining that enables multiple benefits to future Programs of Record (PORs).
- Depending upon the success of the projects, they may create new technology investment areas increasing performance (e.g., higher strength joints), reducing cost and / or applicability to other materials and joint designs.
- Follow-on direction / opportunities will be based upon project success.

Accomplishments:

- See individual project descriptions

Introduction:

The lightest weight structure is the one that utilizes the lightest and most cost effective material that meets the engineering design requirements, i.e., a multi-material vehicle structure. Several workshops and studies [1, 2] have documented that one of the greatest barriers to the multi-material vehicle is the lack of effective joining technologies for dissimilar materials. While there are various cost effective materials, the technology to physically join them while meeting production and engineering requirements has been lacking.

Approach:

The five breakthrough techniques (and their performers) are:

- Collision Welding of Dissimilar Materials (Ohio State University) – develop a process that applies current to a suitable metallic foil (e.g. aluminum) and vaporizes the foil to create a rapidly expanding plasma gas. The expanding gas moves one material with rapid force to explosively bond with the dissimilar mating material.
- Advanced carbon fiber to aluminum joining (Oak Ridge National Laboratory) – Develop rapid process to use a laser to burn a surface pattern into carbon fiber composite parts to increase adhesion to aluminum components.
- Active, Tailorable Adhesives for Dissimilar Material Bonding, Repair and Assembly (Michigan State University) – Development of a nano-platelet doped adhesive that can be cured (assembly) and “uncured” (disassembly) using magnetic fields.
- Upset Protrusion Joining Techniques (Chrysler Corporation) – develop a fast and economical process to “squash” cast protrusions from a precision casting that can fit through holes in a composite (or other dissimilar material) thereby creating a bond similar to rivets.
- Brazing Dissimilar Metals With A Novel Composite Foil (Johns Hopkins University) – development of a foil that will braze two steel to aluminum and magnesium without pre-wetting through a self-propagating chemical process.

References:

- AVPTA Workshop, July 2011
- National Research Council, Committee on Benchmarking the Technology and Application of Lightweighting (2012) *Application of Lightweighting Technology to Military Vehicles, Vessels, and Aircraft*.

AVPTA Technology Focus Area 2: Lightweight Structures & Materials

Breakthrough Techniques for Dissimilar Material Joining – Brazing Dissimilar Metals with a Novel Composite Foil

DOE-VTO TFA Lead: William Joost
TARDEC TFA Lead: Dr. Richard Gerth

Principal Investigator:
Timothy P. Weihs

Johns Hopkins University (JHU)
3400 North Charles St
Baltimore MD, 21218
Phone: (410) 516-4071
E-mail: weihs@jhu.edu

Start: Q1FY14
Projected Completion: Q4FY17

Objective:

- To develop, characterize, and assess novel reactive foils that are based on reduction-oxidation (redox) chemical reactions for use in dissimilar alloy bonding applications.

Strategic Context:

- This technology will be applied to future Programs of record (PORs) requiring dissimilar material lap joints.
- The technology supports the TARDEC Strategy enabling new capability in the design and application of dissimilar material lap joints.
- A patent application has been submitted with the intent of licensing the technology to a materials manufacturer, who will then sell to the automobile industry.
- Follow-on activities may include further AVPTA interest to investigate increasing joint strength, reducing cost and / or developing foils for other material combinations. TARDEC-specific follow-on may include lap joint ballistic shock evaluations.

Accomplishments:

- Fabricated 23 batches of Redox Foil representing 11 unique chemistries by mechanical consolidation and processing of elemental powders. (FY 2014).

- Determined baseline strengths for bonding aluminum (Al) 6061, magnesium (Mg) AZ31 (aluminum 3% and zinc 1%), aluminum coated boron steel (ACBS), and hot stamped boron steel (HSBS) with Al:CuO-based, Al:Cu_2O-based and Al:NiO-based Redox Foils using initial Redox Foil fabrication techniques. (FY 2014).
- Quantified the mass ejected from the Redox Foils as a function of dilution. (FY 2014).
- Obtained high energy ball mill to mechanically fabricate composite thermite particles, thus increasing the reactivity of starting powders before mechanical consolidation and fabrication of Redox Foils. (FY 2014).

Introduction:

Joining of dissimilar engineering materials can be challenging due to differences in chemistry and melting temperatures. Joining can also be complicated by mismatches in thermal contraction on cooling, which can introduce unacceptably high stresses to the bond interface or prevent joining altogether. Brazing and soldering methods can limit thermal mismatch with low melting temperature materials such as Al, Mg, and related alloys. The last two decades have seen the development and commercialization of reactive, self-propagating multilayer foils as local heat sources for joining materials [1-2]. When used in conjunction with solder or braze, these foils can join dissimilar materials without heating either component significantly, as only the area near the interface is heated [3-4]. The standard NanoBond® practice of pre-wetting components with solder, however, adds cost, slows dissemination of the technology, and limits bond strength. Ideally, no pre-wetting would be required and stronger braze bonds would be enabled.

The aim of this project is to develop, characterize, and assess novel reactive foils that are based on redox chemical reactions. Many redox reactions are noted for their exothermic heats of reaction and molten metallic products, making them intriguing candidates for solder-free bonding applications. These are typically known as thermite reactions. Figure 1 gives a schematic of a possible bonding configuration using a Redox Foil. In addition, the reactive properties of thermite foils may be tailored in a controllable manner by altering the chemistry of the reactants and refining the foil microstructure. The relationships between foil properties and bond characteristics for several thermite systems and dissimilar alloys, including Al 6061, Mg AZ31, ACBS, and HSBS need to be understood. Of particular interest are the shear strengths of the bond, mass ejection (gas and particle) during the reaction, wettability of braze materials, and extent of joint corrosion.

Approach:

A technique was developed to produce self-propagating Redox Foils via mechanical processing of metal and oxide powders with initial diameters on the order of tens of microns. These powders are mixed and packed into steel tubes, where they are further compacted into foils through swaging and rolling. Figure 2 illustrates the process for one redox chemistry. Foils are typically rolled to thicknesses between 0.4 millimeter (mm) and 0.6 mm, although the final thickness is adjustable. Following rolling, the steel jackets are removed and the bare samples (Figure 2) are used for testing or bonding. Cross-sections

of the powder compacts in Figure 2 show the refinement of microstructure resulting from the swaging and rolling steps.

The stoichiometry of the reactants is determined from the complete chemical reaction (e.g. 2 Al + 3 CuO → Al_2O_3 + 3 Cu); however, the ratio of the metallic product to the oxide product may be altered by diluting the reactants with excess metal (e.g. 2 Al + 3 CuO + X Cu → Al_2O_3 + [3+X] Cu where X Cu is the excess copper). Ideally, the metal diluent acts as an inert, heat-sinking material, decreasing the temperature of the reaction. The phase of the diluent at the maximum reaction temperature depends on a number of factors, including heat of reaction, specific heat and amount of diluent, melting/vaporization temperature, and efficiency and modes of heat transfer. As expected, dilution has multiple effects on the reactive properties of the foils, including reducing reaction velocity and mass ejection. These effects will be discussed later.

Work at JHU in FY2014 has focused on three redox systems, Al:NiO, Al:CuO, and Al:Cu_2O. Samples from each system were fabricated at several levels of dilution and ignited in bonds to establish baseline bond strengths. Reaction velocities were measured to assess the effect of dilution on reactivity. Furthermore, experiments were performed to quantify the degree of mass ejection for each redox system, an effect generally not seen in systems that self-propagate via intermetallic formation reactions. Mechanical fabrication of composite thermite particles via high-energy ball milling was begun in an effort to reduce reactant spacing before swaging and rolling.

Results and Discussion:

The focus of FY 2014 was fabricating various chemistries of Redox Foils and analyzing the properties of the reactions, as well as performing some baseline bonding experiments. Before fabricating Redox Foils, however, loose compacts of the starting powders were analyzed to determine the effect of dilution on the reactivity of powders, as illustrated in Figure 3. As the Al:NiO powders are diluted with excess Ni, the amount of heat released (J/g), which is the time integral of the differential scanning calorimeter (DSC) trace, decreases. In addition to combining pure elemental and oxide powders, compacts were fabricated using core-shell powders, whereby elemental nickel was oxidized in air for a given amount of time. These core-shelled particles contained an inner core of elemental nickel, surrounded by a layer of nickel oxide. DSC traces of core-shell particles, red in Figure 3, have earlier onset temperatures, indicating a more reactive structure due to the intimate contact of the aluminum fuel and oxide. Increasing the reactivity of the reaction is important since it allows for more dilution, and therefore more braze material, to be added to the reactive structure without the risk of quenching during bonding.

As seen in the DSC traces from Figure 3, if the system is diluted with too much inert material, then the total heat released decreases substantially. The dilution also decreases the rate of heat production. During bonding, if the Redox Foil does not produce heat

faster than it is dissipated into the rest of the foil or the surroundings (the bonding substrates and atmosphere), then the reaction will quench. In this case the reaction no longer self-propagates across the Redox Foil and much of the foil remains unreacted. To understand the limitations of the current Redox Foils, bonds were performed on Al 6061 and Mg AZ31 to determine the amount of dilution that could be added while the reaction still self-propagates in a bonding configuration. Figure 4(a) displays a table of the results from the quenching experiment and an image of a reacted foil that quenched as it entered the bond interface is at Figure 4(b). The CuO system can be diluted the most while still self-propagating in the bond.

Another key reason to increase dilution is to decrease the amount of gas generated by the reaction. Thermites can generate a significant amount of gas [5] as a result of the reaction. Gas generation can also lead to particulate ejection from pressure build up during the reaction. Gas production and particulate ejection are detrimental to the strength of the bond because together they lead to the formation of pores and a non-continuous braze interface. Figure 5 displays the normalized mass ejection fraction as a function of dilution for the three oxide chemistries examined so far. Normalized mass ejection is defined as the mass of the ejected material collected divided by the mass of the original Redox Foil for the experiment. For all three systems, as dilution increases, the average particulate ejection decreases. For the Al:NiO:Ni system, the particle ejection becomes negligible once dilution increases above 10% by mass, whereas for both CuO systems there is still considerable mass ejection even as dilution is increased. Copper (I) oxide ejects less mass than copper (II) oxide, but because copper (I) oxide is more copper-rich, it is a less energetic formulation and thus is harder to self-propagate with added dilution.

To assess the reactivity of as-rolled Redox Foils, velocity measurements were performed on samples from the Al:NiO, Al:CuO, and Al:Cu_2O systems. The results are plotted in Figure 6. Trends are similar to those seen for mass ejection. Al:CuO foils appear relatively insensitive to dilution, with average velocity values between 1-2 meters per second (m/s) until 40% Cu, while velocity in Al:NiO foils drops off considerably after only 10% Ni dilution. Differences in velocity between the Al:NiO and Al:CuO systems increase by nearly an order of magnitude as the respective diluents are added. In theory, increasing the dilution will also increase the average reactant spacing between the metal fuel and oxide powders. Studies on reactive multilayer foils [6-7] confirm that velocity is inversely proportional to reactant spacing and increases with maximum temperature of the reaction. However, the use of powders with micron scale dimensions, coupled with extensive mechanical processing, yield reactant spacings that are not nearly as uniform as those observed in sputter deposited foils. Studies on Redox Foils deposited via magnetron sputtering will be needed to establish the effects of microstructure on reactivity.

In addition to analyzing the properties of the Redox Foils in FY 2014, preliminary bonds were made using Redox Foils. The Al:CuO foils created porous braze interfaces due to the mass ejection caused by the gas generated by the thermite reaction. Even the heavily diluted case of Al:CuO:40%Cu resulted in substantial particulate ejection from the bond interface. Despite these limitations, the Al:CuO:40%Cu foil was still able to bond all substrates, including Al 6061, Mg AZ31, HSBS, and ACBS. The Al:NiO foils did not produce any noticeable particulate ejection, but the strength of the resulting bonds was less than that of the Al:CuO system as depicted in Figure 7(a). There are two reasons that the NiO-based foils did not perform as well as the CuO-based foils. First, the Al:NiO systems produced more alumina, by volume than the Al:CuO system due to their lower reactivity and smaller degrees of dilution that still allow propagation within a bond. Second, the molten nickel from the thermite reaction does not wet the bonding substrates as well as the molten copper as shown in Figure 7(b) where a high speed camera captures the molten nickel balling up on the surface of the aluminum substrate.

Conclusions:

The initial fabrication of Redox Foils during FY2014 shows that it is possible to make heavily diluted reactive foils whose reaction products can be utilized to braze metals together. Initial testing has found that added dilution does decrease the amount of gas generated by the reaction. However, more dilution can be achieved by further refining the average reactant spacing within the Redox Foils. Methods for refining reactant spacing and thereby allowing for more diluent include ball milling powders to make composite particles that will enhance the reactivity of the systems. With enhanced reactivity, more diluent can be added to the foil to increase the quantity of braze available for joining. The diluent chemistry can also be altered to specifically tailored to enhance wetting of the components by the resulting braze product, which will be explored in detail in subsequent years of the project.

Publications / Presentations:

- N/A Slusarski, K.A.; Woll, K.; Kinsey, A.H.; Gibbins, J.D.; Ku, A.Y.; Weihs, T.P. (2014) “Quantifying Reaction Velocity and Mass Ejection in Thermite Composite Foils.” Presented at the Energetic Materials Gordon Research Seminar and Conference, Newry, ME, 2014.
- Kinsey, A.H.; Gibbins, J.D.; Slusarski, K.A.; Ku, A.Y.; Woll, K.; Weihs, T.P. (2014) “Optimizing Mechanically Processed Thermite Foils for Bonding Dissimilar Metals.” Presented at the Energetic Materials Gordon Research Seminar and Conference, Newry, ME, 2014.

References:

- Ma, E.; Thompson, C. V.; Clevenger, L. a.; Tu, K. N. *Appl. Phys. Lett.* 1990, *57*, 1262.

- Duckham, A.; Newson, J. E.; Brown, M. V.; Rude, T. R.; Knio, O.; Heian, E. M.; Subramanian, J. S. Method For Fabricating Large Dimension Bonds Using Reactive Multilayer Joining, 2008.
- Wang, J.; Besnoin, E.; Duckham, a.; Spey, S. J.; Reiss, M. E.; Knio, O. M.; Powers, M.; Whitener, M.; Weihs, T. P. *Appl. Phys. Lett.* 2003, *83*, 3987.
- Swiston, a. J.; Hufnagel, T. C.; Weihs, T. P. *Scr. Mater.* 2003, *48*, 1575–1580.
- Fischer, S. H.; Grubelich, M. C. *Int. Pyrotech. Semin.* 1998.
- Knepper, R.; Snyder, M. R.; Fritz, G.; Fisher, K.; Knio, O. M.; Weihs, T. P. *J. Appl. Phys.* 2009, *105*, 083504.
- Adams, D. P. *Thin Solid Films* 2014.

Figures and Tables:

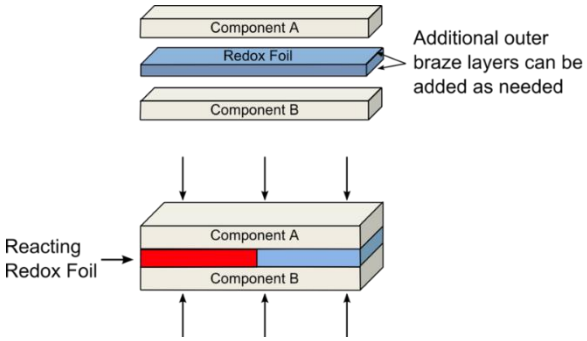

Figure 1: A schematic representation of bonding with a Redox Foil. After ignition, the foil self-propagates through the bond interface.

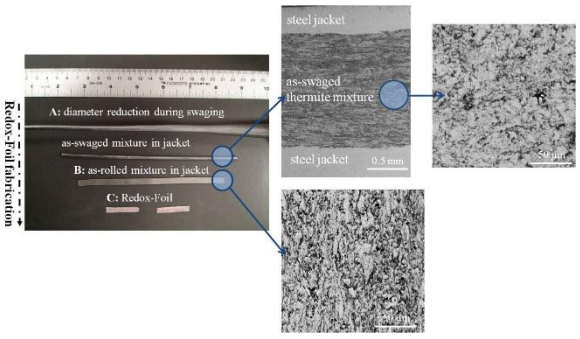

Figure 2: Sequence of swaging and rolling steps. Typical microstructures of cross-sections taken from as-swaged and as-rolled Al:CuO samples are shown.

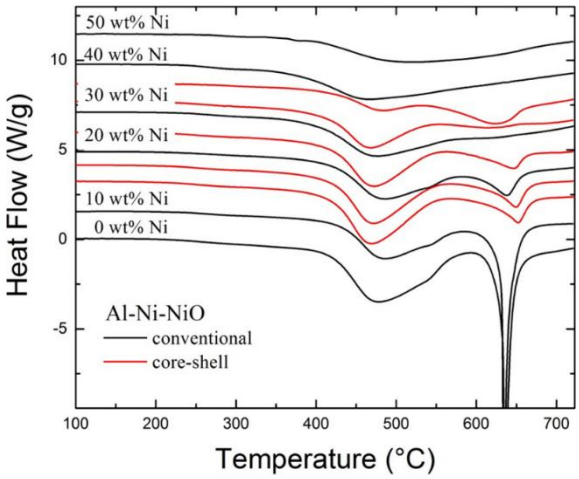

Figure 3: DSC traces of loose compacts of Al, NiO, and Ni powders for various Ni dilutions. Exothermic reactions are identified by a negative heat flow. However, most curves are offset vertically for clarity.

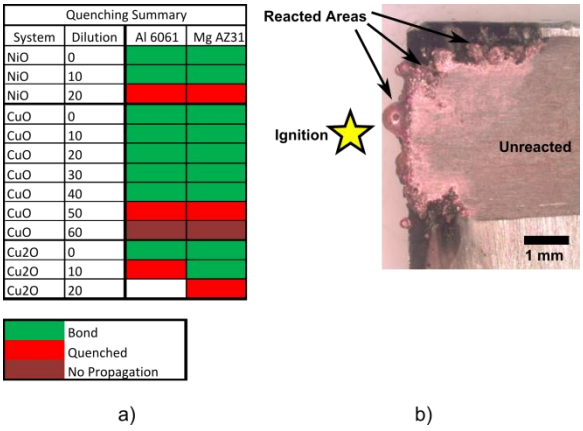

Figure 4: a) A summary of chemistries that either Propagated and produced a bond or quenched during joining for Al 6061 and magnesium AZ31 substrates. b) A quenched Al:Cu_2O:10%Cu Redox Foil on an Al 6061 on an Al 6061 substrate. The foil was ignited outside of the bond interface at the location of the yellow star, but quenched once it reached the metal.

Figures Continued on Next Page

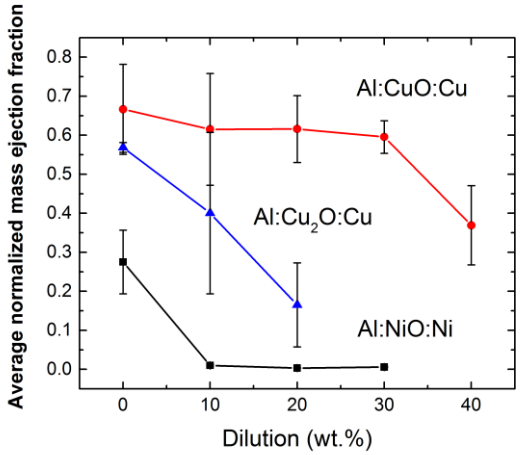

Figure 5: The average normalized mass ejection as a function of dilution for different weight percents of Al:NiO, Al:CuO, and Al:Cu_2O foils, where the diluent is the metal from the starting oxide.

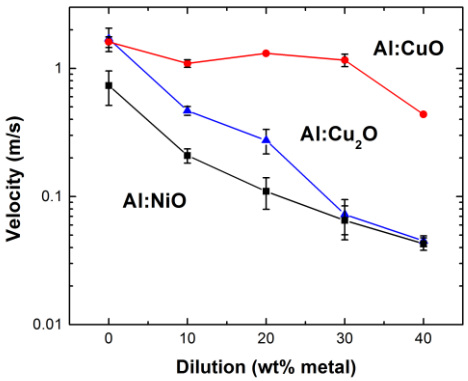

Figure 6: Average propagation velocities of Al:NiO, Al:CuO, and Al:Cu2O foils as a function of dilution.

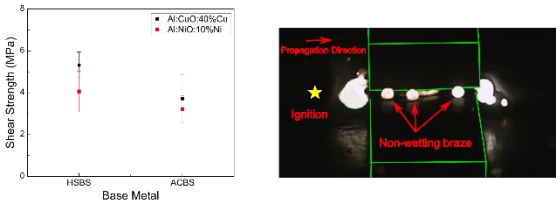

a) b)

Figure 7: a) Shear strengths for bonding HSBS and ACBS with Al:CuO:40%Cu and Al:NiO:10%Ni. b) A frame from high speed video showing molten braze from Al:NiO:10%Ni not wetting the aluminum bonding substrates; bonding substrates have been outlined in green for clarity.

AVPTA Technology Focus Area 2: Lightweight Structures & Materials

Breakthrough Techniques for Dissimilar Material Joining – Collision Welding of Dissimilar Materials by Vaporizing Foil Actuator

DOE-VTO TFA Lead: William Joost
TARDEC TFA Lead: Dr. Richard Gerth

Principal Investigator:
Glenn Daehn

Ohio State University (OSU)
141 Fontana Labs, 116 W 19th
Columbus, OH
Phone: (614) 292-6779
E-mail: daehn.1@osu.edu

With Anupam Vivek
348 McQuigg Labs
105 W Woodruff Avenue
Columbus, OH
Phone: (608) 332-4892
E-mail: vivek.4@osu.edu

Start: Q1FY14
Projected Completion: Q4FY16

Objective:

- To meet the challenge of effectively welding starkly dissimilar materials, namely, steel, aluminum, and magnesium for creating multi-material automotive body structures.

Strategic Context:

- This technology will be applied to future Programs of record (PORs) requiring dissimilar material lap joints.
- The technology supports the TARDEC Strategy enabling new capability in the design and application of dissimilar material lap joints.
- Follow-on activities may include further AVPTA interest to investigate increasing joint strength, reducing cost and / or developing foils for other material combinations. TARDEC-specific follow-on may include lap joint ballistic shock evaluations.

- In addition to discussions with an automotive industry Original Equipment Manufacturer (OEM) and major automotive industry material supplier on material selection and corrosion inhibition strategies, OSU developed a close working relationship with an OEM Tier 1 supplier which is looking to integrate VFAW into its manufacturing process to enable creation of multi-material, lightweight automotive seating structures.

Accomplishments:

- Screened 17 dissimilar metal combinations consisting of magnesium, steel, and aluminum alloys for welding using VFAW. More than 10 combinations were successfully welded.
- Down-selected six material systems based on their weldability and expected resistance to corrosion. (FY2014)
- Created approximately 90 welded samples and subjected samples to mechanical testing and microanalysis. (FY2014)
- Welded high strength steels, such as dual phase (DP) 780 and Boron-quenched steel to aluminum alloy (AA) 6061 T4. Upon peel and lap shear testing, failure occurred in base metal rather than in the weld. (FY2014)
- Collision welding to galvannealed steel was accomplished for the first time. Welded galvannealed steel JAC 270F to aluminum 6061 T4, and mechanical testing resulted in failure in parent aluminum. (FY2014)
- Successfully welded wrought as well as cast magnesium alloys to AA 6061-T4. Additionally, wrought magnesium sheet was also welded directly to uncoated JAC 270F steel. (FY2014)
- Demonstrated the effectiveness of use of interlayers for creating strong bonds with pairs that are relatively difficult to weld. (FY2014)
- Performed welding in lap, as well as spot configurations. (FY2014)

Introduction:

This project aims to meet the challenge of effectively welding starkly dissimilar materials, namely, steel, aluminum, and magnesium for creating multi-material automotive body structures. The primary issue we are addressing in the phase I of this project is the formation of unwanted, brittle intermetallic compounds (IMCs) at the weld interface. Corrosion due to disparate electrochemical potentials is also a major issue with dissimilar material joining. Corrosion mitigation by using intermediate layers, e-coating, and sealing, will be pursued during FY 2015. Traditional fusion-based welding between dissimilar combination of aluminum, steel, or magnesium always leads to formation of IMCs, which are brittle. Upon mechanical testing, failure in such weld samples tends to happen within the weld. For instance, Al-Fe welds made by resistance spot welding often contain IMCs and are not tough enough to be applied in the body in white. Solid-state welding techniques, like friction stir and collision welding, offer a method that avoids or reduces the formation of IMCs.

In this project, a novel method for collision welding, developed at Ohio State University (OSU), is being used. Usually, collision welding relies on the use of high explosives to provide the driving force. However, explosive welding [1] is limited to large scale applications. Besides, there are stringent regulations with respect to transport, storage, and handling of explosives that make it difficult to apply in mass production industries, such as the automotive industry. Magnetic pulse welding [2] can be used for welding at smaller scales; however, actuator longevity at high pressures and operating cycle frequencies have often restricted the application of this technique.

The new technique [3] has been utilized here. A schematic for the VFAW assembly is shown in Figure 2. The main driver of these experiments is a 0.0762 mm thick aluminum foil, which is a consumable, replaced after every experiment. When a high, short-duration current pulse, driven by a capacitor discharge, is passed through the foil, the foil vaporizes rapidly due to Joule heating. This phenomenon, also known as electrically exploding foils [4], creates a high pressure region around the foil, which, in this case, has a thick steel block on one side and the flyer sheet on the other. Therefore, the flyer sheet gets driven to high velocities toward the target plate. Standoff sheets between the flyer sheet and target plate provide the distance over which the flyer is accelerated. Additionally, the height of the standoff sheets and the horizontal distance between them help create an oblique collision, which is necessary for weld creation. Between the two metals to be welded, the flyer is chosen based on density, strength, and ductility of the joining members. Ideally, the flyer materials should be one that is lighter, less strong, and more ductile between the two metals. However, in some cases where all three criteria cannot be met simultaneously, the more ductile material is chosen. Flyer sheet thickness ranges from 0.5 mm to1.5 mm. As for target plates, because they are stationary, they can be as thick as needed.

Approach:

Fifteen different combinations of dissimilar materials were to be screened in order to select five of them for intensive characterization in the second phase. The starting sets of alloys tested include:

Steel: JAC270F (thickness = 0.6mm), DP780 (1mm), high-strength, low alloy (HSLA) 656a (6mm), HSLA 588a (6mm), Boron Quenched Steel (2mm), Aluminum: 6061 T6 (0.8mm and 0.9mm), 6061 T4 (0.8mm and 0.9mm), 5052 (0.8mm), and
Magnesium: AM60B (3mm), AZ31B (0.8mm)

Aluminum was one of the flyer materials when used as a joining member. During the welding of steel and magnesium, steel was chosen as the flyer plate. In most of the cases, OSU worked with uncoated material. However, welding of galvannealed JAC270F with

AA6061 T4 was also done without removing the coating. For each type of flyer, velocity was measured with high temporal resolution by using photonic Doppler velocimetry (PDV). Arcing through work pieces or the backing blocks tends to reduce the efficiency of the process. Therefore, current and voltage were measured in order to ensure that the electric current did not arc through a path other than the foil actuator.

Two types of experimental configurations were implemented for screening: grooved target and flat target welding.

Grooved Target:

Six grooves of angles ranging from 8° to 28° were machined into target plates using electro-discharge machining. These were impacted with aluminum flyer sheets launched by the vaporizing foil actuator operating at varying input energy levels (ranging from 4 kilojoules (kJ) to 10 kJ). With high-resolution measurement of velocity using PDV and microscopic observation of the welded interfaces, a complete welding process window could be created [5]. Assessment of the weld quality was based purely on optical observation, as the samples do not lend well to mechanical testing. The optimal collision parameters determined from such experiments were intended to be utilized to create prototype welds in the second phase. However, some issues were encountered with this method, which rendered it not as useful a screening method as initially envisioned. In order to make this method work, certain variations, such as introducing a vacuum between the joining members, using compliant intermediate layers, and slotting the bottom of the grooves, were implemented.

Flat Target:

This is the more commonly used configuration of VFAW where a flat target plate is used and the angle of collision is created by the standoff distance, which was typically 1.6mm. The part of the flyer sheet directly above the foil actuator is launched flat while the rest of the flyer sheet follows and collapses onto the target plate. Welding takes place in the regions of oblique collapse, where the collision angle and velocity, which are continuously varying, are within the welding process window. Generally, a weld is created above the perimeter of the former position of the active narrow section of the foil actuator. For each material combination tested using this method, the standoff distance was kept at 1.6 mm, and the flyer impact velocity was varied by changing the input energy (between 6 kJ and 12 kJ). Experiments were repeated three times at an intermediate energy level for each set. The samples were sectioned as shown in Figure 3 and subjected to mechanical testing and metallography. Mechanical testing was conducted in lap shear as well as peel mode.

Results and Discussion:

Velocity Measurement:

Velocity-distance curves for each type of flyer launched during this study are shown in Figure 4. Figure 4 shows that the flyer velocity increases with input energy, and the shot-to-shot repeatability is good. In fact, the three traces of the 0.6mm-thick JAC270F flyer obtained at 8 kJ input energy overlap almost perfectly. Although not shown here, increasing the input energy does not always result in a proportional increase in flyer

impact velocity. At very high input energy levels, the electromagnetic interactions between the foil actuator, the backing block, and the flyer plate could substantially deform the flyer plate before foil vaporization, thereby reducing the driving pressure. In any event, driving pressure and impact velocities achieved using this technique are significantly greater than those obtained by magnetic pulse welding, which operates at a similar size scale as VFAW. Because of the ability to reach similar velocities as during explosive welding, VFAW offers the capability to effectively weld a wide range of difficult-to-weld material combinations.

Grooved Target:

This method was used with six material systems. Figure 5 shows the variation of interface structure for AM60B/AA6061-T4 weld. Significant differences in amplitude and frequency of the interfacial waves could be observed. Quite a few of the welded sections, especially ones obtained at lower energies, came apart during sample sectioning. The minimum velocity required to obtain a sample with welds that remained intact after the experiment was 640 meters per second (m/s).

Figure 6 shows typical cross-sections of aluminum/magnesium and aluminum/steel grooved target weldments. While most of the aluminum/ magnesium samples came out welded, generally, the aluminum/steel samples had an air-gap between the target and flyer plates. Peeled surfaces of the aluminum/steel samples depicted significant melting at the interface. Air-rebound, shock heating, and staggered timing of welding in different grooves could have contributed to these weak weldments. Countermeasures, such as introducing a vacuum between flyer and target plates, using an intermediate layer to distribute the energy over two interfaces, and using a slotted target for allowing exit of the compressed air and jetted materials, were implemented. As shown in Figure 6, these modifications enabled successful welding in the grooved targets. However, they also complicated the simple screening method that was initially envisioned. Also, some material systems welded with flat targets but not with grooved targets. Therefore, after the end of the second quarter, flat target welding was preferred for conducting the screening tests.

Flat Target:

This configuration was implemented for 11 disparate material systems. All of them, barring JAC270F/AM60B, welded successfully. The interfacial morphology of some of those welds is shown in Figure 7. All the interfaces were wavy, and IMCs (depicted by intermediate contrast), if any, were intermittent in most cases. Some voids could also be seen in the joints made with AZ31B sheets. OSU successfully welded AM60B magnesium alloy to JAC270F steel with an AA3003 aluminum alloy interlayer in between. Figure 7 also shows, however, that a region where all the layers are continuously welded could not be obtained. By varying the standoff height and input energy, OSU will be continuing the work to join this three-layer system because the interlayer serves the dual purpose of

improving weldability and mitigating corrosion between iron and magnesium Besides, welding of galvannealed steel to ultra-high strength steel was accomplished.

Figure 8 illustrates a typical set of mechanical testing data obtained from peel and lap shear testing of AA6061-T4/JAC270F welded samples. In peel, failure occurred through the weld interface; whereas in lap shear, failure occurred in the JAC270F sheet in a ductile manner. Note that the site of failure in peel testing is in the weld; whereas, the site of failure in lap shear testing occurs where iron (Fe) exists. Table 1 gives the maximum peel and lap shear loads normalized by sample width. Failure in the base metal occurred more frequently during lap shear testing as compared to peel testing. Lap shear testing could not be conducted on some of the weldments due to initial shape of the samples. Nevertheless, the peel strength of those samples was generally very good, if tested in lap shear mode with failures occurring in the parent materials outside the welded region.

Based on the screening tests conducted in FY2014 and their relevance to the automotive industry, OSU down-selected the following material systems for intensive characterization of failure mechanisms, joining induced defects, and corrosion testing in FY2015:

- DP780/AA6061-T4
- JAC270F/6061-T4
- AM60B/AA6061-T4
- AZ31B/AA5052
- Boron steel (1.5 gigapascal (GPa))/AA6061T4
- AM60B/AA3003/JAC270F (uncoated).

Conclusions:

During FY2014, VFAW was utilized for screening 17 dissimilar material systems. Two types of screening configurations, grooved target and flat target, were implemented. While grooved target method was found to be not as robust as initially planned, successful welding was accomplished with almost all the material combinations subjected to flat target welding. Welded interfaces had a wavy morphology, and IMCs, if any, were distributed intermittently along the interface. It is encouraging to be able to effectively weld automotive grade aluminum to high strength steel, as well as galvannealed steel. Mechanical testing of the welded samples yielded varied results. Welds were stronger in lap shear mode than in peel mode; in some cases, samples would fail across the weld interface during peel testing but fail outside the weld during lap shear testing. Aluminum/steel welds were generally strong in peel mode, and during testing of some of the combinations, failure even occurred in base metal. With aluminum/magnesium samples, maximum peel strengths as high as 32.5 N/mm and as low as 6 N/mm were obtained. We have selected six systems for making a larger number of prototype welds in FY2015 in order to study their failure mechanisms and develop corrosion inhibition strategies for them. We have also developed processes for creating lap and spot welds, which will enable faster industrial adaptation of the VFAW technique. With the automated

system under development, a future objective will be to create many welds per hour and obtain statistically viable data on the process.

Publications / Presentations:

- Vivek, A., Hansen, S., Benzing, J., He, M., & Daehn, G.S., (2014) "Impact Welding of Aluminum to Copper and Stainless Steel by Vaporizing Foil Actuator: Effect of Heat Treatment Cycles on Mechanical Properties and Microstructure." *Metallurgical and Materials Transactions A*, pp.1-11.
- Vivek, A.,Daehn, G.S., Liu, B.C., et al., (2014), "Impulse Manufacturing: Multi-material Joining.", presented at *Global Lightweight Vehicle Manufacturing Congress 2014, May 28-29, 2014, Detroit, MI*. http://www.global-lightweight-vehicle-manufacturing-2014.com/
- Liu, B.C., Vivek, A., Daehn, G.S., (forthcoming 2015). "Use of Vaporizing Foil Actuator for Impact Welding of Aluminum Alloy Sheets with Steel and Magnesium Alloys." *TMS Light Metal*.
- Vivek, A., Daehn, G.S., (2014),."Welding in Lap and Spot Configurations with Vaporizing Foil Actuator". Provisional patent application, *The Ohio State University*.

References:

- Findik, F., "Recent developments in explosive welding." *Materials & Design*, (*32*:3), 2011; pp. 1081-1093.
- Psyk, V., Risch, D., Kinsey, B. L., Tekkaya, A. E., & Kleiner, M., "Electromagnetic forming—A review." *Journal of Materials Processing Technology*, (*211*:5), 2011; pp. 787-829.
- Vivek, A., Hansen, S. R., Liu, B. C., & Daehn, G. S." Vaporizing foil actuator: a tool for collision welding." *Journal of Materials Processing Technology* (213:12), 2013:pp 2304-2311.
- Chace, W. and Moore, H., 1959, *Exploding Wires*, 4 vols. Plenum Press.

  Vivek, A., Liu, B. C., Hansen, S. R., & Daehn, G. S. "Accessing collision welding process window for titanium/copper welds with vaporizing foil actuators and grooved targets." *Journal of Materials Processing Technology*, (214:8), 2014; pp. 1583-1589.

Figures Start on Next Page

Figures and Tables:

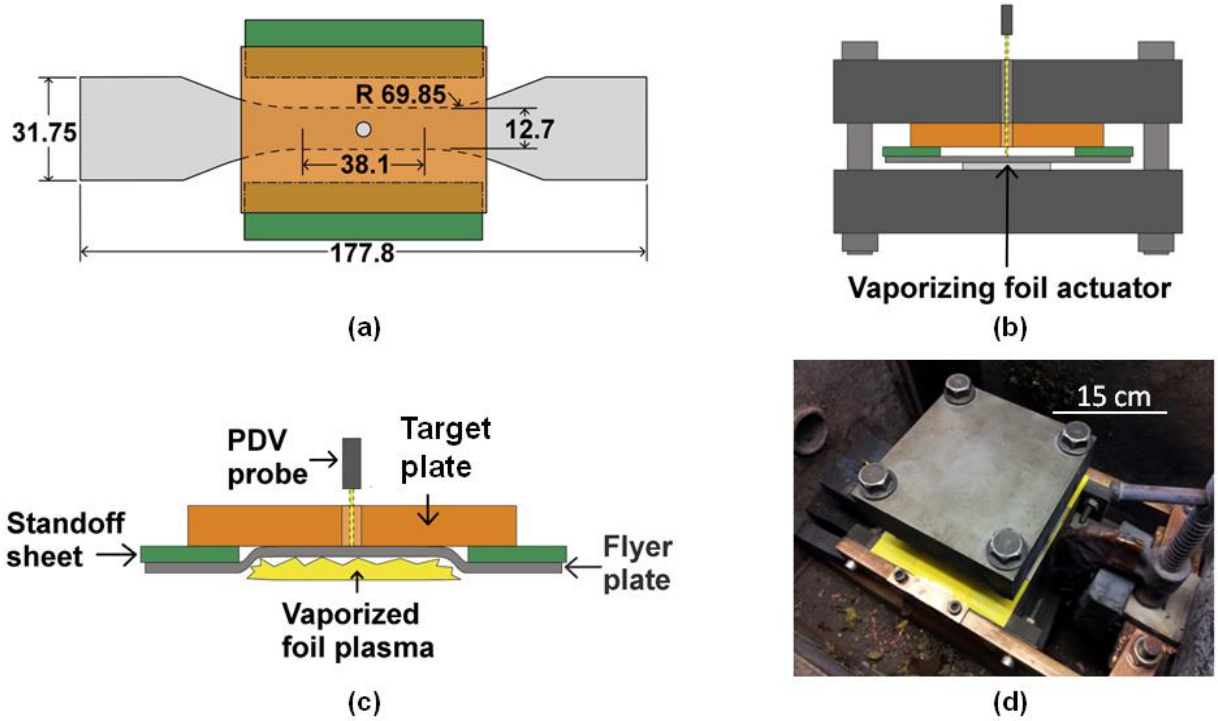

Figure 1: Efforts toward technology transfer: (a) lap weld without overhangs, (b) spot weld, (c) a schematic of the automated VFAW system.

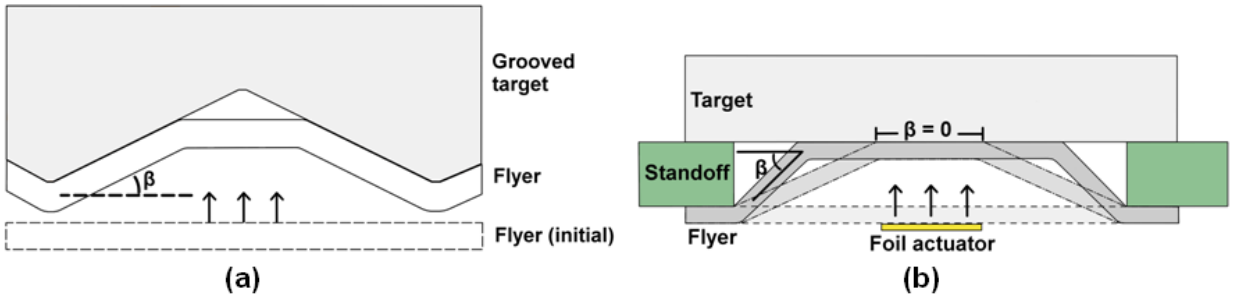

Figure 2: Vaporizing foil actuator welding (VFAW) set up: (a) top view of the foil actuator, flyer sheet, standoff, and target stack, (b) side view of the stack along with the positioning of the photonic Doppler velocimeter (PDV) probe, (c) formation of weld after foil actuator's vaporization, (d) VFAW set up inside the experimental chamber.

Figures Continued on Next Page

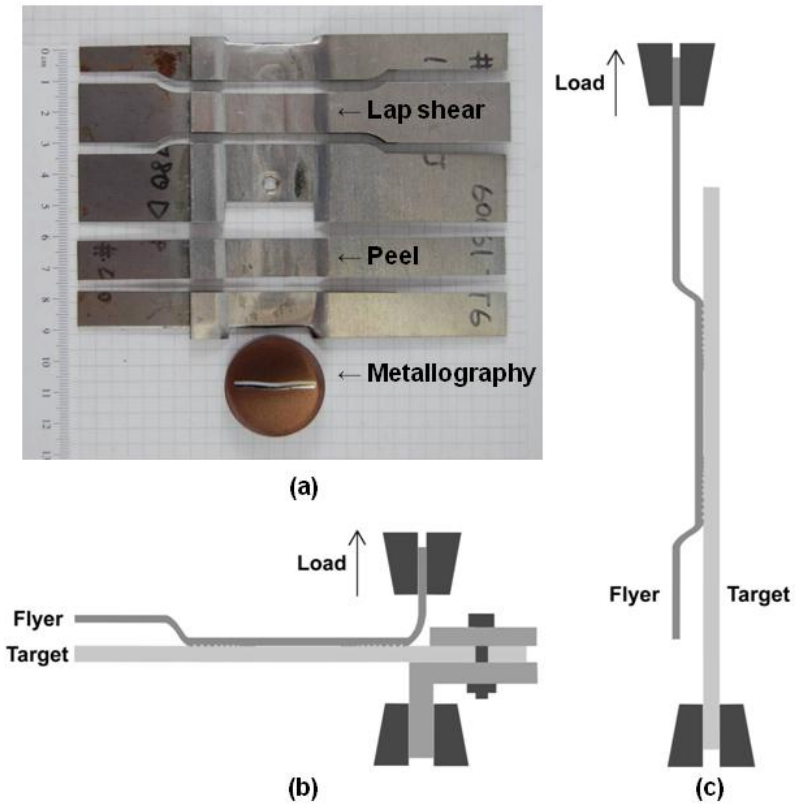

Figure 3: (a) Sectioned sample for mechanical testing, (b) peel testing setup, (c) lap shear testing setup.

Figures Continued on Next Page

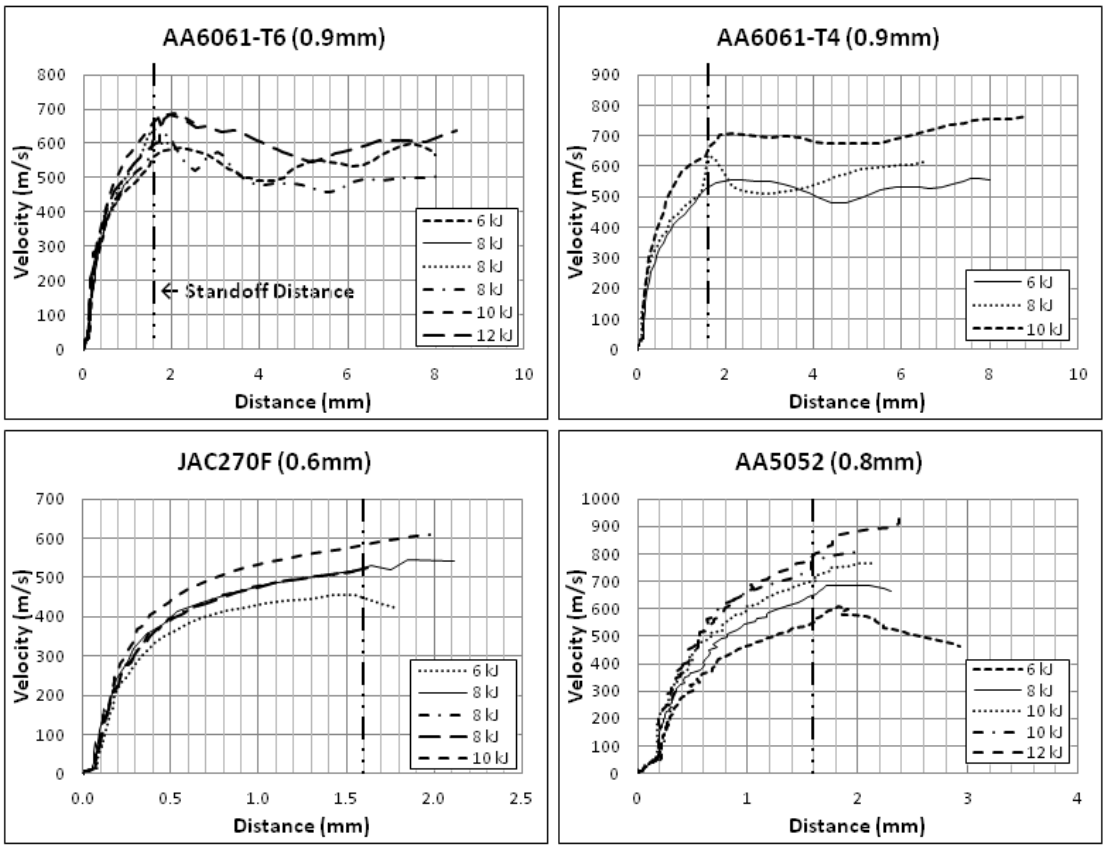

Figure 4: Velocity vs Distance curves for each flyer material.

Figures Continued on Next Page

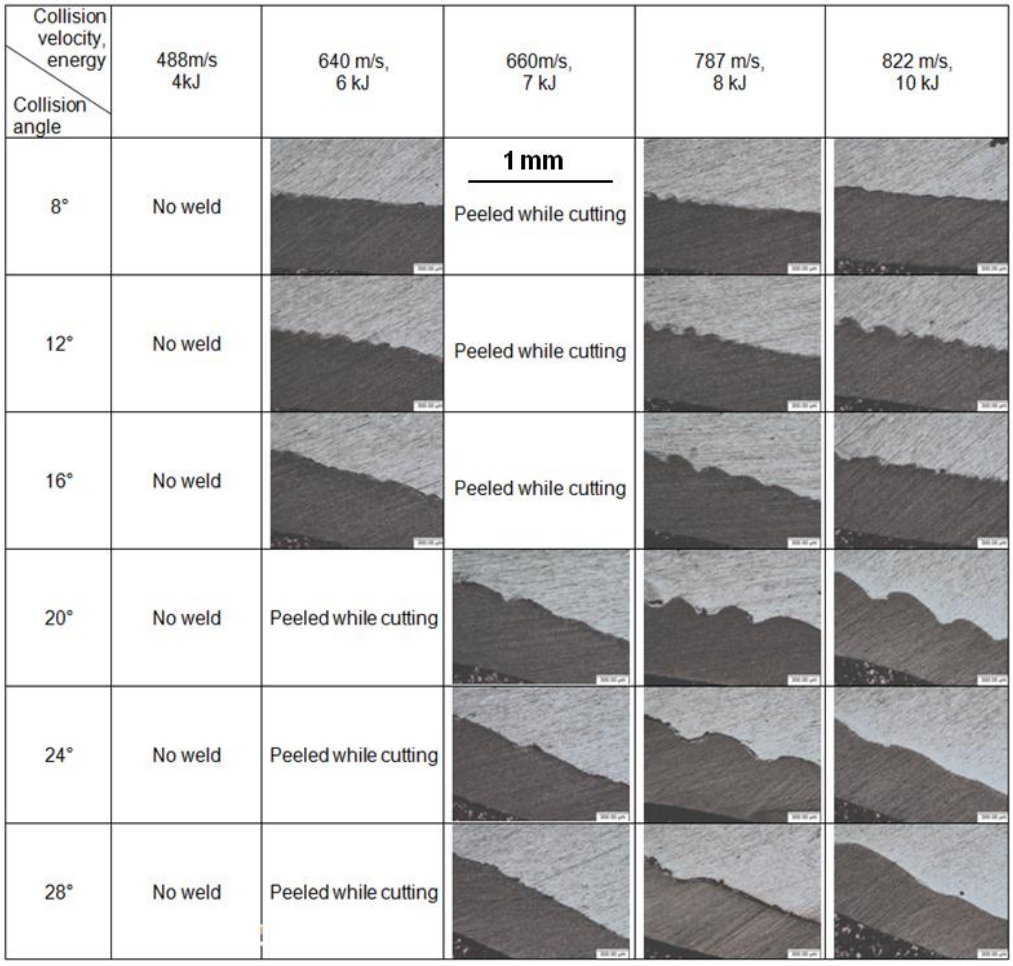

Figure 5: AA6061-T4 Flyers (0.8mm thick) impacted with AM60B grooved targets.

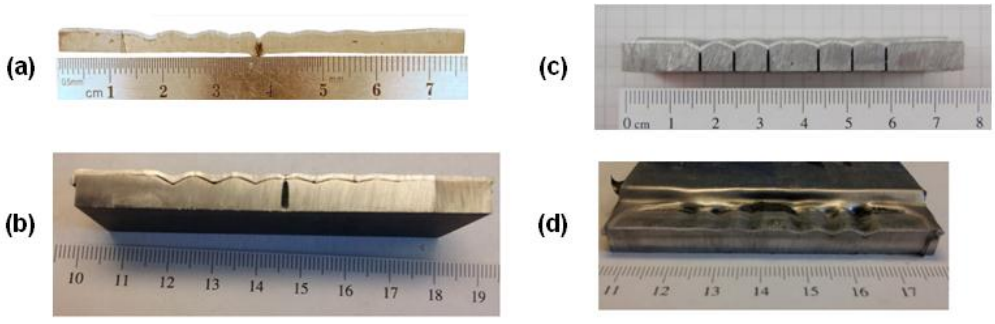

Figure 6: Grooved target welds with material combinations and Experimental conditions: (a) AA6061-T4/AM60B, no vacuum, (b) AA6061-T4/HSLA 656a, no vacuum, (c) AA6061-T4/HSLA656a, slotted target, no vacuum, (d) AA6061-T4HSLA 656, AISI 1018 steel interlayer.

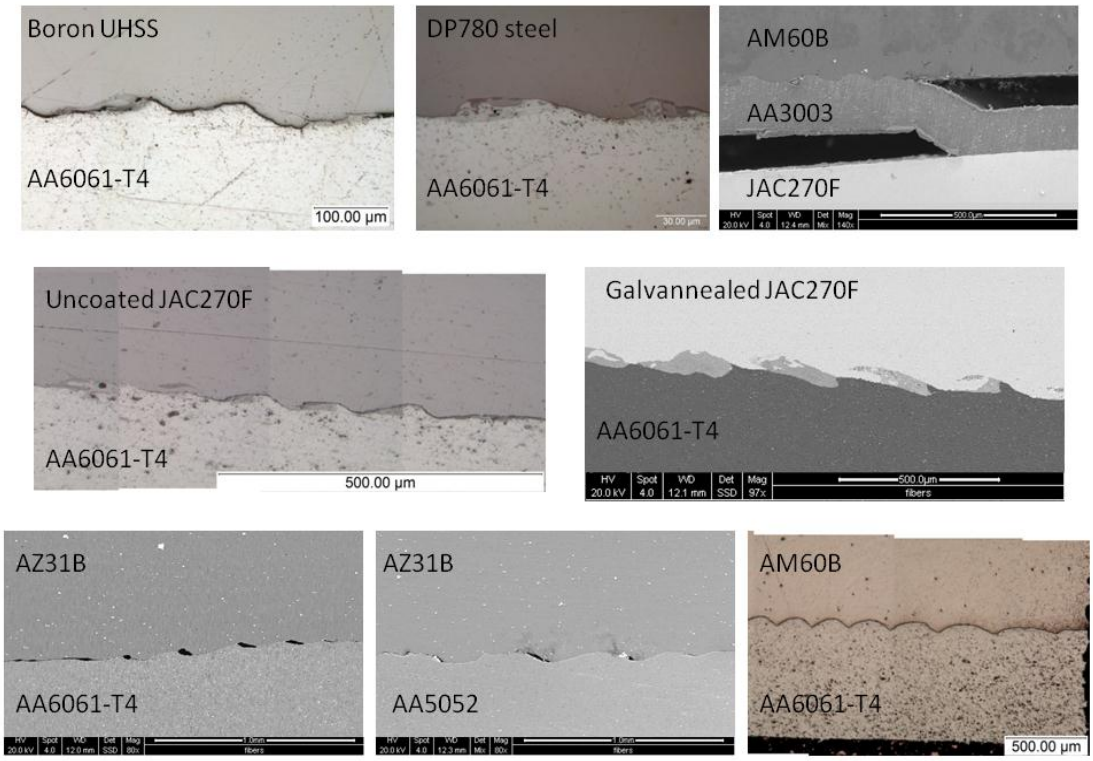

Figure 7: Scanning electron and optical microscope images of the wavy welded interfaces between dissimilar materials (Note: UHSS is ultra-high strength steel).

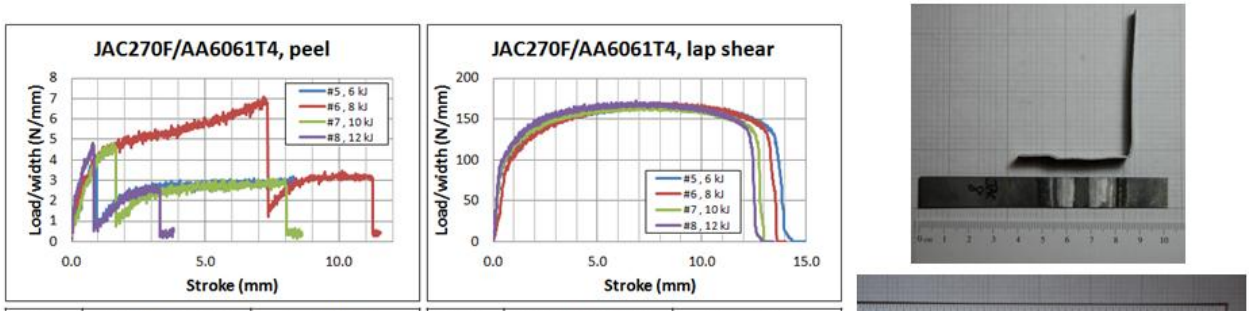

Sample	Peak peel load (N/mm)	Site of failure
#5, 6 kJ	4.20	weld
#6, 8 kJ	7.11	weld
#7, 10 kJ	4.85	weld
#8, 12 kJ	4.83	weld

Sample	Peak shear load (N/mm)	Site of failure
#5, 6 kJ	169.39	Fe
#6, 8 kJ	169.86	Fe
#7, 10 kJ	167.34	Fe
#8, 12 kJ	172.31	Fe

(a) (b)

Figure 8: Mechanical testing data for JAC270F (uncoated)/AA6061-T4 welds: (a) test data, (b) tested samples.

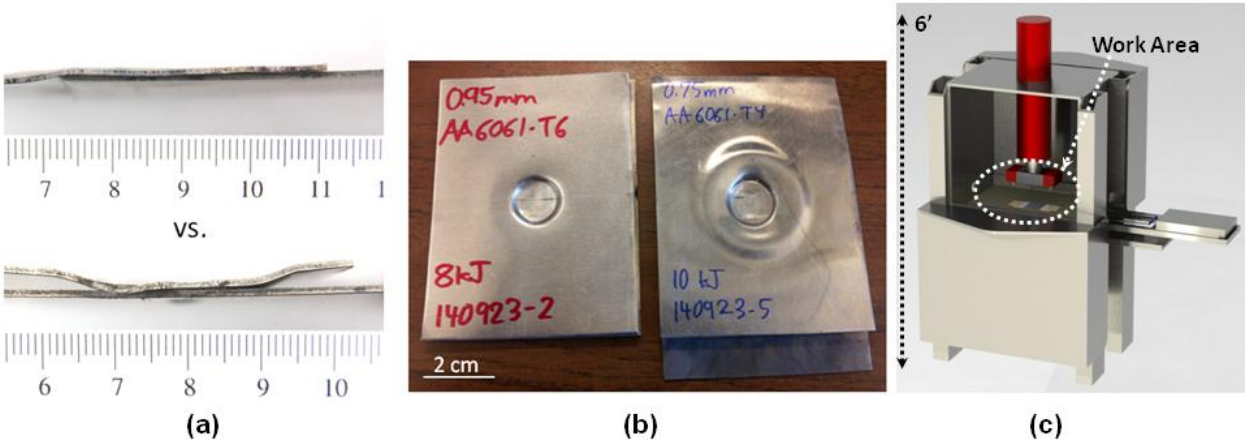

Figure 9: Efforts toward technology transfer: (a) lap weld without overhangs, (b) spot weld, (c) a schematic of the automated VFAW system.

Material System	Peel		Shear	
	Peak load normalized by width (N/mm)	Location of failure	Peak load normalized by width (N/mm)	Location of failure
DP780/AA6061-T6	12.3	Weld	303.9	Al
DP780/AA6061-T4	33.3	Al	187.4	Al
HSLA 588a/AA6061-T4	39.8	Al	--	--
JAC270F/AA6061T4	>18.6	Weld	98.9	Al
AM60B/AA6061T4	32.5	Weld	--	--
AM60B/AA3003/JAC270F	14.9	Weld	--	--
AZ31B/AA6061T4	8.4	Weld	151.3	Al
AZ31B/JAC270F (uncoated)	--	(split during sectioning)	--	--
AZ31B/AA5052	6.0	Weld	119.7	Mg
JAC270F (uncoated)/AA6061T4	7.1	Weld	169.9	Fe
Boron steel (1.5 GPa)/AA6061T4	48.6	Al	--	--

Table 2: Peel and lap shear strengths of material systems welded in flat-flat configuration.

This Page Intentionally Blank

AVPTA Technology Focus Area 2: Lightweight Structures & Materials

Breakthrough Techniques for Dissimilar Material Joining – Upset Protrusion Joining Techniques for Joining Dissimilar Metals

DOE-VTO TFA Lead: Edwin Owens
TARDEC TFA Lead: Dr. Richard Gerth

Principal Investigator:
Stephen Logan

FCA US LLC
800 Chrysler Drive
Auburn Hills, MI 48326
CIMS #482-00-13
Phone: (248) 512-9485
E-mail: stephen.logan@fcagroup.com

Start: Q1FY14
Projected Completion: Q4FY16

Objective:

- To develop and demonstrate a robust, cost effective, and versatile joining technique, known as Upset Protrusion Joining (UPJ), for joining challenging dissimilar metal combinations, especially those where one of the metals is a die cast magnesium (Mg) component.

Strategic Context:

- The project goal is to join Magnesium castings to resin composite structures. The technology and research methodology will be used to develop similar processes for steel or aluminum castings.
- The technology supports the TARDEC Strategy enabling new capability in cost and technically effective joining of metals and composites.
- Follow-on activities may include further AVPTA interest to investigate increasing joint strength, reducing cost and / or developing foils for other casting materials.
- TARDEC-specific follow-on will depend upon project success.
- FCA US LLC (formerly Chrysler Group LLC), an automotive Original Equipment Manufacturer (OEM), is leading this project. Since two of the key obstacles preventing more widespread use of light metals in high volume automotive applications are lack of robust joining techniques (especially for dissimilar metal joining) and susceptibility to galvanic corrosion (also, especially for dissimilar metal joining), successful completion of this project will provide a key enabler to high volume application of lightweight materials, allowing Chrysler to accelerate the

development of new lightweight vehicle designs that utilize multiple lightweight materials in order to aggressively reduce mass on future vehicle programs.

Accomplishments:

- Obtained large plates and sheets of Mg, Al and steel material, and cut them into several hundred 40 millimeter (mm) by 110 mm shear tension (ST) and 40 mm by 120 mm cross tension (CT) joining test coupons to support Self-Pierce Riveting (SPR) and UPJ joint development work. (FY 2014)
- Obtained 200 aluminum-magnesium (AM) 60B and 200 aluminum-zinc (AZ) 91D Mg die castings (each including two bosses for a total of 400 AM60B and 400 AZ91D bosses) and machined them to appropriately sized (11 mm diameter by 14 mm height) cylindrical test samples to support thermo-mechanical characterization being conducted at McMaster University and CANMET-MTL. (FY 2014)
- Completed two repetitions of each measurement of thermo-mechanical compression behavior for die cast AM60B and AZ91D Mg alloys at eight temperatures and two strain rates using cylindrical shaped compression test specimens cut from die-castings to support computer simulations of UPJ forming behavior. (FY 2014)
- Evaluated 17 different SPR designs to down-select those that could join the 2.0 mm thick Mg AM60B to 2.2 mm thick Al6013 T4 materials while minimizing cracking of the Mg material and eliminating cracking of the Al material. (FY 2014).
- Produced over 200 SPR Mg (AM60B) to Al 6013 joint samples to be evaluated as a benchmark comparison for UPJ joints. (FY 2014)
- Conducted 105 initial (pre-corrosion) benchmark SPR mechanical/structural tests, including microstructure evaluations, joining induced defect characterization, and quasi-static, impact, and fatigue tests, of four unique coating combinations each of shear and cross tension joint configurations. (FY 2014)
- Commenced and completed 12 weeks of accelerated corrosion exposure test and evaluation of 122 benchmark SPR joints in four unique coating combinations of shear and cross tension joint configurations. (FY 2014)
- Conducted extensive process modeling and simulation development work and additional experimental work conducted during this reporting period. This simulation work primarily used surrogate thermo-mechanical data established before the start of this program, as well as additional test samples that have been produced at Applied Engineering & Technology Integration, Inc. (AET) during this period. (FY 2014)
- Obtained 500 die cast AM60B magnesium test coupons (each including two bosses for a total of 1000 bosses) with7 mm diameter round bosses and 700 coupons (each including two bosses for a total of 1400 bosses) with 8 mm diameter round bosses to support round boss UPJ joining process development and modeling correlation work as well as to support assembly of joining test coupons for later tasks. (FY 2014)

- Optimized round boss UPJ joint electrode shapes and process parameters using a combination of extensive simulation and actual physical experiments. This included machining and evaluating over 10 unique round boss UPJ electrodes in order to develop optimum robust head shapes for 7.0 and 8.0 mm diameter protrusions. (FY 2014)
- Machined and polished final optimized round boss electrode geometries to support process optimization and production of joined assemblies. (FY 2014)
- In addition to optimizing the electrode shape, conducted numerous simulations and physical experiments comparing the effects on joint development performance of varying force and current rates throughout the process. Several process variations were found to be acceptable. This information is utilized in the final process optimization being used to produce joints for evaluation in the next fiscal year. (FY 2014)
- Pretreated appropriate Mg die castings for round boss UPJ joining. (FY 2014)
- Optimized boss geometry for oval boss configurations using computer aided engineering (CAE) simulation tools. (FY 2014).

Introduction:

The UPJ process, shown conceptually in Figure 1, is somewhat similar to heat staking of plastic components. The simplest form of the process uses a cast-in protrusion on a die cast component, which is aligned with a clearance hole in the mating component prior to application of force and heat which are used to essentially upset forge the protrusion into a larger diameter boss that fills the clearance hole and forms a mushroom-shaped head to solidly lock the two components together.

The process was conceived primarily for the purpose of joining Mg die-castings to each other and to dissimilar metals because die casting is the most common and cost effective process for producing light weight Mg components. This is one of the most common processes for producing aluminum components as well, yet there has been relatively little work aimed at joining components produced from this process (other than bolting).

While alternative dissimilar metal joining processes have been investigated with varying levels of success, galvanic corrosion has consistently been demonstrated to be a key challenge. Particularly:

- Metallic bonding such as fusion or solid state welding processes, which require a clean (no coatings, or a specific coating designed to improve intermetallic bonding rather than corrosion performance) surface on both metals and does not allow for any isolation between the two metals.

- Separate fastener (rivet, bolt, etc.). Typically, the separate fastener is made of steel for high strength and low cost. However, steel fasteners will promote galvanic corrosion in aluminum and will aggressively promote galvanic corrosion in magnesium. This galvanic activity is even worse if one of the two light metals is joined to a steel component. Additionally, any coatings on the steel fasteners intended for corrosion protection tend to get damaged during the installation process and the fasteners also tend to damage any coatings on the components being joined, thus rendering any preliminary coatings to be useless since the isolation has been broken, or even magnifying the galvanic attack on the anode if a small defect is created in the coating of the anode. Figure 2 shows an example of this magnified galvanic attack when a coated steel screw is driven into a coated magnesium component and then exposed to a corrosive environment.

By contrast, the UPJ process relies on a robust mechanical joint rather than intermetallic bonding, so the more cathodic material can be coated prior to joining to protect against galvanic attack on the more anodic material. Additionally, since the UPJ protrusion is going through a hole that can be pre-drilled or pre-punched prior to coating, the UPJ process is much less likely to damage the coating when the joint is being made. Furthermore, since there is no additional cathodic material (such as a steel fastener) used to create the joint, there is no joining induced galvanic activity beyond that between the two parent materials.

Approach:

The project technical approach is summarized as follows:

- Establish benchmark performance of magnesium to aluminum joints produced through SPR, a currently available commercial process, for comparison purposes only.
- Obtain additional knowledge and understanding of thermo-mechanical behavior of magnesium alloys through Gleeble® testing being conducted in Canada at no cost to the U.S. Department of Energy (DOE).
- Take advantage of knowledge that Chrysler has already gained on the UPJ process, as well as additional CAE forming simulations based on the knowledge gained through the Gleeble® testing, to develop optimized cast protrusion and welding electrode shapes to reduce electrical current requirements and provide more robust, repeatable forming performance for each of the joint configurations being considered.
- For each configuration (AM60B to Al6022, Al6013, and high-strength steel (HSS) in bare, pretreated, and coated conditions, and round and oval shaped joints), produce tensile shear and cross tension test coupons, and send select assemblies back for additional coating layer prior to actual start of mechanical/structural and corrosion evaluations.
- Subject a substantial number of samples (five of each configuration) to initial mechanical/structural tests as described above.
- Subject a substantial number of samples to Chrysler's accelerated corrosion tests, reviewing visually every two weeks and removing three samples of each configuration at four week intervals for quasi-static testing.

- Finally, at the end of the 12-week accelerated corrosion exposure, subject select configurations to fatigue and impact testing for comparison to pre-corrosion performance.

Joint performance is validated through:

- Characterization of material microstructure in the joint region
- Characterization of joining-induced defects in the joint region
- Quasi-static tensile shear tests
- Quasi-static cross-tension tests
- Drop tower impact tests of select tensile shear and cross-tension samples Cyclic fatigue testing of select tensile shear and cross-tension samples
- Exposure to 12 weeks of Chrysler's accelerated corrosion test (ASTM G85-A2) with quasi-static lap shear failure and cross tension failure being evaluated after each 4-week increment, and fatigue testing and impact testing to be re-evaluated on select samples at the end of corrosion exposure
- Characterization of failure mechanisms for each of the mechanical tests described above.

Results and Discussion:

As the project approach requires establishing benchmark performance data from a current state of the art joining process that is amenable to joining dissimilar light metals, the SPR process was chosen as being the most likely option for joining dissimilar Mg to Al materials to provide benchmark data. This report will begin by describing the results of the evaluation of the SPR process.

The team developed a test/evaluation matrix to help guide the evaluation of different coating configurations. This test matrix, shown in Table 1, prescribes the evaluation of four different coating configurations in both ST and CT testing configurations. Table 1 is color coded to show the current status of evaluation of these joints. The squares highlighted in ***green*** indicate that pre-corrosion mechanical/structural testing is complete. The squares highlighted in ***yellow*** indicate that corrosion testing has been completed on those configurations but the post –corrosion mechanical/structural evaluation has not yet been completed. The boxes highlighted in ***red*** indicate that those parts were removed from the corrosion test chamber prior to completing the prescribed 12 weeks of testing due to a high number of parts within those configurations experiencing premature failures (i.e., the assemblies were coming apart inside the corrosion chamber without having any load applied to them), and meaningful post-corrosion testing may not be possible. This is certainly true of the post-corrosion fatigue testing, which may not be possible due to an insufficient number of intact assemblies available to produce a fatigue curve.

In order to optimize the SPR joining process to produce high quality dissimilar metal (Mg AM60B to Al6013 T4) joints of 2.0 mm Mg to 2.2 mm Al, 17 different rivet configurations

were evaluated before down-selecting four that looked the most promising (best rivet engagement, fewest cracks, etc.). Figure 3(a) shows cross sections of four different rivet designs evaluated during the optimization of this process while Figure 3(b) shows test results for peak quasi-static loads in Newtons (N) related to the appropriate rivet sections in Figure 3(a). Note that it was not possible to join AM60B to Al6013 T4 without some cracking in the Mg coupons. The slight cracking observed in this configuration has been observed in previous research and development (R&D) projects but has been shown to have no significant effect on the mechanical performance of these joints. Note also that all joints are made by driving the rivet through the Mg plate and into the Al plate. This is because the higher ductility of the Al plate allows for ductile formation of the rivet in the Al plate without damage to the plate, whereas the formation of the rivet would have caused substantial cracking in the less ductile Mg plate.

Over 200 shear and cross tension assemblies were then produced for the purpose of evaluating the mechanical/structural performance of these joints before exposing a substantial number of un-tested joints to an accelerated corrosion procedure.

Figure 4 shows photos of actual tested samples. Figure 4(a) shows the result of a shear tension test, while 4(b) shows the result of a cross tension test. Similar to the results shown in these photos, all SPR joint samples failed in the Mg parent material at the head of the rivet.

Figure 5 shows results of quasi-static shear tension and cross tension testing. The different coating configurations were not expected to show any substantial difference in performance in these pre-corrosion mechanical/structural tests. The primary purpose of this set of tests is to provide the baseline for the post-corrosion tests to be conducted in the next fiscal year.

Figure 6 shows results of quasi-static vs. impact performance results for pre-treated Mg to pretreated Al in (a) ST and (b) CT. In both ST and CT testing, impact performance is significantly better than quasi-static performance. While this is typical for many similar metal joining processes, this behavior was important to validate for the dissimilar metal SPR joints being investigated in this report because these joints will establish the benchmark performance for the UPJ process under development.

Figure 7 shows fatigue results for the same configuration as Figure 6 in (a) ST and (b) CT. As shown in Figure 4, all pre-corrosion joint failures (including fatigue) occurred in the parent material.

While the mechanical/structural evaluation of the SPR joints was typical of results published elsewhere, based on previous experience, we did not expect this type of joint to perform well in accelerated corrosion exposure. In fact, potential for galvanic corrosion in this type of joint was one of the primary reasons for development of the UPJ process.

Figure 8 shows results of SPR rivets that cracked after only 6 weeks (1000 hours) of exposure to Chrysler's ASTM G85-A2 accelerated corrosion procedure. This is a cyclic

salt spray test with the addition of acetic acid. Figure 8 (a) and (b) are sections from a shear tension sample. Figure 8 (c) is from a cross tension sample. These samples were not subjected to any mechanical load. The samples came apart simply as a result of pressure from growth of corrosion products between the aluminum and magnesium plates during the accelerated corrosion exposure. This failure mode was surprising since most previous experience with steel fasteners in Mg (see Figure 2) had exhibited severe erosion of the Mg panel surrounding the rivet as a result of galvanic corrosion. However, in this evaluation, the cracked rivet failure mode was very typical, being displayed by a large number of samples and resulting in many samples being removed from the test prior to the prescribed exposure time.

Further scanning electron microscopy (SEM) evaluation (Figure 9) showed that fracture in the steel rivet was a result of hydrogen-induced cracking (hydrogen embrittlement) as a result of high residual stresses on the inner surface of the rivet from the self-pierce riveting process, and a high level of hydrogen generated during the corrosion process and accumulating in the rivet, which is cathodic to Mg and Al. Figure 9 (a) and (b) show mixed fracture modes: inter-granular + trans-granular (quasi-cleavage) with some secondary cracking along the grain boundaries, while Figure 9 (c) shows inter-granular dominant fracture mode in region A from Figure 9 (b) indicating the hydrogen content was relatively high. The rivet was made from high strength steel, which is more susceptible to hydrogen-induced cracking.

Process optimization and development of the UPJ process began with characterization of the thermo-mechanical behavior of common die cast Mg alloys to be used in numerical forming simulation activities.

McMaster University and CANMET-MTL (both located in Hamilton, Ontario, Canada) conducted thermo-mechanical compression testing of die cast AM60B and AZ91D bosses that were machined from ST and CT plates provided by Meridian. Unfortunately, the bosses from the CT plates exhibited excessive porosity, so only the bosses machined from ST plates were used in producing the stress-strain curves for use in the simulation software. Figure 10 (a) shows results for temperatures below 200^{o}C for slow strain rates of 0.1 per second (s^{-1}) and Figure 10 (b) results for fast strain rates of 1 s^{-1}both with stress in megapascals (MPa). Figure 11 (a) shows results for temperatures above 200^{o}C for slow strain rates of 0.1 s^{-1} and 12 (b) shows results for fast strain rates of 1 s^{-1}.

During this fiscal year, the team investigated literally dozens of boss and electrode design configurations, as well as load/current rate process parameter configurations while attempting to optimize the design and process to provide robust joints requiring minimal energy usage and cycle time, and resulting in minimal damage as a result of heat to coatings on mating components. Figure 12 below shows one example of the type of design and process simulations conducted to develop an optimum electrode shape for the round boss configuration. In this particular example, when comparing the electrode in (a) to the electrode in (b), at the same point in time and using the same process parameters, the electrode shown in (b) results in lower theta stress, which may reduce the risk of cracking during the forming process.

While Figure 12 shows potential for improved joint robustness as a result of electrode shape, actual physical process evaluation showed numerical prediction of damage during the forming process to be more difficult than originally anticipated. Extensive physical experimentation was required in addition to numerical simulations in order to optimize the process. Table 2 shows just one example of numerous experimental evaluations conducted to compare effects of forging force and current rate on joint quality. In this table, the numbers and corresponding colors (1 - green, 2 - orange, and 3 - red) indicate relative subjective ratings for full head formation (larger diameter is better), absence of cracks, and absence of flash, on a scale of 1 (best) to 3 (worst).

Conclusions:

During this fiscal year, extensive thermo-mechanical material characterization, modeling/simulation and physical experimentation has been used to optimize process parameters for round boss UPJ joints, which are currently being produced to support mechanical/structural evaluation and accelerated corrosion evaluation in the next fiscal year.

Additionally, a full test matrix of over 200 SPR joints have been produced and evaluated for mechanical/structural performance and subjected to Chrysler's accelerated corrosion exposure to serve as a benchmark for UPJ design and process development. Most benchmark SPR joints were unable to pass the full test exposure prescribed by Chrysler Corrosion Engineering without losing integrity before the full test was completed.

Figures and Tables:

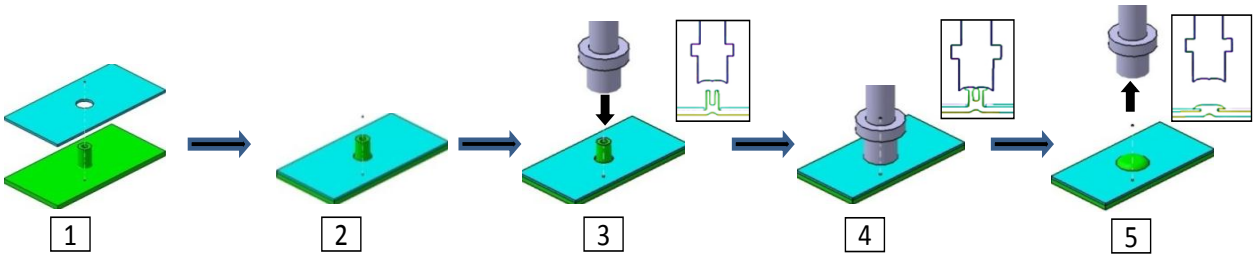

Figure 1: Initial conceptual schematic of UPJ process – assembling parts, applying heat and force, assembly complete.

Figures Continued on Next Page

Figure 2: Galvanic corrosion effects of steel screws in a magnesium component exposed to 240 hours of ASTM B117 salt spray testing.

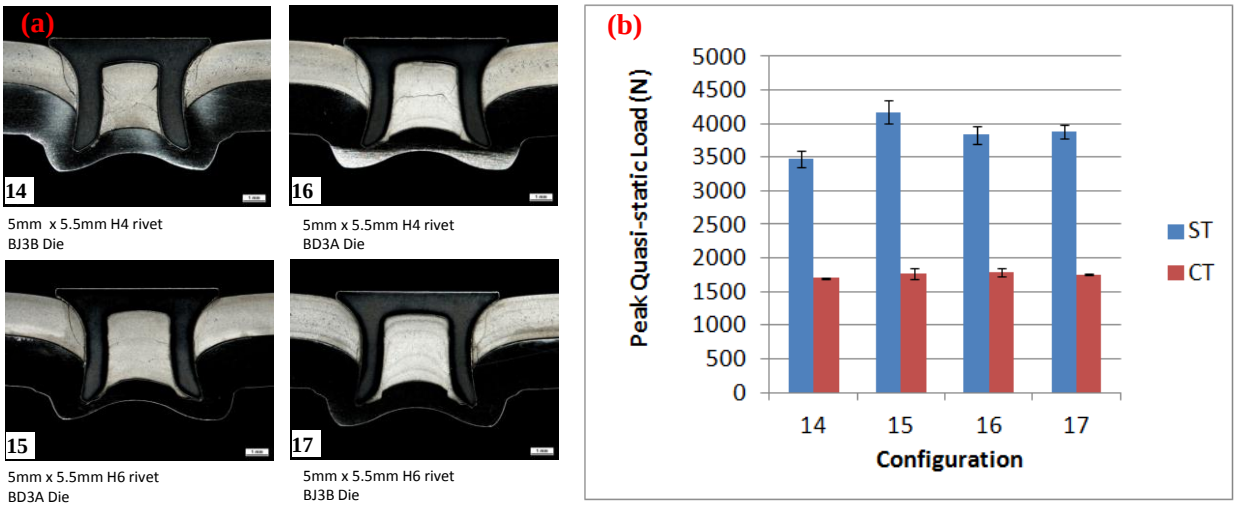

Figure 3: Examples of rivet configurations and joint strengths evaluated for selecting optimum configuration to produce benchmark SPR samples.

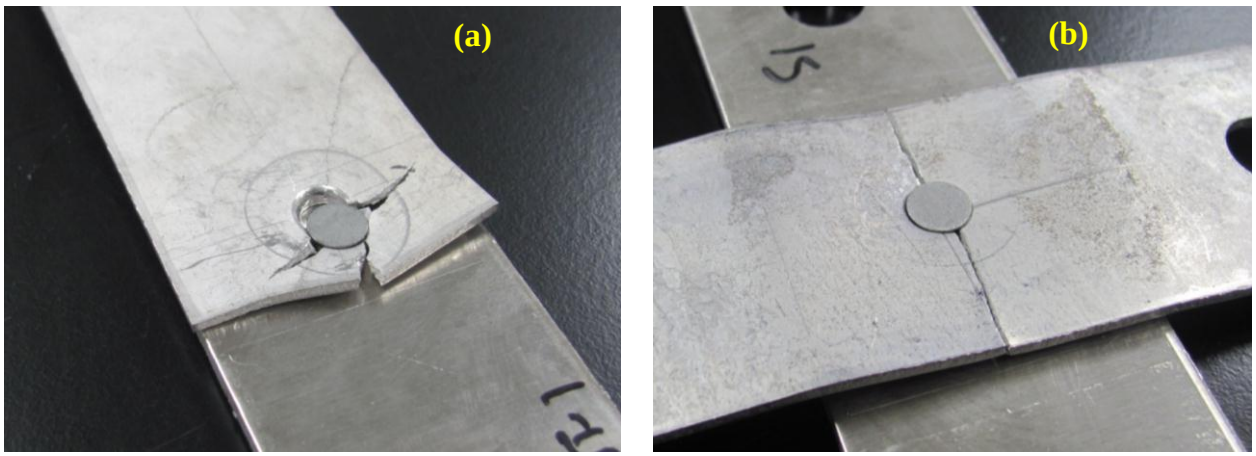

Figure 4: Preliminary test samples of SPR Mg AM60B to Al6013 T-4 joints.

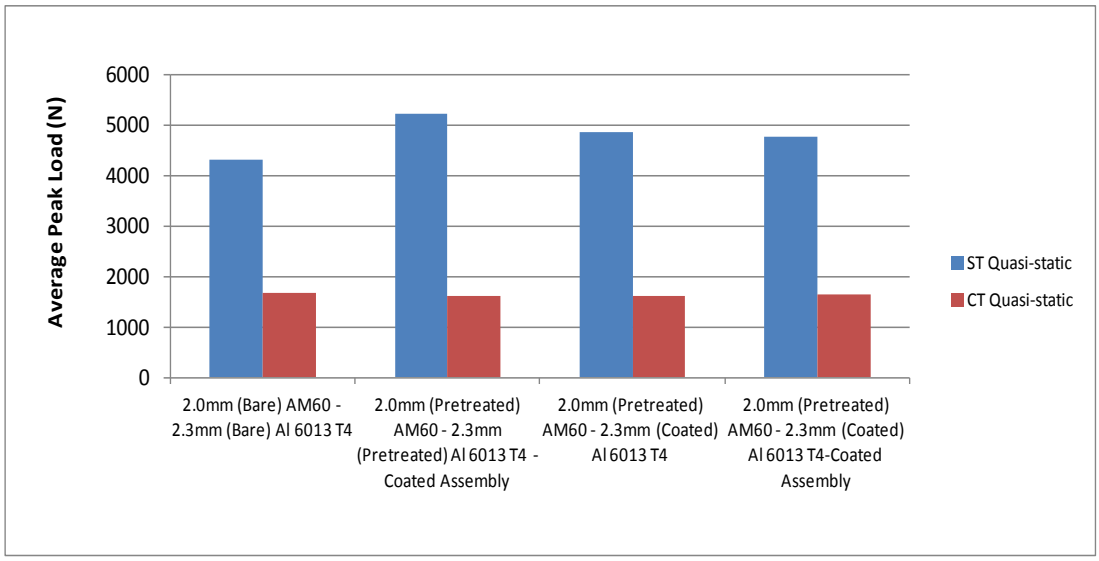

Figure 5: Quasi-static shear tension and cross tension test results for selected coating configurations of Mg AM60B to Al6013 T-4 SPR joints.

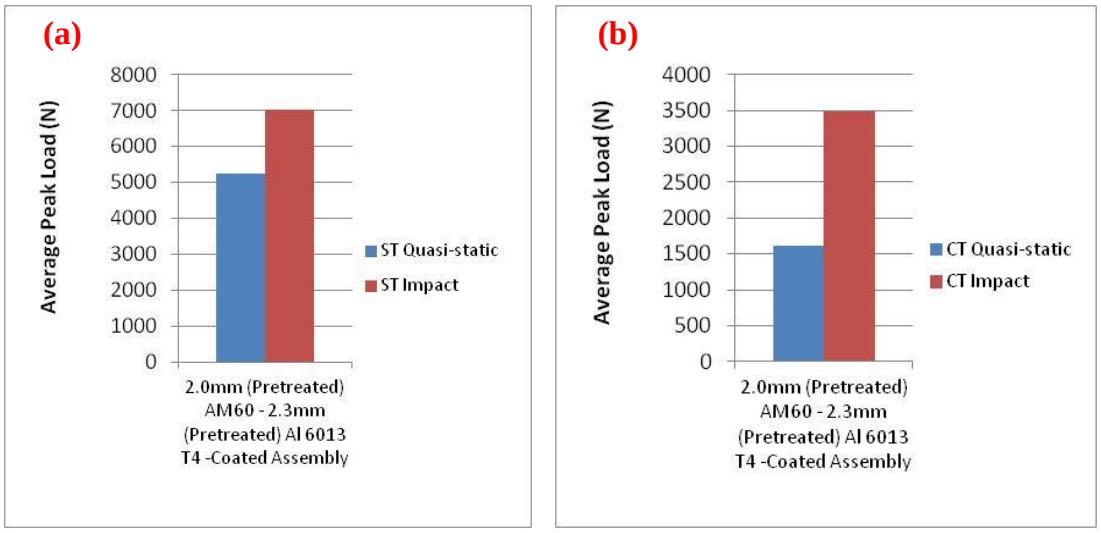

Figure 6: Comparisons of quasi-static vs impact performance for shear tension (a) and cross tension (b) for pretreated Mg AM60B to Al6013 T-4 SPR joints.

Figures Continued on Next Page

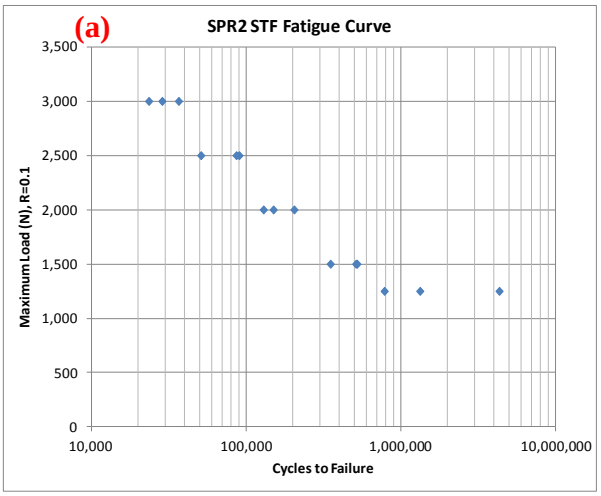

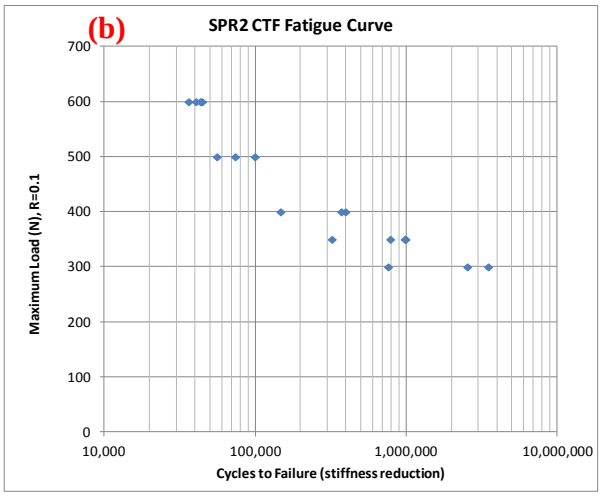

Figure 7: Fatigue curves for pretreated Mg AM60B to Al6013 SPR joints for shear tension joints (a) and cross tension joints (b).

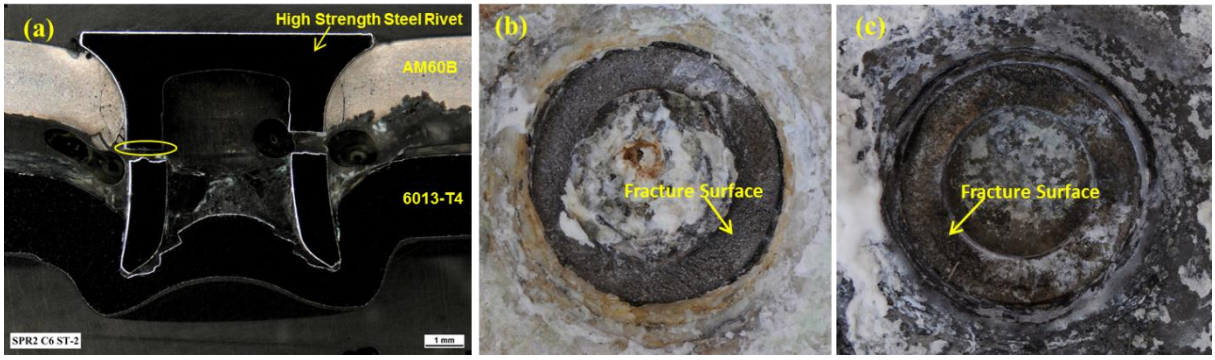

Figure 8: SPR joint failure after 6 weeks of ASTM G85-A2 accelerated corrosion exposure.

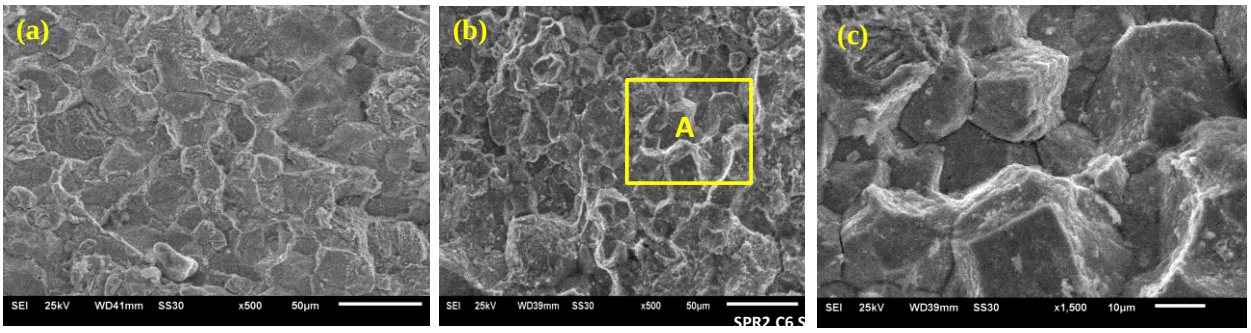

Figure 9: SEM analysis of SPR joints failed after 6 weeks of ASTM G85-A2 accelerated corrosion exposure showing typical fracture morphology near inner surface of rivet.

Figures Continued on Next Page

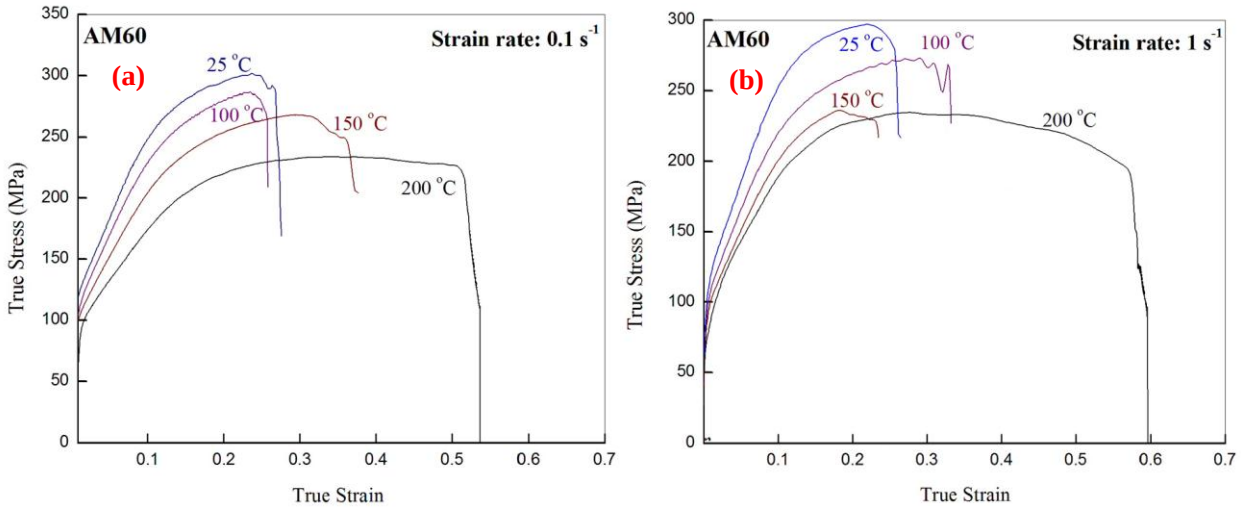

Figure 10: Gleeble® test results for Mg AM60B alloy at low (<=200°C) temperatures.

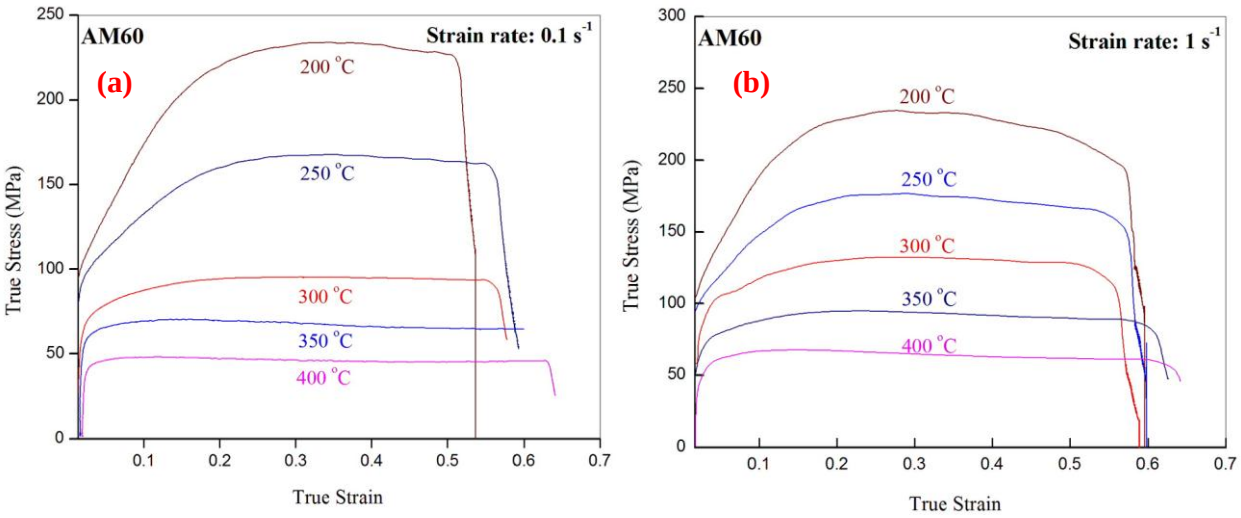

Figure 11: Gleeble® test results for Mg AM60B alloy at high (>200°C) temperatures.

Figures Continued on Next Page

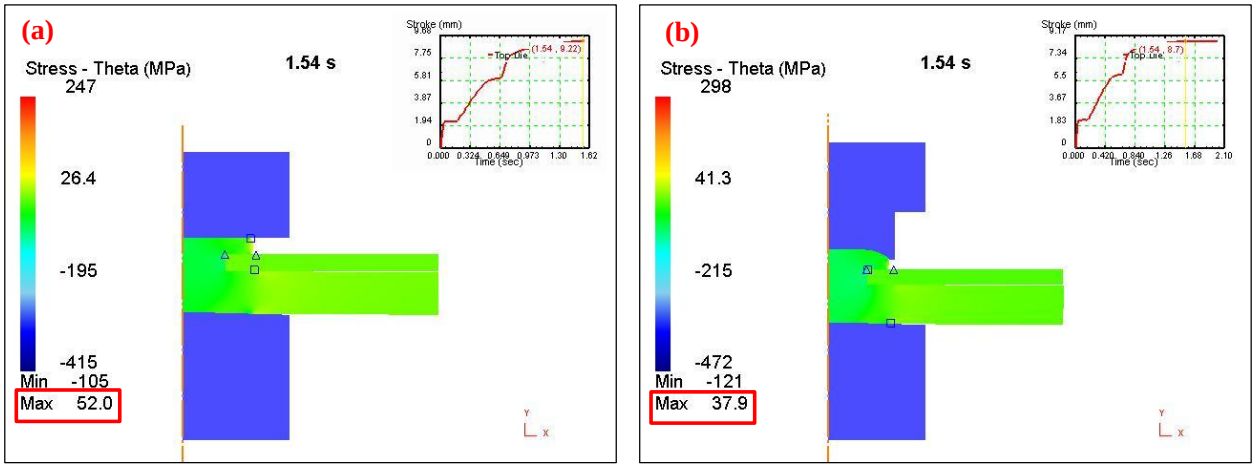

Figure 12: Example simulation comparison of theta (hoop) stress created by two different electrode shapes.

Self-Pierce Riveting - Round Rivet AM60B 2t																							
Base Plate Configuration			Joining Plate			Coated Assem-bly?	Preliminary Evaluations (Prior to Corrosion Exposure)							On-Going Accelerated Corrosion Exposure Evaluation									
														4 wks		8 wks		12 wks					
Material	Test Type Configu-ration	Surface Condition	Material	Thick-ness (mm)	Surface Condition		Micro-structure Charac-terization and Defect Evaluation	Quasi-Static		Fatigue		Impact		Quasi-Static		Quasi-Static		Quasi-Static		Fatigue		Impact	
								ST	CT	ST	CT	ST	CT	ST	CT	ST	CT	ST	CT	ST	CT	ST	CT
Mg AM60B	Shear Tension	Bare	Al 6013 T4	2.2	Bare	No	5	5						3		3		3					
		Pre-Treat			Pre-treat	Yes		5		20		5		3		3		3		20		5	
					Coated	No		5						3		3		3					
					Coated	Yes		5						3		3		3					
	Cross Tension	Bare	Al 6013 T4	2.2	Bare	No			5						3		3		3				
		Pre-Treat			Pre-treat	Yes	5		5		20		5		3		3		3		20		5
					Coated	No			5						3		3		3				
					Coated	Yes	5		5						3		3		3				

Table 1: Benchmark SPR Test and Evaluation Matrix.

Sample	Initial Electrode Force (kN)	Forge Electrode Force (kN)	Forge Timing (ms)	Current 1 (kA)	Time 1 (ms)	Ramp to Current 2 (ms)	Current 2 (kA)	Time 2 (ms)	Current 3 (kA)	Time 3 (ms)	Hold Time (ms)	Head Diameter (mm)	Full Formation	Absence of Cracks	Absence of Flash
D333	8.5	0	0	4	-	3000	8	-	-	-	250	12.0	2	1	1
D357	8.5	15	2500	4	-	3000	8	-	-	-	250	13.0	1	1	1
D354	8.5	22	2500	4	-	3000	8	-	-	-	250	13.2	1	2	1
D356	8.5	28	2500	4	-	3000	8	-	-	-	250	14.0	1	2	1
D355	8.5	35	2500	4	-	3000	8	-	-	-	250	14.3	1	3	1
D339	8.5	0	0	4	1000	3000	6	1000	8	1000	250	12.7	2	1	1
D349	8.5	15	2500	4	1000	3000	6	1000	8	1000	250	13.0	1	2	3
D348	8.5	18	2500	4	1000	3000	6	1000	8	1000	250	13.3	1	2	1
D347	8.5	22	2500	4	1000	3000	6	1000	8	1000	250	13.5	1	3	1
D340	8.5	0	0	5	1000	0	7	1000	9	1000	250	13.0	2	1	2
D334	8.5	0	0	4	-	3000	9	-	-	-	250	12.9	2	1	3
D335	8.5	0	0	5	-	3000	8	-	-	-	250	12.5	2	3	2
D336	8.5	0	0	5	-	3000	9	-	-	-	250	12.9	2	2	2

Table 2: Example of one of many evaluations of forging force and current rate application effect on joint quality.

This Page Intentionally Blank

AVPTA Technology Focus Area 2: Lightweight Structures & Materials

Breakthrough Techniques for Dissimilar Material Joining – Active, Tailorable Adhesives for Dissimilar Material Bonding, Repair and Reassembly

DOE-VTO Lead: William Joost
TARDEC TFA Lead: Dr. Richard Gerth

Principal Investigator:
Mahmoodul Haq

Michigan State University (MSU)
428 S. Shaw Lane, Room 3569
Engineering Building,
East Lansing, MI 48824.
Phone: (517) 402-3409
E-mail: haqmahmo@egr.msu.edu

with
Lawrence T. Drzal
428 S. Shaw Lane, Room 3569
Engineering Building,
East Lansing, MI 48824.
Phone: (517) 353-5466
E-mail: drzal@egr.msu.edu

Start: Q1FY14
Projected Completion: Q4FY16

Objective:

- To demonstrate the feasibility of 'active adhesive' technology for structural joining of dissimilar materials, with the ability to dis-assemble/re-assemble and repair while in-service cast magnesium (Mg) component.

Strategic Context:

- The immediate application target is the Combat Vehicle Prototype (CVP).
- The technology supports the TARDEC Strategy enabling new capability in cost and technically effective joining of dissimilar materials including the potential for joint disassembly.

- Follow-on activities may include further AVPTA interest to investigate increasing joint strength, reducing cost and / or developing adhesives for other material combinations.
- TARDEC-specific follow-on will depend upon project success but is expected to include joint ballistic shock evaluation.

Accomplishments:

- Completed the processing of graphene nanoplatelets (GnP) in thermoplastics. (FY 2014)
- Determined optimal content of GnP to achieve synergy of multi-functional coupling and mechanical properties (e.g. stiffness-toughness balance) (FY 2014)
- Evaluated active adhesives for assembly and repair, bonding/dis-bonding of resulting lap joints. (FY 2014)
- Characterized mechanical and thermo-mechanical properties of the adhesives and the adherends. (FY 2014)
- Manufactured high-temperature resistant glass-fiber composite substrates.(FY 2014)
- Completed morphology analysis for fracture surfaces of both pristine and GnP modified adhesives based single lap joints. (FY 2014)
- Developed nano-homogenization simulations to obtain effective properties of novel adhesives. (FY 2014)

Introduction:

Joining of materials and components is inevitable as it allows versatility in assembly and repair along with reduction in time and cost of manufacturing. However, joints are mostly considered the ‘weak-links’ of the structure due the complex phenomena and interactions of several elements of either similar or dissimilar materials. These complexities combined with the need for lightweight structures and increased safety require better understanding and development of robust dissimilar material joints. The proposed technique uses ‘active adhesives’ and inherits all the advantages of bonded joints, such as lightweight, elimination of holes and associated stress-concentrations, and overcomes the shortcomings of disassembly and repair. Additionally, manufacturing flaws and in-service damage such as impact-induced delamination can be repaired through strategic-targeted heating of the adhesive without affecting the adherends.

The objective of the project is to demonstrate the feasibility of the proposed active adhesive technology for structural joining of dissimilar materials, with the ability to dis-assemble/re-assemble and in-service repair. The outcomes of this work will accelerate the development of efficient active adhesive technology to join multi-materials lightweight structures in different sectors, such as automotive, aerospace, and marine applications.

Approach:

Thermoplastic adhesives modified by the incorporation of electrically conductive GnP at a concentration above the percolation point provide a unique synergy of mechanical,

thermal and electrical properties. While the choice of the thermoplastic is governed by the desired application the addition of the graphene nanoplatelets allows energy to be deposited primarily in the adhesive. The percolated network of graphene particles in the adhesive at less than 2% can quickly couple to UHF □W radiation via non-contact methods and increase the adhesive temperature to above the required processing temperatures. The adhesive melts and flows over the adherends and upon cooling forms a structural adhesive bond. Furthermore, the process can be used to disassemble the adhesive joint if repair or reworking is required. A schematic of the proposed technology is provided in Figure 1. To the best of the investigators knowledge, such active adhesives with repeatable healing/repair and facile disassembly are unique and have not been used in structural joining, and offer a possibility in a wide range of applications.

The approach used in this work follows the “materials by design” philosophy by incorporating an integrated experimental and computational approach to strategically explore the design possibilities and limits of the proposed active adhesive technology. This approach eliminates the costly ‘trial-and-error’ approach and allows a rational development of resulting materials and joints. The EVS developed through this approach will allow exploring material designs beyond the experimental matrix studied. Furthermore, EVS can be used as design tools and can allow prediction of residual strength and design of novel joints. A schematic of the approach is provided in Figure 2.

Most structural joints development studies focus solely on in-plane behavior. This work evaluates the feasibility of proposed technique in: a) in-plane (lap-joints), (b) out-of-plane (three dimensional (3D) woven Pi- shaped or T- shaped joints), and c) torsional/rotatory (super-charger) joints. Measurement techniques such as embedded fiber-Bragg grating (FBG) optic sensors and infrared thermography will be used to accurately measure the in-service performance and observe the repair efficiency of resulting dissimilar material joints. Such a thorough study is directed to cover all possible automotive and ground vehicle applications.

The above mentioned approach of developing ‘active adhesives’ will be achieved through the following sub-objectives/tasks:

Processing, Material Development and Optimization of the Active Adhesives:

- Evaluation of processing parameters, determination of optimal graphene content for synergy of multi-functional, microwave coupling and mechanical properties (e.g., stiffness-toughness balance).

Lab-Scale Evaluation and Detailed Material Characterization:

- Lab-scale evaluation includes strategically selected experiments for characterization of both adhesives and adherends. Also includes low-cost manufacturing of fiber-reinforced composite adherends.

- Detailed experimental characterization of multi-material joints, corrosion analysis of resulting joints, evaluation of assembly and repair using novel non-destructive tools, and evaluation of damage-induced behavior of joints and resulting failure modes.

Design, Testing and Applications:

- Development of design tools and databases using robust, experimentally validated simulations at the nano-, micro- and macro- (large) scale structural simulations.
- Experimental Evaluation of large-scale industrial multi-material joints in: a) in-plane mode (lap-joints), b) out-of-plane mode (T-/Pi- joints) and c) torsional mode (super charger rotor). Also evaluate repair and re-assembly for aforementioned joints.
- Experimental validation /proof-of-concept on an industrial joint and dissemination of results.

Results and Discussion:

Design of Experiments:

The incorporation of nanoparticles in adhesives introduces multi-functionality to the resulting system with enhancements in multiple properties including mechanical (stiffness, strength), fracture (delamination resistance, energy absorption), thermal and moisture diffusion properties along with value added properties such as electromagnetic, MW coupling, etc., On the other hand incorporation of nanoparticles increase the design space for the development and design of the resulting materials and components. Hence a strategic selection of experiments to explore and obtain 'performance bounds/limits' of resulting materials is essential. In this study, GnP are embedded in the thermoplastic adhesive to investigate its thermal response while they are subjected to external □W radiations, while inheriting the enhancements in mechanical properties. Hence, there is a need to understand the influence of GnP concentration on both mechanical properties and on microwave coupling + thermal behavior at both material level and at the component (joints) level.

As mentioned earlier, a detailed characterization of mechanical and thermal properties is essential as it enables identification of "performance limits" of various properties, exploiting the full benefits / synergy in multiple properties (e.g., stiffness-toughness balance) offered by these novel materials while allowing optimal activation of adhesives. Figure 3 illustrates the work-flow adopted to achieve these goals within the project. The acronyms used in Figure 3 are defined as follows: finite element methods (FEM), American Society for Testing and Materials (ASTM), DMA dynamic mechanical analysis (DMA), differential scanning calorimetry (DSC), Fourier Transform Infrared (FTIR), scanning electron microscopy (SEM), and atomic force microscopy (AFM).

Processing of Bulk 'Pristine' and 'GnP Modified' Adhesives:

In this work, the thermoplastic material selected was nylon-6. The choice of thermoplastic depends on the desired application, and instead of studying multiple thermoplastics a single adhesive was selected. The overall approach and the results from this work can be directly extended to other thermoplastics. In this work, prior to the melt extrusion process, the nylon-6 pellets were exposed to 70°C for four hours to eliminate any presence of moisture. Then, melt extrusion of pristine and GnP-modified nylon-6 was carried out in a DSM® Micro 15 cubic centimeters (cc) Compounder, (vertical, co-rotating, twin-screws micro-extruder) operating at 260°C for 3 min at a screw speed of 100 revolutions per minute (rpm). The melted material was then directly transferred in to a DACA® Micro-injector with the barrier temperature ($T_{barrier}$)=260°C and the mold temperature (T_{mold})=100°C. The injection pressure applied for injection molding of tensile, impact, flexural coupons and discs was around 0.97 megapascals (MPa). The melt extrusion and injection molding systems are shown in Figure 4**.** The resulting injection molded samples were used for experimental testing and the discs were used for adhesive film production.

Manufacturing Process of Adhesive Films ('Pristine' and 'GnP Reinforced') Films:

The discs developed from the injection molded specimens were placed between stainless steel plates covered by a high-temperature resistant polyimide film, Kapton® (from DuPont®) to enable ease of adhesive film removal. To control/maintain the adhesive film thickness, 0.09 millimeter (mm) thick Al spacers were placed between the top and bottom plates. To eliminate/reduce entrapped air, the entire setup was covered by a vacuum bag and subjected to vacuum pressure of 1 atmosphere (atm). While maintaining the vacuum pressure, the plates were heated at a rate of 5 degrees Centigrade per minute (°C/min) for up to 260°C, followed by an isothermal process for 5 min. In order to obtain the desired film thickness, successive pressures of 30, 60, and 90 MPa were applied on the plates with a time interval of 3-5 min. One of the challenging problems during film production was inconsistent film thickness. The applied pressure caused the plates to deflect and consequently the central portion of the adhesive film was reduced. To minimize the deflection, additional spacers were also placed at the center, as shown in Figure 5.

Material Characterization of 'Pristine' and 'GnP-Modified Nylon-6:

Tensile and flexural tests were performed using a universal testing system (UTS) electro-mechanical equipment. All tests were performed at room temperature and the results reported here are the average of a minimum of five specimens per case. The tensile tests were performed according to ASTM D638. A 1000 pound (lb) (454 kilogram (kg)) standard load cell attached to the UTS frame and external laser extensometer were used to measure applied force and resulting longitudinal strain, respectively. On the other hand, flexural tests (three-point bending mode) were performed according to the ASTM D770-10 on the same machine with a load cell of 100 lb. (45.4 kg). The dimensions of the samples for flexural tests were 62.7 mm ×12.24 mm×3.2 mm. The span length was set at 50.8 mm. The crosshead speed was calculated based on specimen geometry, according to ASTM standard, and was set at 0.05 inches per minute (in/min) A *linear*

variable differential transformer (*LVDT*) was used to measure the deflection in flexural tests. Impact resistance tests (Izod type) were carried out according to ASTM D256 standard test. The dimensions of the samples for impact resistance tests were 62.7 mm x 10.72 mm×3.91 mm cross-sectional area at the mid-notch.

In order to achieve the desired crosshead velocities as specified by ASTM D638, three testing speeds, namely, 0.05, 0.50, and 5.00 (in/min) were adopted to evaluate the tensile strengths of pristine and GnP-modified nylon-6. Figure 6a provides the tensile strengths of pristine and GnP-modified nylon-6. The tensile strength of pristine nylon-6 was observed to reduce with increasing GnP content. At crosshead speeds of 0.05 in/min and corresponding to 5 wt% GnP content, the tensile strength of nylon-6 reduced by ~19%. As the crosshead speed was increased to 0.50 and 5.00 in/min, the degree of reduction showed slight improvement in the order of ~17% and 15%, respectively. It is evident from Figure 6b that the GnP-modified nylon-6 is more responsive to strain rate than pristine nylon-6. At 5.00 in/min, 3 wt% of GnP-modified nylon-6 exhibited better tensile strengths relative to other material configuration in this study. The reduction in tensile strengths due to addition of GnP was by 'design' and was expected. The GnP used was non-functionalized and the tests were performed to obtain the baseline/control data prior to exploring the benefits of chemical functionalization. On the other hand, the study on effect of strain rate on the adhesives and the improvements observed in GnP modified adhesive shows promise in use of such adhesives for high-strain rate automotive applications, such as crash components etc., Nevertheless, the work is in progress to evaluate the effect of GnP functionalization and to fully explore this benefit before any strong conclusions could be derived.

Figure 7 provides the flexural strength and modulus of pristine and GnP-modified nylon-6. The flexural strength of GnP-modified nylon-6 increases significantly as the GnP content increases. For example, for 5 wt.% GnP, the flexural strength of the adhesive improved by more than 10% relative to pristine nylon-6. Similarly, the flexural modulus of GnP-modified nylon-6 also increases significantly with increase in GnP content. For example, for 5 wt% GnP in nylon, the flexural modulus improved by more than 30% relative to pristine nylon-6.

Figure 8 provides the impact strengths of pristine and GnP-modified nylon-6. Similar to tensile strengths, the impact strength of nylon-6 was observed to reduce with increasing GnP content. This phenomenon can be explained by the fact that the inclusion of rigid filler in a relatively tough polymer has detrimental effect on the impact strength. Similar to the discussion on tensile strengths, improved chemical functionalization can address this issue and possibly improve or at least maintain the toughness similar to pristine nylon-6.

Single Lap-Joints with Pristine and GnP Modified Nylon-6:

Initially, the baseline, or 'control' specimens, corresponding to single lap joints of Al (Al 6061, phosphoric acid anodized) substrates with pristine adhesive were manufactured, followed by dissimilar material (Al-steel) single lap adhesive joints using both pristine and GnP-modified nylon-6. Next, single lap-joints with GFRP (glass-fiber reinforced composite, plain-weave S-glass reinforced with SC-15® from Applied

Poleramics Inc.) adherends were developed. The low temperature resistance of SC-15® resin created problems during melting of nylon-6 and hence high temperature-resistant GFRP substrates with SC-122® resin (Applied Poleramics Inc.) were developed, and resulting multi-material joints have been recently manufactured. The experimental characterization of these high-temperature GFRP joints are in progress and will be provided in the next report. The need for high temperature adherends is only for thermal heating of the adhesives along with adherends. During targeted heating of adhesives only using MW radiations, high temperature adherends need not be used.

Figure 9 provides the lap-shear test results of single lap joints of dissimilar materials (steel-Al). The inclusion of GnP in pristine adhesive film was observed to significantly improve the shear strength of resulting joints. It appears that there was no significant increase in shear strengths beyond 3 wt% GnP. Nevertheless, additional experimental tests are essential prior to making strong conclusions. Statistically significant (sample number (n) > 6) experimental tests for various combinations of adherends are in progress and will be reported in the upcoming report.

Failure Surface Morphology Analysis using Scanning Electron Microscopy (SEM):

The morphology of fracture surfaces of pristine and GnP-modified nylon-6 based single lap joints were observed with a SEM. The SEM samples were coated with a thin layer (3-4 nanometer (nm)) of platinum prior to examinations. The following summarizes the outcomes from SEM observations shown in Figure 10:

- For a given GnP modified nylon-6, the SEM images showed clusters of GnPs with less than tens of micrometers of diameter, indicating a poor interfacial adhesion in the material,
- SEM observation showed that the agglomeration of GnPs is more pronounced when the concentration increases.
- SEM observations revealed that the fracture surfaces of GnPs are smooth.

These observations are consistent with the experimental reduction in tensile and impact strengths. As mentioned earlier, the GnP used was ‘as-received’ and not chemically functionalized to be compatible with the host polymer. Chemical functionalization would improve bonding between the GnP and host polymer, improve dispersion of GnP, eliminate clustering, improve exfoliation and overall improve the mechanical behavior or resulting adhesives and joints.

Nano-scale Simulations and Homogenization:

Nanoscale modeling allows the possibility of understanding and designing materials considering the nanoscale and upwards. One of the main advantages of a computational approach as the one taken in this project is that it eliminates costly trial and error experiments, and provides extrapolation of key experimental data with confidence and in a rational manner. Further, computational analysis provides confidence that the new materials developed possess the desired properties. Most importantly, accurate

nanoscale simulations provide quantitative evaluation of mechanisms that improve or detriment the macroscale properties.

Considerable work on characterization of graphene/polymer nanocomposites for mechanical, thermal and electrical properties exists, but work on fracture/damage resistance is limited. Additionally, the functionalization (for example, coating GnP with rubber) can further improve the toughness and resistance to fracture. While the use the rubber coated graphene is promising, its influence on resulting joints is not fully understood. Furthermore, the development of design tools for structural joints require that the nanoscale properties are fully and accurately transferred to the macro/structural scale. Nanoscale simulations in the form of unit cell homogenization, allow obtaining effective properties of the tailorable adhesive. The unit cell, or representative volume element (RVE) can either be in 2-dimensional (2D) or 3-dimensional (3D).

Figures 11 and 12 show sample 2D and 3D RVEs respectively containing 2.5 weight-percent (wt%) of GnP. While work on thermoplastic development and characterization is in progress, experimental results on vinyl ester (VE) composites with varying graphene contents was readily available in our group. Additionally, the effect of carboxyl terminated butadiene acrylonitrile (CTBN) functionalization on resulting modulus was also available. Nanoscale simulations were developed to compare the predictions with these experimental results. The use of thermoplastic adhesive instead of vinyl-ester is a direct, simple extension, in the form input of material properties. This will be continued as the database of experimental characterization results of GnP reinforced nylon gets populated.

The material properties used for the simulations in Figure 11 and Figure12 are: matrix: Young's Modulus E=3.5 GPa, Poisson's ratio (nu = 0.35, graphene, E=200 GPa (back calculated using rule of mixtures from experimental data), nu = 0.16, rubber coating: E= 1.0 GPa, nu = 0.4. All analyses were performed using Digimat® (MSC software). The 3D simulations were performed in ABAQUS® while the random particle generations was done in Digimat®. Figure 13 shows the comparison of experimental results with numerical predictions. Overall good agreement in experimental and numerical predictions were observed.

Conclusions:

An efficient joining technique that can inherit the advantages of both the bonded (light-weight, elimination of holes and associated stress concentrations) and bolted (ease of repair and re-assembly) techniques while being acceptable to available industrial and assembly line processes is of immediate interest for a wide range of applications. This project deals with the development of 'active adhesives' for dissimilar material joining that would allow reversible bonding of joints through 'targeted heating' of the adhesives. This would allow for inheriting all the network benefits of bonded joints along with ease of re-assembly/dis-assembly, in-situ repair and recovery of micro-cracks or damage over the service life of the joint.

The ‘active adhesives’ were developed by incorporating electrically conductive GnP in a thermoplastic adhesive. The percolated of graphene particles (at less than 2 wt%) can couple with microwave radiations via non-contact methods, thereby increasing the adhesive temperature beyond the required processing temperature. This would allow the adhesive to melt and flow over adherends, and upon curing can lead to a structural bond. Conversely, the microwave/graphene coupling can be used to dis-assemble and repair the joints and resulting components.

During the past year considerable progress was made to develop active adhesive technology for multi-material joints in lightweight structures. The mechanical properties (tensile, strain rate effects on tensile, and impact), thermo-mechanical behavior and processing parameters of both pristine and GnP modified nylon-6 adhesives were experimentally characterized. Additionally, dissimilar material lap-joints with combinations of adherends including Al, steel and composites were manufactured using both pristine and GnP modified nylon-6 adhesives. Experimental lap-shear tests on resulting joints were also performed. Furthermore, a cost-effective, out-of-autoclave liquid molding process was used to manufacture composite adherends with high temperature resistance to achieve the adhesive processing temperatures without affecting or degrading the adherent properties. In parallel, numerical simulations at the nano-scale to obtain effective/homogenized properties of the active adhesives were developed. Experimentally validated numerical simulations for structural lap-joints are also being developed, with the aim that the experimentally validated simulations would allow to extrapolate the material and structural behavior outside the experimental matrix studied in this work.

Experimental characterization of both pristine and GnP modified adhesive showed improvement in tensile and flexural modulus. Reduction in tensile strengths and impact strengths were observed. This reduction was expected as the GnP used was ‘as-received’ and not chemically functionalized to be compatible with the host polymer. This was done by ‘design’ to obtain the lower bound of performance prior to chemical functionalization. In spite of the lack of functionalization, at the structural/joint-level, the lap-shear strengths significantly improved with increasing GnP content.

Overall, the progress and results from this work show great promise in use of GnP reinforced thermoplastics as ‘active’ adhesives for dissimilar material joining. Incorporation of novel non-destructive evaluation tools in experimental characterization and use of such accurate measurements in numerical simulations can provide an excellent tool for ‘rational’ development of design tools and elimination of ‘trial-and-error’ approach. Additional work on optimizing the GnP processing parameters including chemical functionalization, detailed experimental characterization of both adhesives and joints, study of activation, dis-assembly and in-situ repair would allow to fully understand and exploit the benefits offered by these novel active adhesives for a wide range of applications.

Publications / Presentations:

- Haq M. (August 2014) "Active, Tailorable Adhesives for Dissimilar Material Bonding, Repair and Assembly" Presented to U.S. Council for Automotive Research, Southfield, MI.
- Koricho EG, Haq, M, Khomenko A, Drzal LT. (November 2014) "Thermo-mechanical properties and strain-rate dependency of graphene reinforced thermoplastic materials and joints". Manuscript submitted to "*Composites Science and Technology*" (unpublished as of the date of this report).

References:

- N/A Verna, E.; Koricho, E.G.; Cannavaro, I.; Brunella, V.; Belingardi, G.; Roncato, D.; Martorana, B.; Lambertini, V.; Neamtu, V.S.; Ciobanu, R. (2013). "Adhesive joining technologies activated by electro-magnetic external trims." *International Journal of Adhesion and Adhesives* (46); pp. 21-25.
- Rafael, C.S.; Recardo, L.A.; Antònio, F.A.; Marco, A. (November 2007). "Mechanical characterization of glass/epoxy composite material with nanoclay." *Proceedings of COBEM*, *19th International Congress of Mechanical Engineering*, Brasilia, DF, pp. 1-8
- Weibull, W. J. (1951). "A statistical distribution function of wide applicability." *Journal of Applied Mechanics* (18); pp. 293-297.
- Haq, M.; Liu, W.; Patterson, E.A.; Drzal, L.T. (June 2011) "A Computational Approach to enhance the understanding of Novel, Hybrid Graphene/Rubber Nanocomposites." *Engineering Mechanics Institute (EMI) Annual Conference*; Boston, Massachusetts.

Figures and Tables:

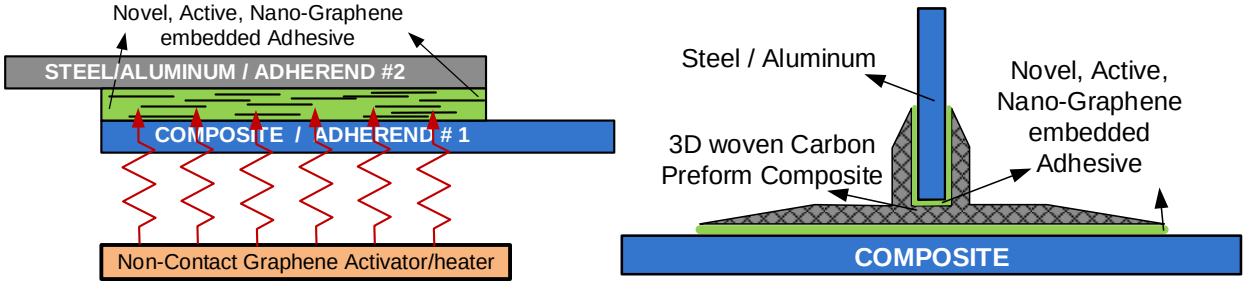

Figure 1. LEFT: Schematic of the concept shown for in-plane joints, RIGHT: out-of-plane joints.

Figures Continued on Next Page

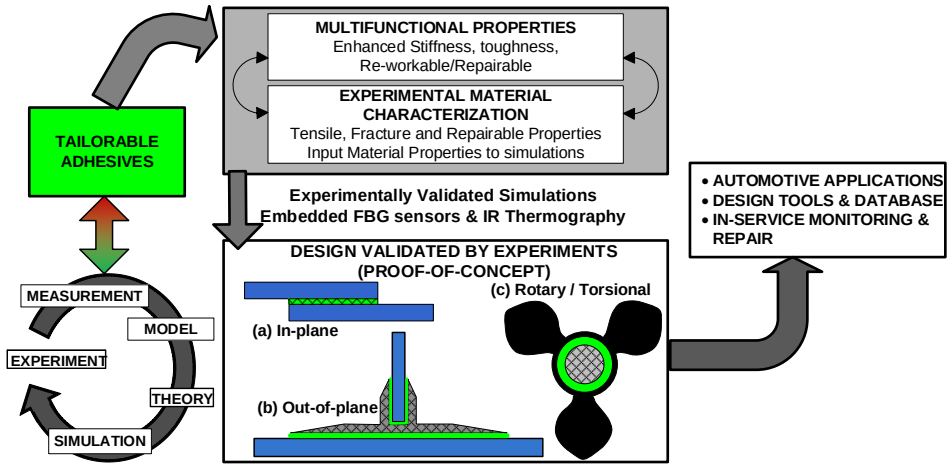

Figure 2. Schematic of Overall Approach.

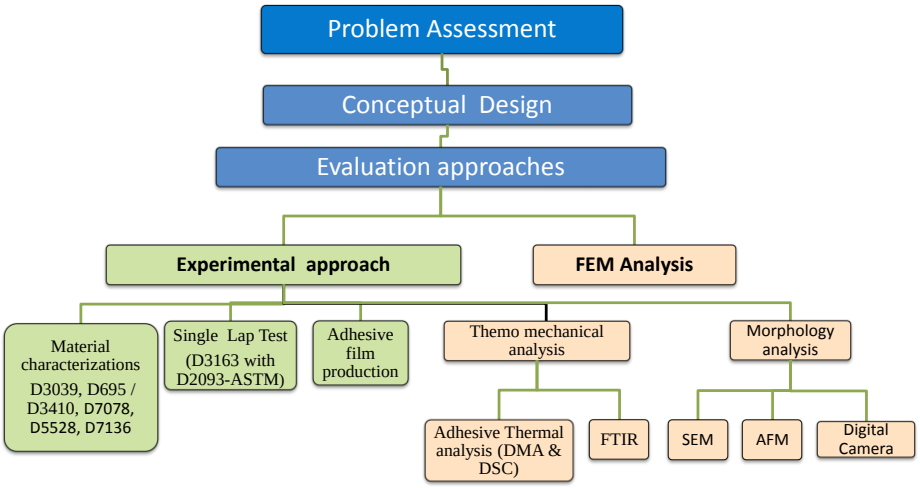

Figure 3. Work-flow adopted to develop active adhesives.

Figures Continued on Next Page

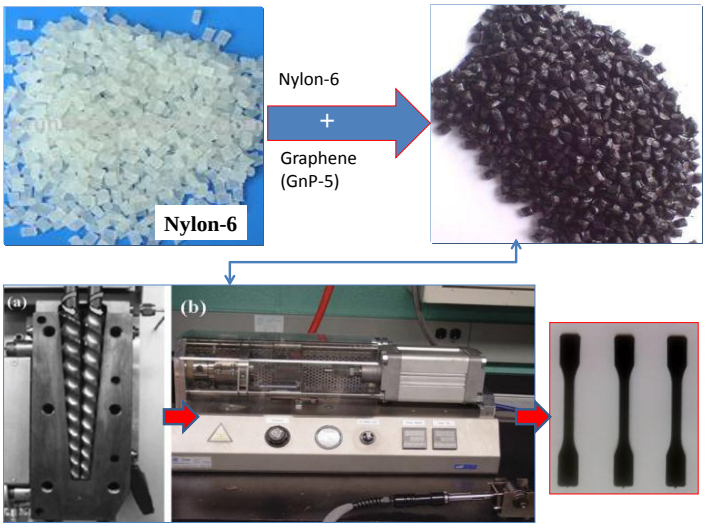

Figure 4. Manufacturing process of pristine and GnP-modified nylon-6 coupons.

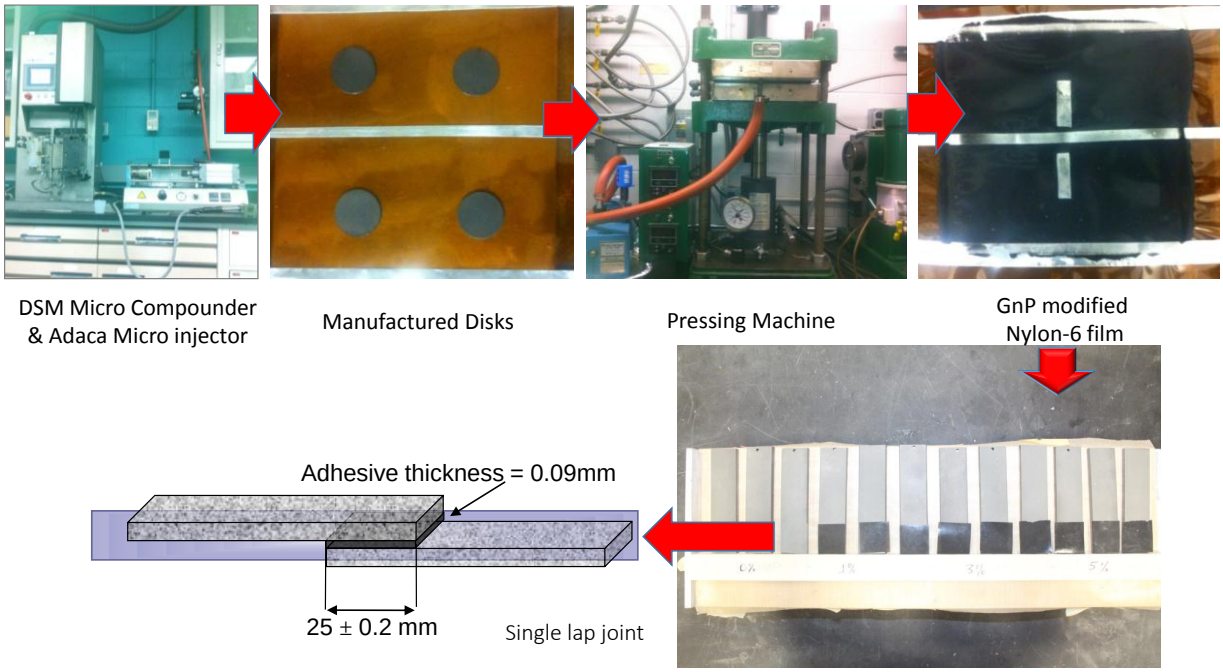

Figure 5. Processing of 'pristine' and 'GnP-modified' nylon-6 films.

Figures Continued on Next Page

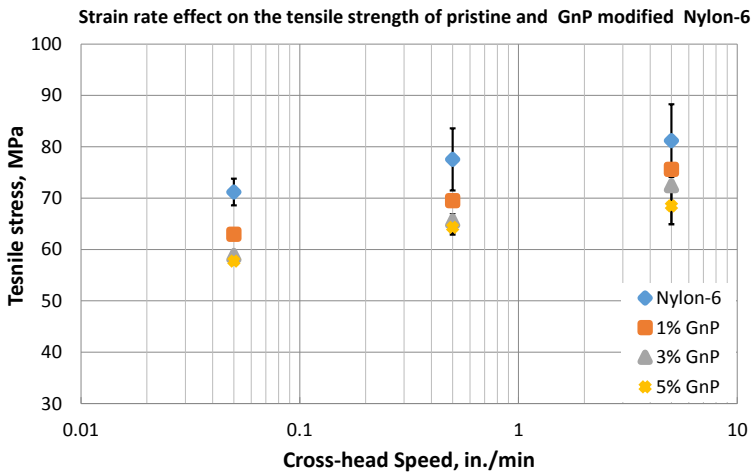

Figure 6a. Strain rate effect on 'pristine' and 'GnP-modified' nylon-6: Tensile Strength.

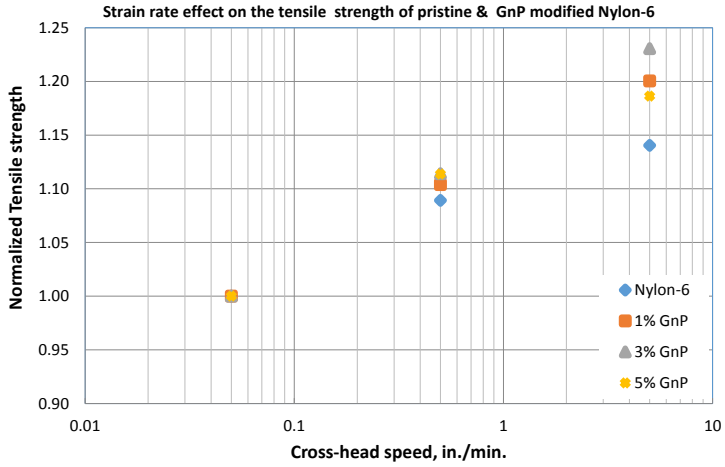

Figure 6b. Strain rate effect on 'pristine' and 'GnP-modified' nylon-6: Normalized Tensile Strength.

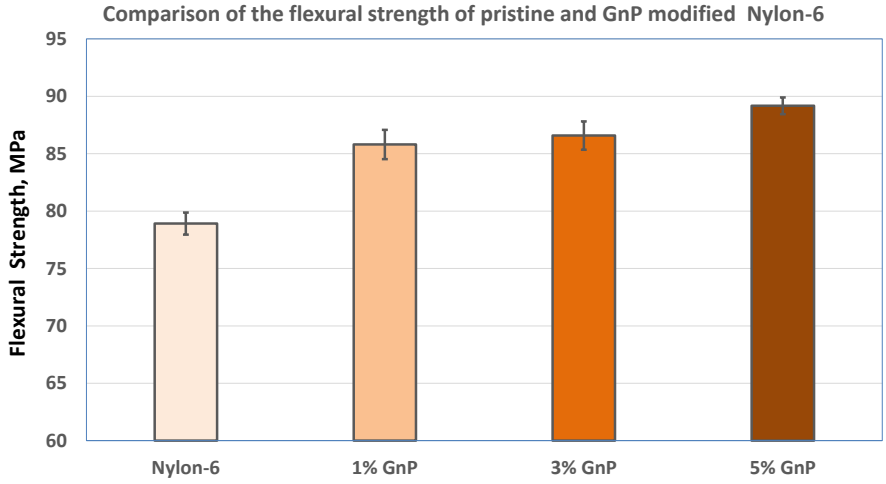

Figure 7a. Comparison of flexural properties of 'pristine'and 'GnP-modified' nylon-6: Strength.

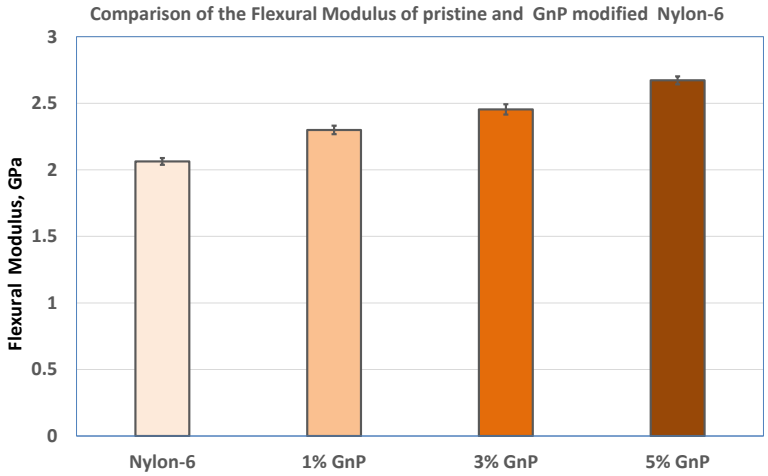

Figure 7b. Comparison of flexural properties of 'pristine' and 'GnP-modified' nylon-6: Modulus.

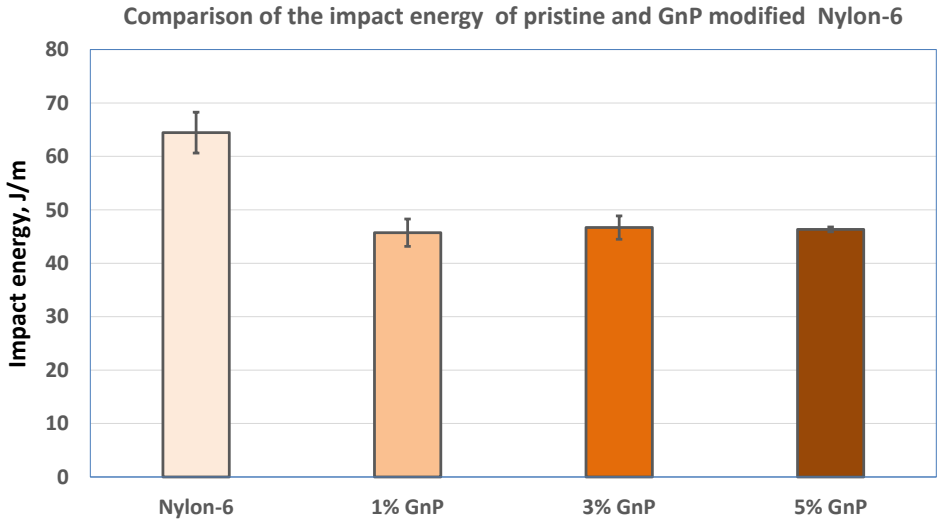

Fig. 8. Comparison of the impact energy in joules per meter (J/m) of pristine and GnP modified nylon-6.

Figures Continued on Next Page

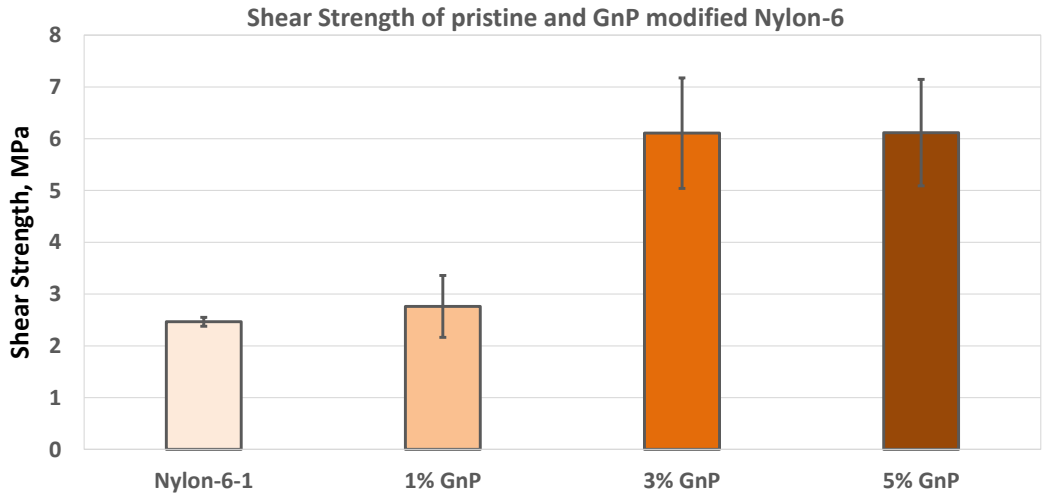

Figure 9. Comparison of shear strengths of 'pristine' and 'GnP-modified' nylon-6.

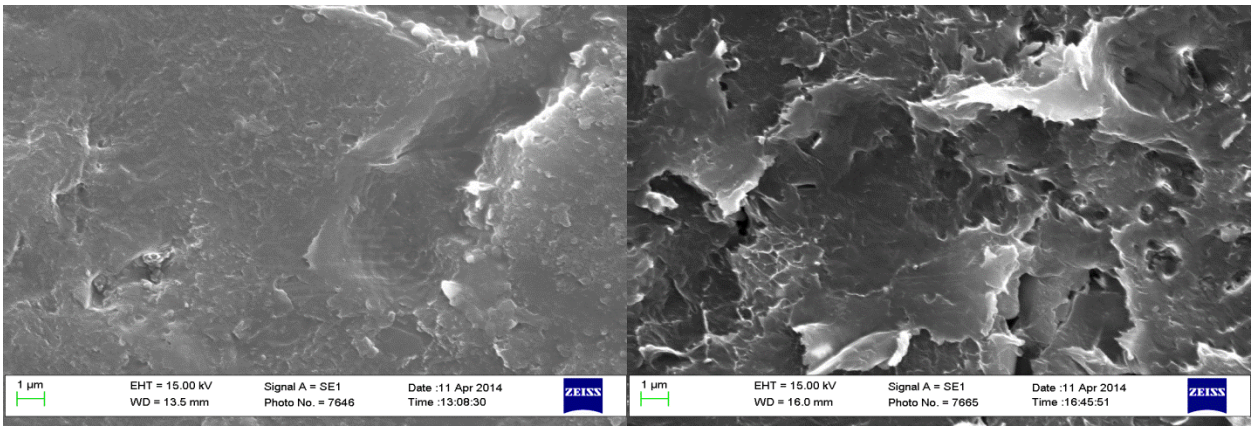

0 wt.% GnP **3 wt.% GnP**

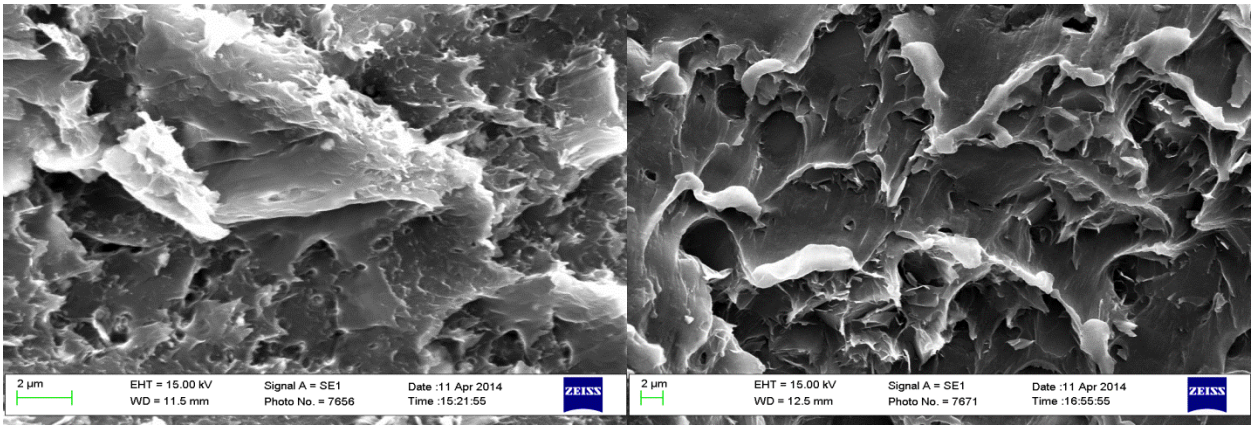

1 wt.% GnP **5 wt.% GnP**

Figure 10. Fracture surface observations, all magnifications at 5000X

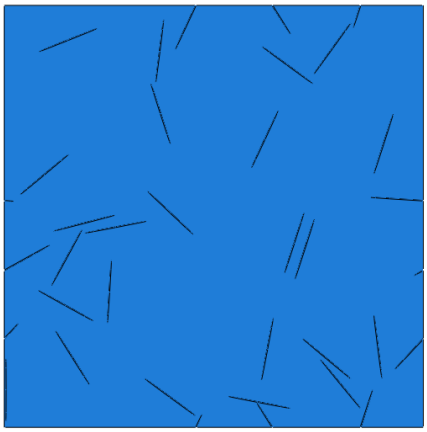

Figure 11. 2D Representative Volume Element (RVE).

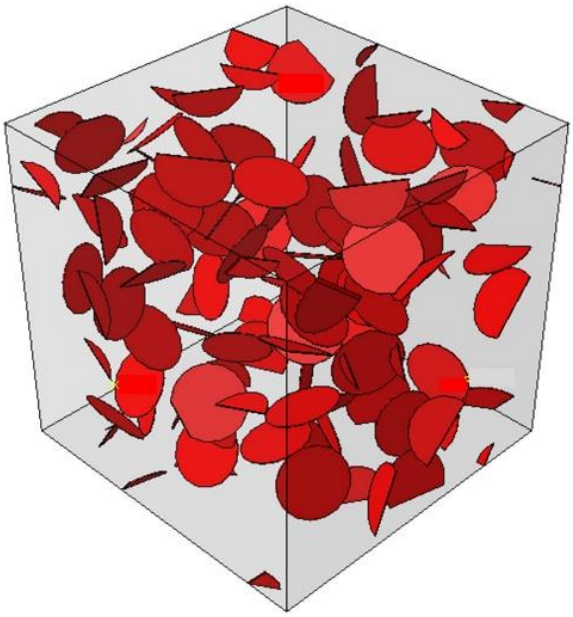

Figure 12. 3D (RVE).

Figures Continued on Next Page

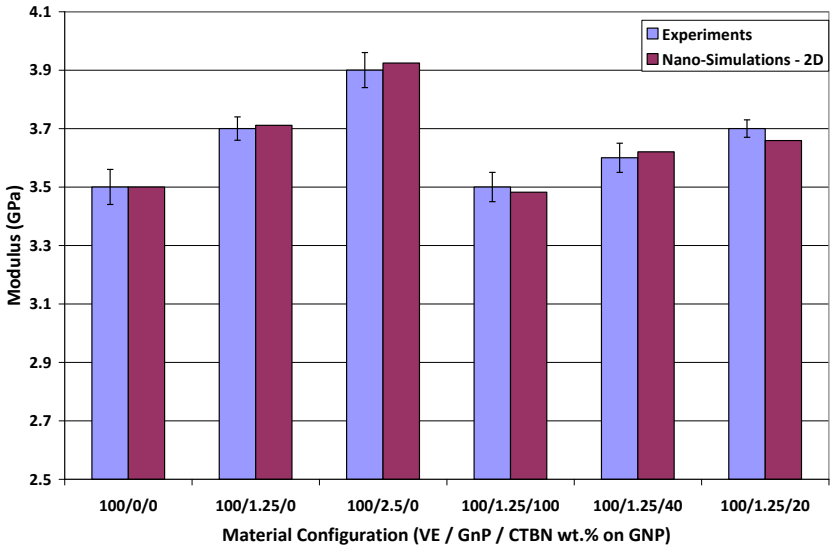

Figure 13. Comparison of Experimental Modulus (E_{11}) with Numerical Predictions.

This Page Intentionally Blank

AVPTA Technology Focus Area 2: Lightweight Structures & Materials

Breakthrough Techniques for Dissimilar Material Joining – Laser-Assisted Joining Process for Aluminum and Carbon Fiber Components

DOE-VTO Lead: William Joost
TARDEC TFA Lead: Dr. Richard Gerth

Principal Investigator:
Adrian S. Sabau

Oak Ridge National Laboratory (ORNL)
1 Bethel Valley Road; Oak Ridge, TN 37831

with
David C. Warren
Oak Ridge National Laboratory (ORNL)
1 Bethel Valley Road; Oak Ridge, TN 37831

Start: Q1FY14
Projected Completion: Q4FY15

Objective:

- To demonstrate a breakthrough laser structuring technology for joining carbon fiber polymer composites (CFPC) and aluminum (Al) components.

Strategic Context:

- The immediate application target for this technology is the Combat Vehicle Prototype (CVP) because it can join thick aluminum with composite resins. No specific CVP design application has yet to be identified.
- The technology supports the TARDEC Strategy enabling new capability in cost and technically effective adhesively bonded composite joints.

- Follow-on activities may include further AVPTA interest to investigate increasing joint strength, reducing cost and / or developing adhesives for other material combinations.
- TARDEC-specific follow-on will depend upon project success but is expected to include joint ballistic shock evaluation.
- Two US-based automotive Original Equipment Manufacturer (OEM) Tier I suppliers that are project participants have the ability to commercialize this technology. This technology is attractive because the use of lighter weight, adhesively joined materials in automotive applications would reduce fuel consumption and the production of greenhouse gasses. Enabling the joining of these lightweight substrates in the process being developed in this work would give credibility to incorporating them in a larger structure for automotive testing. Issues related to the process scale-up will be addressed by the industrial partners. Several steps toward commercialization include:
  - Tier 1 supplier identified materials that are commonly used in the automotive industry and reviewed industrial needs to ensure that the materials used in this project would ensure a straightforward pathway to dissemination of the joining technology developed in this project.

Accomplishments:

- Completed Materials that are commonly used in the automotive industry were selected for this project based on a review of industrial practices conducted at Cosma, Plasan and 3M to ensure a straightforward pathway to dissemination and application of the joining technology that is being developed in this project.
- ORNL measured the single-lap shear strength for baseline specimens.
- Diffuse reflectivity data over a range of wavelengths were obtained for the CFPC and for bare carbon fiber. The data indicated that the optical properties of the CFPC itself do not vary strongly with the wavelength over the range of wavelengths available, while the resin affects the optical properties of the CFPC at wavelengths higher than 280 nm.
- After 13 baseline specimens were joined at 3M using procedures for joining the Al and CFPC specified by 3M, ORNL tested the joint specimens and measured the baseline lap shear strengths.
- Laser structuring of Al 5182 specimens was successfully performed. High-resolution optical profiler images revealed that the surface roughness increased from 226 nm for the as-received surface to 392 nm for the laser interference structured surface.
- Laser ablation of the CFPC was performed with no apparent damage to the carbon fiber. The 3D Keyence optical microscope profiles of laser-ablated specimens showed that the resin rich, composite surface layer had been removed and carbon fibers had been exposed on both the top surface and the side surfaces, creating an ideal bonding surface for the adhesive.
- The increases in the measured lap shear strength compared to the cleaned only baseline and the abraded and cleaned baseline were estimated to be between 560 and 750% and 20 and 54%, respectively.

Introduction:

The proposed technology will enable the increased use of both Al and carbon fiber composites in primary automotive structures. Body structure makes up a significant fraction of the weight of a vehicle and therefore represents a significant opportunity to reduce the weight of a vehicle. According to multiple analyses by the United States Council for Automotive Research, the U.S. Department of Energy, and ORNL, Al alloys have the potential to reduce component weight by 30–60%, and carbon fiber composites have the potential to reduce component weight by 40–70%.

To date, CFPC and Al 5000, 6000, or 7000 series components are joined by simply overwrapping the CFPC over the Al or using specially formulated adhesives coupled with extensive surface preparation techniques. Traditional industrial techniques used to prepare Al surfaces for bonding include grit blasting, solvent wiping followed by abrading, and anodizing. The results from grit blasting and abrasion techniques are inconsistent; a more controlled process would be an improvement. In addition, these processes are empirical, employ several steps, and are labor-intensive surface preparation methods that are incompatible with the degree of automation required in automotive applications.

By using a laser structuring technique [1] prior to the adhesive bonding operation, the untreated smooth adhesive/composite interface of the Al and CFPC was replaced by a rough fiber-reinforced interface, which was expected to increase the bond strength of the CFPC/adhesive interface. Cosma will specify the joint configurations for development of this technology, focusing on carbon fiber/aluminum joints that they believe will be needed for future automotive component designs. The loading conditions and environmental stressors (i.e., corrosion conditions) will be those typically used for validation of those component subsystems.

Approach:

The untreated, smooth adhesive/composite interface between the Al and the CFPC was proposed to be replaced by a rough fiber-reinforced interface, which was expected to increase the bond strength of the CFPC/adhesive interface. The rougher surface would be created by using a laser structuring technique before the adhesive bonding operation.

Cosma supplied Al 5182 samples that were 1.5 mm gauge, 100 mm width, and 300 mm long. Larger sized samples will be provided as needed. Plasan supplied CFPC specimens with T700S carbon fiber and T83 resin (epoxy); the samples were 12 in. × 12 in., 4 plies thick, and 0/90 plaques. Three adhesives were selected for this project based on their compatibility with the Al alloy and the CFPC. The selection process took place at 3M. These adhesives were selected: DP460 (an epoxy), DP620 (a polyurethane), and DP810 (a low-odor acrylic).

A 10 hertz (Hz), Q-switched neodymium-doped yttrium aluminum garnet (Nd:YAG) laser (Quanta-Ray PRO 230, Spectra Physics) was used in this study. With only 10 nanoseconds (ns), the laser pulse duration is very short, creating an extremely high power above 100 megawattt (MW), resulting in greater than 1012 degrees Kelvin per

second (^{0}K/s) heating rates. The beam diameter was 8 mm. The fundamental emission with the wavelength of 1064 nm was transformed to 355 nm and 266 nm using nonlinear crystals. The maximum laser energy per pulse was 0.15 joules (J) at 355 nm and 0.038 J at 266 nm. Patterns can be dot-, line-, and ring-shaped [2–6]. A mechanical shutter selected the number of pulses was selected by a mechanical shutter. In some experiments, the laser pulse fluence was increased by using two identical focal lenses in each path of the split beam to focus laser beams from its original size of 8 mm to smaller sizes. Features of the structured surface morphology include:

- Size: 1–500 nm
- Density: 20–2,000/m^2
- Undulation spacing: 0.5–50 mm
- Structured area of 0.27 cm^2/shot
- Scanning speed: 10,000 lines at a time; 79 million dots at a time; up to 162 cm^2/min.

CFPCs were laser processed using both the one-beam (i.e., without the power interference) and two-beam laser interference setup; Al specimens were processed using the laser interference setup. After laser structuring, the Al and CFPC were joined using the adhesives supplied by 3M. 3M also recommended the procedures for joining the Al and the CFPC. Finally, ORNL tested different joint specimens to obtain the baseline shear lap strength.

Results and Discussion:

Cosma, Plasan and 3M reviewed industrial needs to ensure that the materials used in this project would ensure a straightforward pathway to dissemination of the joining technology developed in this project. These materials were selected:

- Al 5182;
- A CFPC of pre-preg T83 resin (epoxy) and T700S carbon fiber in a 0/90 layup; and
- Three adhesives: DP460 (an epoxy), DP620 (a polyurethane), and DP810 (a low-odor acrylic).

The 5xxx Al alloy series is being used in inner vehicle body structure and it does not age like Al 6xxx series. Plasan has several parts in production using this T700S/T83 CFPC. Using this CFPC material would reduce the mass in more components.

Optical Properties:

Optical measurements were performed on several samples in order to select laser wavelengths that would be appropriate for processing CFPC. Specifically, the absorption properties of the resin were sought. The desired laser ablation wavelengths for the CFPC

were those at which the resin would exhibit high absorption while absorption by the carbon fiber is minimized. The following optical measurements were conducted: (1) normal-

incidence generalized ellipsometry, (2) diffuse reflection, and (3) spectroscopic ellipsometry.

The following samples were studied:

- Carbon fiber composite panel (which is the CFPC, including resin and fiber);
- Carbon fiber modified such that the resin content would be reduced or eliminated (stretched with and without sizing); and
- A carbon fiber sample mounted in an epoxy specimen mold, but epoxy was not allowed to surround the fiber tows.

Diffuse reflectivity data, which is shown in Figure 1, indicate that the optical properties of the carbon fiber itself do not vary strongly in the range of the wavelengths studied. Studies of the CFPC showed fairly consistent absorption above 280–300 nm, but a significant absorption (the converse of diffusivity) below 280 nm. Based on this reflectivity data alone, for an effective ablation of the resin, a laser wavelength of 266 nm be is recommended. However, the variation of the maximum laser power with the wavelength should be taken into consideration.

Baseline Metrics:

After the baseline specimens were joined at 3M Corp., ORNL tested different joint specimens to obtain the baseline shear lap strength in pounds per square inch (psi) (Figure 2). The best results were observed using the DP460NS adhesive, specifically for the cross-ply CFPC joined with Al which is the primary focus of this project.

Surface Morphology of Al and CFPC Surfaces after Laser Processing:

Laser structuring of Al 5182 specimens was successfully attained. Also, laser ablation of CFPC was attained with no obvious damage to the carbon fiber themselves. Both CFPC and Al specimens were laser structured using the interference technique in the as-received condition (i.e., without any additional surface preparation steps). A Wyko™ 9100 vertical scanning interferometer was used to measure the height of the specimen surfaces. Figures 3 and 4 show the profilometry data and the analyzed surfaces of the as-received surfaces and of the surfaces structured using the laser interference technique, respectively. High-resolution optical profiler images revealed that the surface roughness increased from 226 nm for the as-received surface to 392 nm for laser interference structuring surface.

Optical micrographs and 3D Keyence optical microscope scanning depth profiles for the CFPCs are shown in Figures 5 and 6 for the as-received condition and for the laser-ablated condition. The 3D Keyence microscope profile of the laser-ablated specimen shows that the carbon fibers are directly exposed on both the top surface and on side surfaces, creating an ideal bonding surface for the adhesive.

Several joint specimens were made, as shown in Table 1, in order to assess the effect of the laser-structured surface preparation over conventional surface preparations. After they were laser structured, ten CFPC coupons were joined with either cleaned Al coupons or with cleaned laser-structured Al coupons. All the Al coupons that were joined with laser-structured CFPC coupons were only cleaned with ethanol (i.e., they were not abraded).

Conclusions:

Laser structuring of the Al surface was demonstrated. High-resolution optical profiler images revealed that the surface roughness increased from 226 nm for the as-received surface to 392 nm for the laser interference structuring surface.

Laser ablation of the carbon fiber composite was demonstrated. Optical micrographs and 3D Keyence microscope scanning depth profiles for the CFPCs show that the carbon fibers are directly exposed on both the top surface and on the side surfaces, creating an ideal bonding surface for adhesives. A wide range of adhesive compounds was selected, allowing the study of adhesive effect on joint quality and maximizing the chances of success. ORNL measured the shear lap strengths of baseline joint specimens.

A dramatic increase in the lap shear strength compared to the baseline data was observed for the laser-processed specimens, demonstrating the proof of concept for the use of laser structuring and/or ablation technology for surface preparation of both CFPC and Al coupons prior to adhesive joining.

Publications / Presentations:

- Sabau, A. S.; Chen, J.; Jones, J. F.; **Hackett, A.;** Jellison, G. D.; Daniel, C.; Warren, C. D.; Rehkopf, J. D. (March 2015) “Surface Modification of Carbon Fiber Polymer Composites After Laser Structuring”. To be presented by invitation at the 2015 TMS Annual Meeting and Exhibition, Orlando, FL.
- Chen, J.; Sabau, A. S., Jones, J. F.; **Hackett, A.;** Daniel, C.; Warren, C. D. (March 2015) “Aluminum Surface Texturing by Means of Laser Interference Metallurgy”. In preparation to be submitted for presentation to the 2015 TMS Annual Meeting and Exhibition, Orlando, FL.

References:

- Daniel, C.; Mücklich, F.; Liu, Z. (2010) “Periodical micro-nano-structuring of metallic surfaces by interfering laser beams.” *Appl. Surf. Sci.***,** *208–209*, pp. 317–321.
- Daniel, C.; Mücklich, F. (2004) “Quantification of periodical surface structures by white light interferometry.” *Prakt. Metallogr*., (*41*:6), pp. 277–285.
- Mücklich, F.; Daniel, C.; Lasagni, A.; Yu, F. (2004) “Direct Surface Patterning Induced by Interfering Laser Beams.” *Mat. Res. Soc. Symp. Proc.***,** Vol. EXS-2, M11.1.

- Mücklich, F.; Lasagni, A.; Daniel, C. (2005) "Laser Interference Metallurgy—Periodic Surface Patterning and Formation of Intermetallics." *Intermetallics*, (13:3–4), pp. 437–442.
- Mücklich, F.; Lasagni, A.; Daniel, C. (2006) "Laser Interference Metallurgy—using interference as a tool for micro/nano structuring." *Int. J. Mater. Res.*, (97:10), pp. 1337–1344.
- Daniel, C. (2006) "Biomimetic structures for mechanical applications by interfering laser beams—more than only holographic gratings." *J. Mater. Res.*, (21), pp. 2098–2105.

Figures and Tables:

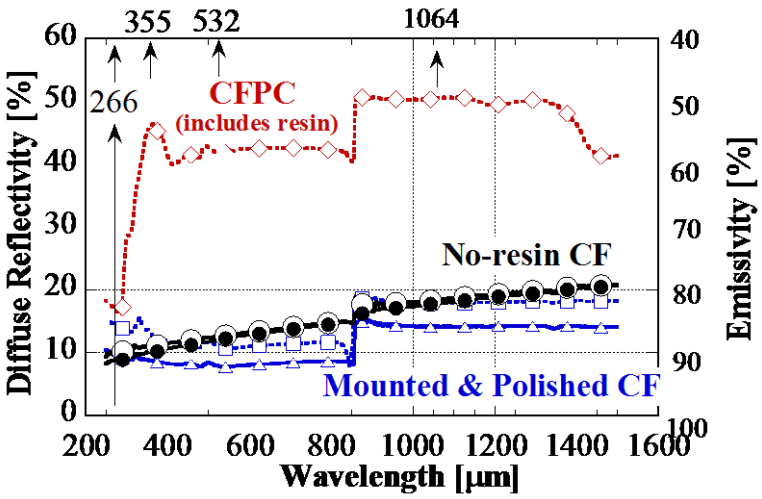

Figure 1. Diffuse reflectivity data for the CFPC samples considered showing variations in the percentages of diffuse reflectivity and emissivity for over several wavelengths in microns (μm).

Figures Continued on Next Page

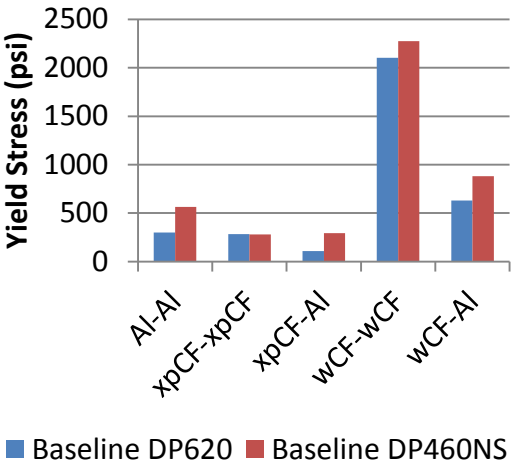

Figure 2. Baseline single-lap shear results for DP620 and DP460 adhesives. (xpCF—cross-ply carbon fiber composite; wCF—woven carbon fiber composite).

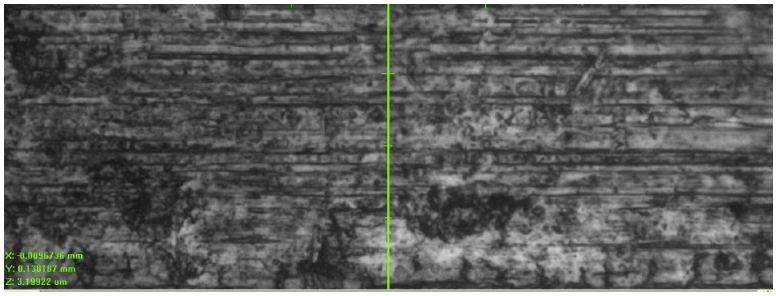

(a)

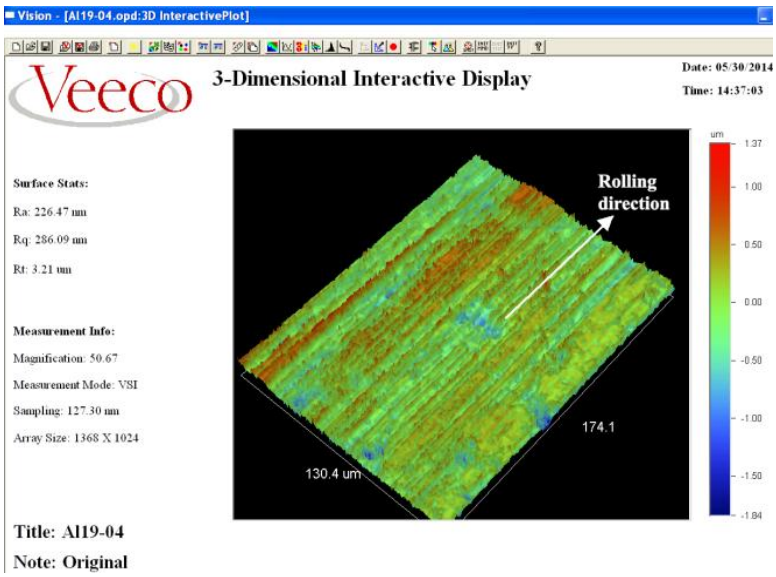

(b)

Figure 3. Profilometry data for an as-received, unprocessed Al specimen: (a) optical micrograph showing the analyzed region (horizontal striations are due to rolling) and (b) profilometry data indicating the rolling direction.

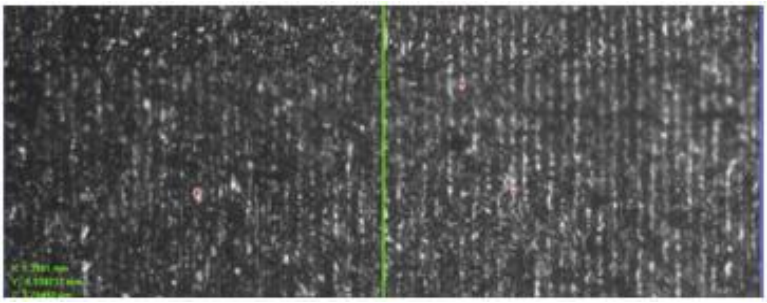

(a)

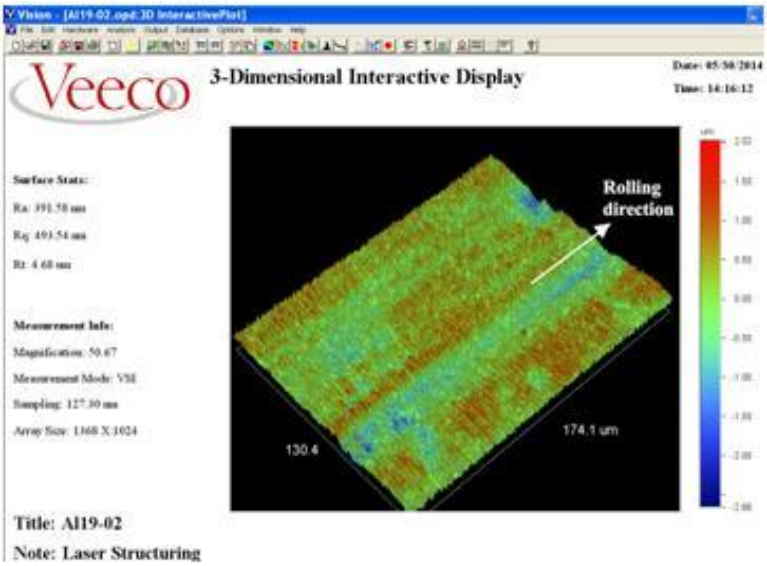

(b)

Figure 4. Profilometry data for a laser-structured Al specimen: (a) optical micrograph showing laser-induced striations and (b) profilometry data also showing laser-induced striations perpendicular to the rolling direction.

Figures Continued on Next Page

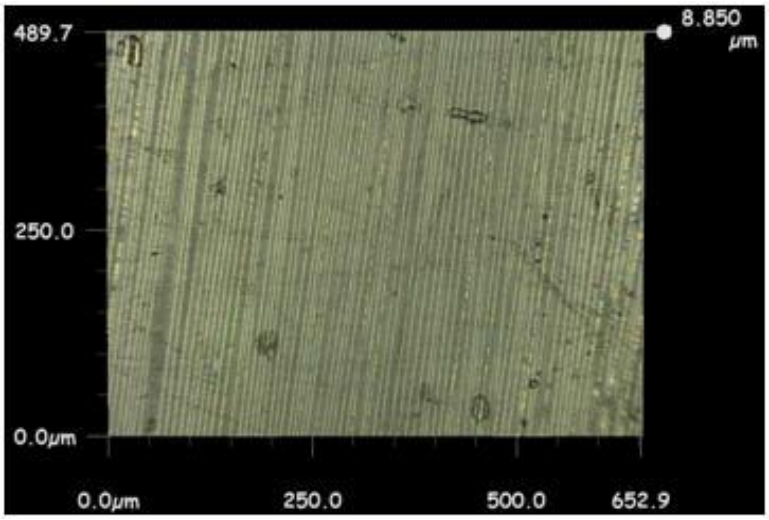

(a)

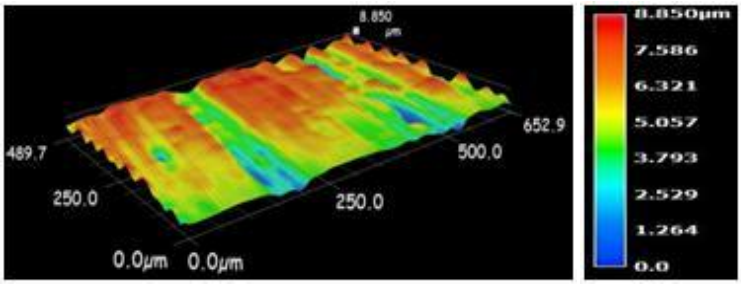

(b)

Figure 5. Data for CFPC specimen in the as-received condition: (a) micrographs and (b) 3D scanning depth profile showing that the surface roughness is mostly less than 8.85 µm.

Figures Continued on Next Page

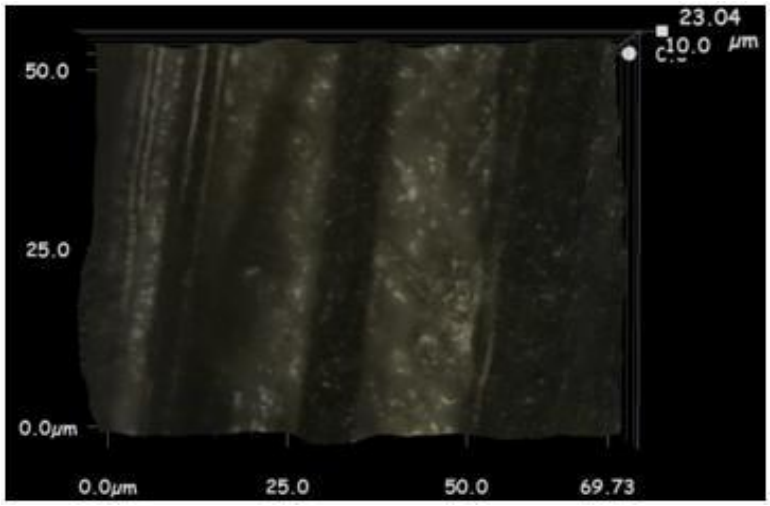

(a)

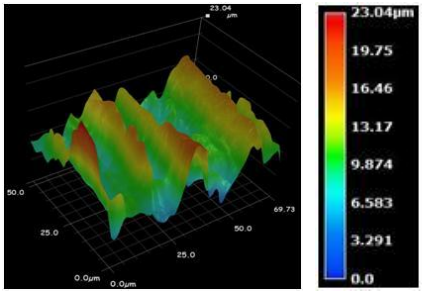

(b)

Figure 6. Surface analysis for a laser-ablated Plasan CFPC specimen: (a) micrographs and (b) 3D scanning depth profile showing that the ablated thickness is 23 µm.

Joint specimens	Preparation of CFPC	Preparation of Al
6	laser structured (not cleaned)	ethanol cleaned only (not abraded)
4	laser structured (not cleaned)	laser structured (not cleaned)
6—baseline	ethanol cleaned only (not abraded)	only cleaned (not abraded)
6—baseline	abraded and ethanol cleaned	abraded and ethanol cleaned

Table 1. Joint specimens made to assess the effect of laser-structured surface preparation over conventional surface preparation.

CFPC	Al	Increase in lap shear strength with respect to "**cleaned only**" **(%)**	Increase in lap shear strength with respect to "**abraded and cleaned**" **(%)**
CFPC ablated	cleaned only (not laser processed)	643–753	34–54
CFPC ablated	laser structured	563–706	20–46

Table 2. Increase in lap shear strength of laser-processed material joints with respect to "cleaned only" baseline and "abraded and cleaned" baseline.

AVPTA Technology Focus Area 3: Energy Recovery & Thermal Management

Thermoelectric Generator (TEG) Enabled Engine (Gentherm)

DOE-VTO TFA Lead: Gurpreet Singh
TARDEC TFA Lead: Mary Goryca

V. Jovovic (Principal Investigator)[1], D. Lock[1], C. Maranville[2], C.Haefele[3], M.Miersch[4]

[1]Gentherm Inc.
5462 Irwindale Ave.
Irwindale, CA 91706
Phone: (626) 593-4532
Email: Vladimir.jovovic@gentherm.com

[2]Ford Motor Company
Scientific Research Lab
Room 2417, MD 3083
201 Village Road
Dearborn, MI 48124

[3]BMW AG
Research and Innovation Center
Knorrstraße 147
80788 Munich, Germany

[4]Tenneco GmbH
Luitpoldstrasse 83
67480 Edenkoben, Germany

Subcontractors:
BMW: Palo Alto, CA and Munich, Germany
Ford Motor Company: Dearborn, MI
Tenneco GmbH: Grass Lake, MI and Edenkoben, Germany

Start: Spring 2008
Projected Completion: Ongoing

Objectives:

- A detailed production cost analysis for TEG for passenger vehicle volumes of 100,000 units per year and a discussion of how costs will be reduced in manufacturing.
- A five (5) percent fuel economy improvement by direct conversion of engine waste heat to useful electric power for light-duty vehicle application. For light duty passenger vehicles, the fuel economy improvement must be measured over the US06 cycle.
- Confirmatory testing of the hardware to verify its performance in terms of fuel economy improvement.

Strategic Context:

- To achieve improved energy efficiency and reduced emissions in advanced combustion engines for passenger / commercial and military ground vehicle applications.
- Build scaled-up thermoelectric generator (TEG) for TARDEC Bradley Fighting Vehicle (BFV).
  - Scale-up to practical device size, as most devices operate in the 10-100 kW range.
  - Designated space claim to fit on large track vehicle
- Component/system durability.

Accomplishments:

- Developed manufacturing processes for fabrication of TE materials.
- Developed manufacturing processes for fabrication of TE engines.
- Designed, built and tested TE cartridges.
- Scaled up manufacturing of cartridges.
- Developed models of cartridge and TEG, integrated these in vehicle.
- Experimentally confirmed cartridge model
- Designed LDV and HDV generators.
- Scaled up TEG fabrication concept by developing mass production design and tooling
- Bench tested partial LDV TEGs.
- Developed test tools.
- Developed and installed materials manufacturing tools.

Introduction:

Rising levels of CO2 in the atmosphere are driving stricter vehicle emission regulations aimed at reducing CO2 generation or providing equivalent fuel efficiency improvements. Engine waste heat recovery strategies are used to manage engine or

transmission oil temperatures in order to minimize friction or to convert portions of waste heat directly into kinetic or electrical energy.

This project focuses on converting exhaust gas thermal energy into electric power. The converter is a solid state device – Thermoelectric Power Generator (TEG). The first objective of this program is to design and implement TEG devices which demonstrate 5% FEI for passenger vehicles. Demonstrating scalability of this design by building and testing a TEG for a Bradley Fighting Vehicle (BFV) for TARDEC is the second objective. The ratio of the engine sizes, and thus the TEG size, for the BFV and passenger vehicles is roughly 20:1.

Approach:

The team is led by Gentherm and structured to follow a traditional automotive supply chain hierarchy. Figure 1 shows the cartridge, the power conversion device developed by Gentherm utilizing Gentherm's new technology of manufacturing thermoelectric materials. Gentherm's goal is to optimize the design of this device by maximizing power output and minimizing manufacturing cost. Products of this development are the cartridge and accompanying performance model. The cartridge (Figure 1) is the fundamental building block, a fully contained power generation device, which can be used in various configurations to design Thermoelectric generators. The role of the tier 1exhaust supplier, Tenneco, is to design and build the complete thermoelectric power generation unit. Tenneco is applying technologies developed in packaging catalytic converters, particulate filters and other exhaust components. Tenneco uses 1D and 3D modeling tools in their design process to minimize the risk of mechanical failures and to optimize the number of cartridges and TEG installation position along the exhaust line. Products of Tenneco's development are the TEG and its 1D performance model. OEMs Ford and BMW North America (BMW) have advisory roles and act as the end customer. In the design process, the OEMs define the vehicle level constraints and analyze the vehicle level performance of the device. In this program NREL has been tasked to perform LDV TEG testing and provide independent confirmation of device performance.

In addition to developing the demonstration TEG platform, the team's long term goal revolves around developing a low cost manufacturing process while improving thermoelectric material performance. In this portion of process Gentherm acts as the process developer while The California Institute of Technology (Caltech) has the role of analyzing fundamental material properties and developing future materials.

Results and Discussion:

The objective of this program is to address the barriers to the widespread market adoption of thermoelectric power generation. This includes the production readiness of TE materials and generators, the underfloor exhaust system bypass valve, gas and liquid heat exchanger integration with the TEG, and the power management strategy for insertion of electrical power onto the vehicle bus.

To fulfill the requirements of this program Gentherm has developed methods of manufacturing TE elements which have the potential of reducing overall device cost. To increase our process throughput, Gentherm has used DOE funds to purchase and install additional powder handling and pressing equipment, doubling the process development capacity. In this program, we are addressing the reduction of TE material manufacturing cost as a parallel activity to working with current production materials required to build TE devices. Basic process parameters are defined and today we have stable processes used to manufacture metalized net shaped TE materials. Our cost studies indicate a significant reduction of the manufacturing cost as shown in Figure 2. Normalizing to cost per kg of TE materials we see that our process results in an approximate 30% reduction of the overall cost when compared to the process in which disks of TE materials are metalized and cut to size.

Process stability is monitored by measuring basic material properties such as Seebeck, electrical conductivity, thermal conductivity and calculating the resulting non-dimensional figure of merit, ZT. This data is used as reference in collaborative work with Caltech and analysis of material properties as a function of the starting materials purity, chemical composition, processing temperatures, etc. In summary, the Caltech group has developed a methodology which is required to better understand N-type CoSb3 based materials. Through systematic analysis of material structure and measured properties they were able to develop material phase diagrams and characterize the electronic structure of these materials. The end result is better control of the materials' ZT as shown in Figure 3. In addition, the ZT values demonstrated by the Caltech team are 10-20% higher than those produced by materials manufactured at Gentherm.

The goal of this program is to develop a TE device concept which can be designed as a scalable system and have power output in the range from approximately ½ to 2 kW. The solution that was developed is the TEG Cartridge shown in Figure 1. This device consists of internal (cold side) and external (hot side) heat exchangers, closely integrated with functional TE materials. The performance of this device shows improvement over that of the previous generation presented in our 2013 report. Tests indicate an additional 10-15% improvement in performance of the cartridge as a consequence of the improved assembly.

As a basic building block, the TEG cartridge is a self-contained power generation unit. This unit is used to build both light duty vehicle TEGs with 10-12 TEG cartridges and a heavy duty vehicle TEG system with 56 cartridges. The power generation of these systems is 500W and 1.5kW, respectively. The complete design of the light duty TEG system is shown in Figure 4. The system is developed by Tenneco and consists of a central canning section used to place ten cartridges, bypass line and two control valves controlling the flow of gas to the TEG. Soft tooling for prototype level manufacturing of stamped components was manufactured by Tenneco and 20 sets of components were prepared for final assembly. A heavy duty vehicle package, design per TARDEC specifications for BFV was prepared in the period covered by this report. The system shown in Figure 5 illustrates the TEG canning designed to hold fifty six cartridges (4x14 units), radiators, fans, water pump and manifolds. This is a self-contained system with integrated cooling designed to fit in 2x2x4ft space allocated by TARDEC. All system components are prepared and are waiting for delivery of cartridges.

The program will conclude by building seven LDV TEG systems which will be tested on vehicles and in Gentherm, Tenneco and NREL laboratories. The HDV TEG will be tested at Tenneco and TARDEC. The ultimate goal of this program is to correlate these test results and results coming from vehicle level performance models in order to calculate the true benefits to fuel efficiency.

Conclusions:

The team is continuing to progress towards final delivery of working systems installed in vehicles.

- Method of producing high performance TE materials is developed and properties are verified in the experiments.
- Material cost model is developed and it will be verified with development of pilot scale equipment.
- Cartridge, as a building block, is designed, modeled and its performance is verified experimentally.
- The TEG system is designed and modeled. Experimental performance confirmation is expected in late 2014.
- Vehicle level integration is modeled. Experimental trials are scheduled for early 2015.

Presentations / Publications:

- *Waste heat recovery in passenger cars* Michael Mirsch, March 31, 2014, presentation at the VDI conference, Dusseldorf Germany.

Figures and Tables:

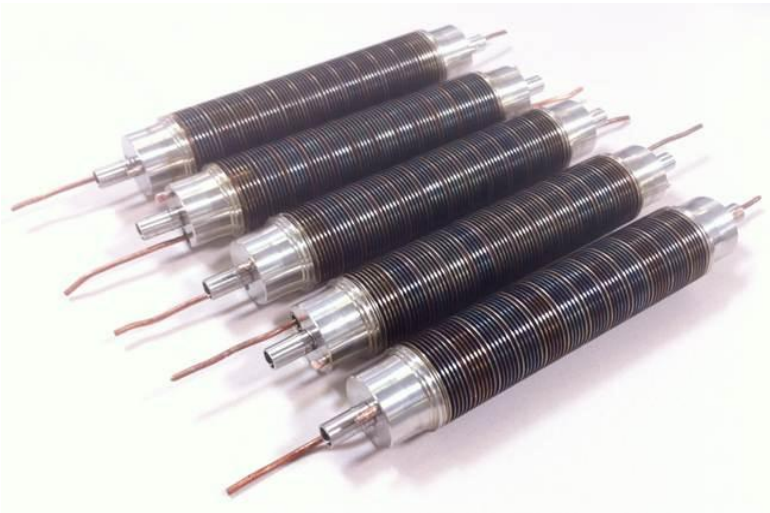

Figure 1: Thermoelectric power generation device – cartridge.

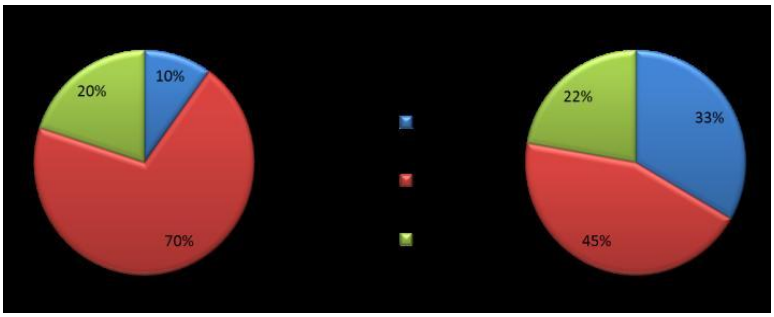

Figure 2: Comparison of manufacturing cost breakdown for traditional TE manufacturing process as compared to new Gentherm process.

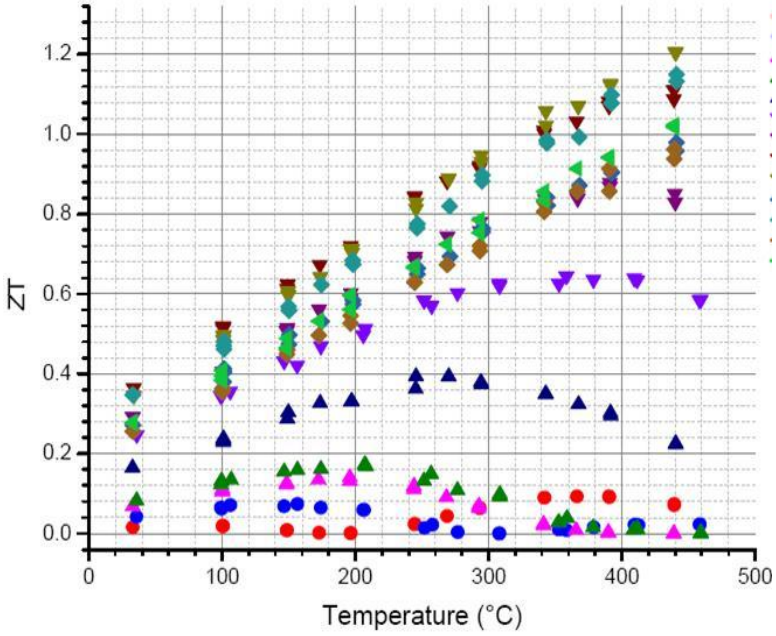

Figure 3: ZT values of n-type Skutterudite materials prepared at Caltech. Variations in ZT values demonstrate ability to control dopant and impurity levels and by doing so vary ZT.

Figures Continued on Next Page

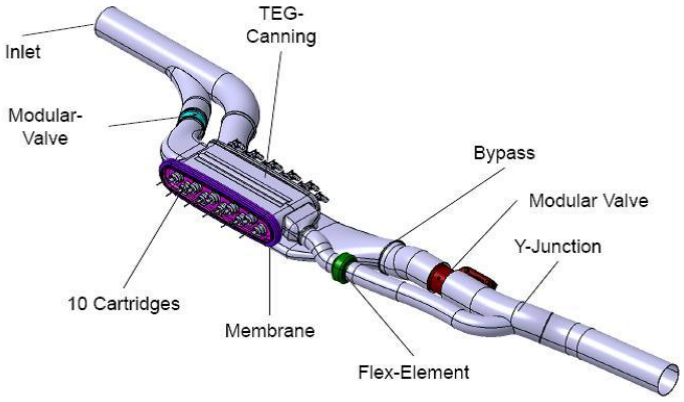

Figure 4: Design of LDV TEG system designed by Tenneco.

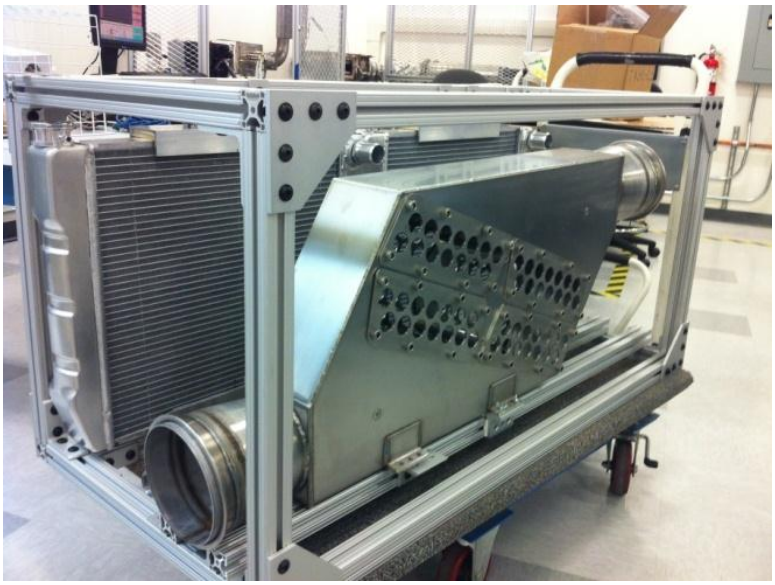

Figure 5: BFV test TEG device in a frame.

This Page Intentionally Blank

AVPTA Technology Focus Area 3: Energy Recovery & Thermal Management

Thermoelectric Generator (TEG) Enabled Engine (GMZ)

DOE-VTO TFA Lead: Gurpreet Singh
TARDEC TFA Lead: Mary Goryca

Principal Investigator
Dr. Martin Cleary

GMZ Energy, Inc.
11 Wall Street
Waltham, MA 02453
Phone: (781) 996-3036 x261
E/M Address: mcleary@gmzenergy.com

Start: FY 2011
Projected Completion: Completed

Objectives:

- A detailed production cost analysis for TEG for passenger vehicle volumes of 100,000 units per year and a discussion of how costs will be reduced in manufacturing.
- A five (5) percent fuel economy improvement by direct conversion of engine waste heat to useful electric power for light-duty vehicle application. For light duty passenger vehicles, the fuel economy improvement must be measured over the US06 cycle.
- Confirmatory testing of the hardware to verify its performance in terms of fuel economy improvement.

Strategic Context:

- To achieve improved energy efficiency and reduced emissions in advanced combustion engines for passenger / commercial and military ground vehicle applications.
- Build scaled-up thermoelectric generator (TEG) for TARDEC Bradley Fighting Vehicle (BFV).
  - Scale-up to practical device size, as most devices operate in the 10-100 kW range.
  - Designated space claim to fit on large track vehicle

Accomplishments:

- Developed manufacturing processes for fabrication of TE materials.
- Developed manufacturing processes for fabrication of TE engines.
- Designed, built and tested TE cartridges.
- Scaled up manufacturing of cartridges.
- Developed models of cartridge and TEG, integrated these in vehicle.
- Experimentally confirmed cartridge model.
- Scaled up TEG fabrication concept by developing mass production design and tooling.
- Developed and installed materials manufacturing tools.

Introduction:

Rising levels of CO2 in the atmosphere are driving stricter vehicle emission regulations aimed at reducing CO2 generation or providing equivalent fuel efficiency improvements. Engine waste heat recovery strategies are used to manage engine or transmission oil temperatures in order to minimize friction or to convert portions of waste heat directly into kinetic or electrical energy.

This project focuses on converting exhaust gas thermal energy into electric power. The converter is a solid state device – Thermoelectric Power Generator (TEG). The first objective of this program is to design and implement TEG devices which demonstrate 5% FEI for passenger vehicles. Demonstrating scalability of this design by building and testing a TEG for a Bradley Fighting Vehicle (BFV) for TARDEC is the second objective. The ratio of the engine sizes, and thus the TEG size, for the BFV and passenger vehicles is roughly 20:1.

Approach:

This past year, GMZ's goal was to finalize their generator design, and focus on the manufacturing process of the thermoelectric material. Its goal was to optimize the design of this process to ensure that they could manufacture enough cartridges in the next year. However, this original plan was insufficient, and early in FY14 a need for a Corrective Action Plan (CAP) was already in place.

GMZ encountered issues with its manufacturing process, namely the material process was too slow when using ½" Half-Heusler disks, and wished to start manufacturing their thermoelectric material in 1" disks. This would increase their return of usable material by a factor of ~4 (2.3g vs 9.2g), but would have a greater chance of increased costs due to a botched process, as smaller batches were "safer" in terms of a successful process. This was talked over with DOE and TARDEC, and ultimately was decided to implement the CAP. The CAP worked exactly as intended, and GMZ made great strides in making up

lost time, and ultimately had no impact in terms of cost, as they stayed within the original cost estimate.

Conclusions:

GMZ completed its 1kW generator and delivered it to TARDEC in 1QFY15. Shortly after, GMZ announced that it would close its doors and exist solely as a shell corporation to for its investors to hold its patents. GMZ is currently working with DOE to work out the financial side of the unfinished project, but with the delivery of the 1kW TEG, TARDEC received its final deliverable and has no cost stake in the program at this time.

This Page Intentionally Blank

AVPTA Technology Focus Area 4: Alternative Fuels & Lubricants

Lubricant Formulations to Enhance Fuel Efficiency

DOE-VTO TFA Lead: Kevin Stork
TARDEC TFA Lead: Dr. James 'Jay' Dusenbury

Principal Investigator:
Allen S. Comfort

Force Protection
US Army TARDEC

Start: FY14
Projected Completion: Ongoing

Objective:

- To develop novel lubricant formulations that are expected to improve the fuel efficiency of, medium -duty, commercial and military vehicles by at least 2% (improvement based on comparative results from engine dynamometer testing, chassis dynamometer testing or test track, e.g., SAE J1321) without adverse impacts on vehicle performance or durability.

Strategic Context:

- Understand the lubricant parameters that effect fuel economy and their impact on durability.
- Demonstrate a battlefield fuel reduction and reduce the logistics burden
- Increase Power Density and Energy Efficiency resulting in increased vehicle range, endurance and operational tempo, while reducing the number of logistics convoys on the battlefield
- Reduce Life Cycle Costs by reducing fuel consumption

Accomplishments:

- Laboratory testing demonstrated:
  - Feasibility of engine and transmission lubricants improving Fuel Efficiency by 2.85%
  - Novel anti-wear / friction additives can reduce friction by 20% to 40%
  - Novel base oil for axle lubricant can improve Fuel Efficiency and wear performance compared to Original Equipment Manufacturer (OEM) factory-fill or military standard oil.

Introduction:

Significant fuel economy benefits can be realized through optimized lubricant formulations utilizing new additive/base oil combinations to control friction, wear, and traction. In FY13, four awardees: Valvoline, a Division of Ashland Inc, Ford Motor Company, Northwestern University, and Pacific Northwest National Laboratory, were selected to develop novel lubricant formulations to address the objective for improved fuel economy through lubricant design.

Approach:

The approach selected by each of the awardees is summarized below:

- Valvoline, decided to draw upon its significant commercial lubricant experience and develop a suite of fuel efficient products. They are developing a fuel efficient engine, gear, and automatic transmission fluid to meet the goal of 2% fuel economy improvement.
- Northwestern University (NWU) is synthesizing new sulfur and phosphorus free boundary additives to reduce friction under conditions of low speed while, also developing a new shear-thinning additive aimed at lowering frictional losses in the hydrodynamic regime (high speed).
- Ford Motor Company is developing a polyalkylene glycol (PAG) based axle oil, taking advantage of PAG's natural lubricity, high viscosity index, and excellent oxidation and shear stability.
- Pacific Northwest National Laboratory (PNNL) is developing functionalized hyper-branched polymers with the goal of combining low boundary friction and viscosity modification to improve fuel efficiency.

Results and Discussion:

Valvoline has developed two candidate engine oils. Candidate 1 meets API commercial category PC-11 and is a 5W-30. Modeling results predict a 2.04% fuel economy improvement compared to baseline. Candidate 2 is lower viscosity and uses a bio-base oil and friction modifier. Modeling predicts a 2.12% fuel economy improvement. Bench top boundary friction and wear results indicate that candidate 2 has lower overall friction and wear. Traction (tangential stress transmitted across a fluid interface) results show that candidate engine oil1 and 2 have much lower traction than the baseline 15W-40. However, Stribeck curves indicated that in boundary regime, candidate engine oil 1 has higher friction than the 15W-40 baseline,

while candidate engine oil 2 continues to have the lowest friction, traction, and wear. Two candidate axle oils have been developed. Candidate 1 is a field tested 75W-90. Modeling results predict a 0.61% fuel economy improvement. Candidate 2 is field proven chemistry plus Valvoline's proprietary technology; modeling results indicate a 0.73% improvement in fuel economy under conditions of the New European Driving Cycle.

Northwestern University has synthesized three major families of heterocyclic additives for boundary lubrication friction reduction. These compounds are sulfur and phosphorus free and have produced significant reductions in friction (20 – 40%) and wear (~95%) compared to base oils and fully formulated 5W-30 oil. Northwestern University has also developed a method to functionalize solid-state-lubricant nanoparticles (h-BN and B_2O_3) resulting in stable solutions in PAO. Scuffing resistance of the PAO base oil has been increased by a factor of three with 1wt% h-BN nanoparticles.

Ford Motor Company has developed a polyalkylene glycol (PAG) based axle lubricant. The lubricant has low viscosity and improved wear and friction results compared to fully formulated 75W-140 baseline oil. PAG axle oil showed a ~18% improvement in EP load compared to the baseline 75W-140. Initial corrosion testing indicated performance issue but this has been overcome with a corrosion inhibitor that was compatible with the PAG.

Pacific Northwest National Laboratory (PNNL) has been working to understand the role of end group polarity and terminal chain length has on critical solubility requirements for the hyper-branched polymers. They have identified three promising candidates with high VI at relatively low concentrations and these have been sent to collaborators at Oak Ridge National Laboratory for boundary and wear protection studies.

Presentations / Publications:

- Sharma, V., Erdemir, A., Aswath, P.B., "An analytical study of tribofilms generated by the interaction of ashless antiwear additives with ZDDP using XANES and nano-indentation," *Tribology International*, **82A** pp. 43-57 (2015).
- Liu, P., Yu, H., Ren, R., Lockwood, L., and Wang, Q., "Pressure-viscosity coefficient of hydrocarbon base oil through molecular dynamics simulations," submitted to *Tribology Letters*, (2014).
- Wang, Q., Jungk, M., Liu, P., Johnson, B., Zolper, T., Marks, T., Chung, Y.W., and Ren,
- relationships for several lubricants," 2014, National Chung Cheng University, Taiwan.
- Erdemir, A., "Facing the Hard Truth about Friction and Its Impact on Global Energy Consumption," 2014 Distinguished Speaker Series, University of Texas-Arlington, Arlington, TX.
- Johnson, B., He, X., Jin, D., Lv, J., Desanker, M., Song, C., Greco, A., Delferro1, M., Erdemir, A., Chung, Y.W., Marks, T. J., and Wang, Q., "Novel friction modifiers for steel contact," 2014 Tribology Frontiers Conference, Chicago, IL.
- Jin, D., Investigation of several boundary lubrication additives, MS Thesis, Northwestern University, 2014.

- Cosimbescu, L., Robinson, J., “Modified Thermo-Responsive Hyperbranched Polymers for Improved Viscosity and Enhanced Lubricity of Engine Oils”, ACS Meeting, August 2014.

AVPTA Technology Focus Area 4: Alternative Fuels & Lubricants

An Integrated Friction Reduction Technology to Improve Fuel Economy without Sacrificing Durability

DOE-VTO TFA Lead: Kevin Stork
TARDEC TFA Lead: Dr. James 'Jay' Dusenbury

Principal Investigator:
Dr. Stephen Hsu

George Washington University
20101 Academic Way
Ashburn, VA 20147
Phone: (240) 351-6579
E-mail: stevehsu@gwu.edu

Start: FY15
Projected Completion: Ongoing

Objective:

- To develop friction reduction technology capable of improving fuel efficiency of legacy vehicles by at least 2% over the baseline technology using low viscosity lubricants and material technology options (surface textures, diamond-like carbon films, and bonded lubricant films) without sacrificing durability.

Strategic Context:

- Understand the lubricant parameters that effect fuel economy and their impact on durability.
- Demonstrate a battlefield fuel reduction and reduce the logistics burden
- Increase Power Density and Energy Efficiency resulting in increased vehicle range, endurance and operational tempo, while reducing the number of logistics convoys on the battlefield
- Reduce Life Cycle Costs by reducing fuel consumption

Accomplishments:

- New start project. No results to report.

Introduction:

In lubricant formulations, base oils of various purities are the solvent and additives are the solute. Additives are added to the solution to impart various performance bench marks. Two types of additives are used, those that control the bulk property such as antioxidants, dispersants, detergents, viscosity modifier (VM), and antifoam; and those that control surface properties, such as anti-wear, friction modifiers, corrosion inhibitors, rust inhibitors, and surface deactivators. The bulk property control agents are either neutrally charged or less polar than the surface active agents; the surface active agents have somewhat hierarchical polarity stacking order to arrange themselves against the sliding surfaces. The anti-wear agent has to be able to adsorb and react with the metal surface to perform its anti-wear function, so the decomposition products of the anti-wear agent; ZDDP (zincdialkyl dithio-phosphate) have to react with the surface active sites (3). The formulation has to be delicately balanced to avoid precipitations and adverse additive-additive interactions rendering some or most of the additives non-functioning.

Over the decades, the basic lubricant chemistries have remained the same but modifications to the molecular structures and finer control have been made. The total amount of additives used, however, has grown steadily to accommodate increasing performance demands. Friction modifiers were introduced in the 1980s and a new engine dynamometer test Seq. VI was developed to measure their effectiveness.

Approach:

Four tasks are implemented to reach the goal (multiple lines of defense against friction deterioration and wear):

Task 1:

Valvoline will supply a commercial SAE 5W-30 GF-5 lubricant to GWU as the baseline formulation. GWU/Valvoline will work jointly to develop a next generation low viscosity fuel efficient lubricant formulation with at least 2% higher fuel efficiency as measured by Seq. VI engine test. GWU will screen new friction reduction chemistry and tougher anti-wear film chemistry in bench tests to identify potential candidates. Valvoline will incorporate the successful candidates into the formulation for testing. The new formulation will be tested to see whether it achieves the fuel efficiency target (as measured by Seq. VI engine tests).

Task 2:

GWU will develop microencapsulation technique (encapsulation, release mechanism, and survivability through engine operation) to create the second line of defense to provide time-release of additives on demand as an option for Task 1.

Task 3:

GWU will work with GMC on controlling engine component surface topography and fabricate surface textures to increase film thickness and enable more hydrodynamic lubrication mode in the most significant engine components (identified by GMC) to reduce friction throughout a selected engine model. When the specific engine component operation requires additional durability, GWU will deposit DLC film with bonded chemical film on the engine component to provide robust durability.

Task 4:

The team will integrate the improved engine component (friction surface technology in Task 3) with the new energy efficient lubricant to evaluate the combined benefits and robustness of the system durability by bench scale simulation tests for a selected engine component. If the results warrant further testing and development, the industrial partners/and or DOE may consider further investment to commercialize the technology.

Results and Discussion:

New start project. No results to report.

This Page Intentionally Blank

AVPTA Technology Focus Area 4: Alternative Fuels & Lubricants

Power Cylinder Friction Reduction Through Coatings, Surface Finish and Design

DOE-VTO TFA Lead: Kevin Stork
TARDEC TFA Lead: Dr. James 'Jay' Dusenbury

Principal Investigator:
Dr. Arup Gangopadhyay

Ford Motor Company
2101 Village Road
Dearborn, MI 48121
Phone: (313) 322-6986
E-mail: agangopa@ford.com

Start: FY15
Projected Completion: Ongoing

Objectives:

- To develop and demonstrate friction reduction technologies for light, and medium, vehicles that improve fuel efficiency of future vehicles by at least 4% without adverse impacts on engine durability.

Strategic Context:

- Understand the lubricant parameters that effect fuel economy and their impact on durability.
- Demonstrate a battlefield fuel reduction and reduce the logistics burden
- Increase Power Density and Energy Efficiency resulting in increased vehicle range, endurance and operational tempo, while reducing the number of logistics convoys on the battlefield
- Reduce Life Cycle Costs by reducing fuel consumption

Accomplishments:

- New start project. No results to report.

Introduction:

The power cylinder and crankshaft components account for approximately 80-90% of the mechanical friction of an internal combustion engine and therefore, offer a great opportunity to reduce friction by controlling surface asperities interactions. The objective of the proposed research is to develop and demonstrate friction reduction technologies for light, and medium, vehicles that improve fuel efficiency of future vehicles by at least 4% over currently used technologies based on comparative results from chassis dynamometer testing without adverse impacts on engine durability. Experience through years of research in this area leads us to believe that full benefit potential can be achieved only by considering a systems approach.

Approach:

The starting point is the identification of deposition conditions which can produce reliably two levels of porosity in PTWA coatings in addition to nanocomposite coatings. This will be followed by coating characterization including surface roughness, microstructure, hardness etc.

The friction and wear evaluation will start in laboratory bench test rig (Plint TE77) where a section of piston ring slides against a section of the liner. This will provide friction coefficient under boundary lubrication condition. This piece of work will be done at Argonne National Laboratory (ANL). Next, we move to little more complex evaluation involving a motored single cylinder friction rig where the friction force between cylinder surface and piston and rings is measured. This will provide friction under boundary and mixed lubrication regimes. The results from these tests will allow selection of material pair for further evaluation. In parallel, we plan to measure connecting rod bearing friction with different surface textures using the motored bearing test rig where a single connecting rod is dynamically loaded. This is expected to show clearly if the surface textures show any benefits and how much. This evaluation will be followed by multi-cylinder motored friction evaluation where torque to turn the crankshaft in an engine block is measured with GF-5 and PAG oils. This includes friction contributions from piston rings and cylinder interface, piston skirts, main and connecting rod bearings (with surface textures). The results from this test can be used as an input to Ford proprietary software tool to estimate fuel economy benefit in FTP cycles.

In parallel, wear assessments on PTWA coating, and piston rings, pistons, and bearings will be performed using a motored multi-cylinder engine block coupled to a radiotracer method.

The next step would be to go the next higher level of complexity involving fired single cylinder friction evaluation. This test measures the friction force between the cylinder surface and piston and rings. The most promising material pairs can be selected from previous tests can be further evaluated here. In addition to friction, oil consumption will also be measured. The ranking of technologies (PTWA with different porosity levels, low friction ring coatings, piston skirts) and the magnitude of benefits could alter due to the combustion load. This piece of work will be contracted out at Federal Mogul.

Results from previous tests will allow selection of final material pairs for evaluation in engines, first with motored friction tests followed by chassis roll dynamometer tests for demonstration of final fuel economy benefit. The motored engine friction data can be used to estimate fuel economy benefit using the Ford software tool.

We believe this work structure will allow systematic evaluation of each technology providing a better understanding of its friction reduction contribution, wear performance, and oil consumption.

We believe this work structure will allow systematic evaluation of each technology providing a better understanding of its friction reduction contribution, wear performance, and oil consumption.

Results and Discussion:

New start project. No results to report.

This Page Intentionally Blank

AVPTA Technology Focus Area 4: Alternative Fuels & Lubricants

Development of Ionic Liquid-Additized, GF-5/6 Compatible Low-Viscosity Oils for Automotive Engine and Rear Axle Lubrication for 4% Improved Fuel Economy

DOE-VTO TFA Lead: Kevin Stork
TARDEC TFA Lead: Dr. James 'Jay' Dusenbury

Principal Investigator:
Dr. Jun Qu

Oak Ridge National Laboratory
1 Bethel Valley Road
Oak Ridge, TN 37831

Start: FY15
Projected Completion: Ongoing

Objectives:

- To further develop the ionic liquid-additized low viscosity engine oil meeting the GF-5/6 specifications and possessing superior lubricating characteristics.
- Expand the ionic liquid additive technology to rear axle lubricant to gain a combined 4% improvement in vehicle fuel economy.

Strategic Context:

- Understand the lubricant parameters that effect fuel economy and their impact on durability.
- Demonstrate a battlefield fuel reduction and reduce the logistics burden
- Increase Power Density and Energy Efficiency resulting in increased vehicle range, endurance and operational tempo, while reducing the number of logistics convoys on the battlefield
- Reduce Life Cycle Costs by reducing fuel consumption

Accomplishments:

- New start project. No results to report.

Introduction:

On 9/28/2013, the ORNL-GM team successfully concluded a 4-year joint project sponsored by DOE Vehicle Technologies Office (VTO) under a Cooperative Research and Development Agreement (CRADA) for developing ionic liquids as next-generation AW additives for engine lubrication. This team made a major breakthrough in developing new groups of oil-miscible ionic liquids (ILs)3-7, with high thermal stability, ashless, non-corrosiveness, and most importantly effective AW characteristics. Fundamental investigation has correlated the anti-wear and friction reduction mechanisms of IL additives to their physical (absorption) and chemical (tribofilm formation) interactions with the metallic bearing surfaces3-5. In addition, accelerated catalyst aging tests of the IL suggested potentially less adverse effects on three-way catalysts compared to ZDDP6. Working with Lubrizol, the team had developed a prototype IL-additized fully-formulated automotive engine oil (the first ever in the literature). The IL-additized engine oil has low-viscosity (comparable to the pending SAE grade 8) and has demonstrated promising lubricating performance6. High-temperature, high-load (HTHL) engine tests showed similar engine wear and oil aging behavior between the IL-additized low-viscosity engine oil and the Mobil 1 5W-30 engine oil6. Further, Sequence VID engine efficiency dynamometer tests of this prototype IL-additized engine oil demonstrated an improved fuel economy by 2.01% benchmarked against the Mobil 1 5W-30 engine oil6. The initial success of our ionic liquid additive technology has been highlighted at Inside Science8 and Green Car Congress9, and starts gaining interest from both academia and industry.

Approach:

There are a number of bearing components in an automotive vehicle. The second largest parasitic friction induced energy loss is the 3-5% at the rear axle (next to the 10-12% in the engine)1,2, and therefore is identified as the next application for the IL additive technology. GM's modeling predicts a potential recovery of 0.75-1.5% vehicle fuel economy by using a lower viscosity oil. This study proposes to apply ionic liquids to mitigate the challenge of wear protection induced by the reduced oil viscosity. The bearing interface for the rear axle is very different from that in the engine, therefore the IL chemistry will be tailored to better handle the much higher contact stress and longer oil service life required for the rear axle lubricant. This study will also provide us the opportunity to gain deeper fundamental understanding of ILs' anti-wear mechanism such as the roles of the cations and anions, and their advantages in surface absorption and tribofilm formation compared to conventional neutral AW additives. Such understanding will strengthen the scientific basis that we have been building for further material optimization and product development.

ORNL will be leading this joint project with main responsibilities for IL design and synthesis, tribological bench tests, tribofilm characterizations, lubrication modeling, and emission analysis. GM will work with Lubrizol to formulate IL-additized engine and rear axle

lubricants. GM will conduct complementary tribological bench tests, multi-cylinder engine dynamometer tests, and vehicle tests.

Results and Discussion:

New start project. No results to report;

This Page Intentionally Blank

AVPTA Technology Focus Area 4: Alternative Fuels & Lubricants

Methods to Measure, Predict, and Relate Friction, Wear, and Fuel Economy

DOE-VTO TFA Lead: Kevin Stork
TARDEC TFA Lead: Dr. James 'Jay' Dusenbury

Principal Investigator:
Dr. Steven Gravante

with Dr. George Fenske
Ricardo, Inc.
40000 Ricardo Drive
Van Buren Charter Township, MI 48111
Phone: (630) 468-8712
E-mail: Steve.Gravante@ricardo.com

Start: FY15
Projected Completion: Ongoing

Objectives:

- To provide the lab-scale fundamental data (open source), model correlations, and full scale verifications to enable more accurate predictions of friction coefficient and wear for a wider range of engines, lubricants, and operating conditions than currently exists.
- To extend the approach to sliding and rolling friction in gears.

Strategic Context:

- Understand the lubricant parameters that effect fuel economy and their impact on durability.
- Demonstrate a battlefield fuel reduction and reduce the logistics burden
- Increase Power Density and Energy Efficiency resulting in increased vehicle range, endurance and operational tempo, while reducing the number of logistics convoys on the battlefield
- Reduce Life Cycle Costs by reducing fuel consumption

Accomplishments:

- New start project. No results to report.

Introduction:

Friction forces and wear performance in engines and other driveline components can be calculated from equations that capture the understanding of the fundamental physics involved. However, accuracy of the results is dependent on measurement or estimation of the friction coefficient used in the calculations. For contacting surfaces in any component system (piston ring or skirt and liner; bearings; gears, etc.) the friction coefficient is a function of lubricant viscosity, relative speed, surface properties and load, which is captured in a Stribeck curve.

For a given set of operating conditions the curve provides a friction coefficient which can be used to calculate FMEP (Friction Mean Effective Pressure). FMEP is a quantification of losses due to friction during engine operation. It combines all types of friction losses from asperity or boundary friction (caused by metal to metal contact) to hydrodynamic friction (caused by viscous losses) and mixed regimes between. Once FMEP is quantified, whether predicted or measured, it can be used to calculate friction impacts on fuel economy.

Approach:

In this program Ricardo will use existing computer models to specify relevant Stribeck conditions (speed and load) for light duty and heavy duty OEM engines (one or more of each). ANL and EMA will make careful measurements of friction and wear using high-precision lab-scale test rigs as a function of surface and lubricant properties over a range of operating temperatures, loads, and speeds typical of engine (or other) components. The data generated will be used, with some processing, as input to Ricardo's codes to improve correlations between model FMEP predictions and measurements of FMEP in full scale engine or driveline tests.

FMEP is equal to the difference between IMEP (Indicated Mean Effective Pressure), which is the theoretical amount of power the engine can produce from the amount of fuel burned, and BMEP (Brake Mean Effective Pressure), which is the amount of power delivered by the crankshaft. Because FMEP is the relatively small difference between two relatively large numbers, accuracy can be poor when determining FMEP by calculating IMEP and subtracting measured BMEP. It can be measured directly in motored tests, but they lack some of the physical realities (temperatures, combustion forces, etc.) of fired engines. Methods to calculate FMEP from well verified models are needed.

The "technology" developed in this project will be FMEP maps as a function of load and speed which, when coupled with IMEP, can be used with suitable weighting factors to predict fuel consumption for any user-specified driving cycle. The lab-scale rig data will be used to predict wear loads (cycle averaged as a function of speed and load) to compare with wear-load-sliding distance calculations. Lubricant effects will be evaluated in terms of both friction losses and wear performance. The models will be used to predict fuel savings and wear, as validated with engine dyno tests by Ricardo and Navistar using an off-the-shelf high viscosity lubricant and a friction-modified low-viscosity synthetic lubricant. Engine tear-down tests at INL will provide data on engine component wear in fleet-tested vehicles.

Results and Discussion:

New start project. No results to report.

This Page Intentionally Blank

AVPTA Technology Focus Area 4 Adjunct: Tire Efficiency

Improved Tire Efficiency Through Elastomeric Polymers Enhanced with Carbon-based Nanonstructured Materials

DOE-VTO Lead: Leo Breton
TARDEC TFA Lead: Dr. James 'Jay' Dusenbury

Principal Investigator:
Georgios Polyzos

Oak Ridge National Laboratory (ORNL)
Oak Ridge TN 37831-6054

Start Date: FY15
End Date: Ongoing

Objectives:

- Reduce hysteretic losses for reduction of rolling resistance
- Sharply enhance the wear resistance of the tire without compromising its viscoelastic properties.

Strategic Context:

- Develop lower rolling resistance tire materials that increase Fuel Efficiency while maintaining traction and wear characteristics
- Enhance TARDEC's Tire Laboratory capability for rolling resistance testing and enable unique tire characterizations for modeling and simulation.

Accomplishments:

- New start project. No results to report.

Introduction:

In materials science of elastomers the influence of manufactured nanomaterial filler particles is of utmost significance for the performance of innovative rubber products, i.e., passenger and commercial tires with ultralow rolling resistance but high traction. Advances in both performance areas are imperative for the development of improved

tire efficiency to meet Department of Energy's (DOE) fuel consumption reduction target of 4%, all while maintaining or improving wear characteristics of the tire. The unique geometrical configuration of the graphene fillers makes them the most promising carbon based fillers for breakthrough reduction of the rolling resistance.

Approach:

The approach capitalizes on the recent advances in nanomaterial and graphene synthesis and functionalization to suggest a promising avenue for the amalgamation of cutting-edge nanotechnologies that can be utilized towards DOE's technical targets. Recent research efforts focus mainly on the development of composite tires based on carbon black and silica. The project goal is to replace existing fillers (such as carbon black and silica) with higher performance materials (viz., graphene and silica nanofibers). At the conclusion of the project, the team will deliver prototype fuel-efficient tires and control tires. These tires will be evaluated at the Tank Automotive Research Development and Engineering Center (TARDEC). This project will be conducted in collaboration with Michelin Americas Research Company.

The project will enable the fabrication and testing of scalable structures, which are anticipated to demonstrate unprecedented improvements in the rolling and wear resistance of tires. The successful implementation of the project will deliver scalable composite materials and will provide processing conditions that can be utilized in advanced tire manufacturing for breakthrough fuel savings.

Results and Discussion:

- New start project. No results to report.

AVPTA Technology Focus Area 4 Adjunct: Tire Efficiency

Advanced Truck and Bus Radial Materials for Fuel-Efficiency

DOE-VTO TFA Lead: Leo Breton
TARDEC TFA Lead: Dr. James 'Jay' Dusenbury

Principal Investigator:
Dr. Justin Martin

PPG Industries, Inc
Monroeville Technical Center
440 College Park Drive
Monroeville, PA 15146
E-mail: justin.martin@ppg.com

Start Date: FY15
End Date: Ongoing

Objectives:

- Develop a novel surface-modified silica technology and demonstrate 4-6% improved fuel efficiency of truck and bus radial (TBR) tires built from the technology.
- Proposed fuel efficiency increase will be achieved while maintaining or improving tear strength and tread wear.

Strategic Context:

- Develop lower rolling resistance tire materials that increase Fuel Efficiency while maintaining traction and wear characteristics
- Enhance TARDEC's Tire Laboratory capability for rolling resistance testing and enable unique tire characterizations for modeling and simulation.

Accomplishments:

- New start project. No results to report.

Introduction:

Fuel-efficient silica fillers were adopted for passenger tires over 20 years ago. However, similar fuel-efficient benefits have not been realized for truck and bus radial

tires. This project is focused on modifying silica to create an affinity for natural rubber as well as synthetic rubbers so that new, fuel-efficient truck and bus radial tires with optimized wear and tear properties result.

Approach:

This project begins with the team systematically and thoroughly investigating the properties that enable uniform dispersion of silica in both natural and synthetic rubbers. This knowledge will drive custom silica synthesis. Once novel silicas are developed that can be uniformly dispersed throughout multiple rubber types, the team will develop new TBR tread compound formulas. The formulas will be tested at bench scale to predict performance with the best performers being built in actual tires so that on-tire testing can be completed. Two rounds of formulation and tire builds will be conducted during the project to confirm viability. At the conclusion of the project, the team will deliver prototype fuel-efficient tires and control tires. These tires will be evaluated at the Tank Automotive Research Development and Engineering Center (TARDEC).

This project will be conducted in close collaboration with Bridgestone Americas Tire Operations. Bridgestone's technical lead is Dr. Amy Randall, Manager of Advanced Materials.

Results and Discussion:

- New start project. No results to report.

AVPTA Technology Focus Area 5: Electrified Propulsion Systems

Non-Rare Earth Materials for Motors (Integrated Starter / Generator)

DOE-VTO TFA Lead: Susan Rogers
TARDEC TFA Lead: Dean McGrew

Principal Investigator:
Dr. Wesley Zanardelli

Ground Vehicle Power & Mobility
US Army TARDEC

Start Date: October 2012
Projected Completion: Ongoing

Objectives:

- The TARDEC Advanced Propulsion Team, in collaboration with the DOE Vehicle Technologies Office, is working to develop and demonstrate two Integrated Starter Generators (ISG) without rare-earth permanent magnet materials suitable for onboard vehicle power generation.
- Most high-performance electric machines in hybrid electric applications use rare-earth magnets (NdFeB & SmCo) to achieve the required power and torque densities.
- This effort will additionally explore alternate electric machine topologies to achieve its goals.

Strategic Context:

- Reduce / eliminate reliance on non-domestically-sourced rare-earth materials required for power electronics and machines.
- Develop and demonstrate increased on-board and exportable power for vehicle and auxiliary needs.

Accomplishments:

- In FY14, the Critical Design Review (CDR) was held at TARDEC and included participation from SBCT, GVPM Advanced Propulsion, VEA, Remy, and DCS. The detailed designs for both Switched Reluctance (SR) and Spoke Interior Permanent Magnet (Spoke IPM) Integrated Starter Generators (ISGs) were reviewed and the build phase commenced. Confirmed during the review was that the cost of the SR ISG to be less the half that of ISGs utilizing rare-earth permanent magnets.
- Suppliers for both ISG inverters were identified. A subcontract relationship was formed with The Power Electronics & Electric Machinery Research group from Oak Ridge National Laboratory (ORNL) to write the control algorithms and software for the SR ISG inverter and test the ISGs. A Test Plan Review meeting was held and the test plan was finalized.
- An issue surfaced and was resolved related to lower-than-expected material properties (tensile strength, flux density, & core losses) on the iron-cobalt lamination material. Compared with traditional silicon-steel, iron-cobalt offers considerably higher saturation flux density, making it possible for a non-rare-earth generator to approach the performance of a traditional permanent-magnet generator. The iron-cobalt lamination material is not commonly used outside of aerospace due to its higher cost and limited availability. An extensive investigation of the lamination material properties was conducted with the original steel supplier to verify the ISG structure will have adequate safety margin beyond the maximum rated speed. Additionally, the original ISG models have been further refined based on the test results quantifying the electromagnetic properties of the lamination material.
- A novel high temperature plastic was chosen for the coil isolators to assist with meeting motor thermal targets. After initial injection molding difficulties, a new plastic formulation was developed with the plastic supplier to provide the desired thermal conductivity and allow for easier injection molding with thin wall thicknesses.
- A Test Plan Review was conducted at Remy which walked through the verification methods to be employed for all of the requirements. Part of this effort will involve acoustic testing and simulation to establish a baseline for follow-on optimization. The SR motors are known to be loud, but not much empirical data appears to be available to quantify the sources or possible mitigation paths for the follow on work.
- A contract modification adding 5 optional tasks to the contract was awarded to optimize the performance of the SR ISG being developed and demonstrated. The first two options have been exercised. The first option includes a trade study and analysis to identify the five most promising methods to optimize the SR ISG, completion of preliminary designs of three down-selected hardware methods, and one software/control system optimization. The second option funds the detailed design, build and demonstration of the highest ranked SR ISG method identified in the Trade Study to reduce the audible noise signature and cogging torque during operation.
- All hardware has been received by Remy to complete the build activities. The SR stator and rotor assemblies are complete. The Spoke IPM rotor assembly is complete. Both the SR and Spoke IPM ISG builds are scheduled to be completed during January 2015.

Introduction:

The Non-Rare-Earth ISG project has the opportunity to reduce the cost of high-performance power generation hardware. This project seeks alternatives to rare earth designs in case of a supply disruption of rare-earth permanent magnet materials similar to events in 2010-2011. In July 2010, China cut its exports rare earth minerals by 72%. In September 2010, China temporarily cut rare earth exports to Japan due to a maritime dispute. In 2011, China had cut exports further and raised export tariffs for rare earths. The world remains almost completely dependent on China for rare earths.

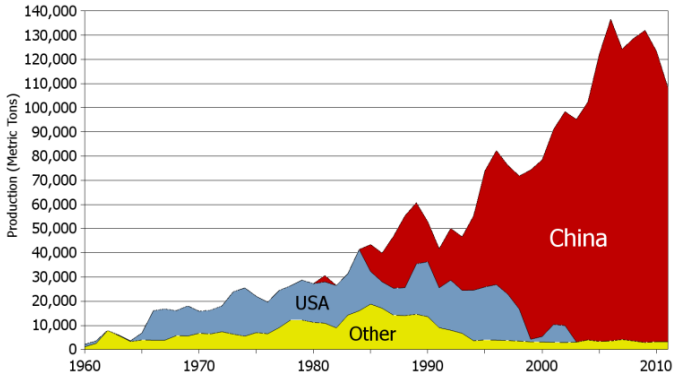

In 2010, The Department of Energy had published a Critical Materials Strategy, ranking Neodymium and Dysprosium among the most critical from an importance and supply risk perspective. Both materials are used in the highest performance Neodymium Iron Boron (NdFeB) permanent magnets available today.

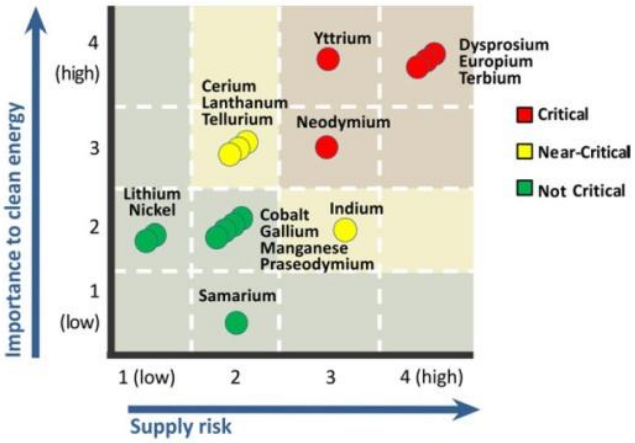

Approach:

This project commenced with trade studies to identify the two most promising ISG architectures without rare-earth permanent magnets and to identify permanent magnet materials which could be leveraged for this effort. The two ISG architectures which were down-selected

include the Switched Reluctance (SR) and Spoke Interior Permanent Magnet (Spoke IPM). The SR architecture does not include permanent magnets. The Spoke IPM is leveraging ferrite magnets which have approximately 1/10 the energy product of high performance rare earth magnets.

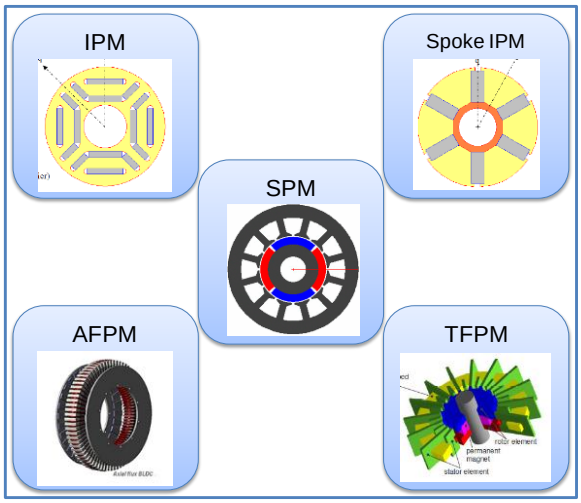

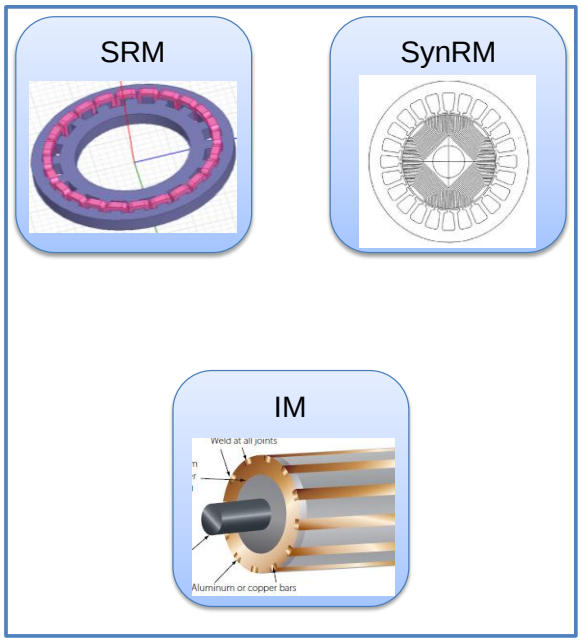

A study on permanent magnets revealed that ferrite and Alnico permanent magnets are the only non-rare-earth permanent magnets available in sufficient quantities to achieve the program goals. Due to the low coercivity of Alnico magnets, ferrite was determined to be the most promising choice for the design.

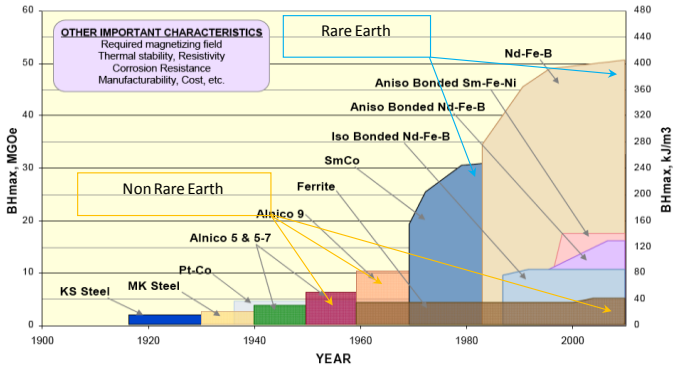

The SR ISG has emerged as the more promising of the two designs evaluated and now being built under the effort. The SR topology is more cost effective than any other known generator architecture - approximately 1/3 the cost of comparable rare earth permanent magnet based designs.

Results and Discussion:

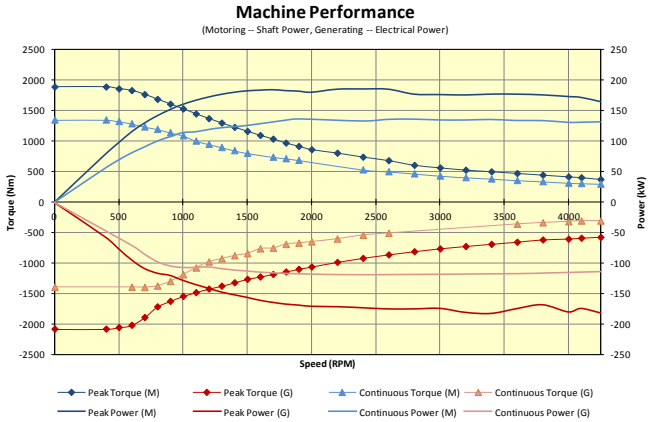

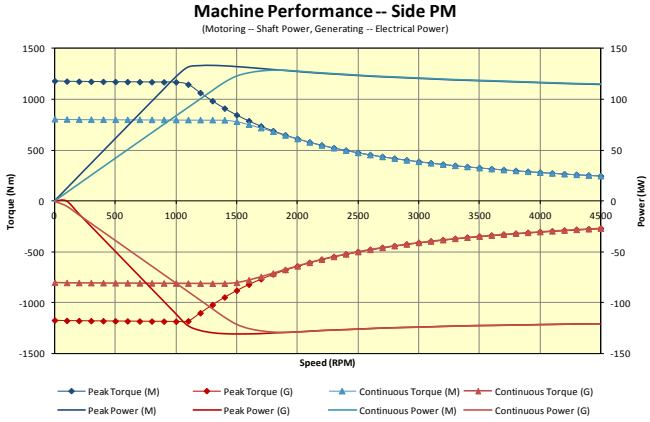

Performance projections for the two ISGs based on Finite Element Analysis are shown above. The Spoke IPM peak torque is presently below the threshold value, however, analysis

is underway to determine the potential for improved performance using emerging non-rare-earth permanent magnets, such as MnBi and FeN. The build status of the SR ISG is at approximately 90% and the Spoke IPM at approximately 80%. Final motor assembly for the SR ISG is expected to be completed during December 2014. Final stator assembly for the Spoke IPM is expected to be completed during December 2014 and final motor assembly during January 2015.

Phase I Deliverables include:

- Switched Reluctance (SR) ISG and ISG controller with associated software for operation, fixtures, couplings, mating connectors, plumbing interfaces, drawings, and documentation (March 2015).
- Spoke Interior Permanent Magnet (Spoke IPM) ISG and ISG controller with associated software for operation, fixtures, couplings, mating connectors, plumbing interfaces, drawings, and documentation (March 2015).

Follow-on work includes two more optimized SR ISG builds and optimized control algorithms to reduce the audible noise and torque ripple of the ISG.

Conclusions:

The hardware builds of both motors are scheduled to be completed by mid-January, 2015. The Spoke IPM ISG will be characterized and tested at Remy's facility in Anderson, IN. The SR ISG will be delivered to Oak Ridge National Laboratory (ORNL) to leverage their controls expertise with SR drives for characterization and testing. Control algorithm and Graphical User Interface (GUI) development and tuning for the first hardware builds is scheduled to be completed in January 2015. The motors will then be delivered to TARDEC no later than March 31, 2015 and integrated with a dynamometer for validation in one of the TARDEC motor evaluation laboratories.

The next phase of work will be beginning in January 2015, which is focused on hardware and control algorithm optimization of the SR design to reduce audible noise and torque ripple leveraging:

- Electromagnetic design optimization
- Higher performance magnetic materials
- Incorporation of mechanical gears
- Methods to optimize inverter and control strategy
- Acoustic prediction study

The trade studies and preliminary designs for the SR optimization tasks will be in progress by the end of Q1FY15.

Publications / Presentations:

- Quarterly Status Updates
- Critical Design Review (CDR)
- Start of Work Meeting for Optimization Task

This Page Intentionally Blank

AVPTA Technology Focus Area 6: Energy Storage & Batteries

Computer-Aided Engineering of Batteries for Military Vehicles

DOE-VTO Lead: David Howell
TARDEC TFA Lead: Dr. Laurence Toomey

Principal Investigator:
Ahmad Pesaram

National Renewable Energy Laboratory (NREL)
15013 Denver West Parkway
Golden, CO 80401

NREL Collaborators:
C. Yang, G.H. Kim, S. Santhanagopalan & K. Smith

Advanced Energy Solutions Collaborator:
Andreas Vlahinos

Start Date: June 2012
Project Completed: January 2014

Objective:

The overall objective was to extend the existing Computer Aided Engineering of Batteries (CAEBAT) tools sponsored by Department of Energy Vehicle Technologies Office to military vehicles. TARDEC's objective was the development of tools to accelerate comparative analysis of alternative lithium-ion batteries designed as drop-in replacements for existing lead-acid cells in 6T battery modules. As part of this effort, NREL objectives were:

- Modify and extend DOE-CAEBAT battery simulation tools to predict the response of lithium- ion battery modules under situations experienced in military vehicles including hot environments, bullet penetration, and mechanical stress.
- Develop models and tools to address response of batteries to abuse conditions such as heating and bullet penetration.
- Extend exiting electrochemical models to include mechanical degradation.

- NREL's eventual goal was to develop tools and procedures so TARDEC staff can accelerate fielding safe, high-performance, and long-lasting lithium-ion batteries in electrified vehicles for military applications.

Strategic Context:

- Reduce battery development time and cost to deployment while improving safety and performance.
- Develop computer-aided engineering tools available to commercial and military product Original Equipment Manufacturers and suppliers for the design and development of battery systems.

Accomplishments:

- Under thermal runaway due to heating, a MATLAB model to generate kinetic parameters for the abuse reactions from experimental DSC/ARC data was developed. This model can be used by the end-user in combination with experimental data for a variety of chemistries to regress the activation energies, rate-constants, and orders of reaction among individual cell components.
- For bullet penetration modeling two approaches were pursued:
  - Developed a "multi-layer puncture" response model to provide a physics-based, flexible, and efficient simulation methodology to predict electrical-thermal-chemical responses of battery cells/packs subject to sudden mechanical failures, such as crush or penetration.
  - Developed an approach to use an explicit dynamics finite element analysis (FEA) model in LS_DYNA to predict bullet penetration geometry and then linking it to the thermal response of the cell.
  - To check the validity of these models, tests were conducted with a 0.308-caliber NATO rifle and ammunition. 25 Ah cylindrical NMC cells and 20 Ah soft pouch prismatic iron- phosphate cells were tested.
  - Only the cells at 100% SOC showed signs of high temperatures or thermal runaway after bullet penetration. Full 3D CT scans of the cylindrical cell at 100% SOC penetrated by a bullet showed the shock wave from the bullet heavily damaged electrodes throughout the entire cell, and was not limited to the bullet penetration site.
  - Generally, the pouch prismatic cells saw much less damage than the wound cylindrical cells, perhaps due to lack of destructive shock waves.
- To link degradation of a lithium ion battery due to internal mechanical stress, a new finite element model to capture swelling/shrinking in cathodes/anodes due to thermal expansion as well as in-plane and out-of-plane deformation was developed. This model could eventually be used to predict the cycle life expectancy of li-ion batteries.
- The developed models provided an insight for TARDEC engineers on evaluating various 6T battery module designs.
- The insight and models developed under this project was transitioned into CAEBAT- 2 project with industry and other stakeholders.

Introduction:

DOE's Vehicle Technologies Office (VTO) has been supporting development of software design tools for accelerating development of batteries for electric drive vehicles for civilian applications under the Computer Aided Engineering of Batteries (CAEBAT) project. Extending the CAEBAT tools for vehicles in military applications was chosen as one the areas for collaboration between VTO and TARDEC under the AVPTA partnership.

The DOE National Renewable Energy Laboratory (NREL) has been lead national laboratory for coordinating CAEBAT. TARDEC provided funding to NREL in June 2012 with the ultimate goal of further enhancing physics- based simulation tools developed by DOE to predict battery response to accelerate fielding optimized batteries in electrified military vehicles. Particularly, TARDEC's objective was the development of tools to accelerate comparative analysis of alternative lithium-ion battery designs as drop-in replacements for existing lead-acid cells in 6T battery modules. In support of TARDEC, NREL's objective was to modify and extend the DOE- CAEBAT battery simulation tools to predict the response of lithium-ion battery modules under abuse conditions experienced in military applications (including hot environments and bullet penetration) and mechanical stress.

In The project was divided into two major tasks: 1) Safety and Abuse Modeling of Cells and 2) Multi-scale Electrochemical Modeling with Mechanical Degradation. Task 1 was further divided into two subtasks: Task 1a Modeling Thermal runaway due to heating and Task 1b Modeling Bullet penetration. The purpose of Task 1a was to extend the chemical kinetics models of CoO_2 cathodes developed under CAEBAT to other chemistries using a differential scanning calorimeter (DSC) and an accelerating rate calorimeter (ARC).

Task 1b:

The objective of Task 1b was to simulate the physics of bullet penetration into a battery cell. Simulating all of the physics of a bullet penetrating into a cell or battery, and subsequent mechanical damage and potential thermal runaway resulting from short circuit heat release, is very complex.

Because of this complexity, Task 1b examined two approaches for modeling. Two subtasks were created: Task 1b.i, Multi-layer Puncture Model, and Task 1b.ii, Mechanical Crush Model.

Task 1b.i:

Assumed that bullet penetration resulted in the puncture of electrode layers, creating statistically-identical short-circuited layers that could be modeled electrochemically-thermally; an NREL CAEBAT model was extended for this subtask.

Task 1b.ii:

Captured the physical state of a cell after bullet penetration using mechanical crush models and then predicting the thermal response using the dynamic modeling commercial software LS_DYNA; bullet penetration data for validation was obtained through field tests performed by Lockheed Martin in Littleton, Colorado, for this subtask. For Task 2, after initial investigations to include stress in life modeling, it was determined that it would be more productive to collaborate with experts at the University of Colorado at Boulder to include electrode mechanical stress in NREL's multi-scale electrochemical-thermal model to investigate the magnitude of stress factors on the degradation and loss of capacity in cells.

The following section provides the results for each of the tasks and subtasks discussed above.

Results and Discussion:

Safety and Abuse Modeling of Cells – Thermal runaway due to heating:

A MATLAB model to generate kinetic parameters for the abuse reactions from experimental DSC/ARC data was developed. This model can be used by the end-user in combination with experimental data for a variety of chemistries to regress the activation energies, rate-constants, and orders of reaction among individual cell components. Experimental data for the different reactions pertaining to the NMC chemistry were generated. Results from this task will serve as input to computational fluid dynamic simulations in calculating the self-heating rate for the different abuse reactions.

Bullet Penetration - Modeling using Multi-Layer Puncture Approach:

NREL researchers developed the multi-layer puncture response model to provide a physics-based, flexible, and efficient simulation methodology to predict electrical-thermal-chemical responses of battery cells/packs subject to sudden mechanical failures, such as crush or penetration. A co- simulation environment, linking NREL's electrochemical, electro-thermal and abuse reaction kinetics models, has been established to simulate battery responses to mechanical abuse. We demonstrated the model capability, applicable to various form factor cells (e.g. pouch, cylindrical, and wound prismatic cells), via three complementary approaches for electro-thermal modeling. The model validation was carried out against experimental data provided by Navy Research Lab and Sandia National Laboratories (SNL).

Bullet Penetration - Modeling using Dynamic Structural Analysis Tools:

The main objective of this research effort is to evaluate and select finite element analysis modeling techniques that can effectively simulate bullet penetration into batteries. The following tasks were completed:

- A parametric solid model of a prismatic battery cell was generated. The number, thickness, and height of the battery cell layers will be parameters of the model.
- A parametric solid model of a bullet was generated. The length, diameter, and conical transition shape will be parameters. This will allow the bullet to be modified to a specified caliber.
- A parametric solid model of the battery and bullet assembly was generated. The bullet height and orientation will be variables of the model. This will allow the bullet position to be modified to a specified line of fire.
- A finite element mesh using the battery and bullet assembly was generated. The elements are solid, and the mesh is appropriate for explicit dynamics simulations.
- A material data set with the appropriate material properties for impact simulations was developed.
- The explicit dynamics software LS_DYNA was used to investigate the failure modes of the battery when penetrated by a bullet. The simulations will predict the impact crater geometry for a specified velocity and caliber bullet.
- Several models for various bullet heights and line of fire orientations, thicknesses, and failure strains of the battery materials were generated and executed.
- Several animations of the bullet penetration were generated to explore the deformed geometry and the strain distributions. Various camera positions such as top, side isometric, and section views were used. The wave propagation was captured.
- For selected cases, the explicit dynamics model transferred the bullet-deformed cell geometry to an electrochemical-thermal finite element model that can predict the electric resistance and transient thermal behavior of the battery.
- A new finite element mesh using the battery and bullet assembly was generated. Shell elements are used that allow delamination of the layers.

Bullet Penetration - Testing for "Validation":

In order to check the validity of these models, we tried to obtain data on the state of a cell after bullet penetration. Except for some limited data from an Army Research Lab (ARL) report on bullet strike with a lithium-ion pack containing cylindrical cells, we could not obtain any public-domain bullet penetration test results for the cells in which TARDEC was interested. Lacking data meaningful to our efforts, we decided to perform bullet penetration tests under this task to gain more insight for "validation" of the models.

To conduct these tests, we subcontracted Lockheed Martin Corporation (LMCO) in Littleton, Colorado. 25 Ah cylindrical cells from Saft and 20 Ah soft pouch prismatic cells from A123 Systems were tested. LMCO performed bullet tests with stringent safety procedures using a 0.308-caliber NATO rifle and ammunition. Cells were tested at 0%, 50%, and 100% SOC. Data were collected with high-speed instrumentation and videos. Most cells lost voltage after bullet penetration.

Only the cells at 100% SOC showed signs of high temperatures or thermal runaway. Full 3D CT scans of the cylindrical cell at 100% SOC penetrated by a bullet at 90° showed the shock wave from the bullet heavily damaged electrodes throughout the entire cell, and was not limited to the bullet penetration site. Generally, the pouch prismatic cells saw much less damage than the wound cylindrical cells, perhaps due to lack of destructive shock waves. The bullet penetration tests provided insight on how cells are impacted physically and potential subsequent thermal events depending on situational geometry, chemistry, SOC, and angle of attack.

3D CT scans provided insightful information to further understand what happened to the cells upon bullet impact. The number of tests performed was limited, due to budget constraints and availability of cells, but the tests provided useful information on improving bullet penetration models.

Multi-scale Electrochemical Modeling with Mechanical Degradation:

Batteries suffer from capacity and power fade due to mechanical-, thermal- and electrochemical-coupled physics. To date, no battery CAE model exists that is capable of predicting large-format cell lifetime and providing design feedback for 3D cell and module design. As an initial step towards filling this gap, NREL and the University of Colorado at Boulder developed and linked new solid mechanics models to explore mechanical phenomena in lithium-ion batteries. The new finite element model captures swelling/shrinking in cathodes/anodes due to thermal expansion and lithium intercalation, as well as in- plane and out-of-plane deformation. Transport of lithium, transport of heat, and generation of heat are provided through linkage with NREL's pre-existing electrochemical-thermal Multi-Scale Multi-Domain (MSMD) model. Example simulations are run for an 8Ah Dow-Kokam pouch cell.

Conclusions:

- Under thermal runaway due to heating, a MATLAB model to generate kinetic parameters for the abuse reactions from experimental DSC/ARC data was developed. This model can be used by the end-user in combination with experimental data for a variety of chemistries to regress the activation energies, rate-constants, and orders of reaction among individual cell components.
- For bullet penetration modeling a "multi-layer puncture" response model was developed to provide a physics-based, flexible, and efficient simulation methodology to predict electrical- thermal-chemical responses of battery cells/packs subject to sudden mechanical failures, such as crush or penetration.

- Developed an approach to use an explicit dynamics finite element analysis (FEA) model in LS_DYNA to predict bullet penetration geometry and then linking it to the thermal response of the cell.

- To check the validity of these models, tests were conducted with a 0.308-caliber NATO rifle and ammunition. 25 Ah cylindrical NMC cells and 20 Ah soft pouch prismatic iron-phosphate cells were tested.

Only the cells at 100% SOC showed signs of high temperatures or thermal runaway after bullet penetration. Full 3D CT scans of the cylindrical cell at 100% SOC penetrated by a bullet showed the shock wave from the bullet heavily damaged electrodes throughout the entire cell, and was not limited to the bullet penetration site.

Generally, the pouch prismatic cells saw much less damage than the wound cylindrical cells, perhaps due to lack of destructive shock waves.

To link degradation of a lithium ion battery due to internal mechanical stress, a new finite element model to capture swelling/shrinking in cathodes/anodes due to thermal expansion as well as in-plane and out-of-plane deformation was developed. This model could eventually be used to predict the cycle life expectancy of li-ion batteries.

The developed models provided an insight for battery OEMs and TARDEC engineers on evaluating various 6T battery module designs.

The insight and models developed under this project was transitioned into CAEBAT-2 project with industry and other stakeholders such as 1. MIT on coupling mechanical behavior to electrochemical-thermal in cells, 2. ANSYS on incorporating thermal abuse kinetics model in Fluent simulation tool, 3. Ford on modeling of cell and modules, 4 Sandia National Labs on better understanding battery abuse tests, and 5. USCAR Car Safety Work Group on evaluating behavior of batteries during crash of electric drive vehicles.

In FY15, these models and lessons learned through this project funded by TARDEC would be continually be shared with CAEBAT-2 performers for inclusion of models and CAEBAT tools that would be provided to end-users from vehicle makers, battery developers, and pack integrator.

Presentations / Publications:

- Ahmad Pesaran, C. Yang, S. Santhanagopalan, G.H. Kim, K. Smith, A. Vlahinos, “Developing Battery Computer Aided Engineering Tools for Military Vehicles,” Final Report to TARDEC, National Renewable Energy Laboratory, Golden, Colorado, December 2013.

Figures and Tables:

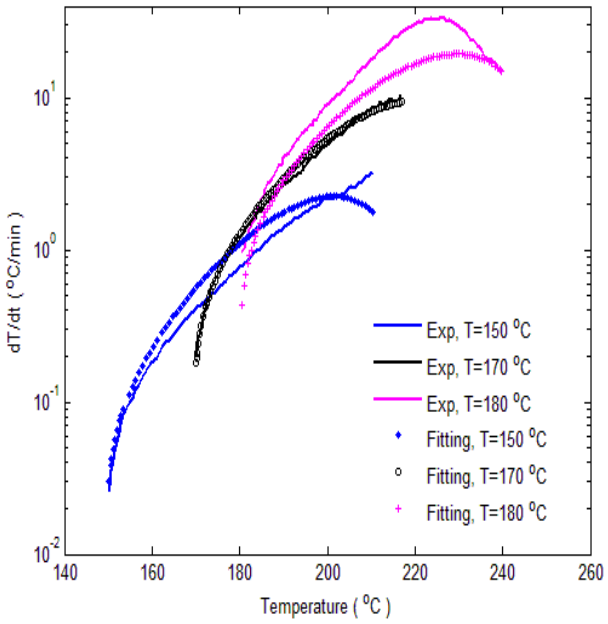

Figure 1. Experimental data and the modeling results used for estimating parameters of cathode-electrolyte reactions. Each color represents a different initial sample temperature for the onset of the abuse reaction.

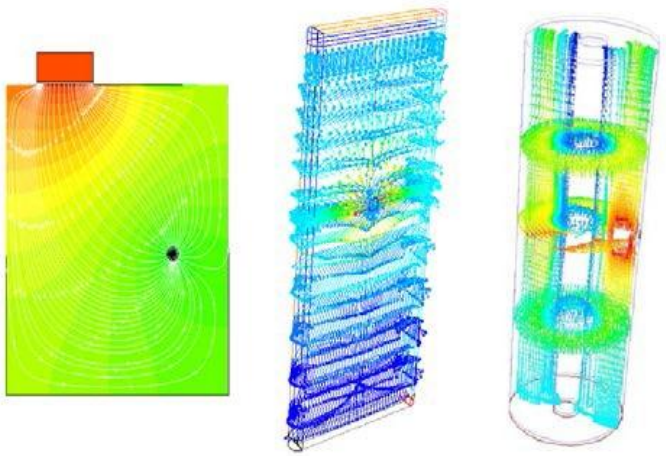

Figure 2. Illustration of 3D fault current flow in a pouch cell, a wound prismatic cell and a cylindrical cell respectively subject to mechanical puncture representing a bullet penetration.

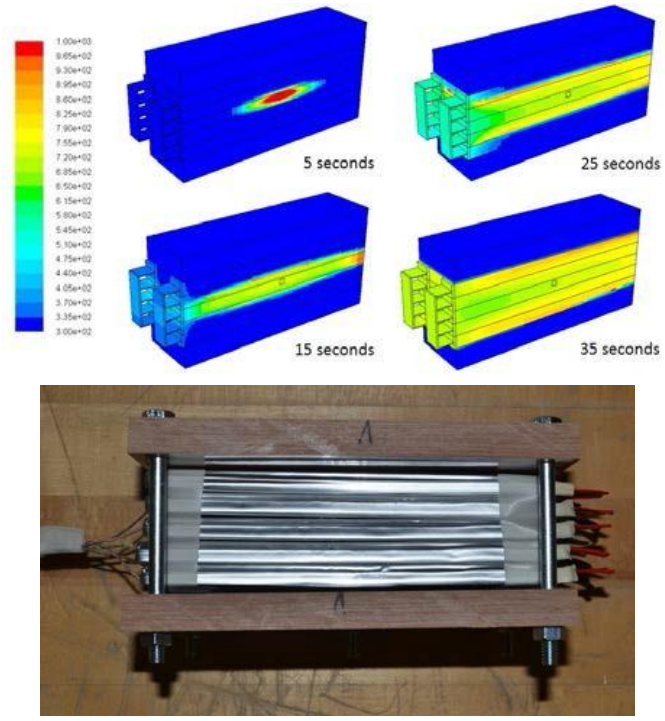

Figure 3. Temperature contours at 5, 15, 25, and 35 seconds respectively after short initialed for in a module, which is modeled based a Sandia National Laboratories' battery module (bottom picture).

Figures Continued on Next Page

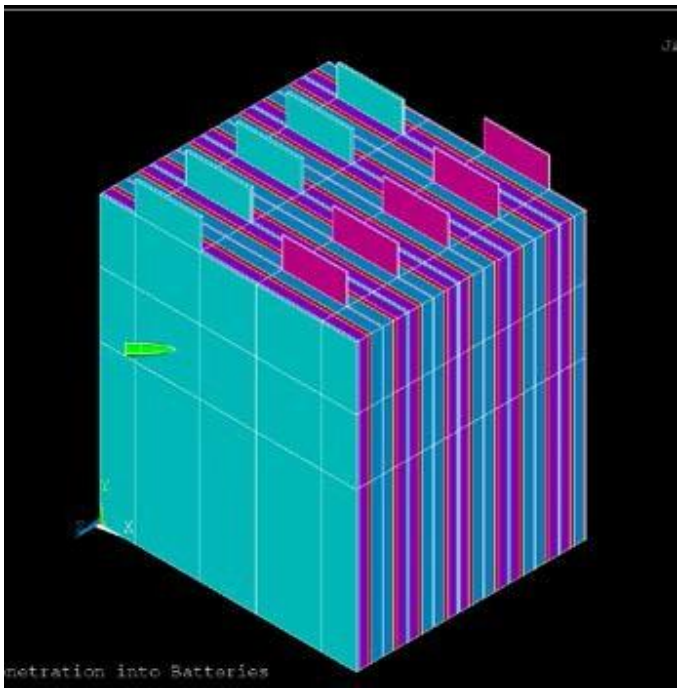

Figure 4. Parametric solid model of a prismatic multi-layer cell (the cell thickness is magnified by 100 times to show details). Also shown is a bullet about to penetrate into the cell.

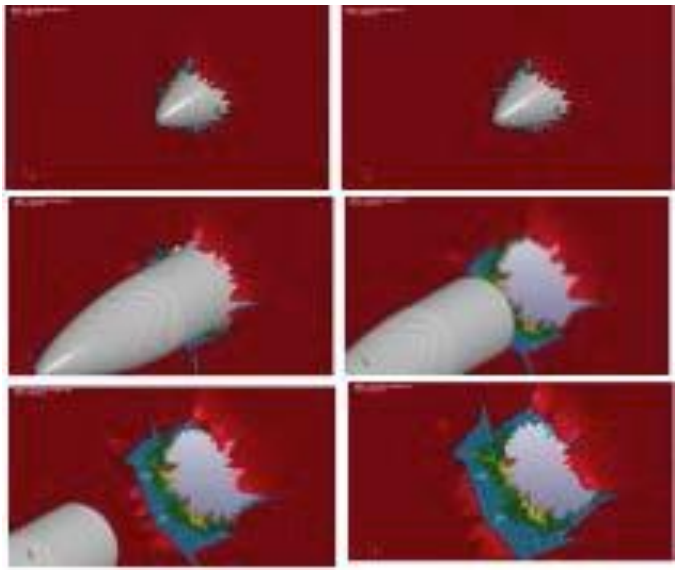

Figure 5. The results of LS-Dyna dynamic mechanical simulation tool showing deformed geometry of a prismatic cell layer after a bullet has struck. (After 0.0008 mili-second (top left), 0.002 ms, 0.004 ms, 0.0044 ms, 0.0056 ms and 0.008 ms (bottom right).

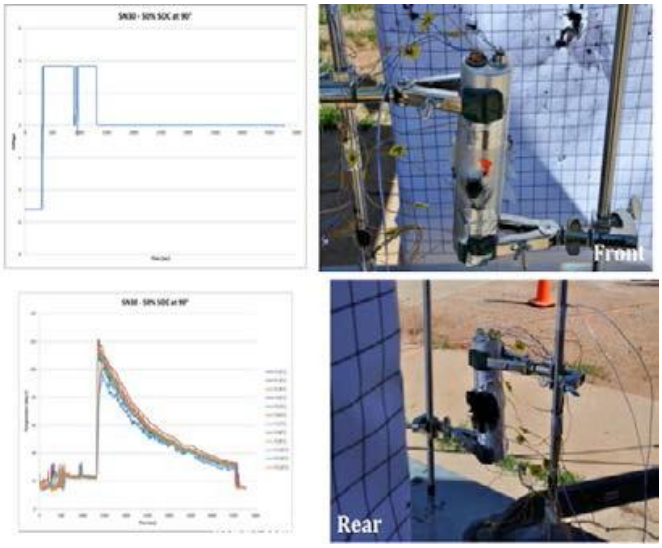

Figure 6. Results from bullet striking a Saft cell at 50% SOC and 90° penetration angle. Voltage drop (top left graph); temperature rise (bottom left graph).

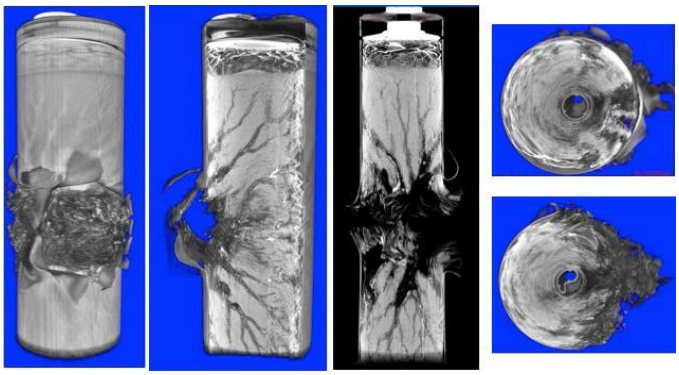

Figure 7. 3D CT Scan of the 100% SOC Saft Cell after Bullet Penetration.

Figures Continued on Next Page

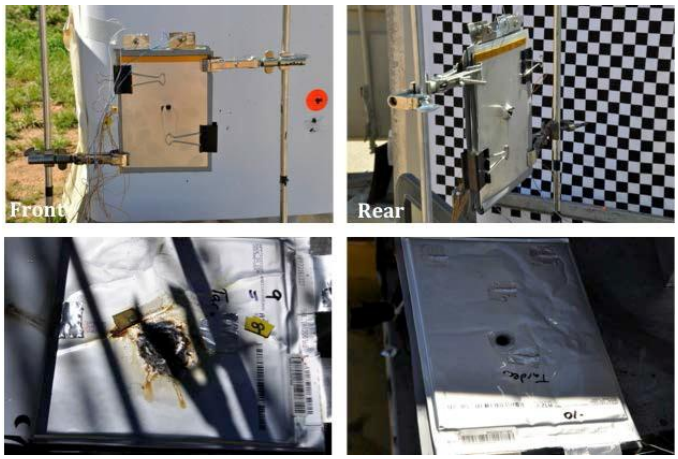

Figure 8. Results from bullet striking a Saft Cell at 50% SOC and 90° penetration angle.

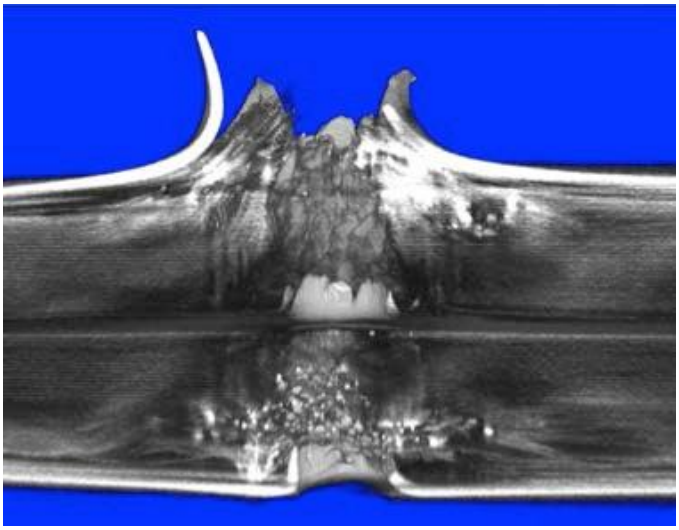

Figure 9. 3D CT scan of the A123 Cell, 50% SOC after bullet strike.

AVPTA Technology Focus Area 6: Energy Storage & Batteries

Efficient Safety and Degradation Modeling of Automotive Li-ion Cells and Pack

DOE-VTO Lead: David Howell
TARDEC TFA Lead: Dr. Laurence Toomey

Principal Investigator:
Christian Shaffer

EC Power
341 N. Science Park Rd.
State College, PA 16803
Phone: (814) 861-6233; Fax: (814) 861-6234
E-mail: ceshaffer@ecpowergroup.com

Subcontractor:
Penn State University, University Park, PA 16802

Start Date: October 2013
Projected End Date: September 2015

Objectives:

- Develop an efficient & robust pack-level safety model.
- Develop abuse and refined life models.
- Perform life, abuse, and safety tests to acquire data for validation.
- Expand extensive materials database by characterizing and adding NCA material.
- Perform co-simulation of our software with structural mechanics software via the Open Architecture Standard (OAS).
- Support DOE CAEBAT activity.

Strategic Context:

- Reduce battery development time and cost to deployment while improving safety and performance.

- Develop computer-aided engineering tools available to commercial and military product Original Equipment Manufacturers and suppliers for the design and development of battery systems.

Accomplishments:

- Successfully validated cell-level safety model with experimental data.
- Successfully completed implementation of pack-level safety model, with coupled electrochemical-thermal physics, which allows user to predict safety of pack using software.
- Investigated ramifications of cell design on safety through large-matrix numerical experiments.
- Completed initial validation of safety and abuse models.
- NCA characterization > 50% complete (-40^{o}C < T < 60^{o}C).

Introduction:

The overarching objective of the ongoing work is to develop experimentally validated, robust, and easy-to-use computation models for Li-ion battery (a) pack-level safety and abuse simulation and (b) advanced and accurate degradation modeling. The commercial need for an efficient pack-level safety and abuse model is best highlighted by the recent Boeing 787 Li-ion battery pack fires, where there has been much debate as to the root cause of the fires, how the failure subsequently spread through the battery pack, and how to avoid such a scenario in the future via enhanced design. The pack-level safety model addresses precisely this type of scenario, yielding great insight as to how an initially local safety-related event such as nail penetration or internal short spreads throughout the pack both thermally and electrically/electrochemically. In addition to pack safety simulation, our team is developing additional chemistry-specific life and abuse models for simulation of blended electrode life and overcharge, for example. The models developed are being extensively validated by generating in-house data from a variety of advanced diagnostics tests. Finally, the team is experimentally characterizing commercially widely-used NCA cathode material (-40^{o}C < T < 60^{o}C) and adding material to the previously developed extensive material database.

Approach:

The EC Power-led team is working to develop physics-based Li-ion battery and pack design software, leveraging EC Power's demonstrated expertise in multi-physics modeling. This physic-based modeling approach results in a *predictive* design software focused on addressing life, safety, and performance barriers over automotive-relevant wide-ranging operating conditions (e.g. -40^{o}C < T < 60^{o}C), which will lead to more widespread adoption of Li-ion batteries in this application. To ensure model accuracy, we also leverage the expertise of the Penn State University team in materials characterization, safety, and life testing, in order to validate the software developed.

Results and Discussion:

Figure 1 highlights the temperature contours from the simulation of a pack-level nail penetration event. This type of a safety test is carried out on new products to ensure safety, and required for several product safety certifications. When the local temperature inside any cell reaches a dangerous level, thermal runaway will ensue, leading to thermal runaway. The predictive design software developed under this project allows users to quickly, cheaply, and safely iterate through various cell and pack designs to optimize safety before a cell is ever built, leading to a more refined and ultimately safer product.

Figure 2 gives an example of the validation of the design software. Figure 6(a) shows the experimental and simulated voltage of a 4Ah cell which has been penetrated with a stainless steel nail; Figure 6(b) gives the temperature inside of the nail and at one location on the cell surface. Overall, good agreement is observed, with the largest discrepancy between experimental and simulated results with nail temperature. Further investigation is ongoing as to the cause of this discrepancy, which could be attributable to experimental noise in the experiment, given the wavy nature of the observed nail temperature. We expect this unprecedented capability of Li-ion battery cell and pack safety simulation will empower manufactures and automakers to reduce time and cost in developing safe Li-ion battery packs.

Finally, as an example of the characterization of NCA cathode material, Figure 7 shows the solid diffusivity of NCA over full depth of discharge (DoD), and at various temperatures ($-40^oC < T < 60^oC$). Note that logarithmic y-axis highlights up to a four orders of magnitude difference in diffusivity over these automotive-relevant conditions; this fact emphasized the importance of the characterization work ongoing in this project, in addition to the software's temperature-dependent materials database developed under previous work.

Conclusions:

EC Power has completed initial software implementation of the models developed under this project, including those related to safety, abuse, and life. Additionally, by working with our partners at Penn State, we have completed our first set of validation testing. The second year of the project will focus on more extensive validation and model refinement, along with completion of the NCA materials characterization. The ultimate goal at the conclusion of the project is to have refined commercial Li-ion battery design software that cuts cost and time from the design phase of automotive Li-ion batteries and packs. As models developed under this project become mature (stable, validated, etc.), they are continually incorporated into our AutoLion™ commercial tool. For example, the pack level safety features developed to date have already been incorporated into the commercial software.

Presentations / Publications:

- 2010 DOE Annual Peer Review Meeting Presentation
- Kalupson, J., Wang, Q., Zhao, W., Sinha, P., Shaffer, C. and Wang, C.Y., "Cell- and Pack-Level Simulation of Large-Format Li-Ion Battery Safety Events," 225th ECS Meeting, Abstract# 160, Orlando, FL, USA, May 11-15, 2014.

Figures and Tables:

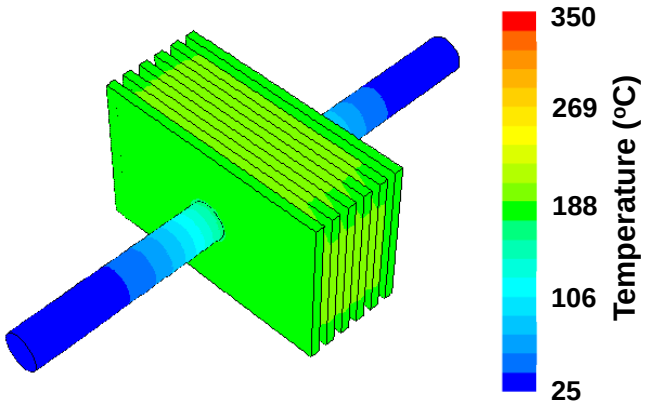

Figure 1: Temperature contours of 6 cell module undergoing nail penetration.

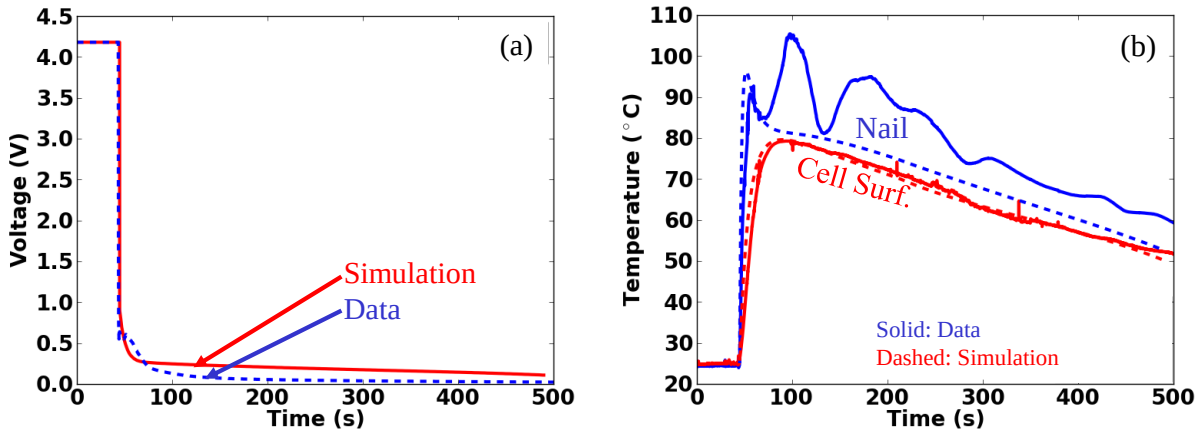

Figure 2: Validation of nail penetration model comparing simulation and experimental data, (a) cell voltage, (b) temperature in nail (blue) and at surface of cell approximately halfway (a) between nail and (b) edge (red).

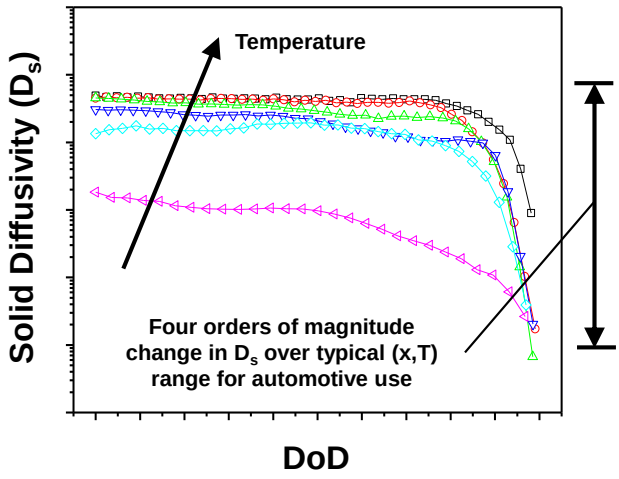

Figure 3: Solid diffusivity of NCA cathode material over full Depth of Discharge (DoD) and temperature.

This Page Intentionally Blank

AVPTA Technology Focus Area 6: Energy Storage & Batteries

Significant Enhancement of Computational Efficiency in Nonlinear Multi-Scale Battery Model for Computer-Aided Engineering

DOE-VTO Lead: David Howell
TARDEC TFA Lead: Dr. Laurence Toomey

Principal Investigator:
Gi-Heon Kim

National Renewable Energy Laboratory (NREL)
1617 Cole Blvd.
Golden, CO 80401

Collaborators:
Kandler Smith, Peter Graf, Myungsoo Jun, Chuanbo Yang
National Reneable Energy Laboratory

Genong Li, Amit Hotchman, Dimitrios Tselepidakis ANSYS

Start Date: October 2013
Projected End Date: September 2015

Objective:

- To develop a computational methodology for a significant enhancement in computation speed of nonlinear multi-scale battery modeling while maintaining or improving the solution accuracy from the most advanced state-of-the-art models.

Strategic Context:

- Reduce battery development time and cost to deployment while improving safety and performance.

- Develop computer-aided engineering tools available to commercial and military product Original Equipment Manufacturers and suppliers for the design and development of battery systems.

Accomplishments:

- Reformulated the model equations using time- scale separation and partial linearization.
- Prototyped ED-GHMSMD and CD-GHMSMD on MATLAB.
- Completed evaluating promising methods for adaptive-SVM.
- Implemented VECTFIT open-source software that improves stability and speed of look-up table identification.
- Developed a method using interconnection-of- systems approach for time-domain realization of nested transfer functions.
- Performed full look-up table identification of all transfer functions associated with Newman model electrode potentials & concentrations
- Developed API to use NREL's SVM and LPD library in ANSYS/FLUENT's CAEBAT module
- Completed GH-PDM and GH-EDM implementation
- Demonstrated stack cell model in the new model framework
- Carried out EDM benchmark tests; x100 speed- up was achieved with the new model framework.
- Performed testing a-SVM prototype code in MATLAB to evaluate tradeoffs in computational efficiency, memory vs. full order model.

Introduction:

Backround and Motivation:

DOE's Computer Aided Engineering for Electric Drive Vehicle Battery (CAEBAT) program has focused on developing innovative modeling capabilities to help industries accelerate mass-market adoption of electric-drive vehicles (EDVs). NREL pioneered the Multi-Scale Multi-Domain (MSMD) model, overcoming challenges in modeling the highly nonlinear multi-scale response of battery systems. The MSMD provides high extent flexibility and multi-physics expandability through its modularized architecture, as well as computational efficiency. NREL also served as a technical advisor/coordinator in transforming the MSMD for industrial use in the first phase of CAEBAT.

However, there are still remaining challenges.

Significant efforts continue being invested to improve energy-power capability and reliability of batteries through engineering at the material level by controlling particulate morphology and size, modifying the particle surface, or redesigning thermodynamics. Due to the complex nonlinear interactions across a wide range and scale of physics, computational cost becomes excessively high to quantify such improvements for the benefits in device level response even

with the state-of-the-art models. The CAEBAT program has resulted in software packages providing 3-D battery pack simulation modeling capability. Because of the system's extreme complexity, the computational cost of simulating a battery pack response is still very high.

Therefore, further improvement of computational efficiency is needed, and the intrinsic nonlinearity of battery physics must be resolved properly. This would enable the use of models in design and management tradeoff studies of performance/life in large vehicle battery systems, which are typically composed of several hundred large-format individual cells.

In this project, we develop a computational methodology for a significant improvement in computational efficiency of nonlinear multi-scale battery modeling while maintaining or enhancing the solution accuracy from the most advanced state-of-the-art models. The project objectives are to:

- Significantly improve the computation speed and stability of multi-scale model framework by eliminating several layers of nested iteration through innovative multi-scale coupling methodology, while still keeping the modular framework architecture.
- Provide a new reduced order model (ROM) that is adaptive to system evolution and identifiable with fewer compound parameters, which is critically needed to improve non-uniformly evolving large battery system life predictions.
- Provide a new ROM that will not fail under severe nonlinear conditions and can achieve compatible speed-up against the state-of-the-art ROMs for battery models.
- Provide multiple options for efficient submodules to improve overall simulation speed while accommodating high-fidelity physics models.

Approach:

The project target will be achieved through complementary parallel efforts in framework efficiency improvement and component efficiency improvement. The team applies an innovative multi-scale coupling methodology (so called, GH-MSMD) using time-scale separation, eliminate several layers of nested iteration, significantly improve the speed and stability upon the original MSMD, and retain the modular framework architecture that is critical to battery behavior simulations. We also develop advanced ROMs for the component models. Computational time is often invested in advance to find reduced order basis in a much lower dimension than that of the full ordinary differential equation systems derived from spatial discretization of the partial differential equation systems. NREL researchers pioneered a reduced-order state space representation of the one-dimensional porous electrochemical model, the State Variable Model (SVM), already having improved the computational speed of the present MSMD model.

The ROM basis is typically restricted to reuse in the system where its characteristics are evolving, such as the battery aging process. In this project, the team develops a new ROM that adapts to system evolution and is identifiable with fewer compound parameters. The state- of-the-art ROMs for battery modeling lose validity when severe nonlinearities arise in the system. In a parallel effort, the team also explores a new ROM that does not fail under severe nonlinear

condition. The project team plans to have the models available to industrial users on a commercial software platform by implementing them in the ANSYS CAEBAT-1 software.

Results and Discussion:

In order to improve the computation speed and stability of multi-scale model framework by eliminating several layers of nested iteration through innovative multi-scale coupling methodology, the original MSMD model governing equations were reformulated using time-scale separation, and variable decomposition. In addition, we established a new technique to identify low order State Variable Model (SVM) that is adaptive to system evolution, such as during aging.

Framework Efficiency Improvement:

An innovative new framework, GH-MSMD, has been developed and implemented up to EDM by the end of FY14. Recent benchmark test performed at EDM level demonstrates that the new GH-MSMD framework could achieve 100 times speed-up while maintaining model accuracy and the modular architecture. The results from EDM benchmark test are presented in Figure 2.

Adaptive ROM Development:

In this task we extend previous work that developed a reduced order model in state variable model form by fitting frequency response of transfer functions representing distributed electrochemical dynamics and use numerical and/or analytical approaches to eliminate the cumbersome pre-processing step required to fit frequency responses and compile results into look-up tables usable only for one battery design at one state of health. Full look-up table identification of all transfer functions associated with Newman model electrode potentials & concentrations has been performed. Adaptive-SVM code has been prototyped in MATLAB to evaluate tradeoffs in computational efficiency, memory versus full order model.

API Development Integrating New Models in CAEBAT Platform:

An application programming interface has been established to integrate NREL's newly developed, computationally efficient physics- based electrochemical model in the ANSYS's CAEBAT-1 software. This opens possibility for industry users to access the most updated NREL's state-of-arts models while using commercially available CAE software suite.

Conclusions:

New quasi-explicit nonlinear multi-scale model framework GH-MSMD has been developed and implemented up to EDM level demonstrating x100 speed up while maintaining model accuracy. In FY15, the model framework will be further refined and extended to CDMs. We will also identify further order reduction opportunities, while developing an algorithm to utilize non-

dimensional form & scaling to circumvent frequent lookup table search or reduce computation upon changes in the parameters. Subsets of the resulting models are used to help industries and transitioned to them through licensing.

Presentations / Publications:

- 2014 DOE Annual Peer Review Meeting Presentation
- M. Jun, K. Smith, P. Graf, “State-space Representation of Li-ion Battery PorousElectrode Impedance Model with Balanced Model Reduction.” J. Power Sources.

Figures and Tables:

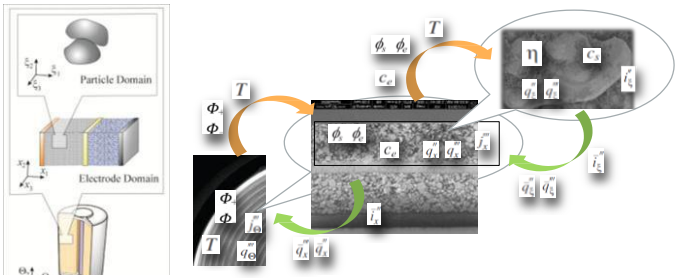

Figure 1: A diagram of intra- and inter-domain coupling coupling protocols used in NREL’s MSMD framework, integrating widely varied scale battery physics in a computationally efficient manner with hierarchical modular architecture.

Figures Continued on Next Page

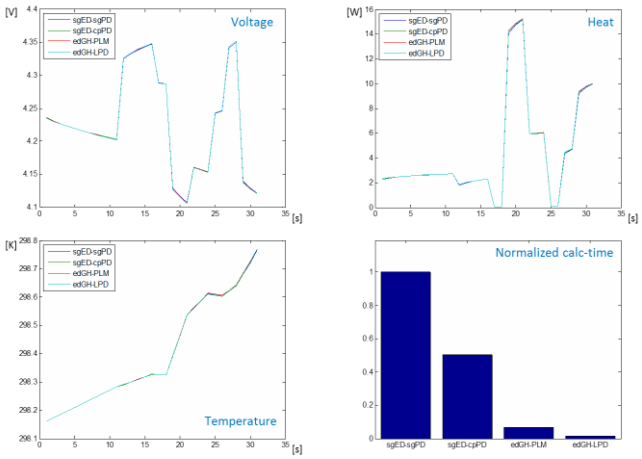

Figure 2: EDM benchmark results shows that, without losing accuracy, x100 speed-up is achieved with the new GH-MSMD framework when the most efficient PDM and EDM submodel combination is chosen.

Figure 2. EDM benchmark results shows that, without losing accuracy, x100 speed-up is achieved with the new GH-MSMD framework when the most efficient PDM and EDM sub-model combination is selected.

Analytical Tools (Modeling & Simulation)

DOE-VTO TFA Lead: David Anderson
TARDEC TFA Lead: Dr. David Lamb

TFA7 Description:

Diverse fuel sources, advanced combustion modes, hybrid/electrified powertrains, energy harvest/waste heat recovery technologies, and using lightweight materials substantially elevate the complexities of efficient vehicle powertrain systems and impose critical challenges for system integration and control. These efficient vehicle powertrain sub-systems, with new characteristics and strongly interactive dynamics, necessitate research on system integration and advanced control strategies. An integrated and analytical systems approach ensure that the various sub-systems of the vehicle work seamlessly, reliably and synergistically to optimize coordination so as to maximize vehicle energy efficiency, power density and emission reduction potential in real-world applications. Through state-of-the-art modeling and analysis, concepts and strategies can be screened during the vehicle design stage, and most promising candidates and key pathways to bring them to realization in an effective time frame can be identified. Critical components and/or systems needing specific development can also be identified and analyzed with simulation tools.

Activities Suspended:

- Eff**e**ctive 21 May 2014, TFA7 activities were suspended by joint agreement of the respective agency Directors. Activities were suspended because no unique, stand-alone projects were identified, and as a regular course of business, Modeling & Simulation is embedded within essentially every AVPTA-related project.
- TFA7 may be reactivated at any time upon respective agency Directors concurrence.

This Page Intentionally Blank

AVPTA Technology Focus Area 8: Advanced / Modular Manufacturing

Advanced / Modular Manufacturing (Proposed)

DOE-VTO TFA Lead: TBD
TARDEC TFA Lead: TBD

TFA8 Description:

As new capabilities, functionalities, materials, structures and related technologies mature and migrate into legacy and next generation ground vehicles, added emphasis will be placed on advanced manufacturing techniques, especially focusing on modularity that enables multiple configurations from a single, basic platform. TFA8 will investigate emerging and unique component, sub-system, system and full-vehicle manufacturing processes and equipment.

Start-up Pending:

- TFA8 start-up is pending obtaining participation interest and directional funding contribution commitment from the DOE Advanced Manufacturing Office (AMO).
- TARDEC has made initial contact with AMO representatives as a prelude to convening a respective agency Subject Matter Experts (SMEs) meeting to identify candidate Areas of Mutual Technical Interest. TARDEC is targeting the 2015 DOE-VTO Annual Merit Review meeting as a forum at which to convene a SMEs 'First Contact' meeting.

This Page Intentionally Blank

AVPTA Technology Focus Area 9: Autonomy-enabled Technologies

Autonomy-enabled Technologies (Starting-up)

DOE-VTO TFA Lead: David Anderson
TARDEC TFA Lead: Robert "Rob" Karlsen

TFA9 Description:

Autonomy-enabled technologies have the promise to significantly decrease fuel consumption through a variety of mechanisms. For example, platooning, where vehicles travel close to each other in order to reduce aerodynamic drag at high speeds, can only be achieved through connectivity and automation. A significant source of excess fuel consumption comes from vehicle operators driving in a sub-optimal manner, such as exceeding optimal speeds and accelerating and decelerating too quickly. Intelligent systems can help increase fuel efficiency by providing information to the driver to improve operational behavior, by determining more efficient routes based on topography or traffic conditions, or by taking control of certain vehicle functions. An automated traffic management system, implement through a system of autonomous vehicles connected with intelligent roadway infrastructure, could greatly reduce vehicle start/stops and slowdowns, optimizing traffic flow, and improving mobility in urban driving. Preliminary research by the National Renewable Energy Laboratory (NREL) indicates that platooning could increase fuel efficiency by 10%, eliminating driver inefficiencies another 15%, and completely automating the vehicle transportation system could yield a 40% improvement. However, these estimates are based on a limited number of experiments, which may not include the full range of variability that a real world system would experience, nor potential second-order effects, such as an increase in vehicle miles traveled. Accordingly, additional analysis and targeted experimentation are needed to more fully explore the limitations that these autonomy-enabled technologies may have in regards to increasing fuel efficiency across the transportation system.

Starting-up:

TFA9 is currently seeking candidate project proposals in Areas of Mutual Technical Interest.

This Page Intentionally Blank

SUSTAINMENT PLAN / TIMELINE

The following figure illustrates the Alliance Sustainment Plan and Timeline for the annual new-start project review and selection process.

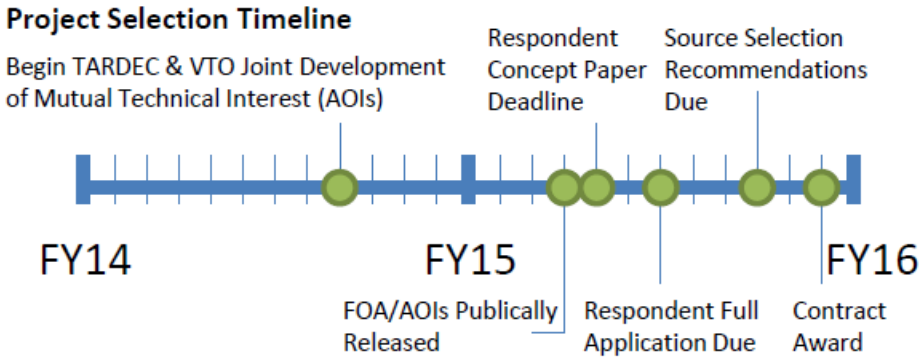

Key Milestone Activities Include:

- TFA Leads & SMEs participate during the VTO Annual Merit Review (June)
- Joint TARDEC / VTO development of next FY FOA/AOI descriptions, scope, deliverables and funds contributions (July – October)
- Directors jointly select new-start projects to add to the AVPTA portfolio (July)
- Sources selected contracts awarded (September)
- Next FY FOA publicly released (January)
- Quarterly: Directors Review Meetings (As convenient during the quarter)
- Quarterly: Technical Status Reports (Published October, January, April & July)
- Annually: Alliance Annual Report (Published during Q1 of the following FY; e.g. FY15 Annual Report published during Q1FY16).

This Page Intentionally Blank

APPENDIX A

Memorandum of Understanding

Between

U. S. Department of Energy

And

U. S. Department of Defense

Concerning Cooperation in a Strategic Partnership to Enhance Energy Security

I. Purpose

The purpose of this Memorandum of Understanding (MOU) is to identify a framework for cooperation and partnership between the Department of Energy (DOE) and the Department of Defense (DOD), hereafter referred to as the Parties, to strengthen coordination of efforts to enhance national energy security, and demonstrate Federal Government leadership in transitioning America to a low carbon economy. This MOU covers, but is not limited to, efforts in the areas of energy efficiency, renewable energy, water efficiency, fossil fuels, alternative fuels, efficient transportation technologies and fueling infrastructure, grid security, smart grid, storage, waste-to-energy, basic science research, mobile/deployable power, small modular reactor nuclear energy, and related areas.

II. Legal Authority

DOE enters into this MOU under the authority of section 646 of the Department of Energy Organization Act (Pub. L. 95-91, as amended; 42 U.S.C. § 7256). DOD enters into this MOU under the authority of DOD Instruction 4000.19 "Inter-Service and Intra-Governmental Support" August 9, 1995.

III. Background

In the 2010 Quadrennial Defense Review, the DOD expressed an intent to partner with other U.S. agencies to research, develop, test, and evaluate new sustainable energy technologies. The DOD aims to speed innovative energy and conservation technologies from laboratories to military end users, and it uses military installations as a test bed to demonstrate and create a market for innovative energy efficiency and renewable energy technologies coming out of DOE laboratories, among other sources. The DOE is currently supporting a range of projects aimed at improving energy efficiency and renewable energy efforts across the military services.

Energy security for the DOD means having assured access to reliable supplies of energy and the ability to protect and deliver sufficient energy to meet operational and Installation energy needs. Energy efficiency can serve as a force multiplier, increasing the range and endurance of forces in the field while reducing the number of combat forces diverted to protect energy supply lines, as well as reducing long-term energy costs. DOD is also increasing its use of renewable energy supplies and reducing energy demand to improve energy security and operational effectiveness, reduce greenhouse gas (GHG) emissions in support of U.S. climate change initiatives, and protect the DOD from energy price fluctuations. Solving military challenges through innovation has the potential to yield spin-off technologies that benefit the civilian community as well.

The DOE is the lead Federal agency responsible for the development and deployment of advanced energy technologies, yet DOD will need to invest in many of these same energy technologies as well as other energy technologies which may be unique to DOD's operational requirements. Partnering with DOD provides DOE the opportunity to accelerate the deployment of its technologies and expertise toward the critical economic and energy security needs of the United States and to promote scientific and technological innovation.

The Parties acknowledge the significant positive collaboration that already exists between DOE and DOD and intend through this MOU to strengthen and broaden that cooperation.

IV. Activities

Specific activities covered under this MOU include, but are not limited to:

A. Evaluate energy systems and technology management solutions that meet DOD objectives including developing energy technologies that meet DOD energy requirements. Work collaboratively to identify a strategy for their development and deployment.

B. Maximize DOD access to DOE technical expertise and assistance through cooperation in the deployment and pilot testing of emerging energy technologies. Technology areas may include, but are not limited to, energy efficiency, renewable energy, water efficiency, fossil fuels, alternative fuels, efficient transportation technologies and fueling infrastructure, grid security (e.g., superconductivity, power, electronics, microgrids, cyber, EMP), smart grid, storage, waste-to-energy, basic science research, mobile/deployable power, small modular reactor nuclear energy, and related areas.

C. Expand cooperation related to energy management practices and knowledge exchange, working to ensure that Federal leadership is in compliance with all statutory and Executive Order goals and objectives, particularly in the area of GHG reductions. Encourage the sharing of data, including, but not limited to, data on internal energy management projects and technical assistance projects.

D. Collaborate on science and technology (S&T) projects at research institutions sponsored by either agency. Synchronize research and development (R&D) of new knowledge and technologies to expand complementary efforts.

E. Develop joint initiatives for major energy technology research, development and demonstration programs of mutual interest to DOD and DOE, such as pilot or demonstration facilities which address military needs and also may address national security needs that transcend military requirements. DOD installations may serve as test beds for such technical demonstrations.

F. Develop human capital within DOE and DOD through teaching and education. Work to integrate respective agency energy training and knowledge exchange practices.

G. Encourage professional exchanges and formal liaison relationships between all DOE and DOD components including, but not limited to, laboratory, headquarters, military installations, combatant command headquarters, and forward operating bases.

H. Collaborate on issues regarding nuclear power, except naval nuclear propulsion, including developing a business, licensing and regulatory strategy as appropriate, and evaluating the integration of energy technologies with other industrial applications that support DOD objectives for energy security and GHG reduction. Collaboration will include NRC review and licensing of nuclear power plants that are deployed for DOD purposes, and are located on or adjacent to DOD U.S. installations.

V. Implementation

DOE and DOD intend to develop and conduct cooperative activities relating to identified high priority energy strategic needs, where such cooperation contributes to the efficiency, productivity, and overall success of the activity. The Parties intend for the activities to be executed under the MOU to be established by a joint DOE/DOD senior-level Executive Committee. This Executive Committee will be co-chaired by a designee of the Under Secretary of Defense (Acquisition,

Logistics and Technology) and a designee of the Deputy Secretary from DOE. The Executive Committee will be responsible for the operations and governance of this MOU. Under the direction of the Co-Chairs, the Committee will include representatives from each of the principal DOE offices, specifically, the Office of the Under Secretary for Science, the National Nuclear Security Administration, and the Office of the Under Secretary for Energy. From the Department of Defense representatives will include the Deputy Under Secretary of Defense (Installations and Environment) and the Director of Operational Energy Plans and Programs. Additional members from both Agencies that may be involved in issues or functions of this MOU may be added. Upon agreement of both Departments, the Co-Chairs will appoint a team to develop, within 60 days, a charter and operating structure, membership, products, and decision processes.

The Executive Committee may establish working groups of Federal employees to perform and execute necessary activities contemplated by this MOU at their discretion. The Executive Committee and its working groups may make consensus recommendations based on their collaboration.

The Executive Committee will determine an appropriate regular meeting schedule, not to be less than four times annually. The Co-Chairs will be responsible for the development and distribution of agendas, presentations, and minutes of each meeting. Action items will be clearly identified and tracked in the minutes.

The Co-Chairs will be responsible for any reporting to the appropriate Departmental Secretarial Officers and will outline accomplishments, issues, redirections, and change assessments. The reporting will be coordinated by the Co-Chairs as appropriate.

The Co-Chairs will be responsible for any reports or presentations that are requested by other organizations, subject to the necessary review of each Party.

VI. Funding

Each party intends to coordinate their individual funding and resource decisions in order to maximize the benefits of cooperation under this MOU. Any transfer of funds or sharing of resources between the parties will be pursuant to a separate or pre-existing agreement.

VII. General

Work under this MOU will be jointly planned and monitored by the DOD and DOE.

In the event any activity undertaken by the agencies to implement the purposes of this MOU involves access to and sharing or transfer of technology subject to patents or other intellectual property rights, such access and sharing or transfer will be provided on terms which recognize and are consistent with the adequate and effective protection of intellectual property rights.

This MOU is strictly for internal management purposes for each of the Parties. It is not legally enforceable and shall not be construed to create any legal obligation on the part of either Party. This MOU shall not be construed to provide a private right or cause of action for or by any person or entity.

This MOU in no way restricts either of the Parties from participating in any activity with other public or private agencies, organizations, or individuals.

This MOU is intended to complement, and not to duplicate, cooperation by the Parties under the Memorandum of Understanding between the Department of Energy (National Nuclear Security Administration)/(Office of Science)/(Office of the Under Secretary) and the Department of Defense (Acquisition, Technology and Logistics) concerning Cooperation in a Strategic Partnership to Enhance National Security of January 26, 2009.

All agreements herein are subject to, and will be carried out in compliance with, all Federal applicable laws, regulations and other legal requirements.

This MOU is neither a fiscal nor a funds obligation document. Nothing in this MOU authorizes or is intended to obligate the Parties to expend, exchange, or reimburse funds, services, or supplies, or transfer or receive anything of value.

VIII. Contacts/Designated Representatives

Under Secretary for Science
U.S. Department of Energy
Washington, DC 20585

Under Secretary for Energy
U.S. Department of Energy
Washington, DC 20585

Under Secretary for Nuclear Security
U.S. Department of Energy
Washington, DC 20585

Deputy Under Secretary of Defense
Installations and Environment
U.S. Department of Defense
Washington, DC 20301

Director of Operational Energy Plans and Programs
U.S. Department of Defense
Washington, DC 20301

Deputy Assistant to the Secretary of Defense for Nuclear Matters
U.S. Department of Defense
Washington, D.C. 20301-3050

IX. Duration of Agreement

This MOU is effective on the date of the final signature and will remain in effect until it is terminated by mutual agreement of the Parties or by either Party providing ninety days written notice to the other. This MOU may be modified at any time by written agreement of the Parties. Nothing in this MOU shall be interpreted to limit or otherwise affect any authorities, powers, rights, or privileges accorded to DOD or DOE or any of the officers, employees, or organizational units under any statute, rule, regulation, contract, or agreement.

Daniel B. Poneman
Deputy Secretary of Energy

JUL 2 2 2010
Date

William J. Lynn III
Deputy Secretary of Defense

JUL 2 2 2010
Date

APPENDIX B

The Deputy Secretary of Energy

and

The Under Secretary of the Army

CHARTER

Advanced Vehicle Power Technology Alliance

I. DESIGNATION

By authority of this charter and effective this date, the Advanced Vehicle Power Technology Alliance (AVPTA) is established. AVPTA shall be active until the charter is rescinded, repealed, terminated or suspended.

II. MISSION

The AVPTA will be a partnership between the Department of the Army (DA) and the Department of Energy (DOE) in accordance with Section IV. E of the Department of Defense (DoD) and DOE Memorandum Of Understanding Concerning Cooperating in a Strategic Partnership to Enhance Energy Security, for the establishment of a joint technology research initiative in the area of ground vehicle power technology research, development and transition. The six focus areas of science and technology are: (1) advanced combustion engines and transmissions; (2) lightweight structures and materials; (3) energy recovery and thermal management; (4) alternative fuels and lubricants; (5) hybrid propulsions systems (including batteries); and (6) analytical tools. Where requirements are common, the two Departments will leverage resources to improve transition of technologies into both the commercial and military marketplace. The Alliance will also leverage industrial research and development (IRAD) involving commercial automotive and defense ground vehicle manufacturers to transition technologies and increase precompetitive research and development.

III. RESPONSIBILITY

The AVPTA is designated as the Department of the Army's and Department of Energy's primary point of contact for automotive power technology in the six areas above. Consistent with applicable law, regulation and policy, the AVPTA may conduct its activities in accordance with such agreements as are deemed necessary for its efficient operation.

IV. AUTHORITY

The AVPTA is jointly led by the Director, U.S. Army Tank Automotive Research, Development and Engineering Center (hereinafter "Director"), and the Department of Energy Program Manager for Vehicle Technologies (hereinafter "Program Manager"). Both the Director and Program Manager maintain authorities over their respective budgets. The AVPTA conducts activities in accordance with the DOD-DOE Energy Security Memorandum of Understanding. DOE enters into this MOU under the authority of section 646 of the Department of Energy Organization Act (Pub. L. 95-91, as amended; 42 U.S.C. § The Army enters into this MOU under the authority of DOD Instruction 4000.19 "Inter-Service and Intra-Governmental Support" August 9, 1995. The Director and Program Manager are the principle and primary points of contact for the prioritization of automotive/ground vehicle power and energy technologies in the six areas above.

V. COORDINATION

The AVPTA shall, as appropriate, coordinate activities and actions with associated government agencies, industries and academia with a focus on efficient vehicle power systems. The DOE and DA leads will meet on a regular basis to coordinate science and technology (S&T) activities, and will align S&T projects and products where requirements are similar. A yearly meeting will be conducted to assess results, update requirements and determine new joint efforts. Results will be reported back to the Under Secretary of the Army and the Deputy Secretary of Energy.

VI. ADVISORY BOARD

The Director and Program Manager may establish a Senior Advisory Board with other government agencies to review strategic planning and make recommendations on future activities. All activities associated with the Senior Advisory Board will comply with the Federal Advisory Committee Act, 5 U.S.C. App. 2 (FACA) and implementing regulation and policy, as applicable. As authorized by law, regulation and policy, the Senior Advisory Board may seek the individual advice of non-Government employees (*e.g.,* individual members of industry or academia) to secure facts and other information to assist the Senior Advisory Board's review.

VII. LEGAL AUTHORITY

The Director and Program Manager will ensure that the activities of the AVPTA are conducted in a manner consistent with all applicable laws, regulations and policies. In particular, all interactions with industry, academia, or other non-governmental entities will be reviewed in advance by appropriate agency counsel to confirm that any necessary enabling

authorities exist and to ensure compliance with the FACA and implementing regulations and policies.

VIII. TERMINATION AND REVIEW

This charter shall terminate automatically on the five-year anniversary date unless expressly approved for renewal by the undersigned. This charter will be reviewed by the Director and the Program Manager biannually on its anniversary date to ensure currency, completeness and adequacy. Changes to mission and/or responsibilities will require the review by and approval of the Secretary of the Army and the Secretary of Energy.

Daniel B. Poneman
Deputy Secretary of Energy

Joseph W. Westphal
Under Secretary of the Army

Dated: July 18, 2011

This Page Intentionally Blank